Photoswitchable glutamate receptors to control neurotransmission with light

Mercè Izquierdo Serra

Aquesta tesi doctoral està subjecta a la llicència ***Reconeixement- SenseObraDerivada 3.0. Espanya de Creative Commons***.

Esta tesis doctoral está sujeta a la licencia ***Reconocimiento - SinObraDerivada 3.0. España de Creative* Commons**.

This doctoral thesis is licensed under the ***Creative Commons Attribution-NoDerivatives 3.0. Spain License***.

Programa de Doctorat en Biomedicina

2010-2014

Photoswitchable glutamate receptors to control neurotransmission with light

Memòria presentada per Mercè Izquierdo Serra per optar al títol de doctor per la Universitat de Barcelona.

Mercè Izquierdo Serra

Nanoprobes and Nanoswitches Group

Institute for Bioengineering of Catalonia

Director

Prof. Pau Gorostiza Langa

ICREA Researcher

Nanoprobes and Nanoswitches Group

Institute for Bioengineering of Catalonia

Tutor

Dr. Artur Llobet Berenguer

Laboratory of Neurobiology

Bellvitge Biomedical Research Institute

Barcelona, March 2014

Himalaya, 2013

Ever tried. Ever failed. No matter. Try again. Fail again. Fail better.

Samuel Beckett

Al Carlo,

Table of contents

Structure of the thesis

The introductory chapter is divided in two main blocks. The first block is focused on the neurotransmission process, where some basic concepts are described related to the presynaptic and postsynaptic terminal. A brief outline of the main techniques used to assay and manipulate this process is also included. The second block is a review of the recently developed photoswitches used to control the activity of neuronal receptors and ion channels. There we explain how they function, their design process and the relevance of each one.

The three following chapters are dedicated to the description of the results obtained in this study. Each chapter focuses on one main objective, starting with the use of LiGluR Ca^{2+}-permeability, then the application of two-photon stimulation, and the last one about the photo-sensitization of endogenous receptors.

Finally, in the fifth chapter the main conclusions of this study can be found. An extended summary in Catalan has been included in a final sixth chapter. Detailed protocols of the techniques and procedures that have been set up in the laboratory during this study are placed in the appendix.

Chapter 1
Introduction

1.1 NEUROTRANSMISSION

When the propagating membrane depolarization (action potential, AP) travels along a neuronal process and reaches the presynaptic terminal, voltage-gated calcium channels (VGCC) open inducing a calcium (Ca^{2+}) entry, which triggers the fusion of neurotransmitter-containing synaptic vesicles. Neurotransmitters are subsequently released to the synaptic cleft, where they bind and activate postsynaptic receptors evoking an electrical response in the postsynaptic cell (**Fig. 1.1a**) (Borst and Sakmann 1996, Katz and Miledi 1967a).

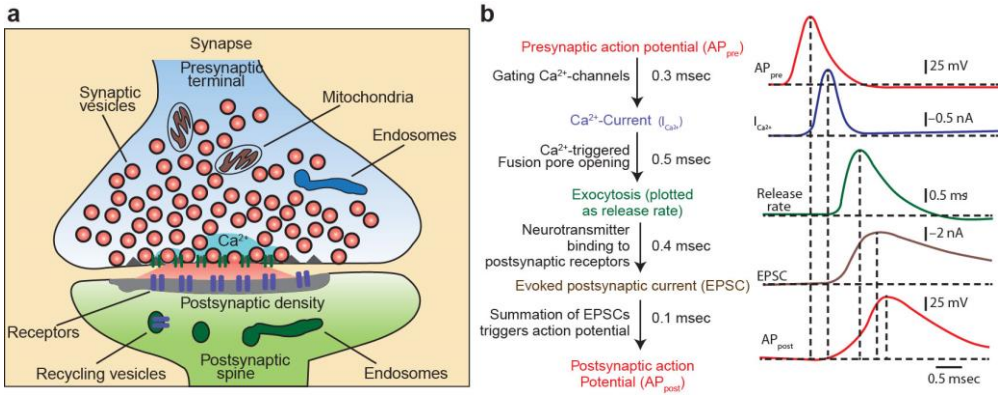

Figure 1.1. The synapses. (a) Schematic representation of a synapse. Presynaptic terminal (in blue) is characterized by synaptic vesicles filled with neurotransmitter and the specialized active zone, containing Ca^{2+}-channels and docked vesicles that will be fused upon AP and the subsequent Ca^{2+} increase (blue). In the postsynaptic neuron (in green), ligand-gated receptors are waiting

for the release of the neurotransmitter (red) to be activated and initiate a membrane depolarization and AP generation in the green neuron. By means of the chemical synapse the AP from the first neuron has successfully been transduced to the subsequent neuron. **(b)** Schematic traces representing the sequence and the fast time course of synaptic transmission. Traces are representative from of pre and postsynaptic patch-clamp recordings at the calyx of Held synapse. From (Südhof 2012).

This process of neurotransmission allows the nerve impulse to propagate from one neuron to another in the chemical synapse, which can be seen as the functional unit of the brain. Since neurotransmission is at the basis of communication between neurons, it must be an extremely fast and synchronized process (**Fig.1.1b**). All the sequential events involved in neurotransmission take place in less than a millisecond, which surprisingly is in the range of the opening time for voltage-channels (Katz and Miledi 1965, Sabatini and Regehr 1996, Borst and Sakmann 1996)

Here we describe the neurotransmission process from a general point of view, focusing on the main topics of the pre- and postsynaptic terminal. However, when taking into account all the particularities of each type of synapses, neurotransmission is a more complex process.

1.1.1 Presynaptic terminal

Neurotransmitters are released in discrete packages called quanta and each quantum of transmitters produces a postsynaptic potential of fixed size (Fatt and Katz 1952, Del Castillo and Katz 1954a). As a consequence, the release of neurotransmitters in a synapse is an all-or-none process, whose occurrence depends on the amount of Ca^{2+} influx after the AP (Katz and Miledi 1967b, Del Castillo and Katz 1954b, Dodge and Rahamimoff 1967). Later on, it was discovered that those quanta of neurotransmitters were packaged in synaptic vesicles. The cargo of the synaptic vesicle varies depending on the synaptic terminal type and, correspondingly to the type of cargo, specific receptors are localized at the postsynaptic site.

Structure of the presynaptic terminal

In a typical presynaptic terminal (**Fig. 1.2a**), synaptic vesicles are the first elements that can be identified using electron microscopy. Usually there are between several

dozens and thousands of 40-nm-diameter vesicles (Takamori et al. 2006). Some of them are placed near an electron-dense region rich of proteins, the so-called active zone where the fusion takes place. The vesicles that are functionally docked to this protein scaffold comprise the readily releasable pool (RRP) (**Fig. 1.3**) (Schikorski and Stevens 2001, Sätzler et al. 2002, Rizzoli and Betz 2005).

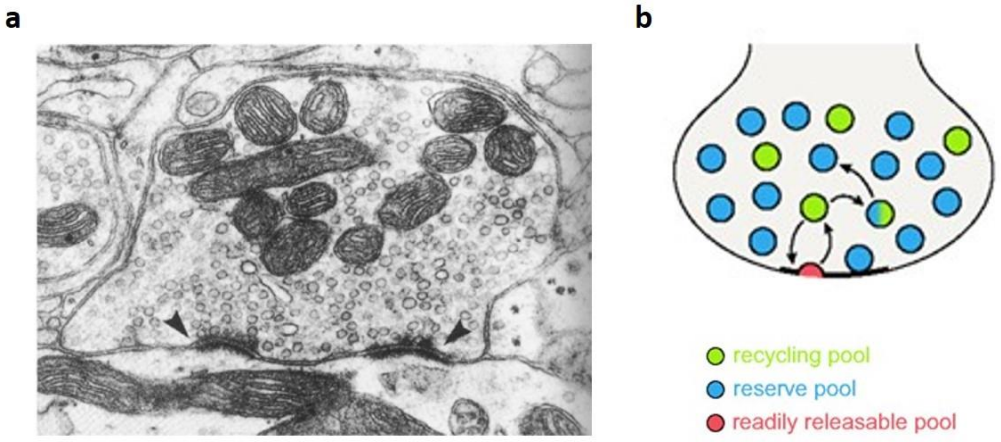

Figure 1.2. Structure of the presynaptic terminal. (a) Electron microscopy image of a synaptic terminal of the cerebellum. The active zone can be identified as a dark band with docked vesicles on the membrane (arrow heads). The large and dark structures are mitochondria. From (Kandel R., Schwartz H., and Jessel M. 1991) **(b)** Scheme of the presynaptic terminal with the different vesicle pools represented on it and its dynamics after stimulation of the neurotransmission. Adapted from (Denker and Rizzoli 2010)**.**

The main functions of the active zone are vesicle recruitment and regulation of release, guaranteeing the close localization between Ca^{2+}-channels and vesicles (Murthy and De Camilli 2003) (**Fig. 1.3a**). Some of the proteins that organize the active zone are piccolo (Wang et al. 1999), bassoon (Tom Dieck et al. 1998) or RIM (rab3-interacting molecule) (Wang et al. 1997). Not all active zones are placed along the cell membrane as shown in **Figure 1.2a** and **1.3a**, instead, presynaptic terminals present different structural organization depending on the functional needs of the synapse. In sensorial synapses (e.g., photoreceptors or hair cells) there is a specialized proteic structure, the sypatic ribbon, which is extended into the cytoplasm and tethers a large pool of releasable vesicles (**Fig. 1.3b**). This specialized structure

with the large number of vesicles attached to it, allows the synapse to be highly sensitive and to support sustained release (Matthews and Fuchs 2010).

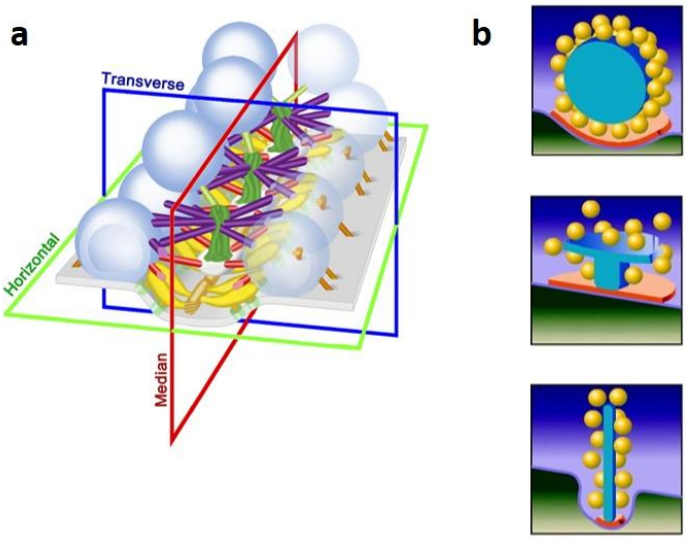

Figure 1.3. Structure of the active zone. (a) Schematic drawing of the components forming the active zone from of the frog's neuromuscular junction. The precise position of each element has been determined by electron tomography. Vesicles are represented in blue. Inserted in the membrane in green there are the VGCC. The scaffolding proteins of the active zone that assemble together the vesicles and Ca^{2+} channels are represented in yellow, brown, purple and green. From (Harlow et al. 2013) **(b)** Schematic drawings of synapses with diverse geometry. Upper: hair cell in frog, middle: photoreceptor from *Drosophila* and lower: photoreceptor from rat. From (Zhai and Bellen 2004).

To maintain the integrity of the typical presynaptic terminal upon continuous activation, vesicles are involved in a dynamic cycle of fusion and retrieval. At least three different groups of vesicles can be distinguished: the RRP, the recycle pool and the reserve (Denker and Rizzoli 2010) or resting pool (Alabi and Tsien 2012) (**Fig. 1.2b**). In an hippocampal synapse, few vesicles conform the RRP (Stevens and Williams 2007), which are immediately available for release. Once this pool is depleted, the release continues with the secondary pool, the recycling pool (10-20% of synaptic vesicles). After fusion is triggered by physiological stimulation, vesicles of this pool are recycled; however, the recycling mechanism is still debated: kiss-and-run, clathrin-mediated endocytosis, endosomal recycling or bulk endocytosis are the

proposed modes (Rizzoli and Jahn 2007) to co-exist, being their contribution largely dependent on the type of stimulation applied. Finally, the third pool comprises the remaining 50-85% of vesicles (Fernandez-Alfonso and Ryan 2008, Harata et al. 2001), and it is only released upon strong stimulation (Schneggenburger, Meyer, and Neher 1999). This pool is not affected by the turnover of vesicles (Harata et al. 2001). Vesicles from the reserve and recycling pool can be exchanged between synaptic boutons (Fernandez-Alfonso and Ryan 2008). Regulation of the dynamics and size of vesicle pools can influence synaptic strength and presynaptic plasticity (Alabi and Tsien 2012).

Exocytosis

The fact that exocytosis is the mechanism behind the neurotransmitters' quanta release was first demonstrated morphologically by using electron microscopy. A key study by Reese and Heuser performed freeze-fracture (Heuser et al. 1979) and electron micrographs (Heuser and Reese 1981) of the neuromuscular junction. They captured structures that corresponded to vesicles just fused with the membrane (Ω-shaped vesicles). Interestingly, the number of these structures increased after a treatment aimed to promote the released of quanta.

Exocytosis is the process by which the cell secretes the content of vesicles or granules to the exterior (Lindau and Gomperts 1991). One type of secretion occurs **constitutively** in the majority of cell types and it serves to deliver newly synthesized proteins on the cell membrane or new components to the extracellular matrix. The other type of exocytosis occurs in the presence of a specific signal – is the **regulated exocytosis**. In excitable cells, this mode of exocytosis is triggered by an intracellular Ca^{2+} increase after an AP. Nevertheless, secretion also exists in non-excitable cells and it occurs as a consequence of the activation of specific membrane receptors. Besides being the mechanism underling the realese of neurotransmitters in synaptic terminals, Ca^{2+}-regulated exocytosis is also the mechanism involved in the secretion of hormones in neuroendocrine cells or in the release of granule content in mast cells and T cells (Pang and Südhof 2010).

Types of release

Calcium induces various types of neurotransmission release in the presynaptic terminal. Two types of evoked release are triggered by APs: one is **time-locked** with the presynaptic AP with a delay of less than 0.5 ms and the second is a **slow asynchronous** release that occurs upon repetitive AP (Goda and Stevens 1994). There is an additional mode called **spontaneous miniature** release that is triggered without stimulation.

The role of voltage-gated calcium channels in exocytosis

The presence of VGCC on synaptic terminals was suggested from experiments done in the giant squid synapse. By stepping the membrane potential of the presynaptic terminal while blocking voltage-sensitive Na^+ and K^+ channels (using tetrodotoxin (TTX) and tetraethylammonium (TEA), respectively), it was observed that the residual inward current of the presynaptic terminal was proportional to the postsynaptic potential recordered. This was the first evidence that neurotransmission is a consequence of the activation of voltage-gated calcium channels (Llinás 1977).

Expression of VGCC is not only restricted to nerve cells, they are also present in other excitable cells such as skeletal and cardiac muscle cells, endocrine cells or retina. In all cells, these channels are activated by membrane depolarization (AP or sub-threshold depolarizations) allowing Ca^{2+} entry into the cell. The intracellular Ca^{2+} rise regulates many cellular events such as contraction, secretion, synaptic transmission or gene expression (Catterall 2000).

VGCCs are a protein complexes formed by four or five different subunits (**Fig. 1.4**) (Catterall 2000). The α_1 is the largest subunit composing the channel and it is homologous to the α subunit from voltage-gated Na^+ channels (Tanabe et al. 1987). It contains the pore, the voltage sensor, the gating apparatus and most of the regulation sites that recognize second messengers, drugs or toxins (Catterall et al. 2005). Although the functionality of VGCCs is sufficient with the α_1 subunit, the presence of $\alpha_2\delta$, γ and β subunits is needed to enhance their expression level and to modulate its kinetics and voltage-dependence (Singer et al. 1991). The nomenclature of these channels indicates the type of α_1 subunit they contain, α_1 subunit are divided

in three structurally and functionally related families (Ca_v1, Ca_v2, Ca_v3) (Ertel et al. 2000).

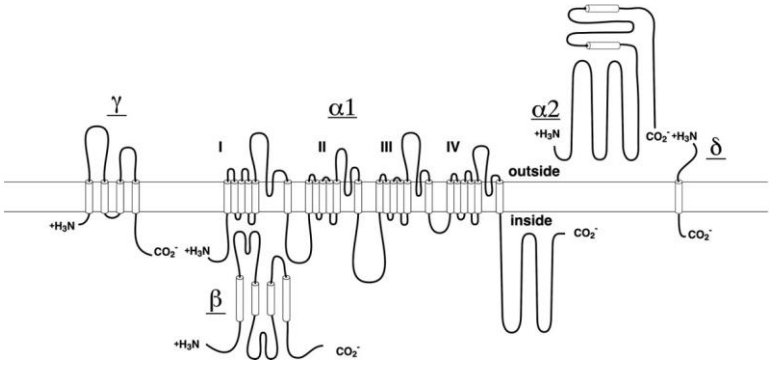

Figure 1.4. Structure of voltage-gated calcium channels. The VGCC complexes are formed by the central subunit α1, the subunit α2γ (carachterized by a single transmembrane segment and a huge extracellular domain), the intracellular β subunit and the optional four-transmembrane subunit γ. From (Catterall 2000).

However, Ca^{2+} currents were first classified by their physiological and pharmacological properties in 6 groups, and still occasionally they are named using the old system (see relationship between Ca^{2+} channel subunits and current types in **Table 1.1**). Although Ca^{2+} current type L is present in most of the excitable cells, it is the main component of Ca^{2+} current in muscle and endocrine cells (Catterall 2000). This kind of current is sensible to organic blockers like phenylalkylamines, dihydroxipyridines (e.g., nifedipine) and benzothiazepines. It is generally characterized by activation with strong depolarizations and a long-lasting current (Catterall et al. 2005). The P/Q-, N- and R-type of currents are mainly found in nerve cells, participating in the neurotransmitter release (Catterall 2000). This three types of Ca^{2+} currents are resistant to L-type organic blockers, but they are sensitive to snail and spider peptide toxins: P- and Q-type are blocked by the spider toxin ω-Agatoxin IVA (Mintz et al. 1992, Randall and Tsien 1995), N-type by the marine snail toxin ω-Conotoxin GVIA (McCleskey et al. 1987) and a specific blocker of R-type was found recently, the SNX-482 a peptide toxin from another spider (Newcomb et al. 1998). P/Q-, N- and R-type of currents are also activated with strong depolarizations. The last type of Ca^{2+} current is the T, it is present in a wide variety of cell types and contrary to L-type

current, this one is activated at much more negative potentials and the current is transient. Ca^{2+} current type T is resistant to all the specific toxins that block the rest of the Ca^{2+} currents. (Catterall et al. 2005).

In synapses, a precisely localization of VGCC is crucial for a proper function of neurotransmission. The millisecond synaptic delay between the arrival of AP at the presynaptic terminal and the release of neurotransmitter has suggested that there is a tight coupling between VGCC and the Ca^{2+}-sensor for exocytosis (**Fig1.1b**) (Eggermann et al. 2012). In some CNS synapses, it has been demonstrated that only few VGCC (around two or three channels) are required to trigger the release of neurotransmitter and that VGCC are coupled to the Ca^{2+}-sensor at a nanometer (20 to 100 nm, e.g. fast GABAergic synapse (Bucurenciu et al. 2008)) or micrometer distance (< 300nm, e.g. calyx of Held (Borst and Sakmann 1996)). However, the coupling distance of the VGCC in a synapse may change to regulate the synaptic strength (Vyleta and Jonas 2014).

Ca^{2+} channel	**Ca^{2+} current type**	**Localization**	**Specific blockers**
$Ca_v1.1–4$	L	Myocytes, endocrine cells, neuronal cell bodies, proximal dendrites, mast cells, pacemaker cells, spinal cord, cochlear hair cells and retina	Dihydropyridines, phenylalkylamines, benzothiazepines
$Ca_v2.1$	P/Q	Nerve terminals, dendrites and neuroendocrine cells	ω-Agatoxin
$Ca_v2.2$	N	Nerve terminals, dendrites and neuroendocrine cells	ω-Conotoxin GVIA
$Ca_v2.3$	R	Neuronal cell bodies and dendrites	SNX-482
$Ca_v3.1–3$	T	Neuronal cell bodies, dendrites and myocytes	None

Table 1.1. Classification of VGCC, their localization and their main specific blockers. (adapted from (A. Catterall et al. 2013)).

The distance between the Ca^{2+}-source and the Ca^{2+}-sensor can be proven by using exogenous Ca^{2+} chelators with different binding rates and similar affinities for the cation (Adler et al. 1991, Eggermann et al. 2012). The couple EGTA and BAPTA is usually employed for this kind of experiments (BAPTA has a binding rate 40 times

faster than EGTA). Intracellular application of these exogenous chelators will block neurotransmitter release by capturing Ca^{2+} on its way from the Ca^{2+}-source to the Ca^{2+}-sensor. Such blocking of neurotransmission will depend on both concentration and binding rate of the chelators used. As a consequence, if the coupling distance is short only a fast chelator will be able to intercept the Ca^{2+} ion. In contrast, for longer distances, both the fast and the slow chelator will inhibit release. By using this method, the presence of nano or micro domains has been identified in different synapses from the CNS (Eggermann et al. 2012).

Mechanism of exocytosis

Besides the tight coupling between VGCC and Ca^{2+}-sensor, neurotransmission needs an effective molecular mechanism to transduce the signal and promote vesicle fusion and release. This exocytic machinery can be divided into three functional groups, represented in **Figure 1.5a** from right to left: the fusion core of machinery SNARE/SM, containing SNARE proteins (synaptobrevin/VAMP, syntaxin-1, and SNAP-25) and the SM protein Munc18-1, the Ca^{2+}-sensor synaptotagmin-1 and its assistant, complexin, and the last group formed by the active zone protein complex containing RIM, Munc13, and RIM-BP and a Ca^{2+} channel (Südhof 2013).

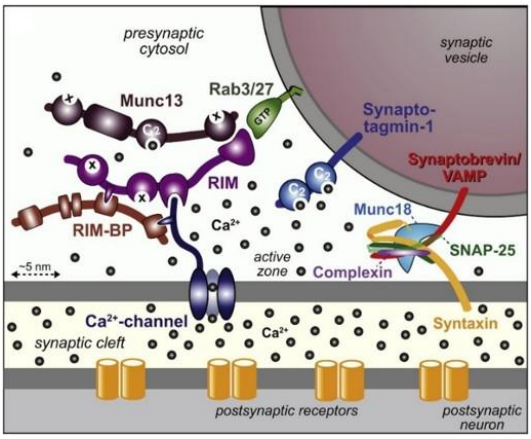

Figure 1.5. The exocytic machinery. Schematic representation of the exocytic machinery involved in the Ca^{2+}-triggered exocytosis. From (Südhof 2013)

- *Fusion process*

Membrane fusion is mediated by the complex SNARE (soluble NSF attachment receptor proteins) and SM proteins (Sec1/Munc18-like proteins) (**Fig. 1.5**).

In the synapse the SNARE complex is formed by the vesicular protein synaptobrevin (or VAMP,vesicle-associated membrane protein) and two proteins located into the targeted plasma membrane, syntaxin-1 and SNAP-25 (Synaptosome-associated protein of 25 kDa) (Söllner, Whiteheart, et al. 1993). During the process of vesicle fusion, the SNARE complex reversibly assembles into a parallel four-helical bundle formed by the α-helical domains of synabtobrevin, syntaxin-1 and two of SNAP-25 (Sutton et al. 1998). Clostridial neurotoxins specifically target the SNARE proteins and inhibit synaptic transmission (Schiavo, Matteoli, and Montecucco 2000), revealing that this complex is essential for neurosecretion. Recently, the number of SNARE complexes necessary to drive fusion has been under debate. Although distinct theoretical studies converge on the fact that three SNARE complex are sufficient (Shi et al. 2012, Hua and Scheller 2001, van den Bogaart and Jahn 2011, Mohrmann et al. 2010), physiological vesicle fusion might involve tens of SNARE complexes. It has been suggested that the amount of SNARE complexes on the vesicle could regulate the speed and Ca^{2+} dependence of neurotransmitter release (Südhof 2013).

The SM proteins are soluble proteins that interact with syntaxin. The SM member Munc-18 binds to the closed conformation of syntaxin-1, prior to vesicle docking and SNARE complex assembly (**Fig. 1.6**) (Dulubova et al. 1999, Misura, Scheller, and Weis 2000). Munc-18 also interacts with the assembled SNARE complex (Dulubova et al. 2007), and it is essential for the fusion. The hypothetical role of Munc-18 during membrane fusion is to mediate lipid mixing (Südhof 2013). Deletion of Munc-18 resulted into a complete loss of neurotransmission and a subsequent neurodegeneration (Verhage et al. 2000). Interestingly, this study showed that neurotransmission is needed for maintaining synaptic connectivity but it is not required for the early stages of brain assembly.

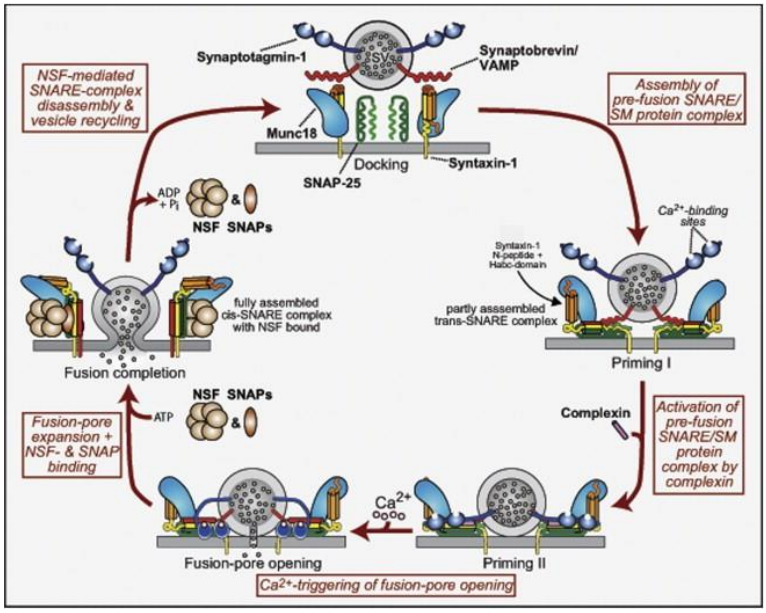

Figure 1.6 Assembly/disassembly cycle of the SNARE/SM complex. Schematic representation of the assembly/disassembly cycle of the SNARE/SM complex and the role each component in all exocytosis stages: docking, priming I, priming II, fusion pore opening and full-collapse of the vesicle. From (Südhof 2013)

SNARE/SM complex are disassembled after fusion to recycle. Some proteins assist them in their assembly/disassembly cycle (**Fig 1.6**). The complex is maintained by chaperones (CSPs and synucleins) (Burré et al. 2010, Sharma, Burré, and Südhof 2011, Sharma et al. 2012), while the ATPase NSF and its adaptors mediate the disassembly (Söllner, Bennett, et al. 1993, Mayer, Wickner, and Haas 1996).

The function of SNARE/SM complex (**Fig. 1.6**) starts with the zippering from the N- to C-terminal of the four-helical proteins from the SNARE complex (Gao et al. 2012, Hanson et al. 1997, Li et al. 2014). The initial zippering of the N-terminal allows vesicle priming and the creation of a RRP (Li et al. 2014, Walter et al. 2010, Gao et al. 2012). In addition, the interaction of other regulatory proteins such as complexin clamps the zippering and prevents membrane fusion. When Ca^{2+} binds to synaptotagmin-1, the clamp is released. In this way, Ca^{2+} triggers a fast zippering of the SNARE complex C-terminal domain, providing the force to overcome the thermodynamic barrier of membrane fusion (Cohen and Melikyan 2004). Membrane

fusion opens a fusion pore (Gao et al. 2012) through which neurotransmitter will be rapidly released (Alvarez de Toledo, Fernández-Chacón, and Fernández 1993) in the first 100-200 μs (Walter et al. 2010). The zippering process follows with the dimerization of transmembrane domains of synaptobrevin and syntaxin-1, inducing the expansion of the pore (Shi et al. 2012). The complete zippering transforms the initial *trans*-SNARE to *cis*-SNARE. The cycle is closed by its disassemby by NSFs and its adaptors.

- *Ca^{2+} triggering*

The Ca^{2+} sensor synaptotagmin is inserted in the vesicle membrane and, upon Ca^{2+} binding interacts with SNARE complex and membrane phospholipids (Lee et al. 2010). It has been reported that synaptotagmin is essential for Ca^{2+}-triggering release *via* SNARE complex (Tucker, Weber, and Chapman 2004, Fernández-Chacón et al. 2001, Geppert, Archer, and Südhof 1991) and that it clamps spontaneous release (Xu et al. 2009, Littleton et al. 1993), but not asynchronous release (Xu et al. 2012). Although first studies indicated that synaptotagmin was the Ca^{2+}-sensor triggering neurotransmission, later on it was demonstrated that Ca^{2+}-regulated exocytosis still takes place once this protein is deleted. Thus the function of synaptotagmin is centered on the regulation of speed and precision of the neurotransmitter release. Several types of synaptotagmin are expressed in the brain with different kinetics and apparent Ca^{2+} sensitivity, that might determine the kinetics and sensitivity of synchronous release and dictate the properties of the synapse (Xu, Mashimo, and Südhof 2007). The action of synaptotagmin is coordinated with complexin, which binds to the SNARE complex (McMahon et al. 1995) and toghether they regulate the activity of SNARE complex by clamping its zippering (**Fig. 1.6**).

- *The active zone protein complex containing*

The principal components of the active zone in the presynaptic, RIM, Munc13, and RIM-BP, are represented on the right of of **Figure 1.5**. They mediate the early stages of the exocytosis (docking and priming) and, notably they are responsible for the recruitment of VGCC close to the synaptic vesicles.

Many studies suggested protein RIM as the main organizer of the active zone due to its interaction with the majority of the proteins forming this scaffold (Mittelstaedt, Alvaréz-Baron, and Schoch 2010). As a cosequence, RIM is essential for wide number of processes like docking, priming or synaptic plasticity. A recent study by Kaeser (2011) has demonstrated that deletion of RIM results in an increased $[Ca^{2+}]_{ex}$ dependence of release, which was also slower and less synchronous, pointing out to a reduction of the presynaptic Ca^{2+} influx.

In summary, RIM tethers VGCC to the active zone *via* two essential interactions: a specific one mediated by the PDZ domain to $Ca_v2.1$ and $Ca_v2.2$ channels, and an unspecific indirect interaction *via* RIM-BP with any VGCCC. Both interactions are essential to keep the VGCC close to the Ca^{2+}-sensor and have a fast and synchronous neurotransmission. However, other important interactions between the exocytic machinery and the VGCC described before. Syntaxin-1A and SNAP-25 bind to $Ca_v2.1$ and $Ca_v2.2$ through a synaptic protein interaction site (synprint), located into a intracellular loop of the VGCC (Bennett, Calakos, and Scheller 1992, Sheng et al. 1994, Rettig et al. 1996, Wiser, Bennett, and Atlas 1996). Disruption of this interaction by competition with peptides containing the synprint site (Mochida et al. 1996) revealed a double effect of the interaction. First, the interaction couples VGCC with the release machinery enhancing neurotransmission and, secondly it serves to reduce Ca^{2+} entry to modulate synaptic strength (Keith et al. 2007, Weiss and Zamponi 2012). Other synaptic proteins such as synaptotagmin-1 or Munc-18 also interact with VGCC in a less critical way (reviewed in (Weiss and Zamponi 2012)).

1.1.2 Methods to study exocytosis

Patch-clamp

The patch-clamp technique was developed by Neher and Sakmann in 1976. As explained in the press release to announce the Nobel Prize in Physiology or Medicine for 1991:

'The two German cell physiologists Erwin Neher and Bert Sakmann have together developed a technique that allows the registration of the incredibly small electrical currents (amounting to picoampere – 10^{-12}) that passes through a single channel. The

technique is unique in that it records how a single channel molecule alters its shape and in that way controls the flow of the current within a time frame of a few millionths of a second.'

Physiology or Medicine 1991 - Press Release

The achievement of recording single-channel currents relies on the electrical isolation of a small patch of membrane (Neher, Sakmann, and Steinbach 1978, Neher and Sakmann 1976). In contrast to using intracellular electrodes to record membrane current, as had been done previously, they pressed a small fire-polished glass pipette against the cell membrane, forming an electrical seal with a typical resistance of 50 MΩ (**Fig. 1.7**). The pipette is filled by Ringer solution, and contains an Ag/AgCl electrode to connect the interior of the pipette with the current-measurement circuitry. Due to the high resistance of the seal, currents originated in the small patch of membrane flow into the pipette and to the circuit. The isolation of the membrane patch with a high-resistant seal allowed them to reduce the background noise with respect to intracellular recordings. In this way they record for first time, single-channel currents. In their first experiments, the potential of the patched membrane was controlled using two-microelectrode voltage-clamp placed near the glass pipette.

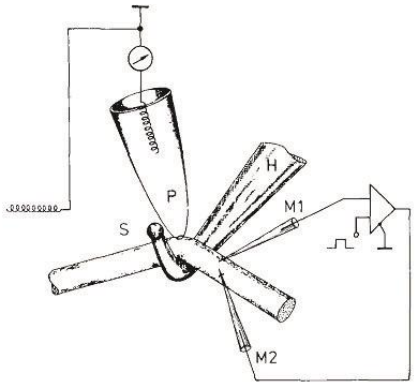

Figure 1.7. **Schematic drawing of the first patch-clamp method described by Sakmann and Neher**. In the image, the nerve fiber is held by a hook (H), while it is voltage-clamped using two-extracellular microelectrodes (M1 and M2). Next to the hook, the fire-polished glass pipette (P) is pressed against the nerve to form a 50 MΩ membrane seal that will allow the isolation of the patched membrane and the recording of the single-channel currents. Note that the end of the hook is protected by a Sylgard ball (S). From (Neher, Sakmann, and Steinbach 1978).

- *The gigaseal*

Few years later, the two Nobel laureates improved the extracellular patch-clamp technique by increasing the seal resistance to 10-100 GΩ (Sigworth and Neher 1980). The tight pipette-membrane seal, called gigaseal, was possible by using a clean pipette surface and applying a gentle suction once the pipette was pressed against the cell membrane.

The implementation of the gigaseal further reduced the background noise by an order of magnitude. In addition, this implementation made possible to voltage-clamp the membrane patch by using the glass pipette and avoiding the use of extracellular microelectrodes.

- *Patch-clamp configurations*

After the implementation of the gigaseal to record single-channel currents with low noise, several new patch-clamp configurations were developed to improve and extend the possibilities of this new technique (Hamill et al. 1981).

The first described configuration is the cell-attached (**Fig. 1.8**). It corresponds to the formation of the abovementioned gigaseal, which is mechanically very stable and it is the precursor to other variants of the technique. From this configuration the pipette can withdrow the patched membrane from the cell membrane, forming a vesicle that occluds the pipette tip (inside-out configuration). Alternatively from the cell-attached configuration the application of a gentle suction through the patch pipette disrupts the membrane, keeping the pipette attached to the cell. The creation of a hole into the plasma membrane allows low-resistance access to the cell interior, while the tightness of the seal prevents leakage of the current and flooding of the cell content with the bath solution. This configuration allows membrane potential recording and voltage-clamp of entire cell and hence named whole-cell configuration (see also **Fig. 1.9**). From the whole-cell configuration, the pipette can also be pulled off, excising a patch and thus obtaining a fourth configuration, the ouside-out (Penner 1995).

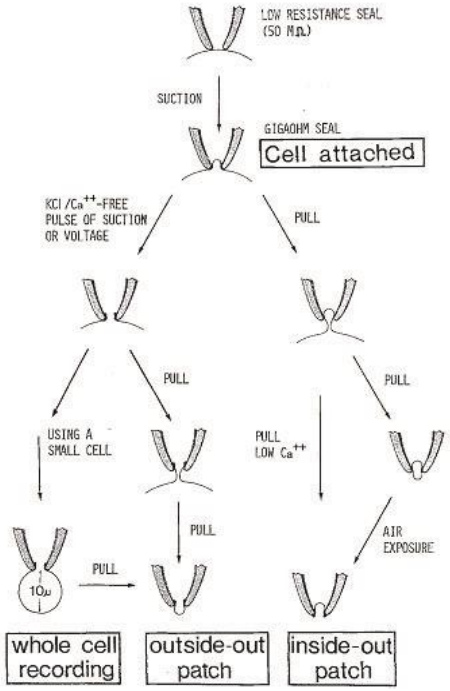

Figure 1.8. Different patch-clamp configurations. Cell-attached, outside-out and inside-out are configurations generally used for single-channel current recording. Cell-attached is the less invasive configuration, outside-out is very useful to easily exchange the extracellular solution, therefore is often applied to study receptor-channels. In contrast, with inside-out one easily exchange the cytosolic solution, and it is the method of choice to study the effects of second-messengers on channels. Finally whole-cell configuration is used to record the electrical activity of the entire cell. From (Hamill et al. 1981).

One of the main disadvantages of whole-cell configuration is the washout of the cytosolic content. To overcome this problem, a different configuration, called perforated-patch, was developed. This technique consists on the selective perforation of the membrane patch by including channel-forming substances in the pipette solution, like amphotericin B (Rae et al. 1991) or other substances (Horn and Marty 1988, Lindau and Fernandez 1986). Perforation of the membrane patch allows a low-resistance access to the cell while preventing the washout of the cytosolic factors. Main weaknesses of this technique are the long time required to perforate the patch and the high-noise recording.

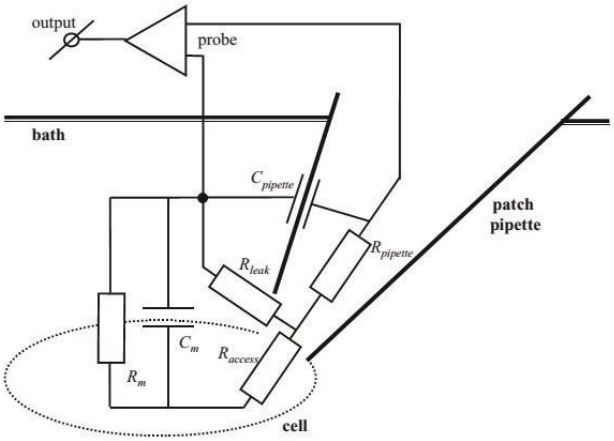

Figure 1.9. Equivalent circuit for the whole-cell configuration. The highest resistance of a circuit determines the current flow. Since R_m is high compared with R_{access} and $R_{pippete}$, it is the one measured with this patch-clamp configuration. Parallel to the circuit, the R_{leak} should be as high as possible to be able to measure current through the cell membrane. Cm: membrane capacitance, $C_{pipette}$: pipette capacitance, $R_{pipette}$: pipette resistance, R_{leak}: leak resistance. Fom (Molleman 2003).

Originally, patch-clamp technique was focused on the voltage-clamp of a small patch of membrane. Now, it refers to both recording of macroscopic whole-cell currents and of microscopic single-channel currents (Penner 1995), as well as including two types of membrane manipulation. The initial technique of voltage-clamp controls the membrane potential and allows direct recording of the membrane current. For voltage-clamping a cell membrane, it is necessary to use an electronic feedback system that measures the membrane potential and compares it with the membrane potential determined by the experimenter (holding potential, V_h). If these values differ, the recorded potential is corrected by an injection of a compensatory current, that is equivalent (but in opposite sign) to the ionic current over the membrane under investigation. Alternatively in current-clamp, changes in the membrane potential can be measured in response to currents flowing across ion channels. In this case, a fixed amount of current can be injected through the intracellular recording pipette without clamping the voltage, and therefore current-clamp recording does not require a feedback system. Current-clamp is used to record action potentials; it is also very useful for those cells in which voltage-clamp it is not allowed because of cells' space

clamp properties (i.e. neurons) or for loose patch recordings with megaohm seals (Penner 1995, Molleman 2003).

- *Capacitance measurements*

Besides current and voltage, other electrical properties can be estimated from a cell by means of the patch-clamp technique, such as capacitance and conductance of the membrane. Monitoring the cell membrane capacitance it is an excellent technique to measure exocytosis and it can be employed for detecting single fusion events with cell-attached configuration or for detecting the entire cellular secretory activity with whole-cell configuration.

The cell membrane acts as an electric capacitor by accumulating charges on both sides of the bilipidic layer. Due to the membrane potential, there are negative charges accumulated onto the intracellular side and positive ones onto the extracellular one, isolated by the cell membrane. Similarly as in capacitors, the ability of the cell membrane to accumulate charges (C_m, membrane capacitance) depends on the membrane surface area. Therefore, measurements of membrane capacitance are good indicators of the membrane surface area. Vesicle fusion induces an increase of the membrane surface area, which then results in an increase of the membrane capacitance.

Capacitance cannot be directly measured from the pipette-cell circuit and it has to be estimated from the voltage and current measurements (Gillis D. 1995). The most popular technique for high-resolution measurements of changes in capacitance is based on the use of a sinusoidal stimulus. Usually, a high-frequency (1 kHz) sinus-wave of 25 mV amplitude is applied together with voltage-clamping, thus the sinus-wave voltage is set to the holding potential (i.e. -70 mV). The resulting sinusoidal current is characterized by its amplitude and phase, which can be resolved using a phase-sensitive detector (or lock-in amplifier) (Neher and Marty 1982). The estimated parameters of the equivalent circuit (C_m, R_m or R_{acces}, **Fig. 1.9**) can be obtained by means of two methods (Lindau and Neher 1988). One method precisely calculates the three estimated parameters using the information from the sinusoidal wave and DC current (Lindau-Neher technique or Sine+DC mode). The second method is simpler

and assumes that C_m is directly proportional to the output signal form the lock-in amplifier in the range of voltages covered by the sinusoidal wave (piecewise-linear technique). Although the second method cannot provide all three estimated parameters, it is computationally less expensive than the first one.

One limitation for the estimation of C_m is due to the fact that changes of capacitance may be caused by other factors besides the increase of the surface area. As a matter of fact, differences in membrane potential or mobilization of charges across the membrane can induce changes on the C_m. To prevent these effects, it is common to stop measuring capacitance during depolarizing pulses.

Using these methods, C_m technique can detect small changes of the capacitance, of the order of magnitude corresponding a single vesicle, at high temporal resolution. The capacitance measurement will report only the net change of the membrane surface area resulting from the combined processes of exocytosis and endocytosis. However, the rate of endocytosis is usually low and therefore exocytosis-driven signal can be distinguished. Some other specific techniques to monitor exocytosis have been developed and are described below, e.g., electrochemical detection of secretion by amperometry or the use of pH-conditioned dyes.

Amperometry

Amperometry is a widely used technique to study exocytosis of neurotransmitters and hormones. It is based on the measurement of an electrochemical current in response to an applied constant voltage (voltammetric technique): the oxidation of the secreted product near a carbon-fiber microelectrode, held at a positive potential, causes the transfer of electrons to the surface of the electrode, producing a measurable current (**Fig. 1.10**) (Evanko 2005). Many of the products secreted by cells (norepinephrine, epinephrine, dopamine or serotonin) are readily oxidizable. Norepinephrine is of the most studied ones (**Fig 1.10a**) and is secreted by the neuroendocrine chromaffin cells, which represent an excellent cell model to study exocytosis.

The first electrochemical electrodes were used to detect neurotransmitters into the brain tissue (Kissinger, Hart, and Adams 1973). However, until the development of smaller carbon-fiber electrodes (8-µm diameter) (Gonon et al. 1978), it was not

possible to apply the technique at the single-cell level. The initial electrochemical measurements of secretion from single cells were done in Millar's and Wightman's laboratories. Placing a carbon-fiber microelectrode near a chromaffin cell, they were able to detect catecholamine release (Duchen, Millar, and Biscoe 1990, Leszczyszyn et al. 1990) and provided the first direct measurement of the quantal release of vesicle content. Later, this technique has been applied to many other secretory cells from mast cells (Alvarez de Toledo, Fernández-Chacón, and Fernández 1993) to neurons (Zhou and Misler 1995)

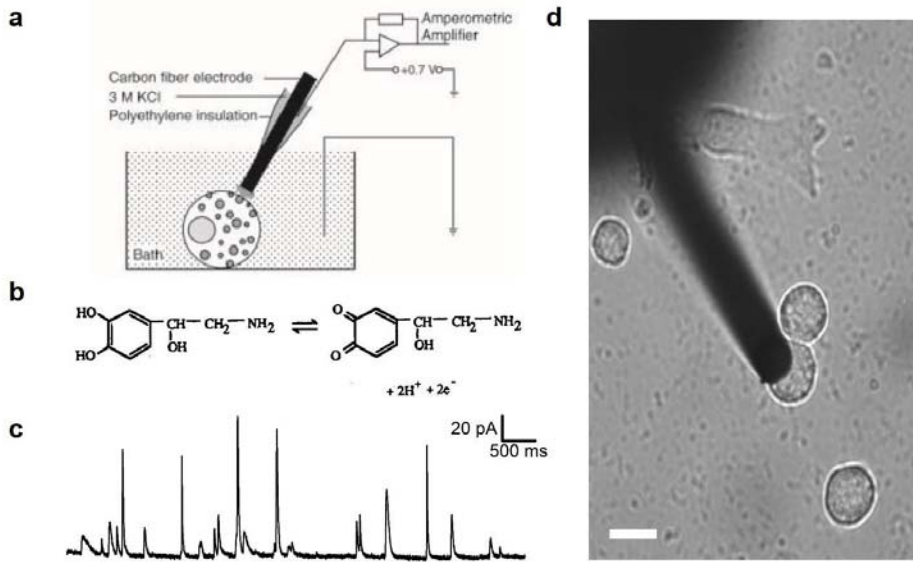

Figure 1.10. Amperometry. (a) Amperometry recordings are usually obtained with carbon-fiber microelectrodes of 5-12 µm diameter, isolated by plastic tubing and connected to an Ag/AgCl electrode through a conductive ionic solution. During experiments, a typical voltage of +700 mV (exceeding the redox potential of the compound) is applied to the carbon-fiber electrode. Then, if the cell is stimulated, norepinephrine is released and oxidized. From (Dernick, Toledo, and Lindau 2007) **(b)** During oxidation of norepinephrine to its quinone product, two electrodes are released and collected by an electrode placed close to the cell. From (Chow H. and von Rüden 1995a). **(c)** The product released per vesicle is detected as spikes in the current signal. The total charge involved in the redox reaction (which equals the integral of the current spike) is proportional to the number of molecules oxidized, making this a quantitative technique. **(d)** Bright field image of a home-made carbon-fiber electrode placed near a cultured chromaffin cell. Scale bar 10 µm.

The extraordinary temporal resolution of amperometry allows to resolve exocytosis of single vesicles as they appear as spikes in the amperometric current (**Fig. 1.10c**) (Wightman et al. 1991). Moreover, analysis of the shape of amperometric spikes provides information about kinetics of the neurotransmitter release (Mosharov and Sulzer 2005). As an example, this techniques has permitted the detection of catecholamine flux through the fusion pore, formed before the full-collapse of the vesicle. This flux is detected in the amperometric current as a 'foot' signal preceding the spike (Chow, von Rüden, and Neher 1992, Alvarez de Toledo, Fernández-Chacón, and Fernández 1993, Neher 1993).

Carbon-fiber electrodes to perform single-cell amperometry are commercially available or can be prepared in the laboratory. There are alternatives manners to obtain the electrodes (Machado, Montesinos, and Borges 2008, Chow H. and von Rüden 1995a). One of the methods consists in isolating single carbon-fiber electrodes with polyethylene, leaving only the very end of the fiber exposed (**Fig 1.10a**). Later, they can be assembled into a glass tube, mounted on the patch-clamp headstage and placed next to the cell to be ready to detect secretion (**Fig 1.10d**). Detailed information about home-made carbon-fiber electrodes is provided in **Appendix A**.

Electrochemical detection of secretion by amperometry complements the C_m technique to assay secretion. Similar to C_m measurements, amperometry has single-vesicle and high-temporal resolution. However, exocytosis measured by amperometry is limited by the oxidation sensibility of the neurotransmitter and by the fact that it can only be assayed the fraction of the cell surface that is close to the electrode. To combine the advantages of cell capacitance and amperometry, patch-amperometry was developed (Dernick et al. 2005). The insertion of the amperometric detector inside the patch pipette allows to measure the vesicle size and fusion pore conductance simultaneously with the quanta content or catecholamine permeability of the pore (Gong, de Toledo, and Lindau 2007, Albillos et al. 1997, Alés et al. 1999).

1.1.3 Postsynaptic terminal

Synaptic vesicles are filled with small-molecule transmitters that are released during neurotransmission. Then, they cross the synaptic cleft and bind to specific receptors located at the opposite site of the active zone, in the postsynaptic neuron. There are two type of neurotransmitter receptors, depending on their response upon activation: ionotropic and metabotropic receptors. The response of ionotropic receptors consists on the opening of an ion channel included in its own structure. Their response is fast and short-lived and their activation changes the charge distribution across the cell membrane by either hyperpolarizing, or depolarizing it. If the depolarization reaches the suprathreshold potential, an action potential is triggered. Alternatively, the response of metabotropic receptors regulates the opening of ion channels indirectly via an intracellular signaling cascade. As a consequence, their response is slow and can persist for long periods. This two types of receptors play essential roles in the neurotransmission process: ionotropic receptors mediate behavior, while metabotropic modulate the synaptic response, being able to induce changes in neural circuits.

Depending on the released neurotransmitter and on the activated receptor, the originated synaptic potential can be excitatory or inhibitory. It is excitatory when it triggers a depolarization current and usually involves glutamate as neurotransmitter. Otherwise, an inhibitory input induces hyperpolarization of the membrane potential and it is normally produced with the release of γ-aminobutyric acid (GABA) or glycine neurotransmitters. Neurons from central nervous system receive both excitatory and inhibitory inputs that must be integrated to generate an appropriate coordinated response.

Structure

Excitatory and inhibitory synapses can be distinguished by their morphology, molecular composition and organization (**Fig. 1.11**). Excitatory synapses are mainly found on tiny protrusions of the dendrites called dendritic spines, wheras the inhibitory synapses are usually directly connected to the dendritic shaft (Gray 1959, Colonnier 1968).

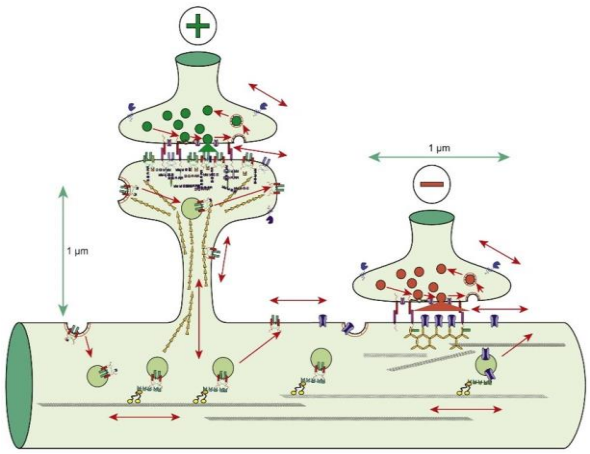

Figure 1.11. Morphology of excitatory and inhibitory synapse. An excitatory synapse (on the left) is characterized by the presence of dendritic spine on the postsynaptic site. Inhibitory synapse (on the right) directly contacts on the dendritic shaft. Arrows indicate the dynamic elements that permit synaptic plasticity. From (Choquet and Triller 2013).

The ultrastructure of the postsynaptic terminal is characterized by the presence of an electron-dense thickening structure adjacent to the postsynaptic membrane, specifically located in opposition to the active zone from the presynaptic terminal (**Fig. 1.12**). It is a specialized matrix of scaffolding proteins that couples together receptors, ion channels and cytoplasmic signaling molecules.

In the excitatory synapse this electron-dense structure is more complex than in inhibitory synapses. It is called postsynaptic density (PSD) and usually presents a perforated disc shape (Ziff 1997). The PSD is formed by many scaffolding proteins (reviewed in (Sheng and Kim 2011)) containing the protein-protein interaction PDZ domain. This type of interaction is at the basis of the postsynaptic scaffolding. In addition, as the PDZ interaction is weak and there is a high number of PDZ domains in the area, it ensures a dynamic organization of the synapse (**Fig. 1.11**). Besides this dynamic organization of postsynaptic elements, the morphology of dendritic spines can also be adapted to the functional needs of the synapse (e.g. changes in the spine volume or the spine neck length). Both structural and morphological changes of the postsynaptic terminal enable synaptic plasticity and, thus learning and memory.

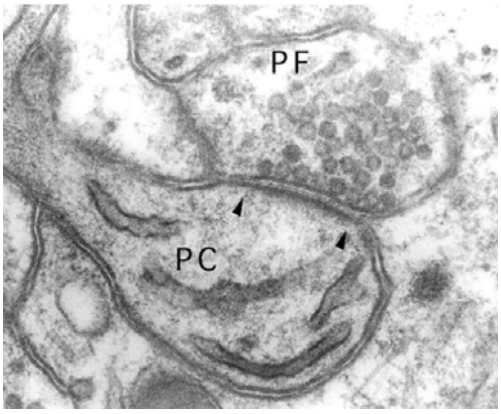

Figure 1.12. Electron micrograph of a synapse. Presynaptic terminal corresponding to a parallel fiber (PF) axon and postsynaptic terminal to a Purkinje cell (PC) from the cerebral cortex. The postsynaptic density (between arrow heads) is located at the opposite site of the active zone from the presynaptic terminal. From (Ziff 1997).

Post-synaptic ionotropic glutamate receptors

Glutamate is the main excitatory neurotransmitter in the mammalian CNS. It binds and activates a highly conserved orthosteric ligand-binding domain (LBD) present in both ionotropic and metabotropic glutamate receptors (Gereau and Swanson 2008). Ionotropic glutamate receptors (iGluRs) are assembled as tetramers where each subunit is composed of four conserved domains: an extracellular amino-terminal domain, the LBD; the transmembrane domain, which includes the ionic pore; an intracellular C-terminal domain. Depending on the pharmacology and structural homology, glutamate receptors are divided in four classes: (1) N-methyl-D-aspartate (NMDA) receptors (NMDARs) have high affinity for NMDA except for the glycine-binding GluN1 subunit, (2) α-Amino-3-hydroxy-5-methyl-4-isoxazolepropionic acid (AMPA) receptors (AMPARs) are activated by AMPA and include GluA1-GluA4 subunits; (3) receptors that can be activated with AMPA and have high affinity for kainate are the kainate receptors (KARs) and include GluK1-GluK5 subunits; and finally (4) the less known family of δ receptors (Traynelis et al. 2010).

Each class is characterized by a kinetics and a neuronal function, briefly described in the following. AMPARs and NMDAR are mainly located at the postsynaptic area and are the basis of the typical glutamate neurotransmission. The postsynaptic response is

mediated by AMPARs. They start the postsynaptic response with their fast current (mainly sodium influx), then the depolarization of the membrane allows the opening of NMDRs and Ca^{2+} entry to modulate synaptic strength and neuronal function. NMDRs are unique receptors because the pore opening is subject to several factors. To a given extent, their function can be associated to coincidence detectors. Two different agonists need to bind the receptor (glutamate and glycine) and, if there is membrane depolarization, it relieves a magnesium ion blockage of the pore, allowing the ion flux through the pore. The role of KAR has not been described until recently, with the development of drugs that specifically target this subunit class. KARs act on the synapses from both the pre-synaptic and postsynaptic sites. Postsynaptically, this receptors contribute to the postsynaptic current together with AMPARs. When KARs are located presinaptically, they regulate the amount of neurotransmitter released (Lerma 2006). Interestingly, KARs have recently been described to induce signaling via G-protein (Lerma and Marques 2013).

The biophysical properties of iGLuRs are mainly determined by post-transcriptional RNA edition, subunit composition and their interaction with auxiliary proteins. Focusing on kainate receptors, since they are the subject of this work, GluK1 and GluK2 subunit mRNA is edited to generate two isoforms. The affected residue is a glutamine located in the membrane reentrant loop M2 that can be edited to an arginine (the Q/R editing site) (Sommer et al. 1991). The unedited isoform, with the glutamine at the M2, has a higher single-channel conductance and Ca^{2+} permeability and it is sensitive to polyamine channel block, displaying an inward rectifying I-V relationship. While the edited isoform, with an arginine, has a lower single-channel conductance and Ca^{2+} permeability and is insensitive to polyamine block (Egebjerg and Heinemann 1993, Swanson et al. 1996, Bowie and Mayer 1995).

Kainate receptors can form functional receptors as homomers of GluK1 to 3 subunits, or as heteromers of GluK1 to 5 subunits. The subunits GluK4 and 5 can only form functional receptors when they are expressed in combination of subunits GluK1 to 3. The subunit composition of KARs influence their functionality, for example, the presence of subunits GluK4 and 5 alters the biophysical and biochemical properties of the heteromeric receptor. Heteromers containing this subunits, with higher affinity to kainate (GluK4 and 5), can be activated at low agonist concentrations without

desensitizing (Fisher and Mott 2011). *In situ* hibrization studies have revealed that kainate subunits are expressed differentlly on tissue (**Table 1.2**). However, due to the lack of subunit specific antibodies, it has been difficult to determine their subcellular distribution.

GluK1	Hippocampal and cortical interneurons, Purkinje cells and sensory neurons.
GluK2	Principal cells: hippocampal and cortical pyramidal cells and hippocampal and cerebral granular cells.
GluK3	Poorly expressed: IV layer of neocortex and dentate gyrus in hippocampus.
GluK4	CA3 pyramidal neurons, dentate gyrus, neocortex and Purkinje cells.
GluK5	Abundantly expressed in the brain.

Table 1.2. Expression of kainate receptors in the nervous system (Lerma and Marques 2013).

The function of glutamate receptors is also affected by the interaction of auxiliary transmembrane subunits, as Neto1 and Neto2 for kainate receptors (Zhang et al. 2009, Tang et al. 2011). Neto proteins reduce the voltage-dependent inhibition by polyamines on KARs (Fisher and Mott 2012). Specifically, Neto1 increases the agonist affinity of the receptors and the rate of recovery from desensitization or increase the steady-state current (Fisher and Mott 2013).

Action potential

Finally, if the postsynaptic current induced by the neurotransmitter released depolarizes the cell membrane to the suprathreshold potential, an action potential is triggered. As it happens with neurotransmitter release, the generation of AP is an all-or-none process.

The action potential is a change in membrane potential caused by the flow of ions through ion channels. It propagates an electrical message along the axons of nerve

cells or over the membrane surface of muscular and gland cells. The generation and propagation of an AP is possible due to differential distribution of ionic charges and species across the membrane in excitable cells.

Excitable cells have an accumulation of positivly charged molecules outside the cell and an accumulation of negativly charged molecules inside, separated by the presence of the lipid bilayer of the membrane. The charge separation originates a difference of electrical potential across the membrane, called membrane potential (V_m). When excitable cells are in resting conditions, they have a characteristic V_m, which in neurons oscillates between -60 mV and -70 mV.

Additionally to the charge separation, ion species are not equally distributed at both sides of the cell membrane. Indeed, Na^+ and Cl^- are more concentrated outside the cell. The opposite happens with K^+ and organic anions (mainly amino acids and proteins), being more concentrated in the cytoplasm (**Fig. 1.13a**). The maintenance of the ionic distribution is due the combination of passive and active mechanisms. The main active mechanism is represented by the Na^+-K^+ pump. This pump uses energy from the ATP hydrolysis to extrude Na^+ from the cell and uptake K^+, it is the main responsible of the differential concentration of these ions inside and outside the cell. The passive mechanism results from the presence of resting channels with selective permeability that makes the cell membrane permeable to only few species of ions (mainly they are selective to K^+ and Cl^-, but there could be some Na^+-selective resting channels), and they counteract the action of the Na^+-K^+ pump. The flux across the membrane is determined by three factors: the electrical driving force, the chemical driving force and the membrane conductance.

Alterations in the Na^+ and K^+ conductance caused by changes on the membrane potential explain the electrical response of nerve cells and are quantitatively described in the Hodgkin-Huxley model of the action potential (Hodgkin and Huxley 1952). The sequence of the events that generate the action potential, according to the mode,l starts when the membrane potential reaches the threshold (around –55mV) and voltage-gated Na^+ channels rapidly open. Then, the Na^+ conductance of the membrane greatly increases and there is a Na+ influx, which exceeds the K^+ efflux causing cell depolarization (rise phase, **Fig. 1.13b**). When the membrane potential

gets close to the Na^+ equilibrium potential (+55 mV), two processes are responsible for the repolarization of the membrane. The inactivation of Na^+ channels, together with the slow opening of voltage-gated K^+-channels, make that K^+ efflux gradually increases until a net efflux of positive ions repolarize the membrane to its membrane potential. In most of the cases, the repolarization phase is followed by a transient hyperpolarization, as a consequence of the slow closing of K^+-channels. Immediately after the action potential, the excitability of the membrane is reduced (refractory period) because of the residual inactivation of Na^+-channels and an increased opening of K^+-channels.

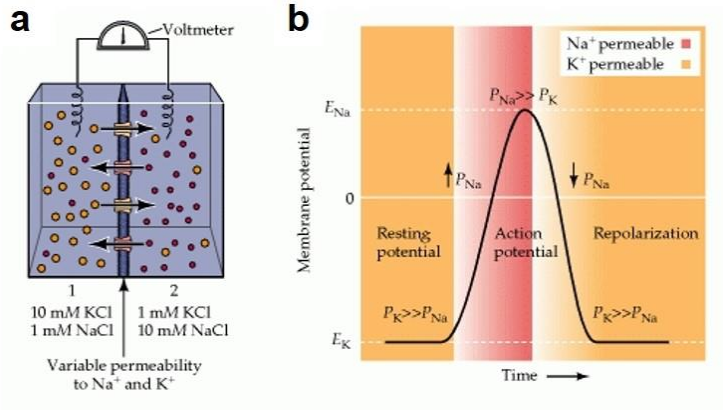

Figure 1.13. Resting membrane potential and action potential. (a) Schematic of the distribution of Na^+ (red) and K^+ (yellow) inside (2) and outside (1) the cell. **(b)** Changes of the Na^+ and K^+ permeability during the action potential. E_{Na} and E_K is the equilibrium potential for each ion, From (Purves et al. 2001)

This general mechanism of the giant squid action potential involves only two different types of voltage-dependent conductances, but it can be broadly used to explain the action potential in mammalian neurons. However, hundreds of different voltage-gated ion channels have been identified in mammalian neurons. The distinct voltage-dependent conductance present in neurons determines their membrane excitability properties. Subcellular regions can also display specific voltage-dependent conductance properties (e.g. the trigger zone of the neuron presents a high-density of voltage-gated Na^+-channels). The diversity of voltage-gated ion channels allows individual neurons to encode information on the different frequencies and patterns of

action potentials (Bean 2007), being essential elements for the understanding of information transfer in the brain.

1.1.4 Methods to manipulate membrane potential

Several methods have been developed to manipulate the membrane potential and thus neuronal activation. These methods are generally focused on the generation of action potentials by means of membrane depolarization. The voltage-clamp technique (see **section 1.1.2**) was the first method developed in 1949 by Kenneth Cole and improved by Alan Hodgkin and Andrew Huxley (Schwiening 2012). Electrophysiological techniques are characterized by their sensitivity and high temporal resolution, as required by the electrical activity of neurons, taking place in the millivolt and millisecond scales. However they are quite invasive and limited by the reduced electrical access to neuronal processes (Scanziani and Hausser 2009). To overcome these limitations, new approaches are being developed based on light stimulation. The most used optical techniques are uncaging of biomolecules and light-gated ion channels, which are described below.

Caged compounds

In the caged technique, a small biomolecule is maintained inactive (or caged) with a chemical modification obtained via attachment of a photolabile protecting group. Upon brief pulses of light, the active functional biomolecule is uncaged and can bind to the targeted receptor. One of the main advantages of this method is that almost all kinds of molecules are susceptible of being caged. The first caged compounds (cyclic-AMP and ATP) appeared in 1977 and 1978 (Engels and Schlaeger 1977, Kaplan, Forbush, and Hoffman 1978). Since then, many important caged biomolecules have been developed such as Ca^{2+}, neurotransmitters, inositols, nucleotides, peptides, enzymes, mRNA and DNA reviewed in (Ellis-Davies 2007).

Caged Ca^{2+} is an exception of the general strategy used for caging compounds. As it is a divalent ion, it cannot covalently bind to a photolabile protecting group. Alternatively, photolabile derivatives of Ca^{2+} chelators have been synthetized, they bind to Ca^{2+} until they are broken with light pulse (**Fig. 1.14a, left**). Two of the most used caged Ca^{2+} are DM-nitrophen (Kaplan and Ellis-Davies 1988), and NP-EGTA

(Ellis-Davies and Kaplan 1994), the last one caging specifically Ca^{2+} over Mg^{2+}. Using this method, a very brief (less than 1 ms) flash of UV light creates a spatially homogeneous Ca^{2+} increase, triggering Ca^{2+}-dependent processes such as exocytosis. As a consequence, caged Ca^{2+} has extensively been used to study the dependence and kinetics of Ca^{2+} during neurotransmission. The first time caged Ca^{2+} was exploited for controlling secretion was in chromaffin cells (Neher and Zucker 1993), then it has been used to study the calyx of Held synapse (Schneggenburger, Meyer, and Neher 1999) and small inhibitory synapse such as Cerebellar basket cells (Sakaba 2008).

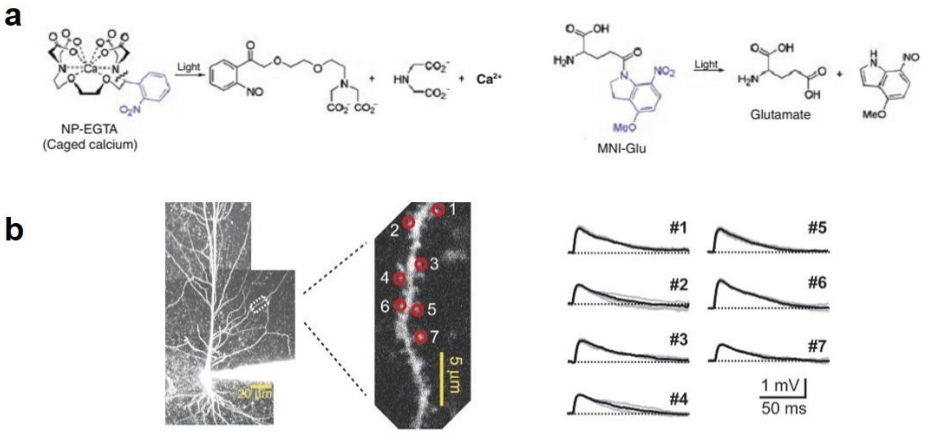

Figure 1.14. Caged compounds. (**a**) Structure of NP-EGTA, left and MNI-Glu, right, before and after photolysis, which releases Ca^{2+} or glutamate. From (Ellis-Davies 2007). (**b**) Example of two-photon glutamate uncaging to simulate individual dendritic spines (red circles, middle image). Then the postsynaptic potential triggered by the stimulation of each one is represented on the right. From (Losonczy and Magee 2006).

Caged neurotransmitters include glutamate, GABA, serotonin and glycine (Ellis-Davies 2007, 2013). Glutamate is the most important neurotransmitter in the mammalian brain. For such a reason it has, together with GABA, several designed caging strategies. Some of the most used compounds are: the first developed CNB-Glu (Wieboldt et al. 1994) or CNB-GABA (Gee, Wieboldt, and Hess 1994), some two-photon sensitive uncaging versions MNI-glu (Matsuzaki et al. 2001) (**Fig. 1.14a, right**) and CDNI-GABA (Matsuzaki et al. 2010) or the also two-photon sensitive compounds with less unspecific effects, RuBi-glu (Fino et al. 2009) or RuBi-GABA (Rial Verde et al.

2008). Caged neurotransmitters have been exploited to functionally map neuronal circuits (Callaway and Katz 1993, Bureau, Shepherd, and Svoboda 2004) either by targeting stimulation on individual neurons (Nikolenko, Poskanzer, and Yuste 2007), individual synaptic inputs on spines (Araya et al. 2006, Matsuzaki et al. 2001, Losonczy and Magee 2006, Branco, Clark, and Häusser 2010) (**Fig. 1.14b**) or on dendrites (Vervaeke et al. 2012).

Additionally to neurotransmitters, other caged ligads with specificity for glutamate receptor sub-type also have been developed (Palma-Cerda et al. 2012). Some of the selective ligands adapted for uncaging are: kainate, AMPA, NMDA or the NMDA receptor antagonist, AP-5 (Murphy et al. 1997).

Optogenetics

Optical stimulation of neurons with light-gated ion channels can mainly be performed by means of two strategies. One relies on the control of neuronal receptors using photoswitchable ligands, as described in detail on **section 1.2**. The second technique is the optogenetic method, which consists in the introduction of natural-light sensitive proteins (ion channels, pumps or GPCRs) in neurons to manipulate the membrane potential with light (Boyden et al. 2005). Apart from overcoming the diffusion limitation that caged compound have, optogenetics has the advantage that light control can be targeted to a specific cell subtype by genetic manipulation.

Optogenetic tools derive from microbial opsins, which, in contrast to animal opsins coupled to G-protein signaling, also include light-driven pumps (bacteriorhodopsins and halorhodopsin) and light-gated ion channels (channelrhodopsins, ChR). Opsins are transmembrane proteins associated with the co-factor all-trans retinal, the light sensitive switch. This chromophore is naturally synthesized in all vertebrate tissues and, thus there is no need to supplement the experimental system with the compound. The first microbial opsins introduced in neuronal cells were Channelrhodopsin-2 (ChR2) (Boyden et al. 2005) and halorhodopsin (NpHR) (Zhang et al. 2007), from the green alga *Chlamydomonas reinhardtii* and from the bacteria *Natronomonas pharaonis*, respectively. ChR2 is a light-gated cation channel (Nagel et al. 2003, Kato et al. 2012) (**Fig. 1.15a**) that, when expressed in neurons, depolarizes

the membrane and triggers action potential time-locked to light pulses (Boyden et al. 2005, Li et al. 2005, Ishizuka et al. 2006). In contrast, NpHR is a chloride pump that, under light activation, transports Cl^- ions from the extracellular side to the citoplasm (**Fig. 1.15a**), hyperpolarizing the membrane and silencing action potentials (Zhang et al. 2007). After the success of these two microbial opsins in the control of neuronal activity, there has been an extensive search for new light-driven pumps and channels in bacteria, alga and fungi. This fact, together with the generation of mutant opsins with improved biophysical and photochemical properties, has bestowed an extensive optogenetic toolbox, as summarized in **Figure 1.15b** (Yizhar et al. 2011, Lin 2011).

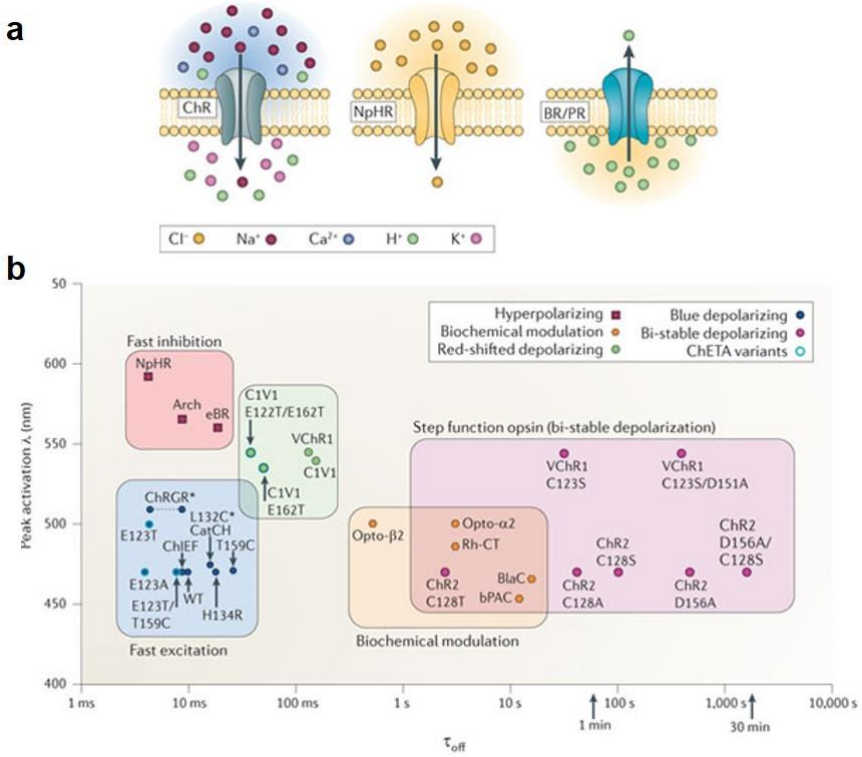

Figure 1.15. Optogenetic tools based on opsins. (a) Scheme of cation-permeable opsin (channelrhodopsin, ChR, left) usually used to depolarize the cell membrane. Cl^--pump (halorhodopsin, NpHR, middle) and the proton pump (bacteriorhodopsins, BR, right) are used to hyperpolarize the membrane potential and silence neurons. **(b)** Variants of available opsins plotted according to their optimal stimulation wavelength (Y-axis) and off kinetics (X-axis). Adapted from (Tye and Deisseroth 2012).

As it has been done with caged compounds, optogenetics has been applied to investigate neuronal circuits (Petreanu et al. 2009, Mao et al. 2011, Packer et al. 2012) and also to manipulate behavior in many animal models: worm, fly, mouse, rat and primates (Fenno, Yizhar, and Deisseroth 2011).

1.1.5 Future challenges

During the last 50 years, our understanding of the neurotransmission process has greatly progressed, prompted by techniques such as patch-clamp (Neher and Sakmann 1976), electron microscopy (Heuser et al. 1979), fluorescence microscopy (Robinson et al. 1995), super-resolution imaging (Liu et al. 2011, Nair et al. 2013), genetic manipulation (Fernández-Chacón et al. 2001) or optical stimulation (Neher and Zucker 1993, Watanabe et al. 2013, Banghart et al. 2004, Szobota et al. 2007). Yet, there are unsolved questions such as: which is the molecular calcium sensor of neurotransmission?, how is neurotransmission so accurately synchronized?, which are the mechanisms of vesicle recycling or how synaptic plasticity is induced and regulated? Synapses are continuously adapted to input signals, processing them and synchronously sending the proper response, making the brain able to learn, to define the behavior of the organism, to store memories or to make decisions. We still don't know which mechanisms are behind the regulation of the brain function, however synapses are playing an important role and new tools are needed to manipulate their activity.

Light offers exceptional advantages to manipulate biological functions (Miesenbock 2009, Gorostiza and Isacoff 2008b): it is non-invasive and usually does not interfere with the system to study; optical control of protein activity provides high spatial resolution. Moreover, light stimuli can be patterned and controlled with a high temporal resolution. Miesenbock visualized the opportunity to control neuronal activity using light-sensitive proteins in 2002 (Zemelman et al. 2002). Few years later, this idea was improved by the development of photoswitchable ion channels (Banghart et al. 2004) and by the introduction of bacterial opsins (natural light-sensitive proteins)

(Boyden et al. 2005) in neuronal cells. Both protein engineering approaches started two new fields in neurobiology: optogenetic pharmacology, and optogenetics.

The use of natural-light sensitive proteins in neurobiology has accelerated our understanding of the brain. Optogenetic actuators, mainly represented by opsins, have been committed to the manipulation of membrane potential, being excellent tools to activate and silence neuronal cells (Kasparov and Herlitze 2013). However, the activity of each neuron is the result of the coordinated action of a large number of endogenous components, e.g., ion channels, membrane receptors and intracellular signaling elements. To further understand neuronal process with minimal invasivity, the endogenous components governing neuronal activity should be the target of the new strategies to optically manipulate their function.

Chemical modification of neuronal proteins with synthetic photoswitches is now addressing the need of developing new tools to study neuronal function. The high interest in extending light control to all known neuronal proteins is reflected in the large number of photoswitchable molecules developed in the last years, which are now available for the majority of ion channels and receptors, as described in the next section.

1.2 PHOTOSWITCHABLE ION CHANNELS AND RECEPTORS

This section reproduces a submitted book chapter submitted for a book entitled Novel approaches for Single Molecule Activation and Detection, which will be published by FOCUS Workshop Proceedings:

Bautista-Barrufet A., Izquierdo-Serra M. and Gorostiza P. Photoswitchable ion channels and receptors. Submitted.

Photoswitchable ion channels and receptors

Antoni Bautista-Barrufet[a,b,+], Mercè Izquierdo-Serra[a,+] and Pau Gorostiza[a,c,d,*]

[a] *Institut de Bioenginyeria de Catalunya (IBEC), Barcelona, Spain.*

[b] *Institut Català d'Investigació Química (ICIQ), Tarragona, Spain.*

[c] *Centro de Investigación Biomédica en Red en Bioingeniería, Biomateriales y Nanomedicina (CIBER-BBN), Zaragoza, Spain.*

[d] *Institució Catalana de Recerca i Estudis Avançats (ICREA), Barcelona, Spain.*

[+] *Equal contribution*

[*] *Corresponding author. E-mail: pau@icrea.cat*

Abstract. The development of photochromic and photoswitchable tethered ligands for ion channels and receptors has made important contributions to optopharmacology and optogenetic pharmacology. These compounds provide new tools to study ion channel proteins and to understand their function and pathological implications. Here we describe the design, operation and applications of the available photoswitches, with special emphasis on ligand- and voltage-gated channels.

One of the major aims of neuroscience is to develop tools to measure and manipulate the activity of neurons in the brain with cellular and action-potential resolution. The synergy of functional mapping and control of neural circuits in the brain will lead to understanding their operation and regulation, and their dysfunction in neurological diseases (Alivisatos et al. 2013). Ion channels and ionotropic receptors are membrane

proteins that directly regulate the excitability of neural cells in response to changes in membrane potential and to binding of a variety of ligands. While neuronal channels and receptors are normally not sensitive to light, it has proven very useful to artificially photoregulate them in order to remotely control neuron excitability with temporal and spatial precision (Gorostiza and Isacoff 2008b). This aim can also be achieved by optogenetics, i.e. expressing non-neuronal natural photoswitchable channels (Tye and Deisseroth 2012).

In this chapter, we review synthetic photoswitchable ion channels and receptors, and the strategies employed to obtain them, with special emphasis on recent reports. Several reviews have been published that discuss photostimulation methods (Kramer, Mourot, and Adesnik 2013, Gorostiza and Isacoff 2007), design and mechanism of photoswitches (Gorostiza and Isacoff 2008a), applications to photocontrol cell signaling and neuronal activity (Gorostiza and Isacoff 2008b, Szobota and Isacoff 2010, Kramer, Mourot, and Adesnik 2013) or specifically focused on ligand-gated ion channels (Szobota, McKenzie, and Janovjak 2013) and potassium ion channels (Mourot, Fehrentz, and Kramer 2013).

Light sensitivity can be achieved by using protein ligands that can be switched between an active and an inactive form with light. Ligands include pore blockers, orthosteric agonists and antagonists, and allosteric modulators. They are linked to a light-regulated moiety formed by a photochromic group like azobenzene, which changes in polarity, geometry and end-to-end distance upon isomerization. This light-regulated change can be designed to alter the ligand properties (affinity, agonist/antagonist character) or the accessibility of the ligand to its binding site in the protein. Synthetic photoswitches can be classified as soluble photochromic ligands (PCLs) if they are free in solution, or as photoswitchable tethered ligands (PTLs) if they are covalently attached to the protein. The development of these light-regulated ligands has given rise respectively to the fields of optopharmacology (including compounds that can act on endogenous receptors) and optogenetic pharmacology (when the PTL is covalently attached to mutated residues in the protein, usually cysteine) (Kramer, Mourot, and Adesnik 2013). Here we have classified photoswitches according to the target channel family, and in each case we specify the methodology used and the reported applications of light regulation.

	Photoswitch	Target	Ligand	Activity	Azobenzene $\lambda_{trans \rightarrow cis}$ / $\lambda_{cis \rightarrow trans}$ (nm)	Active conformation	Refe
PCL	BisQ	nAChR	Quaternary ammonium	Agonist	380/500	*trans*	(Bartels, and Erlanger
	MPC088	$GABA_A$ receptor	propofol	Potenciates, allosteric ligand	500/380	*trans*	(Yue et al. 2
	AP-2	$GABA_A$ receptor	propofol	Potenciates, allosteric ligand	404/fast thermal relaxation	*trans*	(Stein et al.
	Gluazo	Kainate receptor	Glutamate	agonist	380/500	*trans*	(Volgraf et a
	ATA	AMPA receptor	BnTetAMPA	agonist	480/fast thermal relaxation	*trans*	(Stawski, S Trauner 201
	AAQ	Shaker $K_v1.2$, $K_v1.3$, $K_v1.4$, $K_v2.1$, $K_v3.3$, $K_v4.2$	Quaternary ammonium	pore blocker	380/500	*trans*	(Fortin et Banghart et
	BzAQ	Shaker	Quaternary ammonium	pore blocker	380/500	*trans*	(Banghart et
	PrAQ	Shaker	Quaternary ammonium	pore blocker	380/500	*cis*	(Banghart et
	DENAQ	$K_v3.1$	Quaternary ammonium	pore blocker	480/ fast thermal relaxation	*trans*	(Mourot et a
	PhENAQ	Shaker K_v	Quaternary ammonium	pore blocker	480/ fast thermal relaxation	*cis*	(Mourot et a
	QAQ	Shaker Kv Na_v Ca_v	Quaternary ammoniums	pore blocker	380/500	*trans*	(Mourot et a
	2,2'-dimethoxy-QAQ	Shaker K_v Na_v	Quaternary ammoniums	pore blocker	420/fast thermal relaxation	*trans*	(Fehrentz et
	2,2'-dimethyl-QAQ and 2,2',6,6'-tetramethyl-				380/500		

	QAQ						
	ABCTC	TRPV1	BCTC	voltage antagonist	370/420	*cis*	(Stein et al.
	AC4	TRPV1	capsazepin	Capsaicin antagonist	360/440	*cis*	(Stein et al.
				voltage antagonist		*trans*	

Table 1.3. Propierties of the PCLs and its targeted receptors.

	Photoswitch	Target	Ligand	Activity	Ligand reactive moiety	Azobenzene $\lambda_{trans\rightarrow cis}$ / $\lambda_{cis\rightarrow trans}$ (nm)	Active conformation	Re
PTL	QBr	Wild-type AChR	Quaternary Ammonium	agonist	Benzyl bromide group	380/500	*trans*	(Bartels Wasser Erlange
	MAACh	LinAChRs α3β4-E61C α4β2-E61C	AC-5	agonist	Maleimide	380/500	*cis*	(Tochits 2012)
	MAHoCh	LinAChRs α3β4-E61C α4β2-E61C	HoChPE and MG-624	antagonist	Maleimide	380/500	*cis*	(Tochits 2012)
	MPC100	γ-79C $GABA_AR$s	propofol	Potenciates, allosteric ligand	Maleimide	380/500	*trans*	(Yue et
	MAG	LiGluR GluK2-L439C	Glutamate	agonist	Maleimide	380/500	*cis*	(Volgra
		HyLighter iGluR6-p0-C-L439C						(Janovj 2010)
	L-$MAG0_{460}$	LiGluR GluK2-L439C	Glutamate	agonist	Maleimide	445/fast thermal relaxation	*cis*	(Kienzle

	D-MAG-1	LimGluR2-block mGluR2-L302C LimGluR6-block mGluR6-K306C	Glutamate	antagonist	Maleimide	380/500	*cis*	(Levitz
	D-MAG-0	LimGluR2 mGluR2-L300C LimGluR3 mGluR3-Q306C	Glutamate	agonist	Maleimide	380/500	*cis*	(Levitz
	MEA-TMA	P2X2-I328C	-	With ATP: pore blocker Without ATP: channel gating	Quaternary ammonium and maleimide	365/525	*trans*	(Lemoi 2013)
	BMA	P2X2-P329C P2X3-P320C ASICS1-G430C and I428C	-	Channel gating	Maleimide and maleimide	360/440	*trans*	(Brown
	MAQ	SPARK Shaker-E422C	Quaternary ammonium	Pore blocker	Maleimide	380/500	*trans*	(Bangh 2004)
		D-SPARK Shaker-V443Q and E422C						(Chamb 2006)
		Kv1.3- H401Y and P374C Kv3.1-E308C Kv3.4-D420C Kv7.2-E257C SK2-Q339C						(Fortin

		TREK1-K231C					*trans*	(Sandoz
		TREK-PSC TREK1ΔC-S121C					*cis*	

Table 1.4. Propierties of the PTLs and its targeted receptors.

1.2.1 Pentameric ligand-gated receptors

Introduction

The pentameric ligand-gated receptor family (also known as "cys loop" receptors, because they have a conserved extracellular region with a disulfide bridge) are a superfamily of receptors located at the postsynaptic cell membrane, originating both excitatory and inhibitory effects on the mammalian CNS (Connolly and Wafford 2004). This superfamily includes nicotinic acetylcholine receptors (nAChr), serotonin receptors (5-HT_3), γ-aminobutyric acid receptors ($GABA_A$) and glycine receptors (GlyR) (Ortells and Lunt 1995).

The receptors of this family are organized as homo- or heteropentamers, with up to four different subunits α, β, γ, δ and different stoichiometries. In heteromers, the neurotransmitter binding sites are usually located at the interface between α and β subunits. The structure of some prokaryotic homologs of these receptors is known and was reviewed recently (Hilf and Dutzler 2009). Three conserved domains can be distinguished in this protein family. First, a large extracellular N-terminal domain including residues responsible for ligand type specificity, which differs between the family subgroups. The second part is the transmembrane domain with four hydrophobic entities (M1-M4) formed by β-sheet segments. M2 lines the ion channel pore and is responsible for ion permeation and selectivity. And third, a hydrophilic domain between M3 and M4, exposed to the cytoplasm (Brejc et al. 2001, Changeux and Edelstein 1998).

Allosteric ligands bind to a different protein spot than the neurotransmitter (orthosteric ligand), and regulate the activity of the receptor. In pentameric receptors-channels, the three structural domains described above are thought to host allosteric binding sites. Allosteric ligands of nAChrR include ions (Ca^{2+} and Zn^{2+}), ivermectin and steroids. Benzodiazepines and the anesthetic propofol are allosteric modulators of $GABA_A$ receptors (Changeux and Edelstein 1998, Yip et al. 2013).

Nicotinic acetylcholine receptors

nAChRs and serotonin receptors (5-HT_3) are ligand-gated, cation permeable channels with excitatory activity, responsible for the fast synaptic transmission in muscles or nerves (Connolly and Wafford 2004). nAChR was the first ligand gated protein channel to be isolated and greatly helped to understand neurotransmission mechanisms (Hille 2001). This protein was also studied with several chemical biology tools, including photochromic ligands, which originated the first light-gated receptor (Bartels, Wassermann, and Erlanger 1971). This pioneering contribution introduced the PCL and PTL concepts using an azobenzene unit linked to a quaternary ammonium, a receptor agonist. When the quaternary ammonium is present in both sides of the azobenzene, the compound (Bis-Q) acts as a PCL. This symmetry confers cholinergic activity to the *trans* isomer and reduced agonism in *cis*, presumably due to steric hindrance caused by the bent configuration of the azobenzene group. Those results were obtained by measuring the transmembrane potential of electric eel electroplax organs. In order to demonstrate the PTL approach, they used a compound in which azobenzene was flanked by one quaternary ammonium salt and a benzyl bromide group (QBr). Benzyl bromide reacts to a well-characterized native cysteine residue close to the binding-site (Silman and Karlin 1969) and covalently attaches QBr. In this way, QBr produces the same photoregulated activity than a PCL, but with persistent activation-desactivation cycles (Bartels, Wassermann, and Erlanger 1971). Reversible photocontrol of nAChRs was demonstrated using rat myoballs, electric eel electroplaques and frog muscles, and was extensively studied in the following years (Lester and Chang 1977, Chabala and Lester 1986). However, in order to make the target cysteine available for conjugation to the PTL, the use of a strong reducing agent was required (Barrantes, 1980), which limited cellular applications to mechanistic channel gating studies.

The photoswitchable nAChR was recently revisited (Tochitsky et al. 2012), taking advantage of the structural, genetic and computational methods not available at the time of the original design. PTL-anchoring cysteines were selected based on structural homology models and simulations, and introduced by site-directed mutagenesis in nAChRs ($\alpha3\beta4$ and $\alpha4\beta2$ heteromers). Two PTLs including the agonist acetylcholine and the antagonist homocholine were tested in order to respectively photoactivate and photoinhibit the receptors (Tochitsky et al. 2012). Position E61C at the β subunit

of $\alpha_4\beta_2$ receptors led to activation of the receptor using the agonist MAACh (Maleimide-Azobenzene-Acylcholine), which can be photoswitched reversibly between violet (380 nm) and green illumination (500 nm). Attaching the antagonist MAHoCh (Maleimide-Azobenzene-Homocholine) at the same residue produced photoswitchable inhibition between violet and green light. Thus two different nAChR PTLs were rationally designed and synthesized with analogous photoregulation but opposite physiological responses, by varying the linker length and replacing an ester functional group by an ether. This methodology opened a general pathway to photosensitizing pentameric ligand-gated ion channels.

Ionotropic γ-aminobutyric acid receptor ($GABA_A$)

The receptors of γ-aminobutyric acid ($GABA_A$ and $GABA_C$) and glycine (GlyRs) are chloride-selective channel proteins, and thus have an inhibitory effect on the neuronal activity in the central nervous system. They are important targets for anxiety treatment and anesthesia (Connolly and Wafford 2004). Controlling the activity of this receptors with light is attractive because it would allow inhibiting neuronal tissue using designed spatiotemporal patterns, for example to functionally isolate specific neuronal circuits. This aim can be achieved with natural light-gated ion pumps like halorhodopsin or archaerhodopsin (Zhang et al. 2007, Chow et al. 2010), but require continuous illumination, which is not convenient for certain applications (Kasparov and Herlitze 2013). In principle, photoswitchable glycine or $GABA_A$ receptors with slow relaxation lifetimes could be stimulated with a short light pulse, and the open channel would inhibit neurons in the dark. Tethered glycine or GABA receptor ligands are required to design PTLs of these receptors, but adding a tether reduces the affinity in the case of $GABA_A$ agonists (Raster et al. 2013). However, a photoswitchable competitive inhibitor has been used to regulate $GABA_A$ receptors with light (Kramer, Mourot, and Adesnik 2013).

As an alternative to the strategy focused on the orthosteric site, an allosteric binding site like that of propofol (Changeux and Edelstein 1998, Yip et al. 2013) can be the target of photoswitch design. Two recent articles reported a PCL (Yue et al. 2012, Stein et al. 2012) and a PTL (Yue et al. 2012) that potentiate GABA currents in a light-dependent fashion. A series of azo-derived propofol ligands were developed and

applied to $\alpha_1\beta_{2/3}\gamma_2$ heteropentamers. These compounds are active in *trans* and inactive in *cis*, but differ in photostability, therefore in their potential applications. The photochromic AP-2 ligand (Stein et al. 2012), synthesized using the classical diazo coupling, present a red-shifted *cis*-isomerization (404 nm) and a fast *trans* restoration due to para-substituted electro-donating groups that decrease the *cis* thermal stability. The compound was tested in tadpoles where it controlled the anesthetic action of propofol using one wavelength (Stein et al. 2013). On the other hand the PTL MPC088 (Yue et al. 2012) shows *cis-trans* reversibility between 365 nm and 440 nm respectively, and allows modulating GABA currents in retinal neurons and cerebellar Purkinje neurons. Spatiotemporal control of neuronal spike rate was demonstrated using this allosteric PTL.

1.2.3 Tetrameric ligand-gated receptors

Introduction

Glutamate is the main excitatory neurotransmitter in the mammalian CNS. It binds and activates a highly conserved orthosteric ligand-binding domain (LBD) that is present in both ionotropic and metabotropic glutamate receptors (Gereau and Swanson 2008).

The LBD of iGluRs and metabotropic glutamate receptors (mGluRs) are evolutionary related and they might have originated from the same precursor, the periplasmic binding proteins of gram-negative bacteria. The common structure of this module is characterized by two large polypeptide lobes connected via a flexible linker, and the ligand binding site which is formed by the cleft between the lobes. Upon ligand binding there is a conformational change and the two lobes twist and close entrapping the ligand, hence the name Venus flytrap (Felder et al. 1999, Sobolevsky, Rosconi, and Gouaux 2009).

In the case of the iGluRs the two lobes are composed by sequentially separated segments. Closing of the two lobes upon ligand binding induces conformational changes on the transmembrane region, which lead to opening of the pore and receptor activation. The degree of LBD closure is proportional to pore opening and it depends on the ligand bound to the receptor: an agonist allows total closure of the

lobes, partial agonists induce a more open conformation of the LBD and antagonists stabilize the open state of LBD (Felder et al. 1999, Sobolevsky, Rosconi, and Gouaux 2009). Similar conformational changes to the LBD occur upon ligand binding to mGluRs. These receptors have seven-transmembrane helices with the LBD located at the extracellular N-terminus of the protein. They assemble in dimers whose LBDs rest in the open state (in the absence of ligand or stabilized by an antagonist) or in the closed state (stabilized in the presence of an agonist). The change in the relative orientation of the two LBDs in the closed state is determinant for the activation of these receptors (Doumazane et al. 2013).

Glutamate receptors play crucial roles in brain function. They support glutamatergic neurotransmission and are involved in many other fundamental processes such as regulation of synaptic strength, plasticity (memory and learning) and brain development (Gereau and Swanson 2008). Glutamate receptors have been the target of several approaches to control their activity with light, with the aim of controlling and understanding these critical processes.

Kainate receptors

The application of PTL approach to kainate receptors led to the development of the light-gated glutamate receptor (LiGluR) (Volgraf et al. 2006). An agonist (glutamate) was covalently tethered to the protein *via* an azobenzene. The photoswitch MAG (Maleimide-Azobenzene-Glutamate) was conjugated to a cysteine introduced in the LBD of the kainate receptor subunit GluK2. The agonist was able to bind and activate the receptor (open the channel) under violet illumination (380 nm), and green (500 nm) light caused the ligand to unbind and close the channel. Photoswitching occurs in a step function manner due to the slow thermal relaxation of MAG: the channel remains open in the dark for minutes until it is illuminated again with green light. The mechanism of activation and deactivation involves changes in the local effective concentration of the glutamate moiety near its binding site, associated to the isomerization of MAG. The conjugation of MAG to the receptor is mediated by the affinity of the ligand, and can be modulated with illumination (Gorostiza et al. 2007).

Recently, a new PTL has been developed for LiGluR (L-MAG0$_{460}$) with modified functional groups that allow *cis-trans* isomerization by visible light (400-520 nm) and millisecond thermal relaxation in the absence of illumination. This novel MAG derivative enables single wavelength operation of LiGluR (Kienzler et al. 2013).

The PCL strategy was also applied to KARs and allowed to control the activity of native receptors using GluAzo (Volgraf et al. 2007). The design of this KAR-selective ligand is based on the KAR agonist LY339434. *Trans*-GluAzo has a higher affinity to GluK1 and GluK2 than the *cis* isomer, such that receptor-mediated currents can be photoswitched in a certain GluAzo concentration range. This approach has been used to reversibly trigger neuronal firing with light in non-transfected hippocampal neurons (Volgraf et al. 2007).

Computational models of ligands docked in their receptors have been extensively used to understand the action mechanism of photoswitches and to design new actuators (Numano et al. 2009, Tochitsky et al. 2012). However, the crystal structure of a receptor bound to its photoswitchable ligand has been resolved only recently, revealing their detailed molecular interactions (Reiter et al. 2013). The structure of the planar *trans*-GluAzo bound to GluK2 LBD shows a similar interaction as free glutamate, while the bent *cis*-GluAzo might interfere with LBD closure, and subsequent ion channel opening. The molecular contacts show in striking detail how the azobenzene tether of *trans*-gluazo is enclosed within an 'exit tunnel' of the GluK2-LBD. This structure is similar to that of the LBD-domoate complex and displays a conformation of the two lobes that is not fully closed, which explains the partial agonist character of GluAzo.

AMPA receptors

A PCL of AMPARs has also been developed (Stawski, Sumser, and Trauner 2012). The LBD of AMPARs displays high homology with the LBD of glutamate receptors, The LBD of AMPARs and KARs are homologous, but in AMPARs the LBD closes more tightly, which poses difficulties to design a PCL based on GluAzo. The X-ray structure of the AMPAR LBD bound to a modified ATPA agonist, BnTetAMPA, reveals a cleft for ligand exit that is different from that used by GluAzo. A series of PCLs named azobenzene

tetrazoyl ATPA (ATA) was designed to accommodate to this cleft, thus allowing the AMPA receptor clamshell to close for receptor activation. They display red-shifted isomerization and fast relaxation. *Trans*-ATA isomers are strong agonists of GluA2 receptors, and agonism is reduced with 480 nm light (*cis* configuration). These compounds were used in pyramidal neurons to trigger trains of action potentials with light (Stawski, Sumser, and Trauner 2012).

Bacterial iGluRs

An alternative approach to generate new light-activated channels is to take advantage of the modularity of glutamate receptor domains. This strategy was used to generate a K^+-selective light-activated channel termed HyLighter (Janovjak et al. 2010) in which the LBD of GluK2 (including the PTL attachment site) was combined with the pore region of sGluR0 (a K^+-selective prokaryotic receptor homologue to iGluRs). As it happens with LiGluR (Numano et al. 2009), *cis*-MAG0 binds to the LBD and activates HyLighter. In this case, however, photocurrents are mainly due to K^+ and cause the hyperpolarization of the cell membrane. Since the *cis* isomer is thermally stable, continuous illumination is not needed to silence neurons as in the case of light-gated ion pumps. After a brief violet light pulse, HyLighter keeps the membrane hyperpolarized until 500 nm illumination inactivates the receptor.

Metabotropic glutamate receptors

Since glutamate-binding domains are highly conserved among all glutamate receptors, in principle few structural changes are required in order to extend the PTL approach from the LBD of ionotropic receptors to that of mGluRs. In this way, the PTL strategy was extended to the optical control of a G protein-coupled receptor (Levitz et al. 2013). Two distinct enantiomeric photoswitches of MAG-0 and MAG-1 were synthesized, in which the stereochemistry of the glutamate carbon was changed from 4'L to 4'D. In this way, the D-tethers D-MAG-0 and D-MAG-1 (D-maleimide azobenzene glutamate) were obtained that better accommodate in the LBD of mGluRs. These photoswitches were tested on mGluR2 by means of a cysteine introduced in its LBD. The longer photoswitch, D-MAG-1, antagonized glutamate under 380-nm light in the mGluR2-L302C mutant, which they called LimGluR2-block.

In contrast, the short PTL, D-MAG-0, successfully activated the receptor when it was conjugated to mGluR2-L300C mutant (LimGluR) under 380-nm light. These agonist and antagonist photoswitches can also be used to photocontrol the activity of the mGluR3-Q306C (LimGluR3) and mGluR6-K306C (LimGluR6-block) (Levitz et al. 2013).

Applications

LiGluR has been applied to photocontrol a wide variety of systems such as cultured neurons, astrocytes, chromaffin cells, mouse retina and zebrafish locomotive responses. LiGluR contains the non-selective cationic pore of GluK2 and its sodium permeability allows depolarizing neurons and precisely controlling their activity with light. In cultured hippocampal neurons expressing LiGluR, violet light triggers trains of action potentials that are maintained in the dark until the channel is closed with green light. Millisecond photostimulation of LiGluR evokes single action potentials, that precisely correlate with the photoswitch pattern up to a frequency of 50 Hz (Szobota et al. 2007). LiGluR has also been used *in vivo* to investigate the function of neuronal subpopulations of the zebrafish spinal cord (Wyart et al. 2009). The activation by means of LiGluR of each subset of neurons induced different locomotive responses enabling to understand their underlying circuitry.

The relatively high calcium permeability of GluK2 makes LiGluR an effective tool to optically induce calcium currents and trigger calcium dependent processes. Light induced intracellular calcium elevation on LiGluR-expressing astrocytes and a delayed activation of the neighboring cells, and was used to study astrocyte-to-astrocyte communication (Li et al. 2012). LiGluR also allows to increase intracellular calcium concentration with light and directly trigger exocytosis in chromaffin cells independently of voltage-gated calcium channel activation (Izquierdo-Serra et al. 2013a). In this way, the calcium influx through LiGluR can be regulated with the wavelength of illumination and has been used to trigger and modulate neurotransmission in cultured hippocampal neurons (Izquierdo-Serra et al. 2013b).

The therapeutic applications of LiGluR have also been explored. In retinal degeneration, which is characterized by the death of photoreceptors, the surviving non-photoreceptor cells can be utilized to restore visual responses. These cells have

been photosensitized by using electrode arrays in humans or gene therapy with opsins in mice. In an alternative gene therapy approach, Caporale and co-workers inserted LiGluR to retinal ganglion cells in a mice model of blindness and showed that after MAG administration, the animals responded to violet light, (Caporale et al. 2011). New red-shifted PTL L-MAG0$_{460}$ might then be used to restore the response to visible light (Kienzler et al. 2013).

PCLs of glutamate receptors have also been applied to study neuronal systems. The kainate photoswitchable agonist GluAzo allowed photomodulating oscillations in cerebellar Purkinje neurons, a continuously firing neuron that is thought to be an integrator for the motor control system of the brain. When the photoswitchable agonist is added to the system in dark, it induces astability (oscillation between rapid firing and quiescence) in a similar way to other kainate agonists. However, application of 500/380 nm light pulses enabled tuning of astable oscillations by switching on and off the neuronal bursts (Abrams et al. 2012).

On the other hand, the light-gated, K^+-permeable channel HyLighter has been used to silence neuronal activity. It was tested in transgenic zebrafish expressing HyLighter in spinal cord motor neurons, and enabled to reversibly inhibit escape responses when HyLighter was activated under violet light (Janovjak et al. 2010).

1.2.4 Trimeric ligand-gated receptors

Among purinergic receptors, which are activated by Adenosine-5-triphosphate (ATP) or adenosine, P2X receptors are cation permeable non-selective (Na^+, K^+, Ca^{2+}) ion channels, with a trimeric structure that was solved recently (Kawate et al. 2009). They are gated by extracellular ATP, that promotes a conformational rearrangement and pore opening, rendering an excitatory, depolarizing effect on cells. These receptors are involved in various physiological processes having a role in neurotransmission, neurosecretion and are associated with sensory, motor and cognitive tasks.

These receptor-channels are structurally organized in three conserved domains: (1) a pore domain with two transmembrane segments that shares similarities with inward rectifying K^+-channels, (2) an unusually large extracellular fragment containing the

ATP binding site and a cys-loop region similar to that of pentameric receptors, and (3) a short intracellular domain (Conley 1996). Several allosteric ligands have been described for these receptors (Kawate et al. 2009, Valera et al. 1994).

In a series of pioneering optogenetic experiments to manipulate animal behavior, Gero Miesenböck used P2X channels to photocontrol membrane potential using ATP uncaging (Zemelman et al. 2003, Lima and Miesenböck 2005), which had some advantages over his rhodopsin-based chARGe system (Zemelman et al. 2002).

More recently, and guided by the available atomic structure, both PTL and azo-crosslinking strategies have been used to control trimeric ligand-gated receptors with light. In P2X receptors, a symmetric maleimido crosslinker (BMA, (4,4´-Bis(maleimido)azo-benzene)) was introduced between cysteines, changing the conformation of the channel protein in milliseconds upon 440 nm illumination, and reversing the effect at 360 nm(Browne et al. 2014). However, this modification abolishes ATP dependence. The same crosslinker was applied in another trimeric channel, the acid-sensing ion channel (ASICs), which is activated by the acidity of the extracellular medium via structural transitions similar to those of P2X. In ASIC1, BMA was covalently conjugated between introduced cysteines and resulted in *trans* activated, partial photocurrents (Browne et al. 2014).

P2X receptors have also been photocontrolled using a compound with PTL architecture: MEA-TMA has a charged, unspecific "ligand" that is able to modulate channel gating with light of 365 nm and 525 nm. Two photocontrol mechanisms were found: a photomodulation of ATP response, and direct photoactivation in the absence of ATP (Lemoine et al. 2013). Photoswitchable P2X allowed photocontrolling action potentials in hippocampal neurons and open the way to investigate other P2X receptors involved in pain and inflamatory pathologies.

1.2.5 Potassium channels

Introduction

Potassium channels constitute a big and diverse family of ion channels proteins. Among other criteria, they can be classified in three groups by their general architecture: (1) the family of inward rectifying K^+-channels (K_{ir}) are tetramers formed

by subunits with two transmembrane domains that are activated by hyperpolarization, (2) the two-pore (2P) K^+-channels are dimers formed by subunits with four transmembrane domains that assemble forming a two-pore ion channel, and (3) the voltage-gated potassium channel family. This last group is the biggest and is evolutionary related to voltage-gated Na_v and Ca_v channels. All these voltage-gated channels have a conserved motif composed of six transmembrane segments (S1-S4 form the voltage sensor domain and S5-S6 form the pore domain). In voltage-gated potassium channels each motif corresponds to one subunit, and they are assembled as tetramers, whereas in Na_v and Ca_v channels these motifs are repeated four times in a single protein. K_v channels, the small conductance Ca^{2+}-activated potassium channels (SK) and cyclic nucleotide-gated (CNG) channels are members of this family. Voltage-gated potassium channels are responsible for many cellular functions like maintaining the resting membrane potential or repolarizing and hyperpolarizing the cell membrane during the propagation of action potentials in neurons.

K_v Family

The potassium channel blocker tetraethyl ammonium (TEA) was used as the ligand to develop a PTL of potassium channels (Banghart et al. 2004). A cysteine introduced at the extracellular loop of the Drosphila Shaker K^+-channel allowed the covalent attachment of the PTL by means of a maleimide reactive group (Maleimide-Azobenzene-Quaternary ammonium salt, MAQ). The channel pore is blocked in the *trans* configuration, under 500 nm illumination, and this effect is reversed with 380 nm light. This engineered channel was named SPARK (Synthetic Photoisomerizable Azobenzene-Regulated K^+) and is both voltage-gated and light-controlled. It has been used for optically silencing neuronal activity. Introduction of point mutations in the pore of SPARK alters cation selectivity and yielded a depolarizing version of this channel (D-SPARK) which was developed based on the same PTL and allows firing action potentials with light (Chambers et al. 2006).

MAQ was also applied to photosensitize other potassium channels by introducing cysteine mutations at the equivalent position of SPARK (Fortin et al. 2011). The PTL principle was thus extended to four mammalian potassium channels with different cell-type distribution, gating properties, kinetics, and modulatory control. The diverse

physiological functions of K^+-channels suggest that overexpression of light-sensitive versions could be used not only to suppress action potentials with light, but also to fine-tune several aspects of cellular electrophysiology. For example, light-regulated K_v7.2 channels might be useful to control resting potential; K_v1.3 to control repolarization of action potentials, K_v3.1 to control accommodation, and SK2 to control the size of excitatory post synaptic potentials (EPSPs).

PCLs have also been employed to photocontrol native potassium channels, avoiding the cysteine insertion into the protein. Maintaining the azo unit linked to the pore blocker "head" (TEA), several versions of PCLs were synthesized that differ in the "tail" group: The first PCL had an acrylamide moiety (AAQ, acrylamide-azobenzene-quaternary ammonium) that blocked the pore of Shaker and various native K_v channels in its *trans* configuration (Fortin et al. 2008). This PCL acts from the internal TEA binding site, whereas MAQ blocks the ion pore from an external binding site (Banghart et al. 2009). Since it is an intracellular blocker, the functionality of AAQ depends on its ability to reach the cytoplasm. To promote partitioning of the PCL into the membrane, two new molecules were synthesized (Banghart et al. 2009): a hydrophobic benzylamide group (BzAQ) and a propyl group at the end of the molecule (PrAQ) which respectively act as *trans*- and *cis*-blockers. A more recently developed PCL is the QAQ molecule. This molecule has symmetric quaternary ammonium groups and is able to control the excitability of cells by blocking at 500 nm a wide variety of voltage-gated ionic channels (shaker, K_v, Na_v and Ca_v) (Mourot et al. 2012). As a double charged molecule it does not partition in the cell membrane but in analogy to the analgesic lidocaine, QAQ permeates through nociceptive pore channels such as TRPV1 or P2X. The accumulation of QAQ in neurons expressing nociceptive channels like dorsal root ganglion neurons from the spinal cord, offers opportunities to use this photoswitch as a potential drug to control pain. Implanting fiber-optics systems on spinal cords would allow to spatiotemporally regulate the activity of these PCLs (Mourot et al. 2012).

The photoisomerization properties of azobenzene can be adjusted by chemical substitutions like the introduction of electro-donating substituents, and in this way several red-shifted and fast-relaxing PCLs have been described: two AAQ derivatives

named DENAQ and PhENAQ (Mourot et al. 2011) and two derivatives of QAQ (Fehrentz et al. 2012).

A therapeutic application of K^+-channel PCLs is the restoration of visual responses in degenerated retina, where photoreceptor cells have died. AAQ photosensitizes surviving retinal neurons and allow control their firing activity (Polosukhina et al. 2012). AAQ treatment of degenerated retina has the advantage over LiGluR (Caporale et al. 2011) that photosensitization is restored without gene therapy.

2P-potassium channels

The 2P-potassium channel TREK1 was also rendered photoswitchable using the blocker MAQ and a cysteine introduced at the extracellular side by homology with SPARK (Sandoz et al. 2012). Depending on the cysteine position, the PTL blocked the pore in *trans* (TREK1-K231C-MAQ) and a *cis* (TREK1-S212C-MAQ). This channel allowed defining a novel scheme to photocontrol native proteins using a "photoswitchable conditional subunit" (PCS), which contains the PTL anchoring site and a mutation that blocks plasma membrane expression. In cells not expressing native subunits for the protein, the PCS is not functional, but when native subunits are expressed, they coassemble with the PCS, traffic to the plasma membrane, and place the native protein under optical control. Overcoming the lack of specific TREK1 blockers to pharmacologically study their function in neurons, expression of the photoswitchable PCS subunit TREKΔC-S121C allowed to specifically characterize the function of native TREK channels independently of other expressed potassium channels, and related them with GABAergic signaling (Sandoz et al. 2012).

1.2.6 Transient receptor potential channels

Transient Receptor Potential (TRP) channels are a superfamily of cationic channels characterized by their multiple activation mechanisms and roles in sensory physiology. TRP channels have a six-transmembrane structure like voltage-gated cation channels, but they can be considered as integrators of multiple signals because the response of one input can be modified by another. The capsaicin receptor TRPV1 is one of the best studied channels of this diverse superfamily. TRPV1 responds to several stimuli from heat to proinflamatory agents, pH, other chemicals (endocannabinoid,

anandamide, camphor, piperine (from pepper) and allicin (from garlic)) or exocytosis. (Venkatachalam and Montell 2007).

Photocontrol of TRPV1 channels using agonist uncaging was used in early studies to manipulate neurons and behavior with light (Lima and Miesenböck 2005). More recently, two PCLs were developed to reversibly control TRPV1, consisting of azobenzene derivatives of capsazepines and BCTC (AC4 and ABCTC) (Stein et al. 2013). These compounds displayed potent voltage antagonism at complementary conformations, in *trans* for AC4 (440 nm) and in *cis* for ABCTC (370nm). In the presence of the agonist capsaicin, AC4 was able to strongly inhibit TRPV1 responses in the *cis* state and this effect was reversible in *trans* (Stein et al. 2013).

1.2.7 Future challenges

Although the first synthetic photoswitches of ion channel activity were reported more than forty years ago (Bartels, Wassermann, and Erlanger 1971), this field has boomed in the last decade owing to the availability of pharmacology, high-resolution protein structures, recombinant DNA technology, heterologous expression systems and molecular dynamics simulations, which have allowed the rational development of photoswitches for almost every class of ion channel present on neurons. Photocontrol of voltage-gated calcium channels and receptors of NMDA, glycine and serotonin has not yet been described, but will be facilitated by the reported examples of structurally related proteins.

PCLs act on endogenous proteins and can be useful therapeutically (optopharmacology) and to study the physiology of intact tissues and organisms. These applications would benefit from the availability of PCLs for the abovementioned channels and receptors, and from improved photochemical and pharmacological properties (selectivity, potency). In this way it would be possible to study the roles played by each channel in its complex, undisturbed physiological context.

On the other hand, although PTLs provide robust photoswitching that is not subject to diffusion, the current PTL conjugation methodology requires mutating the channel to introduce cysteines, and thus does not allow gaining direct control over the activity of endogenous channels. Channels that have been engineered to conjugate to a PTL

must be overexpressed in tissue or a transgenic or knock-in animal must be developed. Therefore, the interest of PTLs would increase if a conjugation methodology could be developed for endogenous proteins.

An outstanding advantage of synthetic photoswitches is that they are based on chromophores that act on the protein surface, in contrast to the tight binding pockets found in natural light-sensitive proteins. Synthetic photoswitches thus offer excellent opportunities for rationally tuning their photochemical characteristics by chemical substitutions that do not affect the functional properties of the protein. The absorption spectra, photostationary state and relaxation lifetime have been adjusted in several photoswitches (Mourot et al. 2011, Fehrentz et al. 2012, Kienzler et al. 2013), but multiphoton stimulation has not been investigated despite the advances of neurotransmitter uncaging and optogenetics using pulsed illumination. Two-photon switching with infrared light would be attractive to stimulate ion channels deep into tissue (Papagiakoumou et al. 2013), to achieve high three-dimensional resolution (Denk, Strickler, and Webb 1990) and patterned illumination (Oron et al. 2012, Watson, Nikolenko, and Yuste 2009). Finally, while all synthetic photoswitches reported for ion channels so far are based on azobenzene, different photoisomerizable groups have been successfully applied to other proteins (Szymanski et al. 2013) and have advantages of their own that could be exploited with channels.

1.3 Objectives of the Thesis

Recognizing both the need for new optical tools to manipulate neurotransmission, and the opportunities offered by photoswitches, this thesis is focused on the use of light-gated glutamate receptors to control neuronal activity (i.e. the generation of APs) and neurotransmission.

The possibility of using a tethered photoswitch to confer light sensitivity to endogenous receptors would avoid genetically altering the physiological conditions of the neuron by overexpressing exogenous proteins (opsins or mutant receptors). It would also enable studying the role of a receptor *in situ*, and studying the physiological process in which it is involved without any alteration (e.g. the neurotransmission process). Moreover, synthetic photoswitches like azobenzene are often controlled by continuous-wave violet illumination, which does not penetrate deep into tissue, can damage cells and offers a limited ability to focus, especially in the axial direction. An improvement of the stimulation method of synthetic photoswitches is thus needed in order to control receptor activity in intact tissue.

The grand aim of this work is to utilize **endogenous neuronal receptors to optically control neuronal activity and the neurotransmission process**, and being able to **stimulate them in small volumes corresponding to the neuronal functional unit** (i.e. synaptic terminals). In this way, light would emerge as a unique tool to dissect neuronal physiology and to understand the function of neuronal circuits: from the integration of synaptic inputs in individual neurons, to the operation of brain structures. In order to achieve that aim, three separate objectives have been set in this thesis:

- To **directly control neurotransmission with light**, taking advantage of the Ca^{2+}-permeability of glutamate receptors to manipulate intracellular [Ca^{2+}] and to trigger neurotransmitter exocytosis. This objective is developed in **chapter 2**.

- To demonstrate **two-photon stimulation of light-gated glutamate receptors** chemically conjugated to azobenzene-based photoswitches. This objective is the focus of **chapter 3**.
- To develop an efficient and versatile method to **photocontrol endogenous receptors** using targeted covalent ligands, which is described in **chapter 4**.

-

Chapter 2

Reversible control of Ca^{2+}-regulated processes using LiGluR

Ca^{2+} is a secondary messenger of many cellular processes, e.g. it is the trigger for exocytosis, and in consequence for neurotransmission (see **section 1.1**). There are few optical tools devised to manipulate intracellular [Ca^{2+}]. In this chapter, we aim to demonstrate that the Ca^{2+}-permeable LiGluR can be used as a tool to reversibly control neurosecretion by directly affecting the intracellular [Ca^{2+}]. To achieve this goal, LiGluR was expressed in cultured bovine chromaffin cells. These neuroendocrine cells act as a huge presynaptic terminal, being a classical cell model for exocytosis. We measured secretion on chromaffin cells using two techniques, amperometry and membrane capacitance, and controlled LiGluR with 380-nm light illumination to open the channel and 500-nm light to close it. The following step was to refine LiGluR performance and to extend such control to a real chemical synapse, in cultured hippocampal neurons.

The main findings related to this work are:

- Secretion, monitored by means of amperometry, is induced by the opening of LiGluR with light in chromaffin cells, under the block of VGCC. Light-triggered secretion typically achieves a maximum rate of 2-4 Hz, the burst of spikes starts with a delay of few seconds, and it is gradually reduced once LiGluR is closed with 500 nm light. This process can be reversibly repeated until the reservoir of secretory granules is exhausted (see in **section 2.1**, **Fig. 1** and **2**).

- Analysis of the shape of amperometric spikes induced by light revealed that the released charge per event is in agreement with control values for chromaffin cells. Nevertheless light-stimulated events present a slower time profile that could account for either a slower release of the catecholamine or for the diffused detection of a normal event. (**section 2.1**, **Fig. 3**)
- Direct measurement of the Ca^{2+} component of LiGluR photocurrents and the membrane capacitance change showed that:
    - Ca^{2+} current through LiGluR, which account for ~ 10% of the total photocurrent, is responsible for triggering the fusion of chromaffin granules (**section 2.1, Fig. 4**).
    - The dependence of light-evoked secretion on Ca^{2+} influx followed a typical square root function (**section 2.1**, **Fig. 5c**), similar to the dependence described in the calyx of Held synapsis (Leão and von Gersdorff 2009). This finding evidenced that LiGluR is able to artificially activate the molecular mechanism of Ca^{2+}-regulated exocytosis.
    - Fitting the data for depolarization- and light-evoked secretion to the same function, we calculated a two-fold smaller constant in comparison with the value obtained for the depolarization-evoked secretion. This result indicates that exocytosis is more efficiently triggered by Ca^{2+} influx through VGCC.
- The coupling between LiGluR and the Ca^{2+}-sensitive structures that trigger exocytosis was assayed by the intracellular application of exogenous Ca^{2+}-chelators, BAPTA and EGTA (**section 2.1**, **Fig. 6**). The experiments showed that light-induced secretion was more sensitive to both BAPTA and EGTA, than depolarization-induced secretion. These differences in sensitivity point toward a weaker coupling (i.e. larger distance between the release site and LiGluRs) of the light-induced Ca^{2+} influx, which could also explain its lower efficacy in triggering exocytosis and the delay in the onset of secretion observed by amperometry.

- Light-trigged neurotransmission was assayed through the following method in cultured hippocampal neurons: we recorded the membrane potential of a LiGluR(-) neuron that visually overlapped with a LiGluR(+) neuron, and thus was potentially connected to it (**section 2.3**, **Fig. 3b**). We blocked endogenous VGCC to avoid Ca^{2+} entry upon depolarization of the LiGluR(+) neuron. Then, a light pulse was applied which generated a train of AP in the LiGluR(-) neuron, that gradually stopped once LiGluR closed (**section 2.3**, **Fig 3d**). The maximum rate achieved by the AP train is 6 Hz in average; and as it has been observed in chromaffin cells, there is an unusually long delay between the beginning of the light stimulus and the generation of the first AP (Sabatini and Regehr 1996).
- Taking advantage of the dependence of LiGluR-current amplitude on the illumination wavelength (Gorostiza et al. 2007) (**section 2.3**, **Fig. 2a**), the Ca^{2+} influx through the channel can be optically tuned. In chromaffin cells, the secretory rate can be adjusted with the wavelength of light stimuli (**section 2.3**, **Fig. 2b**). Similarly in cultured neurons, light-gated secretion at LiGluR(+) neurons supports color-modulated neurotransmission and, in consequence, control of the postsynaptic firing rate (**section 2.3**, **Fig. 4**).
- The magnitude of LiGluR-mediated Ca^{2+} influx is sufficiently large to trigger regulated exocytosis in chromaffin cells and neurons. In addition, LiGluR-induced (neuro)secretion can be modulated with the wavelength of illumination. This new application of LiGluR opens the possibility to reversibly control the activity of individual synapses, which might help to understand the computational properties of neurons and to unravel how brain circuits work.

This study has been published in two separate articles. The first one demonstrates the optical manipulation of exocytosis in chromaffin cells and investigates its biophysical properties, while in the second one we used the same approach to directly manipulate neurotransmission in cultured neurons.

- In **section 2.1** and **2.2** the following article is reproduced:

Izquierdo-Serra, D. Trauner, A. Llobet, and P. Gorostiza (2013). Optical control of calcium-regulated exocytosis. Biochimica et Biophysica Acta-General Subjects 1830(3):2853-60. doi: 10.1016/j.bbagen.2012.11.003

- **Section 2.3** reproduces the second part of this study:

  Izquierdo-Serra M, Trauner D, Llobet A and Gorostiza P (2013) Optical modulation of neurotransmission using calcium photocurrents through the ion channel LiGluR. Front. Mol. Neurosci. 6:3. doi: 10.3389/fnmol.2013.00003.

2.1 Optical control of Ca^{2+}-regulated exocytosis

Biochimica et Biophysica Acta 1830 (2013) 2853–2860

Contents lists available at SciVerse ScienceDirect

Biochimica et Biophysica Acta

journal homepage: www.elsevier.com/locate/bbagen

Optical control of calcium-regulated exocytosis

Mercè Izquierdo-Serra [a], Dirk Trauner [b], Artur Llobet [c], Pau Gorostiza [a,d,e,*]

[a] Institute for Bioengineering of Catalonia (IBEC), 15-21 Baldiri Reixac, 08028 Barcelona, Spain
[b] Department of Chemistry and Pharmacology, Ludwig-Maximilians-Universität, München, and Center for Integrated Protein Science, 81377 Munich, Germany
[c] Laboratory of Neurobiology, Bellvitge Biomedical Research Institute (IDIBELL), Feixa Llarga s/n, 08907 L'Hospitalet de Llobregat, Spain
[d] Catalan Institution for Research and Advanced Studies (ICREA), Passeig Lluís Companys 23, 08010 Barcelona, Spain
[e] Networking Research Center on Bioengineering, Biomaterials and Nanomedicine (CIBER-BBN), Spain

ARTICLE INFO

Article history:
Received 31 July 2012
Received in revised form 22 October 2012
Accepted 10 November 2012
Available online 20 November 2012

Keywords:
Optical control
Calcium
Exocytosis
Light-gated glutamate receptor (LiGluR)
Neurotransmission
Optogenetics

ABSTRACT

Background: Neurons signal to each other and to non-neuronal cells as those in muscle or glands, by means of the secretion of neurotransmitters at chemical synapses. In order to dissect the molecular mechanisms of neurotransmission, new methods for directly and reversibly triggering neurosecretion at the presynaptic terminal are necessary. Here we exploit the calcium permeability of the light-gated channel LiGluR in order to reversibly manipulate cytosolic calcium concentration, thus controlling calcium-regulated exocytosis.
Methods: Bovine chromaffin cells expressing LiGluR were stimulated with light. Exocytic events were detected by amperometry or by whole-cell patch-clamp to quantify membrane capacitance and calcium influx.
Results: Amperometry reveals that optical stimulation consistently triggers exocytosis in chromaffin cells. Secretion of catecholamines can be adjusted between zero and several Hz by changing the wavelength of illumination. Differences in secretion efficacy are found between the activation of LiGluR and native voltage-gated calcium channels (VGCCs). Our results show that the distance between sites of calcium influx and vesicles ready to be released is longer when calcium influx is triggered by LiGluR instead of native VGCCs.
Conclusion: LiGluR activation directly and reversibly increases the intracellular calcium concentration. Light-gated calcium influx allows for the first time to control calcium-regulated exocytosis without the need of applying depolarizing solutions or voltage clamping in chromaffin cells.
General significance: LiGluR is a useful tool to study the secretory mechanisms and their spatiotemporal patterns in neurotransmission, and opens a window to study other calcium-dependent processes such as muscular contraction or cell migration.

© 2012 Elsevier B.V. All rights reserved.

1. Introduction

Exocytosis is the process by which a cell directs the content of secretory vesicles out of the cell membrane. It is a key process in the expression of membrane proteins, in the secretion of soluble proteins and hormones, and in neurotransmission where exocytosis of transmitter molecules at the presynaptic terminal and the subsequent activation of ligand-gated channels at the postsynaptic neuron allow the propagation of the nerve impulse from one neuron to another.

Exocytic events have been studied in great detail in chromaffin cells, because their size and shape provide good experimental access [1], and the molecular machinery involved in secretory granule exocytosis is homologous to that of synaptic vesicles in neurons [2].

Available methods to manipulate exocytosis can act at two stages of the process. First, by depolarizing the membrane of secretory cells in order to activate the native voltage-gated calcium channels (VGCCs) that mediate exocytosis under physiological conditions. These methods include application of depolarizing solutions, depolarizing pulses by means of patch clamp electrodes, and more recently the activation of the cation-selective channel Channelrhodopsin-2 (ChR2) with light. Alternatively, exocytosis can be manipulated by altering the intracellular calcium concentration with Ca^{2+} ionophores (*i.e.* ionomycin) or Ca^{2+} uncaging. These classical methods directly modify intracellular Ca^{2+} concentrations but are not reversible. Thus, new methods are needed in order to control directly and reversibly intracellular calcium levels, thereby triggering regulated exocytosis.

An appealing possibility is controlling the presynaptic Ca^{2+} concentration with light using photoswitchable ion channels like ChR2 [3] or the light-gated glutamate receptor (LiGluR) [4]. Light stimulation is non-invasive and provides spatial and temporal control at the level of individual synaptic terminals (1 μm) and single action potentials (1 ms). LiGluR and ChR2 are cation-selective channels that upon activation produce large inward currents mainly due to Na^{+} ions at the cell resting potential [5–7]. Light-gated currents readily depolarize the neuron soma and trigger action potentials that propagate along the processes and have been used to investigate neuronal circuits *in vivo* [3,8–11] and to manipulate astrocyte-to-astrocyte communication [12]. However, the Ca^{2+} permeability of light-gated

* Corresponding author at: Institute for Bioengineering of Catalonia (IBEC), 15-21 Baldiri Reixac, 08028 Barcelona, Spain. Tel./fax: +34 934 020 208.
E-mail address: pau@icrea.cat (P. Gorostiza).

0304-4165/$ – see front matter © 2012 Elsevier B.V. All rights reserved.
http://dx.doi.org/10.1016/j.bbagen.2012.11.003

channels has never been exploited to manipulate the intracellular Ca^{2+} concentration without altering membrane potential, which opens up the possibility of directly triggering secretion processes [13]. Here, we demonstrate specific control of Ca^{2+} currents and exocytosis with light using LiGluR and we compare it with exocytosis triggered by VGCCs in the same cells.

2. Materials and methods

2.1. Chromaffin cell culture and infection

Chromaffin cells were isolated from medulla of bovine adrenal glands by enzymatic treatments [14]. Dissociated chromaffin cells were plated at 2.5×10^5 cells $well^{-1}$ density in poly-L-lysine treated coverslips. After 1 day, the cells were infected using an adenoviral construction carrying the fusion protein GluK2-L439C-eGFP. Amperometry and patch clamp experiments in chromaffin cells were performed after 1 to 2 days after infection.

2.2. Conjugation of MAG photoswitch

MAG was synthesized as described [4] and the concentrated stock (10 mM in DMSO) was stored at −20 °C. Before all experiments, the cells were incubated in the absence of light, for 10 min in a Na^+-free and low-Ca^{2+} (0.5 mM) solution with 10–100 μM of MAG (DMSO final concentration <1%) and 0.3 mg mL^{-1} concanavalin A, to block GluKs desensitization [15].

2.3. Carbon microfiber amperometry

Catecholamine release was detected using homemade polyethylene-insulated carbon fiber electrodes of 12-μm diameter [16,17]. Amperometric electrodes were first tested in a solution containing 5 mM ferricyanide in 0.1 M KCl and pH 6.8. Electrodes displaying a current between 1 and 10 nA at a holding potential of +700 mV were selected, and their integrity was verified by voltammetry [18]. Only electrodes showing a symmetric oxidation/reduction current response to a symmetric ramp from +700 to −300 mV (scan rate 100 mV/s) were used to measure exocytosis in chromaffin cells. When necessary, electrodes were freshly cut with a scalpel on a glass surface, and were used for further experiments if the basal current was between 10 and 20 pA (at holding potential +700 mV) in the bath solution. Amperometric current was recorded by applying a holding voltage of +700 mV with an EPC-10 amplifier (HEKA) controlled with Patch Master (HEKA). The sampling rate was 100 kHz and the current was filtered with a Bessel Filter set at 30 kHz. After data acquisition, traces were digitally filtered at 1 kHz. For controls, cells were stimulated by local application of a high-K^+ solution. For light stimulation, illumination was applied using a TILL Photonics Polychrome V monochromator through the side port of an IX70 inverted microscope (Olympus) and using a UApo/340, 40×/1.35 objective. Shutter and wavelength were controlled trough an EtherNet-COM-1 connection to a PC, using TILL Photonics Polychrome V Control (PolyCon) software. The light power measured with a light meter model Newport 1916-C placed next to the objective was 0.9 mW mm^{-2} at 380 nm and 1.7 mW mm^{-2} at 500 nm.

2.4. Voltage-clamp recordings

Recordings of voltage-clamp under whole cell configuration were done using an EPC-10 amplifier and Patch Master software. Pipettes were pulled from borosilicate glass tubing (Harvard Apparatus) with P-97 puller from Sutter Instruments, with a typical resistance of 2–4 MΩ. Membrane capacitance was implemented using the Sine + DC mode of the Patch Master lock-in module. A 1000 Hz, 25 mV sinusoidal wave was applied to a holding potential (V_h) of −80 mV and current was acquired at a sampling rate of 20 kHz. Before each stimulus (depolarization or UV-light) a hyperpolarization of −90 mV was applied to later allow leak subtraction to ion currents. In all voltage-clamp experiments, illumination was set using the same system as for the amperometric. However, light was synchronized with the stimulus, then shutter and wavelength were controlled through photometry module of Patch Master, via Photochromic Manual Control (TILL Photonics) connected to EPC-10 amplifier.

2.5. Data analysis

All analysis was done with IgorPro from Wavemetrics. A macro developed by Eugene Mosharov (http://www.sulzerlab.org) was used for amperometric spike and parameter analysis [19]. Data was exported to Matlab to calculate secretory rate. The membrane capacitance increase was calculated by subtracting the mean basal capacitance to the mean capacitance after stimulus using an IgorPro custom made macro. To calculate the mean membrane capacitance after the stimulus, it was considered a 300 ms time window, starting after 100 ms from the end of the stimulus [20]. All data are expressed as mean ± s.e.m. (standard error of measurement, calculated over the number of n), except for the parameters calculated by curve fittings, where the error is calculated as 95% confidence interval.

We define secretory or exocytic efficacy as the increase of the membrane capacitance divided by the Ca^{2+} charge of the measured Ca^{2+} influx ($\Delta C_m/Q_{Ca^{2+}}$), expressed in fF/pC.

2.6. Solutions

The composition of physiological bath solution (in mM): 140 NaCl, 2.5 KCl, 1 $MgCl_2$, 10 HEPES, 10 Glucose, 2.5 $CaCl_2$ at pH 7.42 and 300 mOsm kg^{-1}. The high-K^+ solution was composed by (in mM): 90 NaCl, 50 KCl, 1 $MgCl_2$, 10 HEPES, 10 Glucose, 5 $CaCl_2$ at pH 7.42 and 300 mOsm kg^{-1}. The Na^+-free and high-Ca^{2+} bath solution contained (in mM): 110 $NMDG^+$, 2.5 KCl, 1 $MgCl_2$, 10 HEPES, 10 Glucose, 30 $CaCl_2$ at pH 7.42 and 300 mOsm k^{-1}. The composition of pipette solution was (in mM): 120 Cesium methanesulfonate, 10 TEA-Cl, 20 HEPES, 3 Na_2ATP, 1 NaGTP and 0.4 BAPTA, pH 7.2 and 290 mOsm kg^{-1}. Except for the experiments with restriction of Ca^{2+}-diffusion, in which EGTA was used instead of BAPTA at (mM): 0.4, 0.6, 0.8, 1.5, 2.7, 5 or 15. In the indicated experiments, the following cocktail of toxins was added to the bath solution: 100 nM ω-agatoxin IVA and 1 μM ω-conotoxin GIVA (Alomone Labs) and 10 μM nifedipine.

All reagents were obtained from Sigma unless otherwise specified.

3. Results

In order to test whether secretion of neurotransmitters can be controlled optically in neurosecretory cells, the receptor-channel GluK2-L439C-eGFP was expressed in bovine chromaffin cells by application of a viral vector. More than 70% of the cells showed GFP expression after 24 h of infection. Prior to the experiments, the receptor was chemically conjugated to the photoswitch Maleimide Azobenzene Glutamate (MAG) as described [4] in order to obtain LiGluR. In 90% of the fluorescent cells evaluated, illumination with 380 nm light resulted in LiGluR opening and visible light of 500 nm closed the channel, indicating that its permeability for Ca^{2+} was susceptible to be controlled by light.

3.1. Expression of LiGluR in chromaffin cells supports optical control of neurosecretion

Exocytosis from chromaffin cells was assayed with amperometry using carbon microfiber electrodes [21,22]. In order to avoid the activation of VGCCs during optical stimulation, cells were bathed in a physiological solution containing nifedipine, ω-conotoxin GVIA and ω-agatoxin IVA, which blocks the three types of VGCCs expressed in

bovine chromaffin cells: Ca_v1, $Ca_v2.2$ and $Ca_v2.1$, respectively [23] (Fig. 1A).

Amperometric recordings of LiGluR-eGFP positive cells, LiGluR(+), showed that shortly after illuminating with UV-light during 5 s, secretory events could be detected as spikes in the amperometric current trace (see Fig. 1B). Shorter light pulse duration decreased the secretion probability (Supp. Fig. 1). Besides the amperometric current, two additional results supported the optical triggering of secretion. First, the amount of released molecules increased with the UV-light pulse duration (calculated by the cumulative integral of the amperometric current) and it stabilized once the channel was switched off (Fig. 1B). And second, we calculated that the frequency of events synchronously occurring upon illumination at 380 nm for 5 s achieved a characteristic maximum secretory rate of 2–4 Hz (green trace in Fig. 1B). Optical stimulation at 380 nm triggered secretion at a rate comparable to control chromaffin cells (non-infected) stimulated *via* perfusion of depolarizing high-K^+ solution (see traces in Fig. 1C and quantitative comparison in Fig. 1D). We also quantified the delay between the beginning of stimuli and the onset of the first amperometric spike, which was about two times longer for LiGluR than for endogenous VGCC stimulation (Fig. 1E). Upon stimulus termination, amperometric spikes remained at its maximum and decayed with a characteristic time constant until cells stopped secreting (Fig. 1F). The decay time τ was again different for light and high-K^+ stimulation (Fig. 1G). These differences were further investigated using patch clamp recordings (see Sections 3.3 and 3.4).

We tested the reversibility of the optical control by alternating stimulation of 5 s pulses at 380 nm with 20 s periods at 500 nm (about three times the decay time constant). Under these conditions, light-triggered secretion could be repeated several times within a

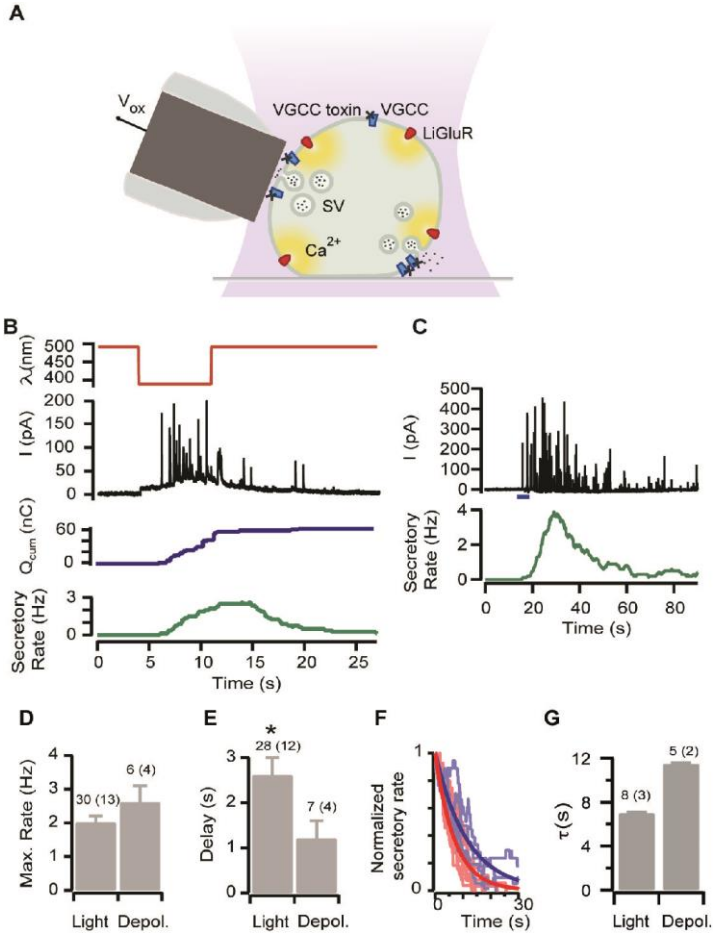

Fig. 1. LiGluR enables optical control of secretion in chromaffin cells. (A) Scheme of the experimental setup to assay light-triggered secretion by carbon microfiber amperometry in individual LiGluR(+) chromaffin cells (V_{ox}: oxidation voltage, SV: secretory vesicle). Depolarizing stimuli were applied by local perfusion of high-K^+ solutions in control amperometry experiments. (B) In LiGluR(+) chromaffin cells, a 380 nm light pulse of 5 s (red plot) produces spikes in the amperometric current recording (black plot) and an increase in the calculated cumulative charge (blue plot) and secretory rate (green plot). When illumination is switched back at 500 nm, spikes are gradually stopped. (C) Amperometric recording (black plot) and calculated secretory rate (green) in response to local application of a high-K^+ depolarizing solution (blue bar) in a wild type chromaffin cell. (D) Average maximum spike rate and (E) average delay between stimuli and the first amperometric spike, for light and depolarization experiments. (F) Upon reaching the maximum, the secretory rate decays exponentially both for light and depolarization experiments (red and blue plots, respectively). Several individual traces (thin lines) and their exponential decay fit (thick line) are shown. (G) Decay time constant for light and depolarization experiments. Numbers on top of each bar indicate the total number of measurements and the number of different cells in parentheses. An asterisk (*) indicates significant differences ($P<0.05$) by Mann–Whitney U test. Error bars are ±s.e.m., except for decay time constant, which is the error propagated from the exponential fitting.

single cell (Fig. 2A). However, rundown of secretion occurred when cells were over-stimulated either with light or depolarization (Fig. 2B and Supp. Fig. 2), in agreement with the known constraints to maintaining a maximum level of secretion, such as the availability of vesicles for release.

Together, these observations evidenced that LiGluR allows reversibly switching secretion of catecholaminergic vesicles, without the need to activate VGCCs.

3.2. Analysis of amperometric spikes

The time course of individual amperometric spikes was quantified by measuring the maximum intensity, the spike half-width and by integrating the spike current to calculate its charge (Fig. 3A). Spikes from independent light-triggered bursts (2243 spikes obtained from 13 cells, 4 different cultures) were analyzed, averaged per cell [24] and compared to control chromaffin cells stimulated by depolarization (1191 spikes, from 5 cells, 1 culture). The corresponding cell-averaged cumulative distributions are shown in Fig. 3B–D. Light-triggered spikes displayed 60% of the amplitude of those obtained by depolarization (80 ± 10 pA and 130 ± 30 pA respectively, Fig. 3F), and a similar increase on half-width (26 ± 1 ms and 16 ± 5 ms respectively, Fig. 3D). However, the averaged charge of exocytic events evoked optically was the same as depolarization-triggered ones (2.1 ± 0.3 pC and 2.1 ± 0.4 pC respectively, Fig. 3G). The fact that depolarization and light stimulation gave rise to spikes with different time profiles (Fig. 3E) but the same charge distribution (Fig. 3C) suggests that the amount of catecholamine released per vesicle is independent of the stimulation method.

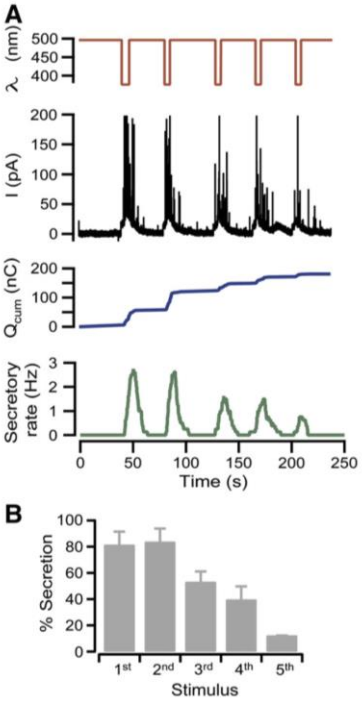

Fig. 2. Reversible control of secretion with light. (A) Example of an amperometric response (black plot) to repetitive light stimulation (red plot). The cumulative charge and spike rate are shown in blue and green respectively. (B) Quantification of rundown of secretion from 4 different cells repetitively stimulated with light (between 3 and 5 light pulses per cell). The total charge released by each stimulus is normalized to the maximum release of the cell before calculating the average. Error bars are ± s.e.m.

3.3. Efficacy of light- and depolarization-induced exocytosis assayed through capacitance measurements

As mentioned above, amperometric recordings showed that light-triggered secretion occurs with a longer delay than when depolarizing stimuli are applied (Fig. 1E). Since release probability in neuroendocrine cells is greatly determined by temporal and spatial characteristics of calcium influx [25], we decided to quantify both calcium influx and the resulting fusion of secretory granules with the plasma membrane, using whole-cell patch clamp and membrane capacitance recordings in chromaffin cells expressing LiGluR (Fig. 4A). Exocytic events increase cell membrane area and are readily detected by membrane capacitance recordings [26].

We started by measuring the current and membrane capacitance during depolarizing stimuli (which activate native VGCCs, see left traces in Fig. 4B) and optical stimuli (pulses at 380 nm and back to continuous 500 nm illumination to keep LiGluR closed, see left traces in Fig. 4C). In both cases, the detection of current influx during stimulation resulted in a jump of capacitance that corresponds to exocytosis (bottom left traces in Fig. 4B and C). However, LiGluR has a cation-selective pore and the photocurrents observed at the holding potential of −80 mV are due to both Na^+ and Ca^{2+} and cannot be directly compared to Ca^{2+}-selective VGCC currents.

In order to isolate the Ca^{2+} influx from other cationic currents of LiGluR, we modified the *physiological bath solution* described in the Materials and methods section by replacing Na^+ with N-methyl D-glucamine ($NMDG^+$) which does not permeate glutamate receptor channels [5]. We also increased Ca^{2+} concentration to 30 mM; this was called *Na^+-free and high-Ca^{2+} bath solution*. LiGluR supports a significant calcium influx at −80 mV [5], and under these experimental conditions Ca^{2+} is the only permeating cation through LiGluR, allowing it to behave as a light-gated Ca^{2+} channel.

As expected, when depolarizing chromaffin cells in Na^+-free and high-Ca^{2+} bath solution, only the fast-inactivating endogenous Na^+ current peak was abolished, while exocytosis was not altered (Fig. 4B, right traces). On the other hand, the amplitude of photocurrents from the cation-permeable channel of LiGluR was substantially reduced in the Na^+-free and high-Ca^{2+} bath solution, without affecting exocytosis (Fig. 4C, right traces).

These results confirm that LiGluR supports substantial Ca^{2+} current to trigger calcium-regulated exocytosis, and other calcium-dependent processes [12], even at resting membrane potential.

3.4. Coupling between calcium influx and exocytosis

We further asked whether LiGluR channels support the same level of neurosecretion as VGCCs. Several studies using a combination of electrophysiological and imaging techniques (reviewed by Olivos and Artalejo [27]) point out the existence of clusters of native VGCCs in the plasma membrane of chromaffin cells, which effectively determine secretion [28,29]. In principle, such level of organization is not to be expected for LiGluR channels overexpressed in chromaffin cells, because these cells do not endogenously express any kainate receptor [30]. In order to evaluate differences in stimulus-secretion coupling, exocytosis was compared for equivalent calcium influxes through the two channel types using the Na^+-free and high-Ca^{2+} bath solution.

A representative example of LiGluR optical stimulation using this solution is shown in the left traces of Fig. 5A, where we recorded the Ca^{2+} entry and increase in the membrane capacitance during a 500 ms pulse of 380 nm light on a LiGluR(+) chromaffin cell. After 90 s to allow cell recovery, we subsequently applied a depolarizing pulse to the same cell and measured the amount of secretion evoked

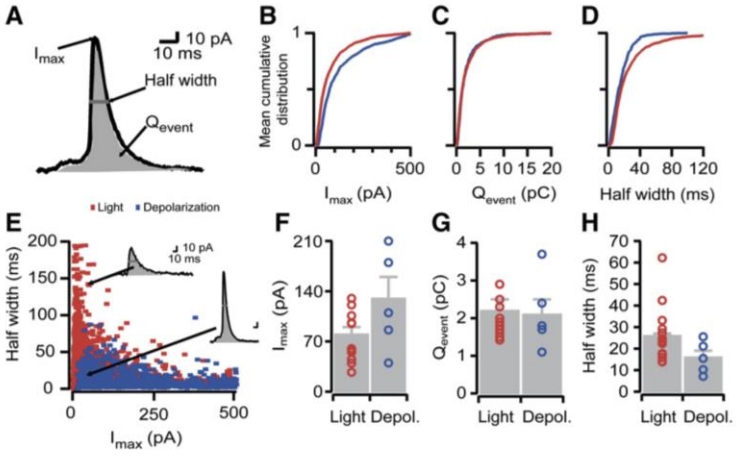

Fig. 3. Analysis of individual amperometric spikes and comparison between light and depolarizing stimuli. (A) Example of an amperometric spike indicating the analyzed parameters: maximum spike current amplitude (I_{max}), spike half width and integrated spike charge (Q_{event}). (B–D) Mean cumulative distribution of I_{max}, Q_{event} and half width for LiGluR(+) cells stimulated by light (red) and control cells stimulated by depolarization (blue). (E) Distribution of amperometry spike parameters: half width *versus* spike amplitude, in depolarization-triggered secretion (●) and light-triggered secretion (●). (F) Mean of I_{max}, (G) Q_{event} and (H) half width of means for LiGluR(+) and control cells stimulated with light or depolarization (red and blue bars respectively). A total of 13 cells were stimulated with light (2243 spikes, 54–323 spikes/cell, 4 different cultures) and 5 cells were depolarized (1191 spikes, 67–658 spikes/cell, 1 culture). Error bars show ± s.e.m.

by activation of VGCCs (right traces in Fig. 5A). To obtain comparable Ca^{2+} charges from overexpressed LiGluR and native VGCC currents, we adjusted the number of opened VGCCs by setting the depolarization pulse between 10 and 30 mV in each cell, until the VGCC charge approximately matched the LiGluR charge. As can be observed in the bottom traces of Fig. 5A, the increase in membrane capacitance was significantly bigger when activating VGCCs. This result was confirmed in a set of experiments where exocytosis could be triggered by light and depolarization in the same cell: Fig. 5B plots the Ca^{2+} charge ($Q_{Ca^{2+}}$) *versus* resulting capacitance increase (ΔC_m) elicited by depolarization and light (blue and red dots respectively; gray lines link responses obtained in the same cell). It can be observed that comparable charges lead to higher depolarization responses, and that a larger light-evoked charge is required to produce similar responses. We further quantified ΔC_m and $Q_{Ca^{2+}}$ in a larger dataset in order to determine how vesicle fusion was correlated with the amount of calcium influx (Fig. 5C). The results show that both depolarization and light-evoked secretion follow the same non-linear behavior, which can be fitted by $\Delta C_m = k\sqrt{Q_{Ca^{2+}}}$ (*i.e.* ΔC_m^2 depends linearly on $Q_{Ca^{2+}}$ in Fig. 5C) [31]. However, the value of the constant k (calculated as the square root of the slope in Fig. 5C, 23.0 ± 0.4 fF/√pC for VGCC and 12.6 ± 0.8 fF/√pC for LiGLuR) is about two fold larger when Ca^{2+} ions permeate the plasma membrane *via* VGCCs than when they do it *via* LiGluR. This difference indicates that secretion is more efficiently triggered by VGCCs, in agreement with Fig. 5A and B.

A possible explanation for the lower secretory efficacy of LiGluR is that native VGCCs are coupled or specifically localized near secretory vesicles, whereas such coupling is not expected from exogenously expressed LiGluR. In order to test whether there are differences in localization between the channels and the release site that could explain the difference in secretory efficacy, we limited intracellular Ca^{2+} diffusion by adding a fast (BAPTA) or a slow (EGTA) exogenous Ca^{2+} buffer in the patch pipette [20,32]. Fig. 6A shows the exocytic efficacy of light- and depolarization-triggered secretion in the presence of 0.4 mM BAPTA and 0.4 mM EGTA. In depolarization experiments, Ca^{2+} buffering did not alter the exocytic efficacy. In light-triggered secretion, the efficacy was significantly reduced in the presence of BAPTA, but remained unaffected in the presence of EGTA (3.3 ± 0.5 and 11 ± 2 fF/pC respectively). The results of Fig. 6A indicate that VGCCs are localized closer to the release site than LiGluR [33], so we further investigated this point. We added increasing EGTA concentrations in the pipette solution in order to gradually limit diffusion of Ca^{2+} and to find the buffer concentration needed to inhibit light- and depolarization-triggered secretion. Exocytosis efficacies are plotted as a function of EGTA concentration in Fig. 6B. In both cases, increasing concentrations of EGTA cause an inhibition of secretion as less calcium is sensed by the exocytic machinery. Data was fitted to a sigmoid function; in the case of light-stimulation we assumed maximum secretion at 0.4 mM EGTA (lower EGTA concentrations could not be assayed due to high secretion variability). Comparing both curves, EGTA has at least a three-fold stronger impact on LiGluR than on VGCCs, with the concentrations corresponding to 50% inhibition being IC_{50} ~ 0.5 mM and 1.5 ± 0.1 mM, respectively.

4. Discussion

LiGluR allows controlling secretion with light in chromaffin cells under physiological extracellular Ca^{2+} concentrations, as demonstrated using amperometry and capacitance recordings. Catecholamine release to the extracellular medium can be reversibly switched on and off with light at 380 nm and 500 nm respectively, and the rate of release events (amperometric spikes) can be controlled between zero and 2.5 Hz, in the range of typical secretory rate of chromaffin cells [34] (Figs. 1 and 2). The maximum optical release rate decreases with each stimulation cycle (Fig. 2B), suggesting that the readily releasable pool of secretory granules [35,36] can be depleted with optical stimulation, which provides experimental access to study their recycling dynamics.

The characteristic spike parameters (Fig. 3) are in agreement with values reported using cell-depolarizing solutions to activate Ca^{2+} channels [21,22]. The fact that depolarization and light stimulation give rise to amperometric spikes with different time profiles (Fig. 3E) but the same charge distribution (Fig. 3C) suggests that the amount of catecholamine released per vesicle is independent of the stimulation method. Although alterations in the time profile of light-triggered spikes could be due to slower catecholamine release caused by UV-generated nitric

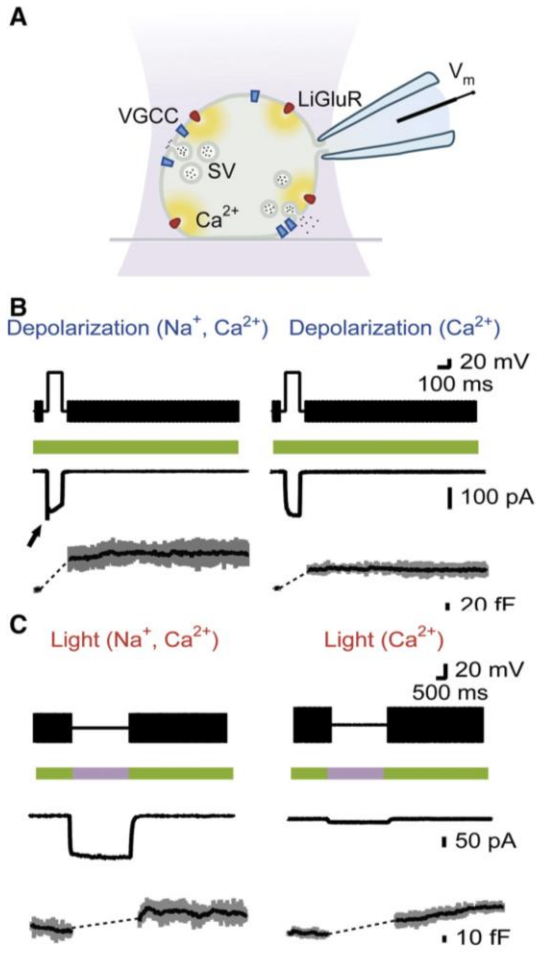

Fig. 4. Whole-cell voltage-clamp measurements reveal that Ca^{2+} current trough LiGluR is sufficient to induce secretion. (A) Experimental setup to measure Ca^{2+} influx and secretion upon UV-light and depolarization stimuli by whole-cell patch clamp in LiGluR(+) chromaffin cells (V_h: holding voltage). (B) Secretion responses of one representative cell to depolarization stimuli in a physiological bath solution (with Na^+ and Ca^{2+}, left panel) and in Na^+-free and high-Ca^{2+} bath solution (with $NMDG^+$ and 30 mM Ca^{2+}, right panel). Top traces represent voltage and display a depolarizing pulse between the 1 kHz, 25 mV sinusoidal wave used for capacitance measurements (bottom traces). Middle traces represent current, which is mainly due to native VGCCs and a fast transient associated to native voltage-gated Na^+ channels (marked with an arrow). In the absence of Na^+, the current transient is abolished but the Ca^{2+} current and secretory responses are maintained. (C) Secretion responses of one representative cell to light stimuli in physiological solution (left panel) and in Na^+-free and high-Ca^{2+} solution (right panel). Top traces represent voltage (held at −80 mV) and display the 1 kHz, 25 mV sinusoidal wave used for capacitance measurements (bottom traces). Middle traces represent current, which is mainly due to Na^+ and Ca^{2+} permeating through LiGluR. Color bars indicate 500 nm (green) and 380 nm illumination (purple). In the absence of Na^+, the current is reduced to reveal the Ca^{2+} component, and secretory responses are maintained.

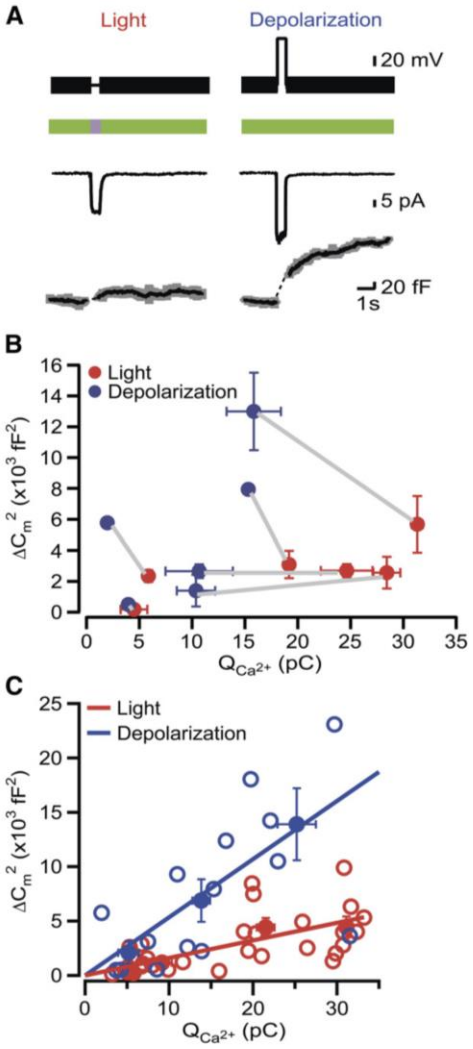

Fig. 5. Efficacy of light- and depolarization-induced exocytosis. (A) Direct comparison in the same LiGluR(+) cell of light- and depolarization-controlled Ca^{2+} influx and resulting secretion in Na^+-free and high-Ca^{2+} solution. Label indicates stimulation by light (left panel) and subsequently by depolarization (right panel). In each panel, upper traces correspond to the sinusoidal voltage applied to the cell at $V_h = -80$ mV, color bar indicates illumination (500 nm in green and 380 nm in purple), middle traces correspond to Ca^{2+} current and bottom traces to membrane capacitance. (B) The Ca^{2+} charge ($Q_{Ca^{2+}}$) and capacitance jump of each secretory response is plotted for depolarization- (blue dots) and light-triggered stimulation (red dots), with gray lines linking responses obtained in the same cell. (C) In order to determine how vesicle fusion was correlated with the amount of calcium influx, a larger dataset of ΔC_m responses to $Q_{Ca^{2+}}$ is shown for depolarization- (○, n = 16 measurements from 9 cells) and light-triggered stimulation (○, n = 32 measurements from 14 cells). The averaged data is shown as ● and ● for depolarization and light stimulation, respectively. Both stimulations follow the same non-linear behavior, which can be fitted by $\Delta C_m = k\sqrt{Q_{Ca^{2+}}}$ (*i.e.* ΔC_m^2 depends linearly on $Q_{Ca^{2+}}$, slope 530 ± 20 fF^2 pC^{-1} and $r^2 = 0.99$ for VGCC; slope 160 ± 20 fF^2 pC^{-1} and $r^2 = 0.9$ for LiGluR). Error bars indicate ± s.e.m.

oxide [37], this change in kinetics is typically related to the detection of diffused events [21], which are likely to occur in our stimulation/detection geometry. While depolarization equally affects all membrane regions, light-triggered events have a higher probability of being generated at the membrane portion in close contact to the glass coverslip, which is more exposed to higher light intensity. The diffusion of the released catecholamines from the triggering site to the carbon microfiber, located at the apical side, might therefore account for the different spike

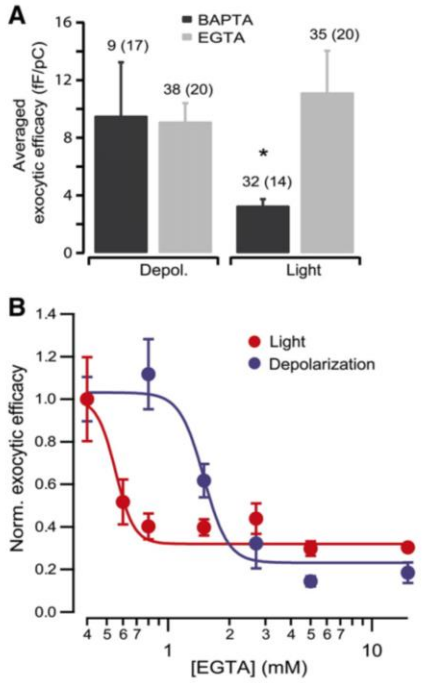

Fig. 6. Coupling between calcium influx and exocytosis. (A) Mean exocytic efficacy of light- and depolarization-triggered secretion was determined in the presence of 0.4 mM of BAPTA or EGTA. In depolarization experiments, calcium buffering did not alter the exocytic efficacy. In light-triggered secretion, the efficacy was significantly reduced in the presence of BAPTA, but remained unaffected in the presence of EGTA. Numbers on top of each bar indicate the total number of measurements and the number of different cells in parentheses. (B) We added increasing EGTA concentrations in the pipette solution in order to gradually limit diffusion of Ca^{2+} during light- and depolarization-triggered secretion (data points indicated by ● and ●, respectively). Exocytosis efficacies are plotted as a function of EGTA concentration. In both cases, data can be fitted to a sigmoid function, with EGTA having at least a three-fold stronger impact on LiGluR than on VGCCs. ($N \geq 6$ cells in all data points, except in 15 mM EGTA where $N = 2$ cells for light and $N = 3$ for depolarization.) An asterisk (*) indicates significant differences ($P < 0.05$) by Student's t-test. All error bars indicate ± s.e.m.

shape. Thus, optical stimulation appears to mobilize a typical population of secretory granules from chromaffin cells, and does not significantly alter their physiology neither by LiGluR overexpression, MAG conjugation or illumination.

The latency in the onset of secretion (Fig. 1E) has been described before in chromaffin cells and it is attributed to the low stimulus-secretion coupling, which results in a slow build-up of intracellular Ca^{2+} [22,38]. The slow decay of amperometric spikes after stimulation (Fig. 1F and G) has also been reported in chromaffin cell secretion [38] and indicates slow cellular metabolism of cytoplasmic Ca^{2+} removal in chromaffin cells. Such slow decay may physiologically limit the maximum frequency of optical secretion cycles, but this limitation is stronger for depolarization-induced secretion (decay rate 7 s for optical stimulation *versus* 13 s for depolarization, Fig. 1G). The later onset and faster recovery of optically-controlled secretion indicate mechanistic differences that prompted a deeper study. Assuming that the molecular identity of vesicles involved in exocytosis is the same in both cases, as shown by amperometric recordings, differences must then be sought in coupling of sites of calcium influx to secretion. For that purpose, we designed experiments to monitor the calcium influx supporting exocytosis.

The ability of LiGluR to control secretion results from its Ca^{2+} permeability, as shown by whole-cell patch capacitance experiments (Fig. 4). Unlike previous reports where whole neurons were depolarized by means of cation permeability of light-gated channels (LiGluR and ChR2) [9,11], here we have specifically controlled Ca^{2+} entry with light in a direct way in order to trigger a Ca^{2+} dependent process. In our experiments, the capacitance increase measured after exocytosis depends on the square root of calcium charge both for electric and optical stimulation (Fig. 4G), similarly to results obtained in the calyx of Held [31]. This result suggests that LiGluR enables optical control of the physiological molecular mechanism governing calcium-regulated exocytosis [39], and this mechanism is altered neither by the presence of LiGluR nor by illumination. The lower secretion yield achieved by photocurrents could be caused by the spatial properties of calcium influx in the submembrane space. This hypothesis was supported by the three-fold higher sensitivity of light-induced secretion when hindering Ca^{2+} diffusion with EGTA (Fig. 5). These results, together with the slower dynamics of vesicle mobilization with light (Fig. 1) are in agreement with a certain molecular organization of secretory granules and native VGCCs. In contrast to LiGluR, VGCCs seem to be directly interacting ("coupled") with chromaffin vesicles, making calcium influx signal more efficient in triggering exocytosis, as co-localization facilitates a faster and more synchronized response. Indeed, it has been reported that VGCCs and vesicle release sites are localized in the same region of the membrane in chromaffin cells [28,29], thereby defining patches of secretion, although with a lower level of organization than synaptic active zones. In addition, L- and P/Q type VGCCs naturally occur in clusters that could enhance this effect [40]. Thus, matching the performance of depolarization-triggered exocytosis will require enhancing LiGluR coupling by incorporating protein motifs that promote molecular localization and/or increase clustering at vesicle release sites [41] or that target cellular compartments like synaptic terminals.

Methods to stimulate exocytosis were limited to cell depolarization using electrodes, applying local perfusion of KCl or agonists, ionomycin and osmotic shock using sucrose, the latter three being quite inaccurate [42]. Important advances were achieved with photolabile compounds that allowed releasing Ca^{2+} to the cytoplasm [43], although the reversibility and physiological relevance of the method is lower than Ca^{2+} entry through the membrane [35]. More recently, ChR2 has been exploited to produce neurotransmission by means of indirect VGCC activation using light-induced cell depolarization [3]. In the present paper, we have described conditions under which LiGluR behaves as a light-gated Ca^{2+} channel that enables controlling the rate of exocytosis remotely, reversibly and in a way that is orthogonal to the control of membrane potential (voltage clamp). We are currently applying the optical control of exocytosis to spatiotemporally manipulate neurotransmission, as it is specially suited to the micrometric size and millisecond timescale dynamics of Ca^{2+}-dependent processes at hippocampal synaptic terminals. One of the challenges of this application of LiGluR is to achieve sufficient presynaptic expression (*i.e.* calcium photocurrent). Reversible control of neurotransmission at individual synapses thus enables studying synaptic integration based on presynaptic stimulation, which is more physiological than activation of postsynaptic receptors with caged neurotransmitters [44]. Light-controlled proteins like LiGluR can also be considered synthetic molecular prosthetics that enable novel nanomedical applications like optically regulated secretion of insulin, lung surfactants, digestive enzymes or skin lubricants.

Supplementary data to this article can be found online at http://dx.doi.org/10.1016/j.bbagen.2012.11.003.

Acknowledgements

We are grateful to Ehud Y. Isacoff for the gift of the GluK2-L439C-eGFP clone, to M. A. Valverde for the $Ca_v2.1$ clone, to C. Manzo and I. Rimmaudo

for the help with data processing, and to M. Segovia and G. Álvarez de Toledo for the help with amperometric recordings. We are indebted to M. Ruíz-Mejías for performing initial experiments, and to C. Solsona, G. Álvarez de Toledo and E. Y. Isacoff for helpful discussions and comments on the manuscript. We acknowledge financial support from the Human Frontier Science Program through a Career Development Award, from the European Research Council through a Starting Grant, from the European Commission through a ICT-FET grant, from the Ministry of Education through a grant (to P.G.) and through a FPU fellowship (to M.I.), from CIBER-BBN through a young investigator fellowship (to M.I.) and from the RecerCaixa foundation.

References

[1] W.W. Douglas, Stimulus-secretion coupling: the concept and clues from chromaffin and other cells, Br. J. Pharmacol. 34 (1968) 451–474.
[2] J.B. Sorensen, Formation, stabilisation and fusion of the readily releasable pool of secretory vesicles, Pflugers Arch. 448 (2004) 347–362.
[3] G. Nagel, M. Brauner, J.F. Liewald, N. Adeishvili, E. Bamberg, A. Gottschalk, Light activation of channelrhodopsin-2 in excitable cells of *Caenorhabditis elegans* triggers rapid behavioral responses, Curr. Biol. 15 (2005) 2279–2284.
[4] M. Volgraf, P. Gorostiza, R. Numano, R.H. Kramer, E.Y. Isacoff, D. Trauner, Allosteric control of an ionotropic glutamate receptor with an optical switch, Nat. Chem. Biol. 2 (2006) 47–52.
[5] J. Egebjerg, S.F. Heinemann, Ca^{2+} permeability of unedited and edited versions of the kainate selective glutamate receptor GluR6, Proc. Natl. Acad. Sci. U. S. A. 90 (1993) 755–759.
[6] G. Nagel, T. Szellas, W. Huhn, S. Kateriya, N. Adeishvili, P. Berthold, D. Ollig, P. Hegemann, E. Bamberg, Channelrhodopsin-2, a directly light-gated cation-selective membrane channel, Proc. Natl. Acad. Sci. U. S. A. 100 (2003) 13940–13945.
[7] H.E. Kato, F. Zhang, O. Yizhar, C. Ramakrishnan, T. Nishizawa, K. Hirata, J. Ito, Y. Aita, T. Tsukazaki, S. Hayashi, P. Hegemann, A.D. Maturana, R. Ishitani, K. Deisseroth, O. Nureki, Crystal structure of the channelrhodopsin light-gated cation channel, Nature 482 (2012) 369–374.
[8] S.Q. Lima, G. Miesenbock, Remote control of behavior through genetically targeted photostimulation of neurons, Cell 121 (2005) 141–152.
[9] S. Szobota, P. Gorostiza, F. Del Bene, C. Wyart, D.L. Fortin, K.D. Kolstad, O. Tulyathan, M. Volgraf, R. Numano, H.L. Aaron, E.K. Scott, R.H. Kramer, J. Flannery, H. Baier, D. Trauner, E.Y. Isacoff, Remote control of neuronal activity with a light-gated glutamate receptor, Neuron 54 (2007) 535–545.
[10] C. Wyart, F. Del Bene, E. Warp, E.K. Scott, D. Trauner, H. Baier, E.Y. Isacoff, Optogenetic dissection of a behavioural module in the vertebrate spinal cord, Nature 461 (2009) 407–410.
[11] F. Zhang, L.P. Wang, M. Brauner, J.F. Liewald, K. Kay, N. Watzke, P.G. Wood, E. Bamberg, G. Nagel, A. Gottschalk, K. Deisseroth, Multimodal fast optical interrogation of neural circuitry, Nature 446 (2007) 633–639.
[12] D. Li, K. Herault, E.Y. Isacoff, M. Oheim, N. Ropert, Optogenetic activation of LiGluR-expressing astrocytes evokes anion channel-mediated glutamate release, J. Physiol. 590 (2012) 855–873.
[13] G. Miesenbock, The optogenetic catechism, Science (New York, N.Y.) 326 (2009) 395–399.
[14] D.T. O'Connor, S.K. Mahata, M. Mahata, Q. Jiang, V.Y. Hook, L. Taupenot, Primary culture of bovine chromaffin cells, Nat. Protoc. 2 (2007) 1248–1253.
[15] P. Gorostiza, M. Volgraf, R. Numano, S. Szobota, D. Trauner, E.Y. Isacoff, Mechanisms of photoswitch conjugation and light activation of an ionotropic glutamate receptor, Proc. Natl. Acad. Sci. U. S. A. 104 (2007) 10865–10870.
[16] B. Sakmann, E. Neher, in: Single-Channel Recording, Plenum Press, New York, 1983, pp. 245–275.
[17] G. Dernick, L.W. Gong, L. Tabares, G. Alvarez de Toledo, M. Lindau, Patch amperometry: high-resolution measurements of single-vesicle fusion and release, Nat. Methods 2 (2005) 699–708.
[18] A. Schulte, R.H. Chow, A simple method for insulating carbon-fiber microelectrodes using anodic electrophoretic deposition of paint, Anal. Chem. 68 (1996) 3054–3058.
[19] E.V. Mosharov, D. Sulzer, Analysis of exocytotic events recorded by amperometry, Nat. Methods 2 (2005) 651–658.
[20] T. Moser, E. Neher, Rapid exocytosis in single chromaffin cells recorded from mouse adrenal slices, J. Neurosci. 17 (1997) 2314–2323.
[21] R.M. Wightman, J.A. Jankowski, R.T. Kennedy, K.T. Kawagoe, T.J. Schroeder, D.J. Leszczyszyn, J.A. Near, E.J. Diliberto Jr., O.H. Viveros, Temporally resolved catecholamine spikes correspond to single vesicle release from individual chromaffin cells, Proc. Natl. Acad. Sci. U. S. A. 88 (1991) 10754–10758.
[22] R.H. Chow, L. von Ruden, E. Neher, Delay in vesicle fusion revealed by electrochemical monitoring of single secretory events in adrenal chromaffin cells, Nature 356 (1992) 60–63.
[23] A.G. Garcia, A.M. Garcia-De-Diego, L. Gandia, R. Borges, J. Garcia-Sancho, Calcium signaling and exocytosis in adrenal chromaffin cells, Physiol. Rev. 86 (2006) 1093–1131.
[24] T.L. Colliver, E.J. Hess, E.N. Pothos, D. Sulzer, A.G. Ewing, Quantitative and statistical analysis of the shape of amperometric spikes recorded from two populations of cells, J. Neurochem. 74 (2000) 1086–1097.
[25] E. Neher, T. Sakaba, Multiple roles of calcium ions in the regulation of neurotransmitter release, Neuron 59 (2008) 861–872.
[26] E. Neher, A. Marty, Discrete changes of cell membrane capacitance observed under conditions of enhanced secretion in bovine adrenal chromaffin cells, Proc. Natl. Acad. Sci. U. S. A. 79 (1982) 6712–6716.
[27] L. Olivos Ore, A.R. Artalejo, Intracellular Ca^{2+} microdomain-triggered exocytosis in neuroendocrine cells, Trends Neurosci. 27 (2004) 113–115.
[28] I.M. Robinson, J.M. Finnegan, J.R. Monck, R.M. Wightman, J.M. Fernandez, Colocalization of calcium entry and exocytotic release sites in adrenal chromaffin cells, Proc. Natl. Acad. Sci. U. S. A. 92 (1995) 2474–2478.
[29] M.M. Wu, A. Llobet, L. Lagnado, Loose coupling between calcium channels and sites of exocytosis in chromaffin cells, J. Physiol. 587 (2009) 5377–5391.
[30] R. Chittajallu, S.P. Braithwaite, V.R. Clarke, J.M. Henley, Kainate receptors: subunits, synaptic localization and function, Trends Pharmacol. Sci. 20 (1999) 26–35.
[31] R.M. Leao, H. von Gersdorff, Synaptic vesicle pool size, release probability and synaptic depression are sensitive to Ca^{2+} buffering capacity in the developing rat calyx of Held, Braz. J. Med. Biol. Res. 42 (2009) 94–104.
[32] E.M. Adler, G.J. Augustine, S.N. Duffy, M.P. Charlton, Alien intracellular calcium chelators attenuate neurotransmitter release at the squid giant synapse, J. Neurosci. 11 (1991) 1496–1507.
[33] E. Eggermann, I. Bucurenciu, S.P. Goswami, P. Jonas, Nanodomain coupling between Ca(2)(+) channels and sensors of exocytosis at fast mammalian synapses, Nat. Rev. Neurosci. 13 (2011) 7–21.
[34] C. Amatore, S. Arbault, Y. Bouret, M. Guille, F. Lemaitre, Y. Verchier, Invariance of exocytotic events detected by amperometry as a function of the carbon fiber microelectrode diameter, Anal. Chem. 81 (2009) 3087–3093.
[35] A. Denker, S.O. Rizzoli, Synaptic vesicle pools: an update, Front. Syn. Neurosci. 2 (2010) 135.
[36] S.O. Rizzoli, W.J. Betz, Synaptic vesicle pools, Nature reviews 6 (2005) 57–69.
[37] J.D. Machado, F. Segura, M.A. Brioso, R. Borges, Nitric oxide modulates a late step of exocytosis, J. Biol. Chem. 275 (2000) 20274–20279.
[38] Z. Zhou, S. Misler, Action potential-induced quantal secretion of catecholamines from rat adrenal chromaffin cells, J. Biol. Chem. 270 (1995) 3498–3505.
[39] T.C. Sudhof, The synaptic vesicle cycle, Annu. Rev. Neurosci. 27 (2004) 509–547.
[40] C.J. Torregrosa-Hetland, J. Villanueva, D. Giner, I. Lopez-Font, A. Nadal, I. Quesada, S. Viniegra, G. Exposito-Romero, A. Gil, V. Gonzalez-Velez, J. Segura, L.M. Gutierrez, The F-actin cortical network is a major factor influencing the organization of the secretory machinery in chromaffin cells, J. Cell Sci. 124 (2012) 727–734.
[41] Z. Szabo, G.J. Obermair, C.B. Cooper, G.W. Zamponi, B.E. Flucher, Role of the synprint site in presynaptic targeting of the calcium channel CaV2.2 in hippocampal neurons, Eur. J. Neurosci. 24 (2006) 709–718.
[42] B. Sakmann, E. Neher, in: Single-Channel Recording, Plenum Press, New York, 1983, pp. 155–198.
[43] E. Neher, R.S. Zucker, Multiple calcium-dependent processes related to secretion in bovine chromaffin cells, Neuron 10 (1993) 21–30.
[44] T. Branco, M. Hausser, The single dendritic branch as a fundamental functional unit in the nervous system, Curr. Opin. Neurobiol. 20 (2010) 494–502.

2.2 Supplementary information

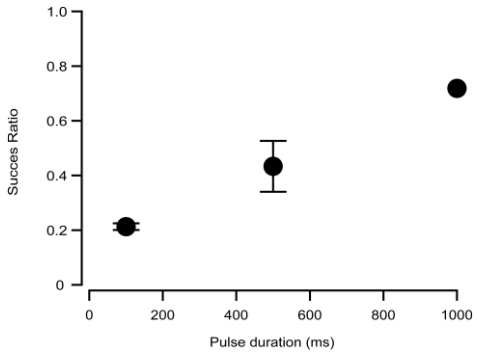

Supplementary Figure.1. Secretion success dependence on light-pulse duration.

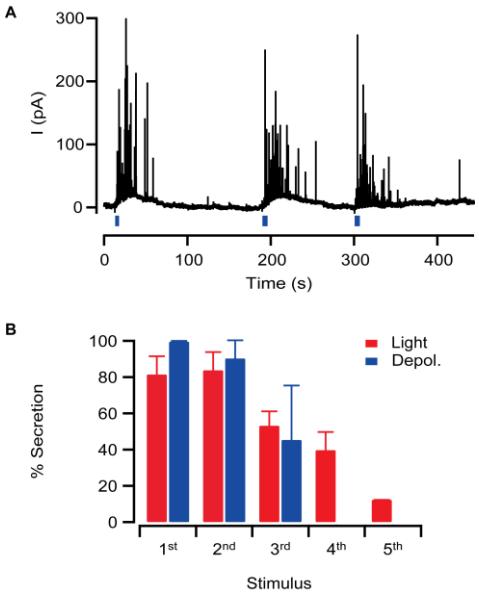

Supplementary Fig.2.Quantification of secretion rundown during depolarization with KCl.

2.3 Optical modulation of neurotransmission using calcium photocurrents through the ion channel LiGluR

frontiers in
MOLECULAR NEUROSCIENCE

ORIGINAL RESEARCH ARTICLE
published: 21 March 2013
doi: 10.3389/fnmol.2013.00003

Optical modulation of neurotransmission using calcium photocurrents through the ion channel LiGluR

Mercè Izquierdo-Serra[1], Dirk Trauner[2,3], Artur Llobet[4] and Pau Gorostiza[1,5,6]*

[1] Institute for Bioengineering of Catalonia (IBEC), Barcelona, Spain
[2] Department of Chemistry and Pharmacology, Ludwig-Maximilians-Universität, Munich, Germany
[3] Center for Integrated Protein Science, Munich, Germany
[4] Laboratory of Neurobiology, Bellvitge Institute for Biomedical Research (IDIBELL), L'Hospitalet de Llobregat, Spain
[5] Catalan Institution for Research and Advanced Studies (ICREA), Barcelona, Spain
[6] Networking Research Center on Bioengineering, Biomaterials and Nanomedicine (CIBER-BBN), Zaragoza, Spain

Edited by:
Piotr Bregestovski, Aix-Marseille Université, France

Reviewed by:
Claire Wyart, Brain and Spinal Cord Institute, France
Fabio Benfenati, University of Genoa, Italy

***Correspondence:**
Pau Gorostiza, Institute for Bioengineering of Catalonia, Edifici Hèlix, Parc Científic de Barcelona, C/ Baldiri Reixac 15-21, Barcelona 08028, Spain.
e-mail: pau@icrea.cat

A wide range of light-activated molecules (photoswitches and phototriggers) have been used to the study of computational properties of an isolated neuron by acting pre and postsynaptically. However, new tools are being pursued to elicit a presynaptic calcium influx that triggers the release of neurotransmitters, most of them based in calcium-permeable Channelrhodopsin-2 mutants. Here we describe a method to control exocytosis of synaptic vesicles through the use of a light-gated glutamate receptor (LiGluR), which has recently been demonstrated that supports secretion by means of calcium influx in chromaffin cells. Expression of LiGluR in hippocampal neurons enables reversible control of neurotransmission with light, and allows modulating the firing rate of the postsynaptic neuron with the wavelength of illumination. This method may be useful for the determination of the complex transfer function of individual synapses.

Keywords: optical control, calcium, firing rate, neurotransmission, optogenetics, synaptic transfer function, neural coding

INTRODUCTION

The investigation of the computational properties of neuronal circuits has required the development of new methods bringing together the morphological properties and physiological activity of neuronal compartments at increasing resolution. As an example, computation of dendritic structures was established with a combination of electrophysiological and imaging techniques (Nikolenko et al., 2007; Branco and Hausser, 2010). More recently, tools to remotely control the activity of neurons with light have been developed (Boyden et al., 2005; Volgraf et al., 2006; Gorostiza and Isacoff, 2008; Deisseroth, 2011). Now, the combination of optogenetic and electrophysiological methods is allowing to test the causality between structure and function: by selectively activating or silencing specific structures like neuronal compartments, one can assess their impact on the function of a neuron, on the dynamics of a circuit, and on the behavior of an organism (Scanziani and Hausser, 2009).

The computational properties of an isolated neuron can be analyzed by postsynaptic activation with compounds caging neurotransmitters, i.e., caged-glutamate (Araya et al., 2006). However, the study of neuronal circuits requires novel tools to gain control of neurotransmitter release by presynaptic terminals. Besides physiological stimulation using patch electrodes or optogenetic approaches, available methods to stimulate exocytosis of synaptic vesicles are restricted to local application of selective Ca^{2+} ionophores (e.g., ionomycin), or Ca^{2+} uncaging (Neher and Zucker, 1993). Dialysis of membrane-impermeant caged Ca^{2+} (e.g., *o*-nitrophenyl-ethylene glycol tetraacetic acid, NP-EGTA) and focused light flashes allow constraining Ca^{2+} release at presynaptic terminals, but this approach is subject to significant intra and inter-experiment variability due to non-homogeneous diffusion of the molecule through the cytoplasm and poor reversibility, thus making this approach virtually non-applicable to a neuronal circuit.

Light-gated ion channels like Channelrhodopsin-2 (ChR2) or the light-gated glutamate receptor (LiGluR) allow optical stimulation with high spatiotemporal resolution. ChR2 has been recently used to map the organization of excitatory connections in the cortex (Petreanu et al., 2009; Mao et al., 2011). LiGluR allows to directly and reversibly control the free concentration of cytoplasmic calcium to trigger regulated exocytosis of large-dense core vesicles in chromaffin cells, showing a comparable efficacy to native voltage-gated calcium channels (VGCCs; Izquierdo-Serra et al., 2012). Calcium-permeable ChR2 mutants have also been identified that should be useful for that purpose (Kleinlogel et al., 2011; Kato et al., 2012). Optical control of calcium influx in neuroendocrine cells opens an experimental window in synapses, as for example, to remotely study the Ca^{2+} dynamics of the process in presynaptic terminals, to gradually trigger neurotransmission and ultimately to modulate the neuronal firing rate by simply changing the illuminating wavelength. All these possibilities would be supported by the ability of LiGluR to efficiently increase submembranous calcium concentration, without requiring the activation of the whole neuron by depolarization.

Here we exploit the wavelength dependence of LiGluR currents (Gorostiza et al., 2007) to achieve a graded control of calcium influx, in order to modulate the secretory rate in chromaffin cells. We also apply this concept to synaptic transmission,

by modulating the firing rate of postsynaptic neurons in a wavelength-dependent manner. This technique allows adjusting the firing frequency in a way that is orthogonal to the control of membrane potential (voltage-clamp), and suggests applications to determine experimentally the frequency-dependent transfer function of individual synapses, that could be useful to model neuronal circuits.

MATERIALS AND METHODS

CHROMAFFIN CELL CULTURE AND INFECTION

Chromaffin cells were isolated from medulla of bovine adrenal glands by enzymatic treatments (O'Connor et al., 2007). Dissociated chromaffin cells were plated at 2.5×10^5 cells well^{-1} density in Poly-L-lysine treated coverslips. After 1 day, cells were infected using an adenoviral construction carrying the fusion protein GluK2-L439C-eGFP. Amperometry and patch clamp experiments in chromaffin cells were performed after 1–2 days of infection.

HIPPOCAMPAL NEURONAL CULTURE AND CELL TRANSFECTION

Hippocampal neurons from Albino Sprague-Dawley rats (P1–P4) were isolated and cultured as described previously (Halliwell et al., 1989). Experimental procedures were approved by the Department of Environment from the Generalitat de Catalunya and registered under DMAH #5131. Neurons were plated at 5×10^5 per 12-mm diameter coverslip, previously treated with poly-D-lysine and they were incubated at 37°C and 10% CO_2. On day 7 to 14 after plating, neurons were transfected with the DNA encoding for GluK2-L439C-eGFP using Lipofectamine 2000 (Invitrogen). Neurons were recorded 2–3 days after transfection.

CONJUGATION OF MAG PHOTOSWITCH

Maleimide-azobenzene-glutamate (MAG) was synthesized as described (Volgraf et al., 2006) and the concentrated stock (10 mM in dimethyl sulfoxide, DMSO) was stored at −20°C. Before all experiments, cells were incubated in absence of light, for 10 min in a Na^+-free and low-Ca^{2+} (0.5 mM) solution with 10–100 μM of MAG (DMSO final concentration <1%) and 0.3 mg mL^{-1} concanavalin A, to block GluK2 desensitization (Gorostiza et al., 2007).

CARBON MICROFIBER AMPEROMETRY

Catecholamine release was detected using homemade polyethylene-insulated carbon fiber electrodes of 12-μm diameter (Chow and von Rüden, 1995; Dernick et al., 2005). Amperometric electrodes were first tested in a solution containing 5 mM ferricyanide in 0.1 M KCl and pH 6.8. Electrodes displaying a current between 1 and 10 nA at a holding potential of +700 mV were selected, and their integrity was verified by voltammetry (Schulte and Chow, 1996). Only electrodes showing a symmetric oxidation/reduction current response to a symmetric ramp from +700 to −300 mV (scan rate 100 mV s^{-1}) were used to measure exocytosis in chromaffin cells. When necessary, electrodes were freshly cut with a scalpel on a glass surface, and were used for further experiments if the basal current was between 10 and 20 pA (at holding potential +700 mV) in the bath solution. Amperometric current was recorded by applying a holding voltage of +700 mV with an EPC-10 amplifier (HEKA) controlled with Patch Master (HEKA). The sampling rate was 100 kHz and current was filtered with a Bessel Filter set at 30 kHz. After data acquisition, traces were digitally filtered at 1 kHz.

CURRENT-CLAMP RECORDINGS

Recordings of current-clamp under whole-cell configuration were done using an EPC-10 amplifier and Patch Master. Pipettes were pulled from borosilicate glass tubing (Harvard Apparatus) with P-97 puller from Sutter Instruments, with a typical resistance of 3–6 MΩ. Voltage was acquired at a sampling rate of 25 kHz and filtered with a Bessel Filter set at 30 kHz. Membrane voltage was held at −70 mV before switching to current-clamp mode, and the injected current was corrected if basal membrane voltage drifted above −60 mV.

VOLTAGE-CLAMP RECORDINGS

Borosilicate glass pipettes were pulled with a typical resistance of 2–4 MΩ. Voltage-clamp recordings under whole-cell configuration were done using an EPC-10 amplifier and the Patch Master. Cell membrane was clamp at a holding potential (V_h) of −80 mV and current was acquired at a sampling rate of 20 kHz. Before each train of light stimulus a hyperpolarization of −90 mV was applied to later allow leak subtraction to ion currents. For the current density–voltage relationship, the following pulse protocol was used: $V_h = -80$ mV, test pulses of 20 ms at steps between −100 and +50 mV (10 mV increment), and P/5 leak subtraction protocol. First, neurons were bathed in a physiological solution with 1 μM of tetrodotoxin (TTX, Ascent Scientific). Then, to quantify the VGCC inhibition, the toxin cocktail was directly added to the bath. Toxins get the maximal VGCC block after 15 min, when current density–voltage relationship was measured again from the same neuron.

ILLUMINATION

Illumination was applied to the entire focused field, using a TILL Photonics Polychrome V monochromator through the side port of an IX70 inverted microscope (Olympus) and with a UApo/340, 40×/1.35 objective. Shutter and wavelength were controlled trough EtherNet-COM-1 connection to PC, using TILL Photonics Polychrome V Control (PolyCon) software. The light power measured with light meter model Newport 1916-C placed next to the objective was 0.9 mW mm^{-2} at 380 nm and 1.7 mW mm^{-2} at 500 nm.

DATA ANALYSIS

All analysis was done with IgorPro from Wavemetrics. For amperometric spike and action potential (AP) detection and parameter analysis (Mosharov and Sulzer, 2005) *Igor Procedures Quanta Analysis* macro from Eugene Mosharov laboratory was used (http://www.sulzerlab.org). Data was exported to Matlab to calculate secretion and firing rate with a custom made macro that calculates the number of events per second in 20 ms windows. Statistical tests were done with Matlab. For all groups of data we applied a non-parametric multiple comparison test

(Kruskal–Wallis) and a multicompare least significant difference (LSD) test. All data are expressed as mean ± SEM (standard error of the mean, calculated over the number of *N*).

SOLUTIONS

Composition of physiological bath solution (in mM): 140 NaCl, 2.5 KCl, 1 $MgCl_2$, 10 HEPES 4-(2-hydroxyethyl)piperazine-1-ethanesulfonic acid, 10 glucose, 2.5 $CaCl_2$ at pH 7.42 and 300 mOsm kg^{-1}. The composition of pipette solution for voltage-clamp was (in mM): 120 Cesium methanesulfonate, 10 TEA-Cl (tetraethylammonium chloride), 20 HEPES, 3 Na_2 ATP, 1 NaGTP, and 0.5 EGTA, pH 7.2 and 290 mOsm kg^{-1}. In current-clamp recordings, the pipette solution contained (in mM): 130 KCl, 5 MgCl, 3 NA_2ATP, 1 NA_2GTP, 20 HEPES, 0.5 EGTA, pH 7.2 and 290 mOsm kg^{-1}. In the indicated experiments, the following cocktail of toxins was added to the bath solution: 100 nM ω-agatoxin IVA (and 1 μM ω-conotoxin GVIA from Alomone Labs and 10 μM nifedipine. When indicated, TTX (Ascent Scientific) was added to the bath solution at 1 μM.

All reagents were obtained from Sigma unless otherwise specified.

RESULTS

MAG OPTICALLY GEARS NEUROSECRETION

Neurosecretion can be triggered by light in bovine chromaffin cells expressing LiGluR [LiGluR(+)], due to the calcium photocurrent (Izquierdo-Serra et al., 2012). Light-triggered exocytic events are detected by amperometry (**Figure 1A**) or by whole-cell membrane capacitance recordings, while keeping the endogenous VGCCs blocked to avoid calcium entry due to depolarization. In order to inhibit the three types of VGCCs expressed in bovine chromaffin cells: Ca_v1, $Ca_v2.2$, and $Ca_v2.1$, cells were bathed into a physiological solution containing nifedipine, ω-conotoxin GVIA, and ω-agatoxin IVA (Garcia et al., 2006). **Figure 1B** shows that a 5-s illumination pulse at 380 nm (red trace), evokes catecholamine release detected as spikes in the amperometric current recording (black trace). The secretory rate (green trace) can be calculated from the amperometric trace and rises up to 2 Hz upon 380 nm light stimulation, gradually decaying once light is switched back to 500 nm. The 380 nm wavelength opens maximally LiGluR and thus triggers a maximal photoinduced secretory rate (Izquierdo-Serra et al., 2012). To gear optical control of neurosecretion, we took advantage of the graded behavior that the MAG photoswitch elicits on LiGluR channels (Gorostiza et al., 2007). As indicated in **Figure 2A**, the amplitude of cationic currents flowing through LiGluR channels is proportional to the illumination wavelength between 420 and 380 nm, which we used to finely modulate secretion.

In **Figure 2B**, secretion was repeatedly triggered with light as in **Figure 1**, but illuminating alternately at wavelengths producing variable Ca^{2+} currents, which account for roughly 10% of the measured cationic current (Izquierdo-Serra et al., 2012). The result is illustrated by the amperometric response (black trace) of a single LiGluR(+) cell to this wavelength range, and the calculated frequency (green trace). As can be seen in **Figure 2B**, secretion was stopped at 500 nm and it could be driven at low (~0.1–0.8 Hz) or high secretory rate (2–4 Hz) depending on whether cells were illuminated at 408 or 380 nm, respectively. The off, low and high rates of neurosecretion were reproducibly alternated.

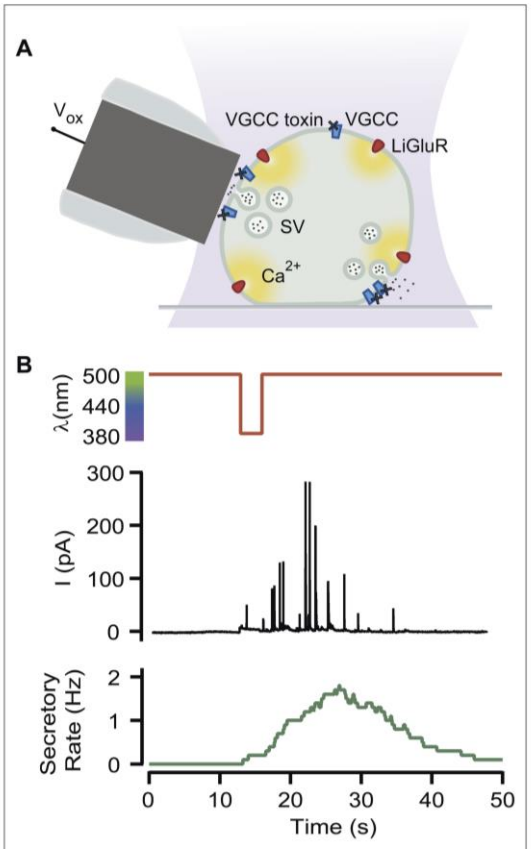

FIGURE 1 | Optical triggering of neurosecretion. (A) Diagram of the experimental approach. Secretion upon light stimuli was detected by amperometry in LiGluR(+) chromaffin cells while VGCC where blocked by toxins (V_{ox}, oxidation voltage; SV, secretory vesicle). **(B)** Amperometric current recording (black plot) from a single LiGluR(+) cell in response to 5 s, 380 nm light pulse (red plot), and the secretory rate (green plot).

The plot on **Figure 2C** summarizes the averaged values obtained from amperometric experiments in several individual chromaffin cells (black). It points out that the light-triggered secretory rate can be directly regulated with the illumination wavelength as a consequence of the control of the photocurrent amplitude (**Figures 2A,C** in gray).

LiGluR-MEDIATED Ca^{2+} INFLUX IN THE PRESYNAPTIC NEURON-INDUCED POSTSYNAPTIC ACTION POTENTIALS

Having shown that exocytosis can be triggered and modulated with light by means of LiGluR-mediated Ca^{2+} influx in chromaffin cells, we aimed at extending such control to neurotransmitter release at chemical synapses.

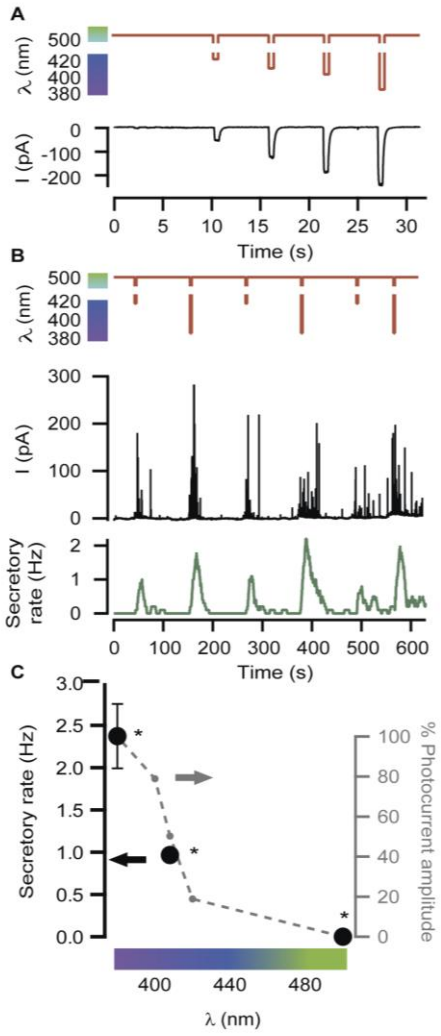

FIGURE 2 | Modulation of secretory rate. (A) LiGluR current amplitude can be adjusted with the illumination wavelength: whole-cell patch clamp current responses (black) to light pulses between 500 nm and different UV wavelengths (sequence of pulses of 420, 408, 400, and 380 nm, red plot). **(B)** The wavelength of light stimuli (red plot) allows adjusting the size of the burst of amperometric spikes (black plot) and thus the maximum secretory rate in each burst (green plot). The exocytosis rate always returns to 0 under 500 nm light, and can be driven reproducibly at 1 or 2 Hz by stepping to 408 or 380 nm, respectively. **(C)** Plot of the averaged secretory rate in response to 380, 408, and 500 nm light (●, left *y*-axis, $N = 4$ cells) measured by amperometry. In gray, photocurrent amplitude dependence on wavelength illumination in LiGluR(+) chromaffin cells measured by whole-cell voltage-clamp (-●-, right *y*-axis, $N = 4$ cells). All pairs are significantly different ($p = 0.12$) and were compared using a non-parametric multiple comparison test (Kruskal–Wallis) and a multicompare LSD test. Error bars indicate ±SEM.

For that purpose, we expressed LiGluR in rat cultured hippocampal neurons, and stimulated them with light while blocking VGCC-mediated Ca^{2+} currents as done in the previous experiments in chromaffin cells. LiGluR expression was observed in the soma and in all processes (**Figure 3A**). Using whole-cell patch clamp in the current-clamp mode, we recorded the membrane potential of non-transfected, LiGluR(−) neuron in the vicinity of a LiGluR(+) neuron and (post)synaptically connected to it (**Figure 3B**). We aimed to record APs generated at the LiGluR(−) postsynaptic neuron, as a consequence of the neurotransmitter release from the LiGluR(+) stimulated by light. To validate this assay, two control experiments were done. First, in order to rule out that the recorded neuron was expressing any LiGluR, we always verified the absence of voltage-clamped current responses to UV stimulation, discarding the cell when it responded to light. In other control experiments, recording from LiGluR(+) neurons we assessed the efficacy of VGCC block by comparing the current density–voltage relationship before and after adding the toxin cocktail. Before the cocktail the current density–voltage curve presents one peak at −30 mV and one at 0 mV corresponding to the activation of low- and high-threshold Ca^{2+} channels, respectively. Currents were reduced to less than 10% at 0 mV (due to Ca^{2+} channels resistant to low ω-agatoxin IVA concentration, 100 nM; Garcia et al., 2006), and 50% at 30 mV with the toxins, and were completely blocked with Cd^{2+}, which corroborates that the remaining currents were due to the presence of Ca^{2+} channels (**Figure 3C**). The total charge mobilized by VGCCs and LiGluR can be calculated taking into account that VGCC currents inactivate and that non-desensitizing LiGluR currents have a 10% calcium component (Izquierdo-Serra et al., 2012). Thus, VGCCs (including low-threshold) give rise to a calcium charge of 9 ± 4 pC ($N = 21$) during 2 s stimulation pulses, which is 10-fold smaller than that of LiGluR during the same time (90 ± 20 pC, $N = 11$). Under these conditions, and in the presence of physiological bath solution, LiGluR(+) neurons can still be depolarized with light (due to the cationic influx), but APs traveling along axons produce a small Ca^{2+} entry through VGCCs in comparison to LiGluR. Therefore, the main pathway for Ca^{2+} influx is controlled by illumination.

We thus proceeded with the experiment described in **Figure 3B**. A representative trace is shown in **Figure 3D**. At the beginning of the recording neurons showed a stable membrane potential or few spontaneous AP. During the light pulse of 2 s at 380 nm, a train of APs was generated, and when the light was switched to 500 nm APs were gradually reduced.

We observed a delay between the beginning of the stimulus and the generation of the first AP (see **Figure 3D**), which was longer (0.74 ± 0.09 s, $N = 4$ neurons stimulated at 380 nm) that the value that has been reported in hippocampal neurons (100 ms). As discussed in detail for chromaffin cells (Izquierdo-Serra et al., 2012), such delay may arise from poor coupling between LiGluR channels and synaptic vesicles, compared to VGCCs. In these experiments, the calculated firing rate on the current-clamped postsynaptic neuron reversibly switched between 0 Hz under 500 nm and a maximum rate under 380 nm illumination. Maximum frequency ranged from 1.3 to 10 Hz, and was 6 ± 2 Hz ($N = 4$

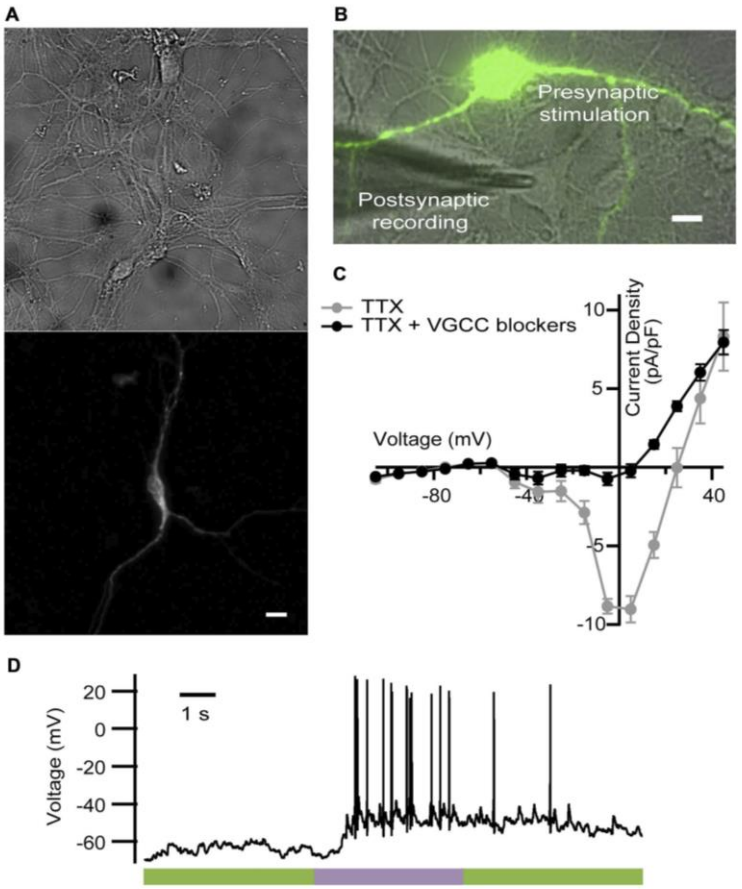

FIGURE 3 | LiGluR-mediated Ca^{2+} influx in the presynaptic neuron-induced postsynaptic AP. (A) LiGluR is expressed in the neuron soma and in all processes, as indicated by fluorescence from green fluorescent protein (GFP) fused to GluK2-L439C under a cytomegalovirus (CMV) promoter (top: bright field image; bottom: GFP). Scale bar, 10 μm. **(B)** Image of the presynaptic LiGluR(+) neuron (green fluorescence), and the glass pipette recording from a LiGluR(−) postsynaptic neuron in contact with the green one. Scale bar, 10 μm. **(C)** Quantification of the voltage-gated Ca^{2+} current inhibition by the toxin cocktail against VGCC in hippocampal neurons. Current density–voltage relationship in absence (gray) and in presence of the toxin cocktail (black) measured in the same neuron. Isolation of the Ca^{2+} current was obtained by blocking voltage-gated Na^{+} channels with 1 μM of TTX in the physiological bath solution, where up to 91.6% of the VGCC currents were inhibited ($N = 4$ cells with cell capacitance between 14.5 and 26.5 pF). Error bars indicate ±SEM. **(D)** Representative voltage recording from postsynaptic neuron in the presence of VGCC blockers, purple bar indicates 2 s, 380 nm illumination.

neurons) on average. Altogether, these results indicate that the LiGluR-mediated Ca^{2+} influx in the presynaptic neuron triggers regulated exocytosis of neurotransmitter containing vesicles, thus supporting the generation of postsynaptic APs.

LIGHT-GATED SECRETION AT PRESYNAPTIC TERMINALS SUPPORTS COLOR-MODULATED NEUROTRANSMISSION AND CONTROLS POSTSYNAPTIC FIRING RATE

In order to further test the ability of LiGluR to adjust the excitatory input, neurotransmission was evoked by 380, 408, and 500 nm light wavelengths, which geared exocytosis at different secretory rates in chromaffin cells (**Figure 2A**). The amount of APs generated by 408 nm illumination was lower than by 380 nm (**Figures 4C,B**, respectively). The postsynaptic firing rate calculated was 2 and 10 Hz for 408 and 380 nm, respectively, and it changed reversibly and reproducibly according to light wavelength (**Figure 4A**).

The average of various responses is represented in the plot of **Figure 4D**, which shows that neurotransmission, assayed through the firing rate, was modulated in proportion to the color of illumination.

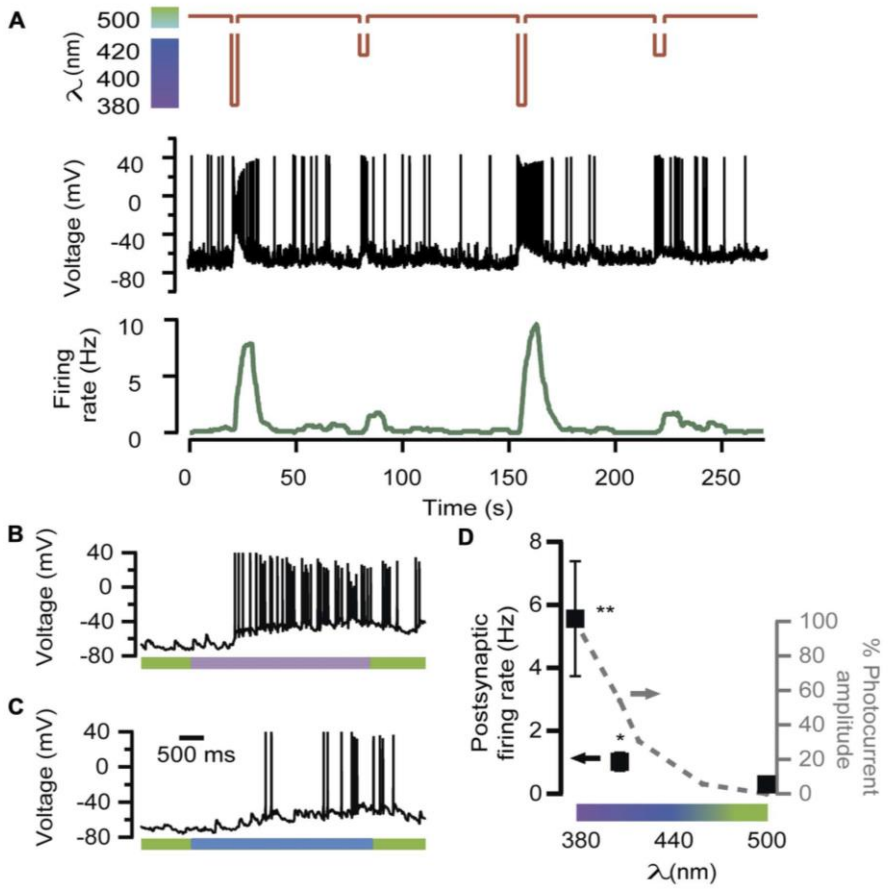

FIGURE 4 | Wavelength modulation of postsynaptic firing rate in hippocampal neurons. (A) Alternated illumination at 380 and 408 nm was spaced by a 45-s period under 500 nm to recover resting membrane voltage (red trace). Voltage recording of the APs on the postsynaptic neuron (black trace) and the calculated firing rate (green trace). Note that AP bursts are associated with light stimulation pulses, and the maximum values of firing rate depend on wavelength illumination. **(B,C)** Two voltage recordings from the same postsynaptic neuron expanded from **(A)**, during illumination at 380 nm (purple bar, up) or 408 nm (blue bar, down). **(D)** Plot of the averaged firing rate from postsynaptic LiGluR(−) neurons, in response to 380, 408, and 500 nm light pulses (●, left *y*-axis, $N = 4$ cells) and photocurrent amplitude of the presynaptic neuron at the same wavelengths measured in LiGluR(+) hippocampal neurons by whole-cell voltage-clamp, following the same protocol described in **Figure 2A** (-●-, right *y*-axis, $N = 4$ cells). **Significantly different from 500 nm with $p < 0.05$; *significantly different from 500 nm with $p < 0.1$. All pairs were compared using a non-parametric multiple comparison test (Kruskal–Wallis) and a multicompare LSD test. Error bars indicate ±SEM.

DISCUSSION

Light-gated glutamate receptor allows controlling secretion with light in chromaffin cells under physiological extracellular Ca^{2+} concentrations, as demonstrated by amperometry and membrane capacitance recordings (Izquierdo-Serra et al., 2012). Interestingly, LiGluR allows a color control of secretory events by adjusting the illumination wavelength between 380 and 500 nm (**Figure 2B**). This maneuver sets the fraction of open channels (*cis*-MAG) and thus the total Ca^{2+} influx. At each wavelength, the relative abundance of *cis*- and *trans*-MAG results from the relative optical absorption of each isomer because inter conversion between them occurs until a photo stationary state is reached (Fischer, 1967; Gorostiza et al., 2007). In chromaffin cells the control of secretory rate with light wavelength was limited to three "gears": no secretion, medium and maximum secretion (**Figure 2B**). Although gating of LiGluR can be finely adjusted by the color of illumination, which would theoretically expand the number of "gears," our results show that in practice such tuning of neurosecretion is not viable. A plausible explanation resides on the fourth power relationship between neurotransmitter release and extracellular

calcium (Dodge and Rahamimoff, 1967). This limitation, however, does not preclude the possibility of using LiGluR to perform a remote color-encoded manipulation of firing rate in neural circuits, which is reminiscent of color-encoding of neuronal identity with the optical probe Brainbow (Livet et al., 2007).

Chromaffin cells constitute a well-established model to study the exocytic processes that occur in presynaptic terminals. We have described conditions under which LiGluR behaves as a light-gated Ca^{2+} channel that mediates a sufficiently large Ca^{2+} influx to support regulated exocytosis (Izquierdo-Serra et al., 2012). Furthermore, the exocytic rate can be geared with the wavelength of illumination (**Figure 2**) and this property can be translated to chemical synapses by utilizing LiGluR as a presynaptic channel (**Figure 4**). Although other light-gated, Ca^{2+}-permeable channels like ChR2 can support neurotransmitter release by depolarizing individual synapses and activating VGCCs (Petreanu et al., 2009), their application could be improved by directly triggering exocytosis in a wavelength-dependent manner, a possibility that is limited in practice by the reduced conductivity and Ca^{2+} permeability of ChR2 (Miesenbock, 2009; Li et al., 2012). On the other hand, Ca^{2+} uncaging to the cytoplasm (Neher and Zucker, 1993) is poorly reversible and less physiologically relevant than Ca^{2+} entry through the membrane (Denker and Rizzoli, 2010), and cannot be genetically targeted to the cells of interest. Thus, LiGluR stands as the best available method to remotely and reversibly trigger Ca^{2+}-regulated exocytosis in neurons. However, the delay observed between illumination and the first AP points to a weak coupling between LiGluR and synaptic vesicles that leads to slow Ca^{2+} buildup (Izquierdo-Serra et al., 2012), and/or to the possibility that light-stimulated neurons and recorded neurons in the preparation are connected polysynaptically or indirectly through the network, and thus the observed optical modulation of neurotransmission probably reflects overall changes in the excitability of the network. Future improvements include LiGluR constructs to enhance presynaptic targeting and coupling to synaptic vesicles, and applying them to preparations where LiGluR(+) neurons establish monosynaptic connections. In these conditions, a systematic correlation between photocurrent amplitude and firing rate could be carried out by paired patch clamp recordings of the presynaptic LiGluR(+) and postsynaptic LiGluR(−) neurons. In that way, the wavelength of light may provide analog control on the synaptic strength, without resorting to changes in the extracellular Ca^{2+} concentration, which affect all synapses in the preparation. Similar progress could be achieved with recently discovered ChR2 variants displaying high permeability to Ca^{2+} (Kleinlogel et al., 2011), or with rationally designed mutants based on ChR2 structure (Kato et al., 2012), although LiGluR has been reported to provide larger photocurrent, shorter illumination required to fire APs, and lack of desensitization (Szobota et al., 2007). LiGluR also has a larger conductivity and is five times ($P^{2+}_{Ca}/P_{Na} = 1.2$; Egebjerg and Heinemann, 1993) more Ca^{2+}-permeable than CatCh ($P^{2+}_{Ca}/P_{Na} = 0.24$; Kleinlogel et al., 2011). In addition, the method based on LiGluR can benefit from synthetic variants of MAG switches with tuned optical properties, as it has been shown for other photoswitches (Mourot et al., 2011).

Understanding the full computational properties of a neuron connected in a circuit requires the characterization of individual synapses by means of the complex transfer function (i.e., with the explicit frequency dependence and not just a measure of "synaptic strength" at low frequencies; Buchanan, 1992; Buchanan et al., 1992; Markram et al., 1998; Abbott and Regehr, 2004). This could be achieved with a large calcium photocurrent channel, by recording the postsynaptic firing pattern in response to a wavelength ramp. Determining the complex transfer function of all synapses in a neuron would allow integrating the overall neuronal transfer function, and lead to cracking neural rate coding.

ACKNOWLEDGMENTS

We thank A. Pérez Jiménez for hippocampal neurons preparation. We are grateful to Ehud Y. Isacoff (University of California at Berkeley) for the gift of the GluK2-L439C-eGFP clone, to C. Manzo for help with data processing, to S. Civit for help with statistical analysis, and to M. Segovia, G. Álvarez de Toledo, and D. Soto for help with experimental methods. We are indebted to M. Ruíz-Mejías for performing initial experiments and to M. I. Bahamonde, C. Solsona, and G. Álvarez de Toledo for helpful discussions and comments on the manuscript. We acknowledge financial support from the Human Frontier Science Program through a Career Development Award, from the European Research Council through a Starting Grant, from the European Union's Seventh Framework Programme [FP7/2007-2013] under grant agreement n° 270483 (Project: FOCUS), from the Spanish Ministry of Education through grant CTQ2008-06160 (to Pau Gorostiza) and through a FPU fellowship (to Mercè Izquierdo-Serra), from CIBER-BBN through a young investigator fellowship (to Mercè Izquierdo-Serra), from RecerCaixa and Marató de TV3 foundations.

REFERENCES

Abbott, L. F., and Regehr, W. G. (2004). Synaptic computation. *Nature* 431, 796–803.

Araya, R., Eisenthal, K. B., and Yuste, R. (2006). Dendritic spines linearize the summation of excitatory potentials. *Proc. Natl. Acad. Sci. U.S.A.* 103, 18799–18804.

Boyden, E. S., Zhang, F., Bamberg, E., Nagel, G., and Deisseroth, K. (2005). Millisecond-timescale, genetically targeted optical control of neural activity. *Nat. Neurosci.* 8, 1263–1268.

Branco, T., and Hausser, M. (2010). The single dendritic branch as a fundamental functional unit in the nervous system. *Curr. Opin. Neurobiol.* 20, 494–502.

Buchanan, J. T. (1992). Neural network simulations of coupled locomotor oscillators in the lamprey spinal cord. *Biol. Cybern.* 66, 367–374.

Buchanan, J. T., Moore, L. E., Hill, R., Wallen, P., and Grillner, S. (1992). Synaptic potentials and transfer functions of lamprey spinal neurons. *Biol. Cybern.* 67, 123–131.

Chow, R. H., and von Rüden, L. (1995). "Electrochemical detection of secretion from single cells," in *Single Channel Recording*, eds B. Sakmann and E. Neher (New York, NY: Plenum Press), 245–276.

Deisseroth, K. (2011). Optogenetics. *Nat. Methods* 8, 26–29.

Denker, A., and Rizzoli, S. O. (2010). Synaptic vesicle pools: an update. *Front. Synaptic Neurosci.* 2:135. doi: 10.3389/fnsyn.2010.00135

Dernick, G., Gong, L. W., Tabares, L., Alvarez de Toledo, G., and Lindau, M. (2005). Patch amperometry: high-resolution measurements of single-vesicle fusion and release. *Nat. Methods* 2, 699–708.

Dodge, F. A. Jr., and Rahamimoff, R. (1967). Co-operative action a calcium ions in transmitter release at the neuromuscular junction. *J. Physiol.* 193, 419–432.

Egebjerg, J., and Heinemann, S. F. (1993). Ca^{2+} permeability of unedited and edited versions of the

kainate selective glutamate receptor GluR6. *Proc. Natl. Acad. Sci. U.S.A.* 90, 755–759.

Fischer, E. (1967). Calculation of photostationary states in systems A ↔ B when only a is known. *J. Phys. Chem.* 71, 3704–3706.

Garcia, A. G., Garcia-De-Diego, A. M., Gandia, L., Borges, R., and Garcia-Sancho, J. (2006). Calcium signaling and exocytosis in adrenal chromaffin cells. *Physiol. Rev.* 86, 1093–1131.

Gorostiza, P., and Isacoff, E. Y. (2008). Optical switches for remote and noninvasive control of cell signaling. *Science* 322, 395–399.

Gorostiza, P., Volgraf, M., Numano, R., Szobota, S., Trauner, D., and Isacoff, E. Y. (2007). Mechanisms of photoswitch conjugation and light activation of an ionotropic glutamate receptor. *Proc. Natl. Acad. Sci. U.S.A.* 104, 10865–10870.

Halliwell, R. F., Peters, J. A., and Lambert, J. J. (1989). The mechanism of action and pharmacological specificity of the anticonvulsant NMDA antagonist MK-801: a voltage clamp study on neuronal cells in culture. *Br. J. Pharmacol.* 96, 480–494.

Izquierdo-Serra, M., Trauner, D., Llobet, A., and Gorostiza, P. (2012). Optical control of calcium-regulated exocytosis. *Biochim. Biophys. Acta* 1830, 2853–2860.

Kato, H. E., Zhang, F., Yizhar, O., Ramakrishnan, C., Nishizawa, T., Hirata, K., et al. (2012). Crystal structure of the channelrhodopsin light-gated cation channel. *Nature* 482, 369–374.

Kleinlogel, S., Feldbauer, K., Dempski, R. E., Fotis, H., Wood, P. G., Bamann, C., et al. (2011). Ultra light-sensitive and fast neuronal activation with the Ca(2)+-permeable channelrhodopsin CatCh. *Nat. Neurosci.* 14, 513–518.

Li, D., Herault, K., Isacoff, E. Y., Oheim, M., and Ropert, N. (2012). Optogenetic activation of LiGluR-expressing astrocytes evokes anion channel-mediated glutamate release. *J. Physiol.* 590, 855–873.

Livet, J., Weissman, T. A., Kang, H. N., Draft, R. W., Lu, J., Bennis, R. A., et al. (2007). Transgenic strategies for combinatorial expression of fluorescent proteins in the nervous system. *Nature* 450, 56–62.

Mao, T., Kusefoglu, D., Hooks, B. M., Huber, D., Petreanu, L., and Svoboda, K. (2011). Long-range neuronal circuits underlying the interaction between sensory and motor cortex. *Neuron* 72, 111–123.

Markram, H., Gupta, A., Uziel, A., Wang, Y., and Tsodyks, M. (1998). Information processing with frequency-dependent synaptic connections. *Neurobiol. Learn. Mem.* 70, 101–112.

Miesenbock, G. (2009). The optogenetic catechism. *Science* 326, 395–399.

Mosharov, E. V., and Sulzer, D. (2005). Analysis of exocytotic events recorded by amperometry. *Nat. Methods* 2, 651–658.

Mourot, A., Kienzler, M. A., Banghart, M. R., Fehrentz, T., Huber, F. M., Stein, M., et al. (2011). Tuning photochromic ion channel blockers. *ACS Chem. Neurosci.* 2, 536–543.

Neher, E., and Zucker, R. S. (1993). Multiple calcium-dependent processes related to secretion in bovine chromaffin cells. *Neuron* 10, 21–30.

Nikolenko, V., Poskanzer, K. E., and Yuste, R. (2007). Two-photon photostimulation and imaging of neural circuits. *Nat. Methods* 4, 943–950.

O'Connor, D. T., Mahata, S. K., Mahata, M., Jiang, Q., Hook, V. Y., and Taupenot, L. (2007). Primary culture of bovine chromaffin cells. *Nat. Protoc.* 2, 1248–1253.

Petreanu, L., Mao, T., Sternson, S. M., and Svoboda, K. (2009). The subcellular organization of neocortical excitatory connections. *Nature* 457, 1142–1145.

Scanziani, M., and Hausser, M. (2009). Electrophysiology in the age of light. *Nature* 461, 930–939.

Schulte, A., and Chow, R. H. (1996). A simple method for insulating carbon-fiber microelectrodes using anodic electrophoretic deposition of paint. *Anal. Chem.* 68, 3054–3058.

Szobota, S., Gorostiza, P., Del Bene, F., Wyart, C., Fortin, D. L., Kolstad, K. D., et al. (2007). Remote control of neuronal activity with a light-gated glutamate receptor. *Neuron* 54, 535–545.

Volgraf, M., Gorostiza, P., Numano, R., Kramer, R. H., Isacoff, E. Y., and Trauner, D. (2006). Allosteric control of an ionotropic glutamate receptor with an optical switch. *Nat. Chem. Biol.* 2, 47–52.

Conflict of Interest Statement: The authors declare that the research was conducted in the absence of any commercial or financial relationships that could be construed as a potential conflict of interest.

Received: 14 November 2012; accepted: 27 February 2013; published online: 21 March 2013.

Citation: Izquierdo-Serra M, Trauner D, Llobet A and Gorostiza P (2013) Optical modulation of neurotransmission using calcium photocurrents through the ion channel LiGluR. Front. Mol. Neurosci. ***6****:3. doi: 10.3389/fnmol.2013.00003*

Copyright © 2013 Izquierdo-Serra, Trauner, Llobet and Gorostiza. This is an open-access article distributed under the terms of the Creative Commons Attribution License, which permits use, distribution and reproduction in other forums, provided the original authors and source are credited and subject to any copyright notices concerning any third-party graphics etc.

2.4 General discussion

In the first part of this work, we demonstrate that LiGluR can be used as a tool to control neurosecretion by directly affecting the intracellular [Ca^{2+}]. Previous studies on Ca^{2+}-permeability of kainate receptors encouraged us to use LiGluR to achieve this aim, as LiGluR is based on the unedited version kainate receptor GluK2, GluK2(Q), it presents a relatively high Ca^{2+} permeability ($P_{Ca^{2+}}/P_{mono}$=1.2, (Egebjerg and Heinemann 1993)). Simultaneously to our work, Li and co-workers showed that LiGluR mediated Ca^{2+}-rises in cultured astrocytes inducing astrocyte-to-astrocyte communication (Li et al. 2012). They argue that in their case, astrocyte activation with LiGluR is due to its Ca^{2+} influx, as the activation was more inefficient with the photoswitchable channel ChR2, which has low calcium permeability. Interestingly, the engineered ChR2 displaying higher Ca^{2+} permeability ($P_{Ca^{2+}}/P_{Na^{+}}$= 0.24, (Kleinlogel et al. 2011)) also activated astrocytes; however in comparison with LiGluR, higher stimulation conditions were needed and amplitude-responses were less reproducible. Subsequently, they studied it further and found that LiGluR activation induced both Ca^{2+} influx and Ca^{2+} release from the intracellular stores, enhancing its ability to increase intracellular [Ca^{2+}].

As a result of all these studies, LiGluR-mediated Ca^{2+}-influx is currently the best tool to reversibly and remotely manipulating the intracellular [Ca^{2+}] independently of VGCC activation. This approach is interesting because it can help to better understand the Ca^{2+} dependence of exocytosis. Moreover, regarding the neurotransmission process, the reversible manipulation of intracellular [Ca^{2+}] with light makes it possible to activate synaptic terminals individually, which could be realized using highly-focusable, two-photon activated photoswitches (see **chapter 3**). In principle, photoactivation could be targeted to either the pre or postsynaptic terminal without affecting the status of the whole neuron, thus enabling the study the brain synaptic circuitry.

There are other intrinsic properties of LiGluR as a neuronal ligand-gated receptor derivative that favor its use as an actuator. The first one is the **higher pore conductance** of the receptor, 5.4 pS (Swanson et al. 1996) in contrast to the 0.05

pS from ChR2 (Nagel et al. 2003). Additionally, LiGluR might **start intracellular signaling** upon activation —kainate receptors have recently been associated to signaling through G proteins (Lerma and Marques 2013)— or reach **specific locations** determined by its own trafficking signals, thereby mimicking the physiological conditions. And last but not least, **glutamate receptors are endogenously expressed in many neuronal cell types**, at locations and expression levels required to accomplish their function. A chemical strategy that allows photosensitizing these endogenous receptors (see **chapter 4**) would provide remote control over neuronal function without altering its physiology, that is, in a truly orthogonal way.

Nevertheless, controlling exocytosis by means of LiGluR can be regarded as an artificial way of manipulating (neuro)secretion. Our results revealed a loose coupling between LiGluR and the secretory machinery. As an exogenously expressed "light-gated calcium channel", LiGluR lacks the interaction domains required to be fully integrated into the native molecular machinery. The main consequences are that a higher Ca^{2+} build-up is required before exocytosis starts, and thus a longer delay, lower efficiency and slower secretion are observed. These observations reinforce the notion that exocytosis and neurosecretion are extremely well coordinated processes. Still, certain modifications of LiGluR might improve the synchronization between optical stimuli and the response process, like genetically introducing intracellular motif that targets LiGluR to the presynaptic area, and more specifically to active zones. An alternative approach to photocontrol exocytosis would be targeting with PTLs the endogenous voltage-gated calcium channels: their high exocytic efficacy has been attributed to strong coupling with the secretory machinery (Eggermann et al. 2012), but no specific PTLs have been described yet (see Futhure challenges of photoswitchable ion channels and receptors, **section 1.2.7**).

Chapter 3

Two-photon cellular stimulation of azobenzene-based photoswitches

An effective method to interrogate the neuronal function in intact tissue with cellular and subcellular resolution should support high-spatial 3D resolution and tissue penetration. Multiphoton excitation with near-infrared (NIR) enables stimulation with these characteristics, and it has been extensively applied to optical actuators such as caged compounds and more recently to optogenetics. However, two-photon stimulation of synthetic photoswitches has not yet been explored. In this chapter, the two-photon stimulation of LiGluR is investigated, including the design, synthesis and applications of two new compounds based on MAG structure intended to enhance the two-photon absorption ability of the azobenzene switch. The compound MAG_{2p} is a red-shifted derivative of MAG.The second one is a modification of MAG_{2p}, which includes a light-harvesting antenna introduced to sensitize the azobenzene isomerization by resonant electronic energy transfer to the photoisomerable group (see structures on **section 3.1**, **Fig. 1**).

The main findings of this project are:

- The photochemical characterization of the new PTLs for LiGluR, MAG_{2p} and $MAGA_{2p}$, revealed a right shift on their absorption spectra with respect to the original MAG (See **section 3.1**, **Fig. 2**), with the peak of maximum absorbance located at ~475 nm. This change in the absorption spectra is accompanied by a shortening of the *cis* isomer lifetime (see **section 3.2**, **Fig S2**). In aquesous

solution and the dark, these new compounds relax from *cis* to *trans* in the millisecond time scale, enabling single-wavelength operation of LiGluR. These photochemical properties are directly translated to LiGluR by conjugation of the compounds. LiGluR can then be activated with 425 nm illumination and deactivates spontaneously after the light pulse (see **section 3.1**, **Fig. 3a** and **section 3.2**, **Fig. S5** and **Table S1**).

- Direct excitation of light-harvesting antenna of the $MAGA_{2p}$ at 355 nm (one-photon) sensitizes the *trans-cis* photoisomerization and gives higher photoconversion of $MAGA_{2p}$ with respect to MAG_{2p}. The enhanced photoconversion is observed in the free compound in solution (see **section 3.1**, **Fig. 2** and **section 3.2**, **Fig. S3** and **S4**), as well as in the compound conjugated to the receptor (see **section 3.2**, **Fig. S5**).
- Two-photon activation of LiGluR-MAG is optimally achieved by repeated stimuli at 820 nm, as observed by patch clamp (see **section 3.1**, **Fig. 3** and **4** and **section 3.2**, **Table S2**). Reversible deactivation can be achieved with 500 nm illumination (one photon). Two-photon current responses of LiGluR-MAG after a single scan are relatively smallpA. However, the thermal stability of *cis*-MAG allows accumulating activated channels by repeated stimulation, and eventually reaching currents above 100 pA.
- Two-photon activation of LiGluR-MAG_{2p} is optimally achieved at 900 nm. A single or few cell-scans are enough to obtain maximal LiGluR current (32 ± 12 pA on average) that reversibly decrease after the stimulation (see **section 3.1**, **Fig 3** and **4** and **section 3.2**, **Table S2**).
- Two-photon activation of LiGluR-$MAGA_{2p}$ can be achieved in two spectral ranges. Saturated LiGluR currents were obtained by single cell-scan at 880 nm (5.8 ± 1.5 pA on average, corresponding to the direct absorbance of azobenzene) and 740 nm (4.8 ± 0.3 pA on average, corresponding to sensitizing antenna) (see **section 3.1**, **Fig. 3** i **4** and **section 3.2**, **Table S2**). Similarly to MAG_{2p}, the current decreases spontaneously after the stimulus.
- The novel red-shifted compounds display higher 2P/1P LiGluR-current ratio compared to MAG (see **section 3.1**, **Fig 4**), indicating their higher efficacy to

activate LiGluR using two-photon stimulation. This fact is also supported by the shorter stimulation and lower laser power required to obtain saturating LiGluR currents with MAG_{2p} and $MAGA_{2p}$.

- The fast relaxing and single-wavelength operated LiGluR-MAG_{2p} can elicit photocurrents and trigger APs in cultured hippocampal neurons using two-photon stimulation (see **section 3.1**, **Fig. 5**). On the other, the step-function, two-wavelength LiGluR-MAG can trigger large currents in cultured astrocytes with cellular and subcellular two-photon stimulation (see **section 3.1**, **Fig. 6**), thereby inducing a calcium wave on the neighboring astrocytes (see **section 3.1**, **Fig. 6** and **section 3.2**, **Fig. S10** and **Movie S1** and **S2**).

This project, coordinated by Pau Gorostiza, has been done in collaboration with the laboratories of Jordi Hernando and Rafael Yuste. The synthesis and photochemical characterization of the new PTLs was carried out by Marta Gascón-Moya, under the guidance of Ramon Alibés, Fèlix Busque and Jordi Hernando from the Chemistry Department of *Universitat Autonoma de Barcelona*. Silvia Pittolo, from our group, and Marta performed one-photon calcium imaging to assay the new compounds on LiGluR-expressing cells. I carried out the electrophysiological characterization of these PTLs on LiGluR with one-photon stimulation in our laboratory and with two-photon stimulation in Rafael Yuste´s laboratory (Columbia University). At Columbia, I was assisted by Jan J. Hirz in electrophysiological assays, and by Kira E. Poskanzer in calcium imaging of astrocytes.

The results of this study have been recently submitted for publication and are currently under review. They are reproduced here in a journal article format. The main text corresponds to **section 3.1**, and supporting information include photochemical characterization of the new PTLs and cellular responses (**section 3.2**). The reference of this work is:

M. Izquierdo-Serra, M. Gascón-Moya, J.J. Hirtz, S. Pittolo, K. E. Poskanzer, È. Ferrer, D. Trauner, R. Alibés, F. Busque, R. Yuste, J. Hernando and P. Gorostiza. Two-photon cellular stimulation of azobenzene-based photoswitches. Submitted (February 28th, 2014)

Two-photon cellular stimulation of azobenzene-based photoswitches

Mercè Izquierdo-Serra[a,+], Marta Gascón-Moya[b,+], Jan J. Hirtz[c], Silvia Pittolo[a], Kira E. Poskanzer[c], Èric Ferrer[a,b], Ramon Alibés[b], Félix Busque[b], Rafael Yuste[c,*], Jordi Hernando[b,*] and Pau Gorostiza[a,d,e,*]

[a] Institut de Bioenginyeria de Catalunya (IBEC), Barcelona, Spain.

[b] Departament de Química, Universitat Autònoma de Barcelona (UAB), Cerdanyola del Vallès, Spain.

[c] Department of Biological Sciences, Columbia University, New York, New York, USA.

[d] Centro de Investigación Biomédica en Red en Bioingeniería, Biomateriales y Nanomedicina (CIBER-BBN), Zaragoza, Spain.

[e] Institució Catalana de Recerca i Estudis Avançats (ICREA), Barcelona, Spain.

ABSTRACT: Synthetic photochromic compounds can be designed to control a variety of proteins and their biochemical functions in living cells, but the high spatiotemporal precision and tissue penetration of two-photon stimulation has never been investigated in these molecules. Here we demonstrate two-photon excitation of azobenzene-based protein switches, and versatile strategies to enhance their photochemical responses. These results enable new applications to control the activation of neurons and astrocytes with cellular and subcellular resolution.

INTRODUCTION

The large number of photoswitchable biomolecules discovered and developed in recent years covers a great variety of cellular functions like catalysis of metabolic processes,[1,2] cytoskeletal polymerization[3] and motors,[2,4] nucleic acids dynamics,[5-7] intracellular signaling[8,9] and perhaps most dazzlingly membrane excitability, which has been at the focus of optogenetics[10] and optopharmacology.[11] The dream of precisely and remotely photocontrolling every aspect of the cell's inner workings in intact tissue appears within reach and offers the promise of interrogating complex cellular processes to discover their molecular mechanisms.[12]

In order to take full advantage of light-regulated proteins, multiphoton excitation with near-infrared (NIR) light provides sub-micrometric resolution in three dimensions,[13] deep penetration into tissue[14] and patterned illumination.[15,16] However, in order to be adapted to two-photon stimulation technology, the light response of natural photoswitchable proteins like Channelrhodopsin-2 (ChR2) must often be adjusted by mutating the tight binding pocket of the natural chromophore, which has fixed photochemical characteristics.[17,18] In contrast, synthetic photoswitches developed by optochemical genetics and optopharmacology are based on chromophores that act on the protein surface and thus offer excellent opportunities for rationally tuning their photochemical behavior by chemical substitutions that do not affect the functional properties of the protein.[19-22] Remarkably, two-photon stimulation of synthetic photoswitchable proteins has not been investigated despite the advances of neurotransmitter uncaging[23] and optogenetics[24,25] using pulsed NIR illumination.

To demonstrate the multiphoton activation of synthetic photoswitches, we chose ion channels because they constitute highly sensitive transducers of chromophore

isomerization (potentially up to the single channel level). In particular, we focused on the well-characterized light-gated glutamate receptor (LiGluR),[26,27] a GluK2 kainate receptor-channel that is chemically conjugated to a maleimide-azobenzene-glutamate photoswitch (MAG **1**, Figure 1a). Azobenzene *trans-cis* photoisomerization[28] of this photoswitchable tethered ligand (PTL) allows the efficient activation of the receptor upon one-photon absorption of violet or blue radiation (open LiGluR, Figure 1b), a process that can be reverted back either by absorption of green light or thermal relaxation in the dark (closed LiGluR, Figure 1b).[21,26,27]

To control LiGluR using multiphoton excitation, here we have investigated the performance of MAG and two new MAG derivatives (**2** and **3**, Figure 1a) upon pulsed NIR illumination. Compounds **2** and **3** were devised to enhance the two-photon excitation response of the symmetrically-substituted azobenzene chromophore in MAG, which is expected to be poor.[29,30] We tested two design concepts using a modular architecture. In compound **2** we introduced an asymmetric aminoazobenzene with sufficiently strong push-pull character as to enhance its two-photon absorption cross-section (MAG_{2p}).[29-32] In addition, the presence of the electron-donating tertiary amine in the 4-position should dramatically decrease the thermal stability of its *cis* state in physiological conditions,[21] thus resulting in fast spontaneous *cis-trans* back-isomerization and, as such, enabling single-wavelength operation of the switch. This behavior is also expected for **3** containing the same azobenzene core as MAG_{2p}. However, a novel scheme was exploited in this compound to enhance its non-linear optical response, which consists in the introduction of a light-harvesting antenna to sensitize the *trans-cis* isomerization of the system by absorption of NIR radiation and subsequent resonant electronic energy transfer (RET) to the *trans*-azobenzene group.[33] Because of its Maleimide-Azobenzene-Glutamate-Antenna structure, we named compound **3** as $MAGA_{2p}$. A naphthalene derivative was selected as antenna because of (i) its high two-photon absorption cross-section,[34] (ii) the large spectral overlap between its emission and the absorption of the

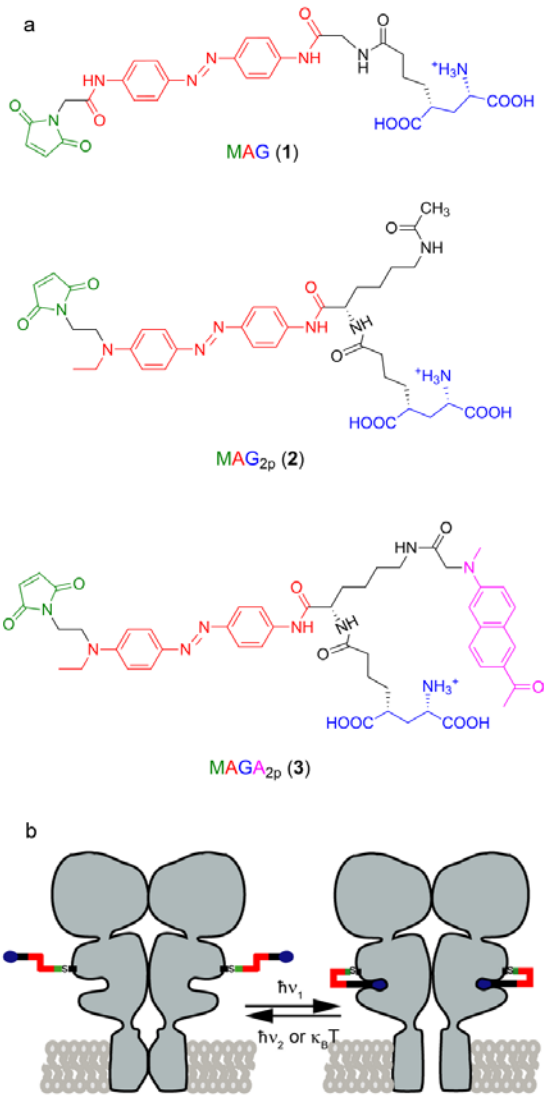

Figure 1. (a) Structures of the photoswitchable tethered ligands applied to the two-photon control of LiGluR: MAG (**1**), MAG_{2p} (**2**) and $MAGA_{2p}$ (**3**). (b) Operating mode of different PTLs on LiGluR. Violet (one-photon) or NIR (two-photon) light excitation induces glutamate recognition and channel opening via *trans-cis* isomerization, which results in ion flow across the membrane. This process is reverted by illumination with visible light (one-photon excitation) for LiGluR-MAG and by thermal back-isomerization for LiGluR-MAG_{2p} and LiGluR-$MAGA_{2p}$.

trans isomer of the aminoazobenzene group in **3**, and (iii) its reduced size, to minimize potential steric hindrance effects on the glutamate-binding site of the receptor.

RESULTS AND DISCUSSION

The preparation of compounds MAG_{2p} and $MAGA_{2p}$ was achieved via a multistep modular synthetic sequence allowing structural diversity in the final compounds as well as the additional incorporation of a photo-harvesting antenna in **3** (Scheme 1). In both cases, we took the *N*,*N*-orthogonally diprotected L-lysine **4** as scaffold, to which the different functional fragments of the target compounds were sequentially introduced via standard peptide coupling and Mitsunobu reactions: *O*-protected aminoazobenzene **5**, fully protected glutamate derivative **6**, naphthalene derivative **7** and furan-protected maleimide **8**. These fragments were obtained from commercial products as described in the Supporting Information. With respect to the synthesis of MAG,[26] several changes were realized in our procedure. First, a branching point was inserted between the glutamate and azobenzene moieties to facilitate the incorporation of additional functional units to the PTL structure. Second, we introduce herein the use of **6** and **8** as more robust, versatile and convenient precursors of glutamate and maleimide moieties during the multistep synthesis of novel MAG derivatives.

Figure 2a plots the electronic absorption spectra of the initial *trans* state of compounds **1**-**3**, while the main photochemical properties of the new ligands MAG_{2p} and $MAGA_{2p}$ are displayed in Figures S1-S4 of the Supporting Information. Owing to the 4-amino substituent introduced in the azobenzene core of these compounds, two main differences are observed with respect to MAG: (i) the absorption maximum of *trans*-MAG_{2p} and *trans*-$MAGA_{2p}$ bathochromically shifts (~50 nm in DMSO); (ii) the thermal stability of their *cis* isomers strongly decreases. Actually, the lifetimes of *cis*-MAG_{2p} and *cis*-$MAGA_{2p}$ drop off down to the millisecond timescale in aqueous buffer at room temperature (τ = 118 and 96 ms in 80% PBS : 20% DMSO, respectively). The optical properties of $MAGA_{2p}$ are further altered by introduction of the photo-harvesting antenna. Thus, *trans*-$MAGA_{2p}$ displays an additional band in the absorption spectrum (λ_{max} = 385 nm in DMSO), which arises from the naphthalene sensitizer. The fluorescence emission of this group is however strongly quenched upon covalent attachment to the ligand, with a ~20-fold decrease in fluorescence quantum yield measured in aqueous buffer. This indicates the occurrence of efficient RET processes from the photoexcited naphthalene antenna to the azo moiety of *trans*-$MAGA_{2p}$, in agreement with the large Förster radius calculated for this donor-acceptor pair (see the Supporting Information). Indeed, upon selective excitation of the naphthalene antenna at 355 nm, the *trans-cis* photoconversion of $MAGA_{2p}$ is ~60% higher than that of MAG_{2p} as a result of photosensitized *trans-cis* isomerization of azobenzene (Figure 2b).

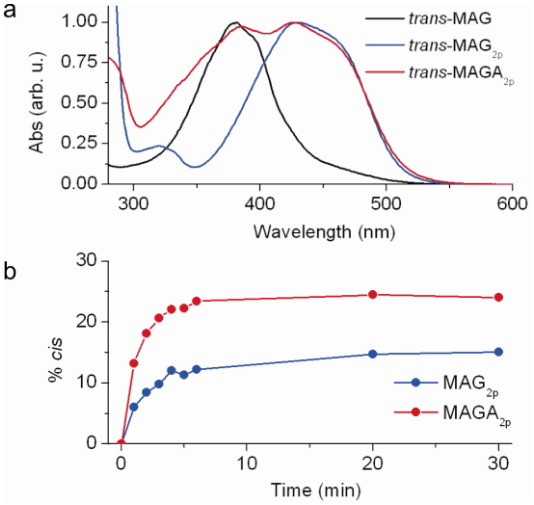

Figure 2. (a) Absorption spectra of *trans*-MAG, *trans*-MAG_{2p} and *trans*-$MAGA_{2p}$ in DMSO. (b) *trans-cis* photoconversion efficiency of *trans*-MAG_{2p} and *trans*-$MAGA_{2p}$ upon irradiation at λ=355 nm in DMSO, which allows nearly selective excitation of *trans*-$MAGA_{2p}$ sensitizer (see Figure S1 in the Supporting Information).

Scheme 1. Total synthesis of MAG_{2p} (2) and $MAGA_{2P}$ (3)[a]

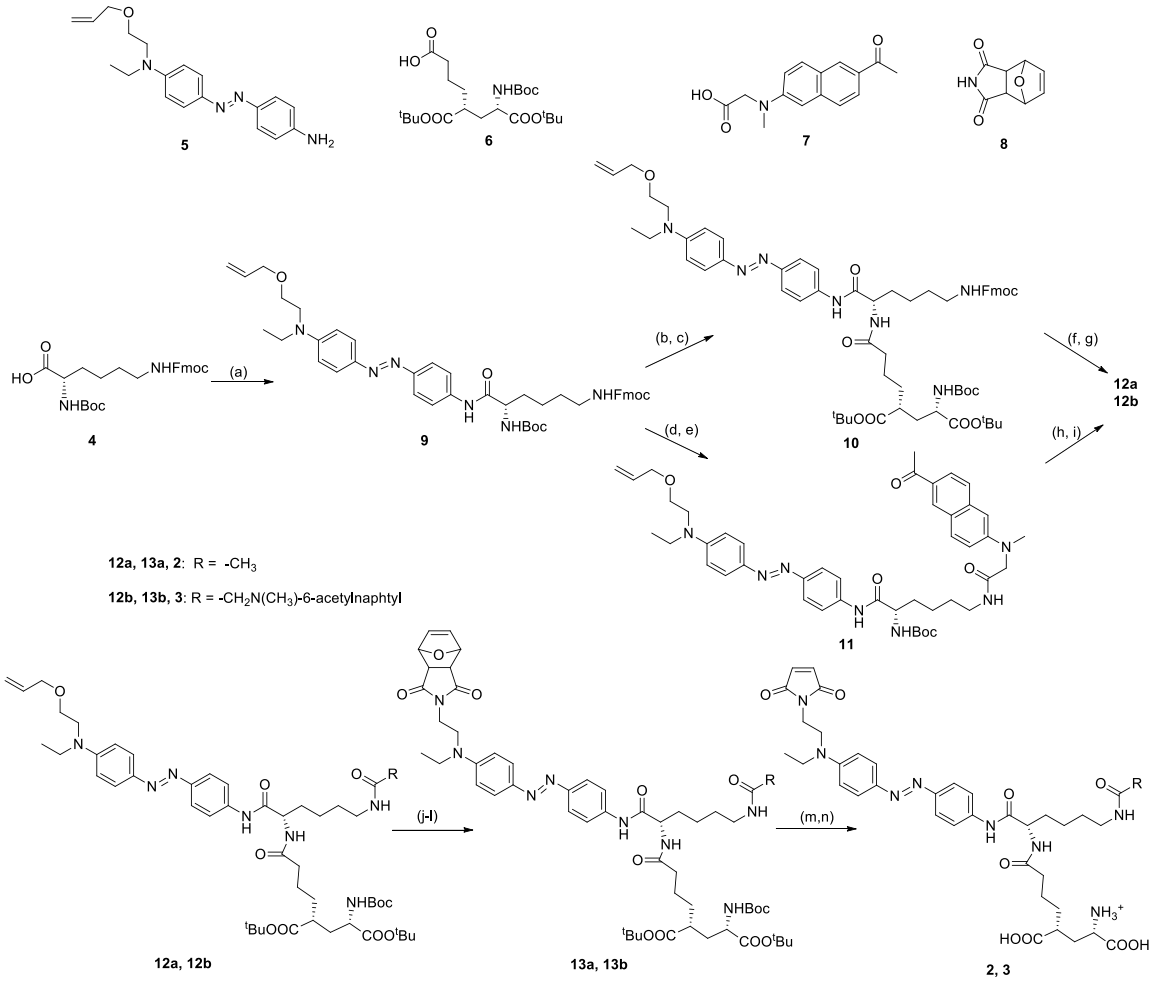

[a]Reagents and conditions: (a) **5**, HATU, DIPEA, THF (89%); (b) 37% HCl, MeOH (93%); (c) **6**, EDCI, HOBt, DIPEA, THF (88%); (d) 20% piperidine/DMF (87%); (e) **7**, EDCI, DIPEA, THF (81%); (f) 20% piperidine/DMF (64%); (g) $ClCOCH_3$, pyridine, THF (69%); (h) 37% HCl, MeOH (93%); (i) **6**, EDCI, HOBt, DIPEA, THF (71%); (j) $RhCl(PPH_3)_3$, $EtOH/H_2O$, reflux; (k) HgO, $HgCl_2$, $acetone/H_2O$, reflux; (l) **8**, Ph_3P, DIAD, THF (81%, over the three steps, for **13a**, 27% for **13b**); (m) toluene, reflux; (n) TFA, CH_2Cl_2 (81% over the two steps for **2**, 86% for **3**). HATU, *O*-(7-azabenzotriazol-1-yl)-*N*,*N*,*N*',*N*'-tetramethyluronium hexafluorophosphate; DIPEA, diisopropylethylamine; EDCI, *N*-ethyl-*N'*-(3-dimethyldiaminopropyl)-carbodiimide HCl; HOBt, 1-hydroxybenzotriazole hydrate; DIAD, diisopropyl azodicarboxylate.

We next tested this set of PTLs to photoswitch LiGluR in living cells using one- and two-photon stimulation (Figures 3a and 3b, respectively). We expressed GluK2-L439C-eGFP in HEK293 cells, incubated them in MAG, MAG_{2p} and $MAGA_{2p}$ and recorded the corresponding photocurrents generated upon light-induced opening of LiGluR channels using whole-cell patch clamp[26,27] (see the Supporting Information). Introduction of the 4-amino substituent in the azo core allows the one-photon action spectra of MAG_{2p} and $MAGA_{2p}$ to red-shift ~60 nm with respect to that of MAG, as recently reported for a similar compound[21] (Figure S5 and Table S1 in the Supporting Information). An additional peak is observed for $MAGA_{2p}$ at λ=370 nm, which coincides with the absorbance band of the naphthalene moiety. Thus, sensitization of the azobenzene photoisomerization by the antenna also occurs when the photoswitch is conjugated to LiGluR. In addition, the time course of the MAG_{2p} and $MAGA_{2p}$ one-photon currents (blue and red traces in Figure 3a) confirms that fast spontaneous *cis-trans* back-isomerization and channel closure takes place after the illumination is switched off, while it requires irradiation with green light for MAG (black trace in Figure 3a). By fitting the one-photon current decays in the dark with monoexponential functions, the lifetimes of *cis*-MAG_{2p} and *cis*-$MAGA_{2p}$ tethered to LiGluR were determined to be 150 ms and 265 ms, respectively (Table S1 in the Supporting Information). These values are larger than those measured in solution (see above), which suggests that the ligand-binding site interaction slows down the thermal *cis-trans* isomerization of the azobenzene-based switches.

Using a custom-built multiphoton setup where a tightly focused fs laser is raster scanned over the cells of interest, all three PTLs display robust and LiGluR-specific photocurrents in living cells (Figure 3b and Figure S7 in the Supporting Information) that first demonstrate two-photon stimulation with NIR light of a synthetic photoswitchable protein. The amplitude of the responses follows the characteristic power-dependence of two-photon absorption processes (Figure S8 in the Supporting Information) and corresponds to 10-20% of the photocurrent under one-photon excitation (Table S2 in the Supporting Information). In order to optimize the multiphoton stimulation conditions we characterized the two-photon action spectrum of each PTL (Figure 4a). The wavelength that yields maximal two-photon responses of MAG is around 820 nm. Repeated cell raster scans are required to get a saturating photocurrent from all available receptors (black trace in Figure 3b). Then, the current remains stable without laser illumination until LiGluR is closed with 500 nm light via one-photon *cis-trans* back-photoisomerization. The MAG_{2p} two-photon action spectrum is red-shifted and yields maximum current amplitude around 900 nm. The reduced currents obtained from

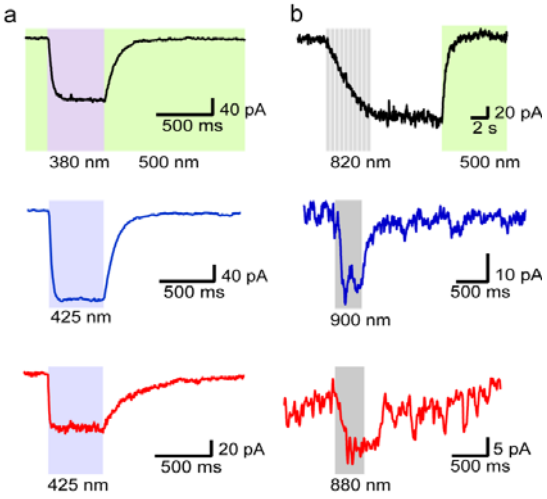

Figure 3. (a) One- and (b) two-photon whole-cell voltage-clamp recordings on HEK293 cells expressing LiGluR conjugated with MAG (black), MAG2p (blue) and MAGA2p (red). Bars indicate stimulation pulses applied to open (one-photon pulses in violet and blue, two-photon pulses in grey) and close LiGluR (one-photon pulses in green). Irradiation wavelengths are given in each case. Two-photon excitation conditions: MAG (λ=820 nm, 10 scans of 0.4 s, 38 mW on sample), MAG2p (λ=900 nm, 0.4 s scan, 30 mW on sample) and MAGA2p (λ=740 nm, 0.4 s scan, 42 mW on sample).

$MAGA_{2p}$ hindered the acquisition of a detailed action spectrum, but are sufficient to identify two spectral ranges allowing two-photon activation of LiGluR: the first can be found at ~880 nm (corresponding to the direct

absorbance of azobenzene, as in MAG_{2p}), and the second is located around 740 nm, and is consistent with the naphthalene-sensitized photoisomerization.[34]

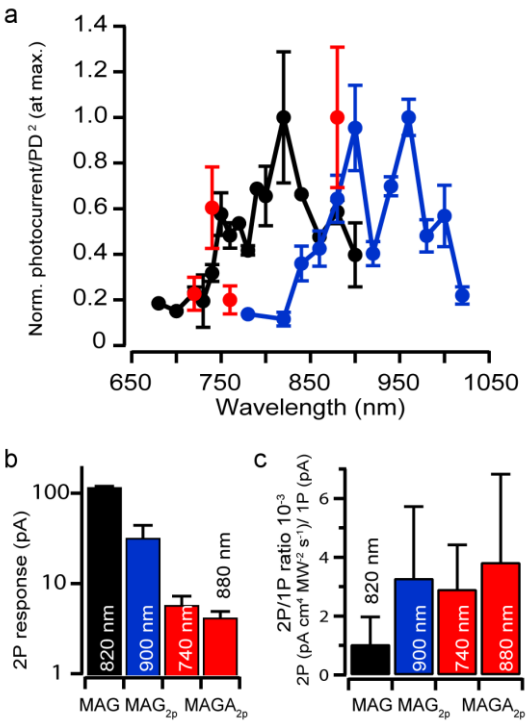

Figure 4. (a) Two-photon action spectra of LiGluR-MAG (black) and LiGluR-MAG2p (blue) and two-photon activation of LiGluR-MAGA2p (red) at selected wavelengths. Photocurrent amplitudes were corrected for the different power densities used (PD), averaged over all cells measured and normalized to the spectral maximum. (b) Absolute two-photon (2P) responses at the optimal wavelength. For MAGA2p values are given for sensitized (λ=740 nm) and direct (λ=880 nm) azobenzene excitation. (c) Ratio between the two- and one-photon responses (2P/1P). To compare between different LiGluR-tethers, two-photon responses were corrected for the distinct power densities and excitation times used and averaged over all cells measured. In (a-c) *N*=1-6 cells and errors are s.e.m.

Remarkably, multiphoton currents mediated by MAG_{2p} and $MAGA_{2p}$ completely saturate after few laser scans of the recorded cell (blue and red traces in Figure 3b). In addition, their rapid relaxation allows LiGluR to close immediately after the end of each stimulus, with time constants similar to those obtained with one-photon illumination (Table S2 in the Supporting Information). Thus, the novel compounds MAG_{2p} and $MAGA_{2p}$ enable single-wavelength, multiphoton gating of LiGluR. However, MAG achieves higher two-photon current amplitudes than MAG_{2p} and $MAGA_{2p}$ in the long term (Figure 4b), because the thermal stability of its *cis* isomer allows building up a larger population of open-state channels upon repeated cell raster scans (Figure S9 in the Supporting Information). To compare the efficacy of LiGluR activation between PTLs, we calculated the ratio between two-photon and one-photon maximal responses (Figure 4c). Noticeably, MAG_{2p} and $MAGA_{2p}$ (both via direct and sensitized azobenzene excitation) display a higher ratio than MAG, thereby demonstrating that the efficiency of multiphoton isomerization was enhanced by the design of the new photoswitches.

After characterizing the two-photon stimulation of LiGluR, we pursued physiological applications that exploited the ability of this receptor to rapidly activate neurons[35] and trigger calcium-regulated processes.[36,37] The stimulation of individual neurons in micrometric volumes and millisecond timescales has been demonstrated using two-photon neurotransmitter uncaging[23] and optogenetics.[24,25] To complement this set of tools for investigating brain connectivity, we applied two-photon activation of LiGluR in neuronal and non-neuronal cells of the brain using the high photocurrents provided by MAG and MAG_{2p}. We expressed GluK2-L439C-eGFP in cultured hippocampal neurons, incubated them in MAG_{2p} and recorded neuronal activity using whole-cell patch clamp (Figures 5a-d). Excitation of the soma with 900 nm light elicits inward currents in voltage-clamp experiments (Figure 5c). In current-clamp mode, these photocurrents triggered action potentials in two thirds of the neurons tested (Figure 5d). Although several properties of LiGluR-MAG_{2p} must be improved in order to reliably photocontrol whole neurons and individual presynaptic terminals (lifetime of the *cis* isomer, receptor expression level and subcellular localization), these results

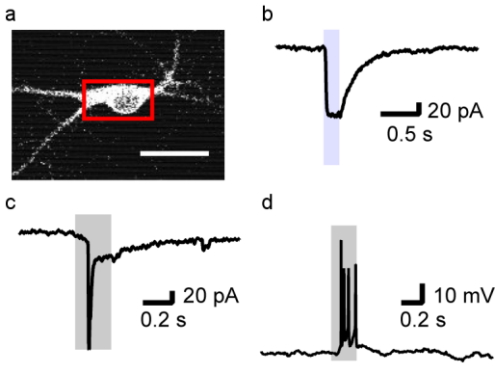

Figure 5. (a) Two-photon image (λ=1000 nm) of a cultured LiGluR-MAG$_{2p}$ hippocampal neuron filled with Alexa Fluor 594. Red square limits the raster scan area of two-photon stimulation. Scale bar is 20 µm. (b) Voltage-clamp recording during one-photon stimulation (blue bar). (c-d) Two-photon raster scan (grey bars) of the same neuron during: (c) voltage-clamp recording, which shows basal two-photon current with a transient current spike (two-photon mean current amplitude: 21±3 pA, 19±2% of one-photon current, *N*=3), and (d) current-clamp recording (resting potential=-45 mV). Two-photon excitation conditions: λ=900 nm, 0.25 s scan and 15 mW on sample.

indicate that it is possible to activate neurons using two-photon stimulation of synthetic photoswitchable proteins.

In the same experimental conditions, no spikes were elicited by two-photon stimulation of LiGluR-MAG, probably due to the slow photoresponses shown in Figure 3b. However, the large, step-function photocurrents provided by MAG and the calcium permeability of GluK2[38] make LiGluR-MAG more attractive to trigger calcium-regulated processes[37,39] including astrocyte activation[36] (see also Figure S6 in the Supporting Information). In cultured astrocytes expressing LiGluR-MAG (Figures 6a-h), two-photon excitation at 820 nm triggered bistable currents

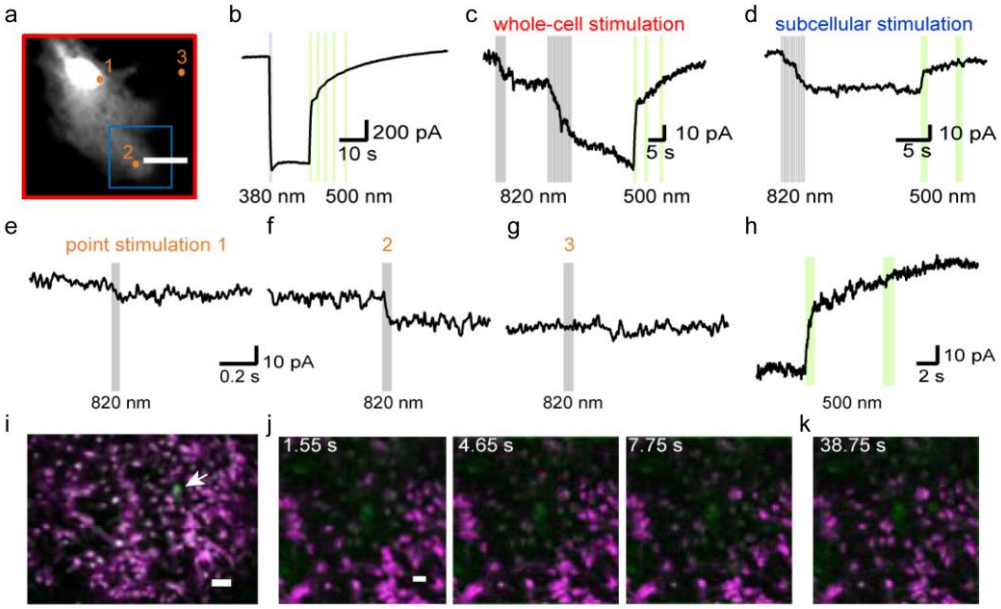

Figure 6. (a) Two-photon image (λ=1000 nm) of a cultured LiGluR-MAG astrocyte filled with Alexa Fluor 594. Red and blue squares limit the whole cell and subcellular raster scan areas, respectively. Location of point stimulations are shown with orange dots. Scale bar is 10 µm. (b) Whole-cell voltage-clamp recording of the astrocyte during one-photon stimulation (LiGluR opening: purple bar, LiGluR closing: green bar). (c-h) Two-photon currents measured on the same astrocyte (LiGluR opening: grey bar, one-photon LiGluR closing: green bar): (c) whole-cell scan stimulation at λ=820 nm, 10 scans of 0.7 s and 37 mW on sample (mean current amplitude: 60±20 pA, 30±10% of one-photon current, *N*=2); (d) subcellular scan stimulation at λ=820 nm, 10 scans of 0.25 s and of 68 mW on sample (mean

current amplitude: 17±9 pA, *N*=2); (e-g) Single point stimulation (grey bar) at λ=820 nm, 50 ms and 68 mW on sample (points 1 and 2 are on the cytoplasm and 3 out of the cell as control); (h) LiGluR closing at the end stimulation protocol (green bar) (i-k) Two-photon calcium imaging of cultured astrocytes loaded with Fura-2 (in purple, λ=800 nm) overlapped with an image of GFP fluorescence (in green, λ=900 nm) to identify astrocytes expressing LiGluR-MAG. Scale bar is 20 µm, except 50 µm in (i). (j) Images at 1.55, 4.65 and 7.75 s after targeting the astrocyte pointed with the arrow in (i) with two-photon stimulation (20 targets, 16-pixel diameter, 10 ms per point at λ=800 nm, 60 mW on sample). (k) Recovery of intracellular calcium levels 38.75 s after stimulation.

(Figure 6c). Interestingly, whole-cell photocurrents can also be measured during the stimulation of a subcellular region (Figure 6d) or a spot (Figures 6e-g) and these responses are reversible by illuminating the cell at 500 nm (Figures 6c-d and h). In order to verify whether such stimuli were enough to activate an intracellular calcium response in the astrocyte,[36,40] we performed two-photon calcium imaging together with two-photon stimulation of astrocytes expressing LiGluR-MAG. When we stimulated an expressing astrocyte, LiGluR activation caused a calcium increase that propagated to neighboring cells, generating a calcium wave that expanded to astrocytes throughout the field of view (Figures 6i-k and Movie S1 in the Supporting Information). This effect, which is not observed when locally stimulating non-expressing astrocytes (Figure S10 and Movie S2 in the Supporting Information), demonstrates that two-photon LiGluR activation can be used to manipulate cytosolic calcium levels in cultured astrocytes.

CONCLUSIONS

We have demonstrated the two-photon activation of azobenzene-based photoswitches in living cells expressing the light-gated receptor LiGluR.[26] Although a symmetrically-substituted azobenzene was reported to photoisomerize under continuous-wave NIR excitation,[41] in general these chromophores present low two-photon absorption cross-sections.[29,30] However, synthetic PTLs like MAG[26] offer great flexibility to adjust their photochemical properties without altering protein function. We have rationally designed MAG derivatives with visible absorption, fast thermal relaxation and high two-photon isomerization efficacy based on push-pull substitutions[31,32,42,43] and sensitization[33] of the azobenzene photoisomerization. These modifications and the reported multiphoton excitation conditions should be directly applicable to all azobenzene-based bioactive ligands,[11] including intracellular photoswitches known to penetrate into cells directly[44] or through specific ion channels,[45] and hyperpolarizing step-function photoswitchable channels like SPARK[46] or LiGABA.[11] Our findings thus enable the use of synthetic photoswitches to manipulate extra- and intracellular biochemical processes with the spatiotemporal precision provided by two-photon stimulation.

EXPERIMENTAL SECTION

Synthesis. A detailed description of the synthesis of target photoswitchable tethered ligands is given in the Supporting Information.

Photochemical characterization. *Trans-cis* isomerization of MAG_{2p} and $MAGA_{2p}$ in solution was investigated by: (i) ^{1}H NMR for the elucidation of the photostationary state mixtures; (ii) steady-state UV-vis absorption spectroscopy for *trans-cis* photoisomerization and slow *cis-trans* thermal back-isomerization processes; (iii) transient absorption spectroscopy for fast *cis-trans* thermal back-isomerization processes.

LiGluR on cultured cells. HEK293 tsA201 cell line, cultured hippocampal neurons and astrocytes plated on glass coverslips were transfected with GluK2-L439C-eGFP. Prior to each experiment, they were incubated with one of the PTLs to allow the chemical conjugation with the receptor channel and light sensitization. A second incubation with concavalin A was done in order to inhibit desensitization of the glutamate receptor.

Electrophysiology. For two-photon stimulation, voltage-clamp and current clamp recordings under whole-cell configuration were done with an Axon Multiclamp 700B amplifier

(Molecular Devices) and data was acquired at 10 kHz. Borosilicate glass pipettes were pulled with a typical resistance of 4–6 MΩ for HEK293 tsA201 cells and neurons or 7–8 MΩ for astrocytes. Bath solution was composed of (in mM): 140 NaCl, 1 MgCl, 2.5 KCl, 10 HEPES, 2.5 CaCl2 and 10–20 mM glucose to fix osmolarity to 310 mOsm·kg–1, pH 7.42 adjusted with NaOH. For HEK293 tsA201 cell line, pipette solution contained (in mM): 120 cesium methanosulfonate, 10 TEA-Cl, 5 MgCl2, 3 Na2ATP, 1 Na2GTP, 20 HEPES, 0.5 EGTA, 290 mOsm·Kg–1 and pH 7.2 was adjusted with CsOH. For neurons and astrocytes it consisted on (in mM): 130 potassium gluconate, 5 NaCl, 10 HEPES, 0.1 EGTA, 2 MgSO4, 4 Mg-ATP, 0.4 NaXGTP, 7 Na2-Phosphocreatine, 2 Pyruvic acid 0.1 Alexa Fluor 594 (Molecular Probes), and pH 7.3 adjusted with KOH.

Two-photon stimulation. All two-photon experiments were performed with a custom-made two-photon laser scanning microscope based on a modified Olympus BX50WI microscope with a Ti:sapphire laser as light source (Coherent Chameleon Ultra II, 140-fs pulses, 80-MHz repetition rate). Laser power was modulated by a Pockels cell (Conoptics) and adjusted for each wavelength to be close to 40 mW for MAG2p and MAGA2p and 50 mW for MAG. In experiments with MAG, we used a 20x/0.5-NA objective (Olympus) and with the red-shifted compounds, we used a 20x/0.95-NA objective (Olympus) in Figures 3-4 and a 40x/0.8-NA objective (Olympus) in Figures 5-6. For two-photon stimulation we defined a ROI and applied a unidirectional raster scan using FluoView software or we performed point stimulations with a costum written LabView Software.[47]

Calcium imaging of astrocytes. 50 µL DMSO was added to a 50 µg aliquot of Fura-2-AM (Life Technologies). 0.2 µL of this solution and 0.2 µL of Pluronic acid (20% in DMSO), in 2 mL supplemental media was added to the culture dish and incubated at 37°C for 30 min., before washing and LiGluR conjugation with MAG and concanavalin A treatment. We raster-scanned Fura-2 (100 frames, 1.55 s/frame) at 800 nm and 40 mW on sample with a 20x/0.5-NA objective for recording the activity of astrocytes and stimulated single non-expressing or GFP-positive astrocytes using custom written software,[47] with a protocol of 20 stimulation targets on the cell with a16-pixel diameter, corresponding to approximately 11 µm diameter.

Data analysis. Amplitudes of LiGluR currents were analyzed using IgorPro (Wavemetrics), closing time constants of LiGluR were determined with a custom made software using LabView. In the two-photon action spectrum of each compound, every set of data from one cell was normalized to the action spectrum integral from a chosen representative before cell average. Finally we normalized each action spectrum to its maximum. Calcium imaging of astrocytes was analyzed using custom written software (Caltracer) and ImageJ.

ASSOCIATED CONTENT

Supporting Information

General materials and methods, detailed description of the synthesis of MAG_{2p} and $MAGA_{2p}$, and additional photochemical (Figures S1-S7) and biological (Figures S8-S13, Tables S1-S2 and Movies S1-S2) measurements. This material is available free of charge via the Internet at http://pubs.acs.org.

AUTHOR INFORMATION

Corresponding Author

*rmy5@columbia.edu (R. Y.), jordi.hernando@uab.cat (J. H.), pau@icrea.cat (P. G.)

Author Contributions

+ Equal contribution

Notes

The authors declare no competing financial interests.

ACKNOWLEDGMENTS

We thank Dirk Trauner for providing us the MAG compound, Ehud Isacoff for supplying us with the GluK2-L439C-eGFP construct, Ariadna Pérez-Jiménez and Núria Camarero for subcloning it into pcDNA3, Yeonsook Shin, Alexa Semonche and Masayuki Sakamoto for preparation of primary cultures and cell transfection, and Sònia Parés for synthesis at initial stages of the project. We are grateful to Darcy S. Peterka and Artur Llobet for helpful discussions. We acknowledge financial support from the RecerCaixa foundation

(2010ACUP00378), the "Marató de TV3" foundation (111531), the Human Frontier Science Program (CDA022/2006), the European Research Council (ERC-2007-StG-210355 and ERC-2012-PoC-335011), the European Commission (FP7-ICT-2009-270483), the Catalan government (grant 2009-SGR-277 and fellowship 2012-FI_B 01122), the "Universitat Autònoma de Barcelona" (pre-doctoral fellowship of M.G.-M.) and the Spanish government (grants CTQ2008-06160, CTQ2012-30853 and CTQ2010-15380 and FPU fellowship AP2008-03313). The R.Y. laboratory is supported by the Kavli Institute for Brain Science, NIH Director Pioneer Award, NEI, NINDS, NIMH, NIDA, Keck Foundation and NARSAD. This material is based upon work supported by, or in part by, the U. S. Army Research Laboratory and the U. S. Army Research Office under contract number W911NF-12-1-0594

REFERENCES

(1) Harvey, J. H.; Trauner, D. *ChemBioChem.* **2008**, *9*, 191.
(2) Yamada, M. D.; Nakajima, Y.; Maeda, H.; Maruta, S. *J. Biochem.* **2007**, *142*, 691.
(3) Wu, Y. I.; Frey, D.; Lungu, O. I.; Jaehrig, A.; Schlichting, I.; Kuhlman, B.; Hahn, K. M. *Nature* **2009**, *461*, 104.
(4) Umeki, N.; Yoshizawa, T.; Sugimoto, Y.; Mitsui, T.; Wakabayashi, K.; Maruta, S. *J. Biochem.* **2004**, *136*, 839.
(5) Schierling, B.; Noël, A. J.; Wende, W.; Hien, l. T.; Volkov, E.; Kubareva, E.; Oretskaya, T.; Kokkinidis, M.; Römpp, A.; Spengler, B.; Pingoud, A. *Proc. Natl. Acad. Sci. U S A* **2010**, *107*, 1361.
(6) Asanuma, H.; Liang, X.; Nishioka, H.; Matsunaga, D.; Liu, M.; Komiyama, M. *Nat. Protoc.* **2007**, *2*, 203.
(7) Ito, H.; Liang, X.; Nishioka, H.; Asanuma, H. *Org. Biomol. Chem.* **2010**, *8*, 5519.
(8) Airan, R. D.; Thompson, K. R.; Fenno, L. E.; Bernstein, H.; Deisseroth, K. *Nature* **2009**, *458*, 1025.
(9) Oh, E.; Maejima, T.; Liu, C.; Deneris, E.; Herlitze, S. *J Biol Chem* **2010**, *285*, 30825.
(10) Miesenbock, G. *Science*, **2009**, *326*, 395.
(11) Kramer, R. H.; Mourot, A.; Adesnik, H. *Nat. Neurosci.* **2013**, *16*, 816.
(12) Toettcher, J. E.; Gong, D.; Lim, W. A.; Weiner, O. D. *Nat. Methods* **2011**, *8*, 837.
(13) Denk, W.; Strickler, J. H.; Webb, W. W. *Science* **1990**, *248*, 73.
(14) Papagiakoumou, E.; Begue, A.; Leshem, B.; Schwartz, O.; Stell, B. M.; Bradley, J.; Oron, D.; Emiliani, V. *Nat. Photon.* **2013**, *7*, 274.
(15) Oron, D.; Papagiakoumou, E.; Anselmi, F.; Emiliani, V. *Prog. Brain Res.* **2012**, *196*, 119.
(16) Watson, B. O.; Nikolenko, V.; Yuste, R. *Front. Neural Circuits* **2009**, *3*, 6.
(17) Yizhar, O.; Fenno, L. E.; Prigge, M.; Schneider, F.; Davidson, T. J.; O'Shea, D. J.; Sohal, V. S.; Goshen, I.; Finkelstein, J.; Paz, J. T.; Stehfest, K.; Fudim, R.; Ramakrishnan, C.; Huguenard, J. R.; Hegemann, P.; Deisseroth, K. *Nature* **2011**, *477*, 171.
(18) Wen, L.; Wang, H.; Tanimoto, S.; Egawa, R.; Matsuzaka, Y.; Mushiake, H.; Ishizuka, T.; Yawo, H. *PLoS One* **2010**, *5*, e12893.
(19) Gorostiza, P.; Isacoff, E. Y. *Physiology* **2008**, *23*, 238.
(20) Mourot, A.; Kienzler, M. A.; Banghart, M. R.; Fehrentz, T.; Huber, F. M.; Stein, M.; Kramer, R. H.; Trauner, D. *ACS Chem. Neurosci.* **2011**, *2*, 536.
(21) Kienzler, M. A.; Reiner, A.; Trautman, E.; Yoo, S.; Trauner, D.; Isacoff, E. Y. *J. Am. Chem. Soc.* **2013**, *135*, 17683.
(22) Fehrentz, T.; Kuttruff, C. A.; Huber, F. M.; Kienzler, M. A.; Mayer, P.; Trauner, D. *ChemBioChem* **2012**, *13*, 1746.
(23) Judkewitz, B.; Roth, A.; Häusser, M. *Neuron* **2006**, *50*, 180.
(24) Packer, A. M.; Peterka, D. S.; Hirtz, J. J.; Prakash, R.; Deisseroth, K.; Yuste, R. *Nat. Methods* **2012**, *9*, 1202.
(25) Prakash, R.; Yizhar, O.; Grewe, B.; Ramakrishnan, C.; Wang, N.; Goshen, I.; Packer, A. M.; Peterka, D. S.; Yuste, R.; Schnitzer, M. J.; Deisseroth, K. *Nat. Methods* **2012**, *9*, 1171.
(26) Volgraf, M.; Gorostiza, P.; Numano, R.; Kramer, R. H.; Isacoff, E. Y.; Trauner, D. *Nat. Chem. Biol.* **2006,** *2*, 47.
(27) Gorostiza, P.; Volgraf, M.; Numano, R.; Szobota, S.; Trauner, D.; Isacoff, E. Y. *Proc. Natl. Acad. Sci. U S A*, **2007,** *104*, 10865.
(28) Szymanski, W.; Beierle, J. M.; Kistemaker, H. A. V.; Velema, W. A.; Feringa, B. L. *Chem. Rev.* **2013**, *113*, 6114.
(29) De Boni, L.; Rodrigues, J. J.; dos Santos, D. S.; Silva, C.; Balogh, D. T.; Oliveira, O. N.; Zilio, S. C.; Misoguti, L.; Mendonça, C. R. *Chem. Phys. Lett.* **2003**, *374*, 684.
(30) De Boni, L.; Misoguti, L.; Zilio, S. C.; Mendonça, C. R. *ChemPhysChem* **2005**, *6*, 1121.
(31) Antonov, L.; Kamada, K.; Ohta, K.; Kamounah, F. S. *Phys. Chem. Chem. Phys.* **2003**, *5*, 1193.
(32) Magennis, S. W.; Mackay, F. S.; Jones, A. C.; Tait, K. M.; Sadler, P. J. *Chem. Mater.* **2005**, *17*, 2059.
(33) Jiang, D. L.; Aida, T. *Nature* **1997**, *388*, 454.
(34) Kim, H. M.; Cho, B. R. *Acc. Chem. Res.* **2009**, *42*, 863.
(35) Szobota, S.; Gorostiza, P.; Del Bene, F.; Wyart, C.; Fortin, D. L.; Kolstad, K. D.; Tulyathan, O.; Volgraf, M.; Numano, R.; Aaron, H. L.; Scott, E. K.; Kramer, R. H.; Flannery, J.; Baier, H.; Trauner, D.; Isacoff, E. Y. *Neuron*, **2007**, *54*, 535.
(36) Li, D.; Herault, K.; Isacoff, E. Y.; Oheim, M.; Ropert, N. *J. Physiol.*, **2012**, *590*, 855.

(37) Izquierdo-Serra, M.; Trauner, D.; Llobet, A.; Gorostiza, P. *Biophys. J.* **2013**, *104*, 497A.
(38) Egebjerg, J.; Heinemann, S. F. *Proc. Natl. Acad. Sci. U S A* **1993**, *90*, 755.
(39) Izquierdo-Serra, M.; Trauner, D.; Llobet, A.; Gorostiza, P. *Biochim. Biophys. Acta* **2013**, *1830*, 2853.
(40) Cornell-Bell, A. H.; Finkbeiner, S. M.; Cooper, M. S.; Smith, S. J. *Science* **1990**, *247*, 470.
(41) Zhang, Y.; Erdmann, F.; Fischer, G. *Nat. Chem. Biol.* **2009**, *5*, 724.
(42) Venkataramani, S.; Jana, U.; Dommaschk, M.; Sonnichsen, F. D.; Tuczek, F.; Herges, R. *Science* **2011**, *331*, 445.
(43) Sakamoto, R.; Kume, S.; Sugimoto, M.; Nishihara, H. *Chem. Eur. J.* **2009**, *15*, 1429.
(44) Nevola, L.; Martín-Quirós, A.; Eckelt, K.; Camarero, N.; Tosi, S.; Llobet, A.; Giralt, E.; Gorostiza, P. *Angew. Chem. Int. Ed.* **2013**, *52*, 7704.
(45) Mourot, A.; Fehrentz, T.; Le Feuvre, Y.; Smith, C. M.; Herold, C.; Dalkara, D.; Nagy, F.; Trauner, D.; Kramer, R. H. *Nat. Methods* **2012**, *9*, 396.
(46) Banghart, M.; Borges, K.; Isacoff, E.; Trauner, D.; Kramer, R. H. *Nat. Neurosci.* **2004**, *7*, 1381.
(47) Nikolenko, V.; Poskanzer, K.E; Yuste, R. *Nat. Methods* **2007**, *4*, 943.

3.2 Supporting information

Photochemical and Biological Supporting methods.

Photochemical characterization of MAG_{2p} and $MAGA_{2p}$.

All spectroscopic and photochemical experiments were carried out in HPLC or spectroscopy quality solvents and in Ar-degassed samples. Steady-state UV-vis absorption measurements were recorded on a HP 8453 Spectrophotometer. Transient absorption measurements were registered in a ns laser flash-photolysis system (LKII, Applied Photophysics) equipped with a Nd:YAG laser (Brilliant, Quantel) as pump source, a Xe lamp as probe source and a photomultiplier tube (Hamamatsu) coupled to a spectrograph as detector. Fluorescence emission spectra were measured in a custom-made spectrofluorometer, where the above-mentioned pulsed laser is used as excitation source and the emitted photons are detected in an ICCD camera (Andor) coupled to a spectrograph. Fluorescence quantum yields were determined relative to DAPI in DMSO (4',6-diamidino-2-phenylindole, Φ_{DAPI} = 0.58 (Härd, Fan, and Kearns 1990)). Different excitation sources were used in the photochemical experiments depending on the spectral requirements: a Xe lamp coupled to a spectrograph, the third harmonic of the Nd:YAG laser (λ_{exc} = 355 nm), and a cw DPSS laser (λ_{exc} = 473 nm, SciTec).

Molecular cloning

The expression plasmids for GluK2-L439C and GluK2-L439C-eGFP were kindly provided by Ehud Y. Isacoff (University of California). GluK2-L439C was subcloned into EcoRI site of the pCDNA3.1 expression vector. To obtain the GluK2-L439C-eGFP-pCDNA3 construct, a fragment spanning the C-terminal domain of GluK2-L439C and eGFP was amplified by PCR using AfeI/XbaI flanked primers and subcloned into GluK2-L439C-pCDNA3 plasmid by replacing the former AfeI/XbaI cassette.

Cell line and transfection

HEK293 tsA201 cell line (SV40-transformed, Human Embryonic Kidney 293 cells) was maintained at 37 ºC in a 5% CO_2 humid incubator with Dulbecco's Modified Eagle

Medium/Nutrient Mixture F-12 media (DMEM) (1:1, Invitrogen) supplemented with 10% Fetal Bovine Serum (FBS) and 1% Penicillin/Streptomycin. Cells were transfected with pcDNA3-GluK2-L439C-eGFP for electrophysiology or pcDNA3-GluK2-L439C for calcium imaging.

- *Transfection of one-photon electrophysiology and calcium imaging.*

For transfection DNA–X-tremGENE 9 Transfection Reagent (Roche) mix was prepared following manufacturer's instructions with a Transfection Reagent:DNA ratio of 3:1. The mix was incubated for 20 min at room temperature, meanwhile cells were placed into a 12-mulltiwell plate at a density of $3 \cdot 10^5$ cells per well. After incubation, the mix was added dropwise into each well. For electrophysiology, experiments were performed after 24–48h and 16 h before cells were plated at low density on 15-mm coverslips treated with Poly-L-lysine (PLL). For calcium imaging, we waited expression for 72–96 h and 16 h before experiment, cells were plated on PLL-coverslips at high density.

- *Transfection of two-photon electrophysiology*

Cells were plated the day before transfection at a density of $2 \cdot 10^5$ into a 12-multiwell plate. Per each well, 2 µg of DNA were mixed with 3.75 µL 2M $CaCl_2$ (250 mM final concentration) in a final volume of 30 µL adding H_2O. Then, 30 µL of 2x HBS (Hepes Buffered Saline) were bubbled, added dropwise to the DNA-$CaCl_2$ mix and incubated 20 min at room temperature. Before the mix was added dropwise into each well, cell media was removed and replaced with 800 µL minimal essential media (MEM). Cells were placed back into the incubator, and after 36 h they were plated on 12-mm coverslips treated with PLL at low density, to do experiments the day after.

Hippocampal neuronal and astrocyte culture preparation and transfection

Animal handling and experimentation were done according to the US National Institutes of Health and Columbia Institutional Animal Care and Use Committee guidelines. Low-density primary hippocampal cultures were prepared from newborn P0 pups from C57/BL6 mice and maintained in cell culture for 1-3 weeks in coverslips coated with PLL, as described previously (Lester et al. 1989).

Cultured astrocytes were prepared from the hippocampal of newborn P0 pups from C57/BL6 mice as described elsewhere(Li et al. 2012). Cells were plated in PLL coated coverslips with complete medium (MEM, 10% Fetal Calf Serum, high Glucose, 2 mM glutamine, serum extender, penicillin (5 U ml^{-1}) and streptomycin (5 µg ml^{-1})) and within 24 h the medium was changed to the MEM solution with 5% FBS, penicillin (5 U ml^{-1}) and streptomycin (5 µg ml^{-1}). After 1 week, 0.15 mM dibutyryl cAMP (Sigma) was added.

Transfection of neurons was done 7 to 9 days after dissection and for astrocytes it was done 5 to 7 days after differentiation. Per each well, 2.3 µg of DNA were mixed with 1.875 µL 2 M $CaCl_2$ (250 mM final concentration) in a final volume of 15 µL adding H_2O. Then, 15 µL of 2x HBS were bubbled, added dropwise to the DNA-$CaCl_2$ mix and incubated 20 min at room temperature. Cell media was replaced with 400 µL MEM. The mix was added dropwise into each well and incubated 45 min, for neurons, and 2 h for astrocytes at 37 ºC, after that each well was washed three times with 1 mL of pre-warmed MEM and finally the old media was returned to the well.

Conjugation of LiGluR with photoswitched tethered ligands

All compounds were stored at 10 mM in DMSO at –20 ºC. Before each experiment cells were incubated with one of the compounds for 10 to 30 min in absence of light in extracellular solution composed by (in mM): 140 NaCl, 1 MgCl, 2.5 KCl, 10 HEPES, 0.5 $CaCl_2$ and 10–20 mM glucose to fix osmolarity to 300 mOsm·kg^{-1}, pH 7.4 adjusted with NaOH. For cell line, MAG or MAG_{2p} were added at a concentration of 50 µM and $MAGA_{2p}$ at 150 µM. For neurons and astrocytes MAG or MAG_{2p} were added at 20 µM. After compound incubation, cells were washed three times with extracellular solution and incubated 10 min with 0.3 mg mL^{-1} Concanavalin A (Sigma) —to block GluK2 desensitization— on an extracellular solution based on $NMDG^+$ (to avoid depolarization due to open LiGluRs, in mM): 110 NMDG+, 2.5 KCl, 1 MgCl2, 10 HEPES, 10–20 mM glucose to fix osmolarity to 300 mOsm·kg^{-1}, pH 7.4 adjusted with HCl. Before placing the coverslip to the recording chamber, cells were washed again three times with extracellular solution.

Electrophysiology

Voltage and current-clamp recordings under whole-cell configuration were done using an EPC-10 amplifier and data at 10 kHz was acquired with amplifier's software Patch Master (HEKA) —for one-photon stimulation— or using Axon Multiclamp 700B amplifier (Molecular Devices), digitized at 10 kHz with National Instruments 6259 multichannel cards and acquired data using custom software written with LabView (National Instruments) —for two-photon stimulation. Bath solution was composed of (in mM): 140 NaCl, 1 MgCl, 2.5 KCl, 10 HEPES, 2.5 $CaCl_2$ and 10–20 mM glucose to fix osmolarity to 310 $mOsm \cdot kg^{-1}$, pH 7.42 adjusted with NaOH. Borosilicate glass pipettes were pulled with a typical resistance of 4–6 MΩ for HEK293 cells and neurons or 7–8 MΩ for astrocytes. For HEK293 cell line, pipette solution contained (in mM): 120 cesium methanosulfonate, 10 TEA-Cl, 5 $MgCl_2$, 3 Na_2ATP, 1 Na_2GTP, 20 HEPES, 0.5 EGTA, 290 $mOsm \cdot Kg^{-1}$ and pH 7.2 was adjusted with CsOH. For neurons and astrocytes it consisted on (in mM): 130 potassium gluconate, 5 NaCl, 10 HEPES, 0.1 EGTA, 2 $MgSO_4$, 4 Mg-ATP, 0.4 Na_X-GTP, 7 Na_2-Phosphocreatine, 2 Pyruvic acid 0.1 Alexa Fluor 594 (Molecular Probes), and pH 7.3 adjusted with KOH.

Photostimulation

- *One-photon*

One-photon action spectrum characterization was done by illumination of the entire focused field using a Polychrome V monochromator (TILL Photonics) connected through the back port of an IX70 inverted microscope (Olympus) with a CP-ACHROMAT 40x/NA-0.65 objective (Zeiss). For automatically controlling wavelength, the monochromator was connected to the EPC-10 amplifier via Photochromic Manual Control (TILL Photonics) and controlled with photometry module of Patch Master. Then during voltage-clamp recordings we applied a train of 500 ms light-pulses at different wavelengths (for the whole action spectrum we ranged wavelengths from 325 to 572 nm, with 25 nm steps and for a higher resolution spectrum of the UV-light region of MAG_{2p} and $MAGA_{2p}$ we scanned from 300 to 450 with 10 nm steps) with 4 s delay between pulses in which light was switched to 500 nm for MAG (to close LiGluR) or 690 nm for MAG_{2p} and $MAGA_{2p}$. Light power measured with the Newport 1916-C light meter after the objective was 1.6 mW mm^{-2} for 425 nm, 0.8 mW mm^{-2} for 380 nm and 1.8 mW mm^{-2} for 500 nm.

- *Two-photon*

All two-photon experiments were performed with a custom-made two-photon laser scanning microscope based on a modified Olympus BX50WI microscope with a Ti:sapphire laser as light source (Coherent Chameleon Ultra II, 140-fs pulses, 80-MHz repetition rate). Laser power was modulated by a Pockels cell (Conoptics). For control one-photon stimulation we used mercury arc lamp with different band-pass filters: FURA cube for activation and TRITC cube for closure of LiGluR–MAG, and FITC cube for LiGluR-MAG_{2p} and LiGluR-$MAGA_{2p}$ activation. Light was triggered for 1 s illumination using a MASTER-8 (A.M.P.I.) to control a Uniblitz Shutter with D122 driver (Vincent Associates).

After checking response under one-photon stimulation, two-photon fluorescence images of cells filled with Alexa Fluor 594 were acquired with FluoView software (Olympus) using a photomultiplier tube (Hamamatsu) connected to a signal preamplifier (Model 5113, Signal Recovery AMETEK Advanced Measurement Technology) and low laser power illumination at 1000 nm. For simultaneous two-photon stimulation and electrophysiology, we defined a ROI enclosing the whole cell, typically of 20x20 µm, and applied a unidirectional raster scan. When we defined the ROI, we took into account that the Fluoview system slightly overscans the ROI area in the left and right direction. Duration of the scan was between 0.4 and 1.25 s for the red-shifted compounds and a 0.4-s scan was repeated 10 times in the case of LiGluR-MAG. Two-photon point stimulations were carried out using custom written LabView Software(Nikolenko, Poskanzer, and Yuste 2007). In experiments with MAG, we used a 20x/0.5-NA objective (Olympus) and with the red-shifted compounds, we used 20x/0.95-NA objective (Olympus) in Figure 3-4 and 40x/0.8-NA objective (Olympus) in Figure 5-6.

To characterize the wavelength dependence of two-photon LiGluR activation, we checked response at different wavelengths: 660 nm to 900 nm in steps of 20 nm for MAG, 740 nm to 1020 nm in steps of 20 nm for MAG_{2p} and 720 nm to 760 nm in steps of 20 nm and 880 nm for $MAGA_{2p}$.

To characterize the power dependency of the two-photon response we selected a wavelength that showed a good LiGluR current (750 nm for MAG and 880 nm for

MAG_{2p} and $MAGA_{2p}$) and we gradually increased the light intensity to saturation of LiGluR current amplitude.

Calcium imaging

- *Two-photon stimulation of astrocytes*

50 µL DMSO was added to a 50 µg aliquot of Fura-2-AM (Life Technologies). 0.2 µL of this solution and 0.2 µL of Pluronic acid (20% in DMSO), in 2 mL supplemental media was added to the culture dish and incubated at 37°C for 30 min., before washing and LiGluR conjugation with MAG and concanavalin A treatment. For each field of view, we obtained a two-photon image (FluoView) at 900 nm excitation wavelength with a 510/40 emission filter before the PMT to find astrocytes expressing iGluK2-L439C-eGFP. Then we raster-scanned Fura-2 (100 frames, 1.55 s/frame) at 800 nm and 40 mW for recording the basal activity of astrocytes. We stimulated single non-expressing or GFP-positive astrocytes using custom written software(Nikolenko, Poskanzer, and Yuste 2007), with a protocol of 20 stimulation targets on the cell with a 16-pixel diameter (corresponding to approximately 11 µm diameter) at 800 nm with a power on sample of 60 mW. Immediately after stimulation, we imaged Fura-2-loaded cells again as described for baseline. We used a 20x/0.5-NA objective (Olympus).

Data analysis and statistics

Amplitude of LiGluR currents were analyzed Using IgorPro (Wavemetrics). Closing time constant of LiGluR was calculated with a custom made software using LabView. Displayed whole-cell current traces have been filtered using the Inifinte Impulse Response (IIR) digital filter from IgorPro (Low-pass filter with cut off 10-50 Hz).

For the two-photon action spectrum, we corrected the current amplitude by dividing it for the square power density, to take into account the power applied during stimulation and the objectives used with different numerical aperture. To obtain the action spectrum of each compound, before cell average, every set of data from one cell was normalized to the action spectrum integral from a chosen representative.

Finally to normalize magnitude between different compounds, we normalized each action spectrum.

Calcium imaging of astrocytes was analyzed using custom written software (Caltracer) and ImageJ.

Figure S1. Direct *trans*-*cis* photoisomerization.

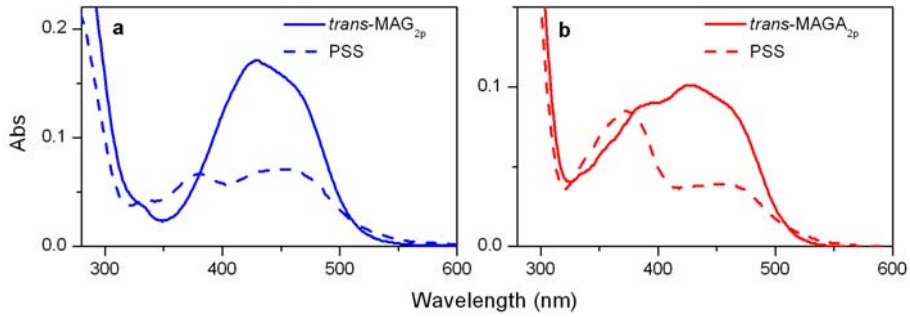

Figure S1. (a) Absorption spectra in DMSO of *trans*-MAG_{2p} and the photostationary state (PSS) obtained upon photoexcitation of this compound at λ_{exc} = 473 nm. ^{1}H NMR measurements in DMSO-d_6 under the same irradiation conditions revealed that the relative concentration of *cis*-MAG_{2p} in the PSS mixture is $\%^{cis}$ PSS = 58%. **(b)** Absorption spectra in DMSO of *trans*-$MAGA_{2p}$ and the photostationary state (PSS) obtained upon photoexcitation of this compound at λ_{exc} = 473 nm. At this irradiation wavelength, the azo group of *trans*-$MAGA_{2p}$ is selectively photoexcited, since the antenna fragment does not absorb. ^{1}H NMR measurements in DMSO-d_6 under the same irradiation conditions revealed that the relative concentration of *cis*-$MAGA_{2p}$ in the PSS mixture is $\%cis$ PSS = 58%. From Marta Gascón-Moya.

Figures S2. *Cis*-*trans* thermal back-isomerization.

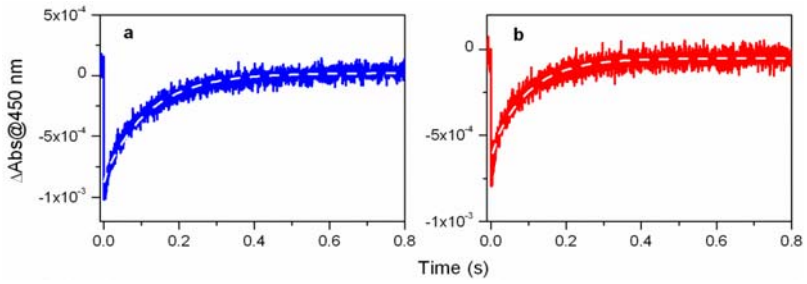

Figure S2. Variation of the absorption of a *trans/cis* mixture of **(a)** MAG_{2p} and **(b)** $MAGA_{2p}$ in the dark at 25ºC in 80% PBS: 20% DMSO. At these conditions,

thermal *cis-trans* back-isomerization takes place, thus restoring the inital concentration of the *trans* state of the ligands, which presents a larger extinction coefficient at λ_{abs} = 450 nm. Solid lines correspond to the experimental data, while dashed lines were obtained from a monoexponential fit (τ = 118 and 96 ms for MAG_{2p} and $MAGA_{2p}$, respectively). As previously reported for other aminoazobenzene derivatives(Schanze, Mattox, and Whitten 1983), the lifetime of the *cis* isomers of MAG_{2p} and $MAGA_{2p}$ dramatically decreases with polarity and it is expected to be in the millisecond range in physiological media. From Marta Gascón-Moya.

Figure S3. Fluorescence emission spectra of *trans*-$MAGA_{2p}$ and the photo-harvesting antenna model 14.

To demonstrate the occurrence of sensitized *trans-cis* photoisomerization in *trans*-$MAGA_{2p}$ via photoexcitation of the photo-harvesting antenna unit and subsequent resonant energy transfer (RET) towards the azobenzene group, the following data are presented: (i) fluorescence measurements on *trans*-$MAGA_{2p}$ and the free antenna model **14** (Fig. S3); (ii) evaluation of the RET efficiency for the antenna-azobenzene donor-acceptor pair (see Fig. S7); (iii) *trans-cis* photoisomerization efficiency upon selective photoexcitation of the antenna unit in *trans*- $MAGA_{2p}$ (Fig. 2b in the article).

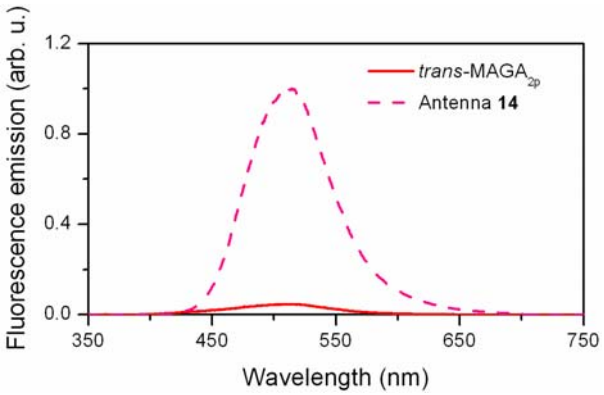

Figure S3. Fluorescence emission spectra of *trans*-$MAGA_{2p}$ and the photo-harvesting antenna model **14** (see Fig. S2) in 80% PBS : 20% DMSO. The spectra are normalized relative to the excitation intensity and the absorption at the excitation wavelength (λ_{exc} = 355 nm). The fluorescence quantum yields of *trans*-$MAGA_{2p}$ and **14** at these conditions were found to be: $\Phi_{trans\text{-}MAGA2p}$ = 0.02 and $\Phi_{\mathbf{14}}$ = 0.43. Therefore, the fluorescence emission of the naphthalene antenna group is strongly quenched upon incorporation into the *trans*-$MAGA_{2p}$ backbone, with a ~20-fold decrease in fluorescence quantum yield measured in

aqueous buffer, which points towards the occurrence of resonance energy transfer processes. From Marta Gascón-Moya.

Figure S4. Resonance energy transfer in *trans*-MAGA$_{2p}$.

To evaluate the efficiency of resonance energy transfer from the photoexcited antenna unit to the azobenzene group in *trans*-MAGA$_{2p}$, we calculated the Förster's radius (R_0) of this donor-acceptor pair in 80% PBS : 20% DMSO using equation S1 (Lakowicz 2006).

$$R_0 = \left(8.88\text{x}10^{-25} k^2 n^{-4} \Phi_D J\right)^{\frac{1}{6}} \quad (in\ cm) \qquad \text{(S1)}$$

The following parameters were used in this calculation: (i) J= 3.99x10^{-14}, which is the spectral overlap integral between the absorption spectrum of the antenna-less *trans*-MAG$_{2p}$ molecule and the emission spectrum of the model antenna group **14** in 80% PBS : 20% DMSO (see Supplementary Fig. 7); (ii) Φ_D= 0.43, which is the fluorescence quantum yield of **14** in 80% PBS : 20% DMSO; (iii) k^2= 2/3, which assumes random orientation between the donor and acceptor units owing to the flexible alkyl chain linking them together in *trans*-MAGA$_{2p}$; (iv) n= 1.365, which is the refractive index of a 80% PBS : 20% DMSO mixture. In this way, we obtained a value of R_0= 37.8 Å for *trans*-MAGA$_{2p}$, which is larger than the center-to-center distance between its antenna and azobenzene groups according to a molecular mechanics calculation with a MM2 force field (r= 10.1 Å). By introducing these parameters into equation S2 (Lakowicz 2006), we calculated that the efficiency of the RET process (E) in *trans*-MAGA$_{2p}$ should be higher than 99%, which would account for the nearly complete suppression of the fluorescence emission from the naphtalene sensitizer of this compound.

$$E = \frac{1}{1+\left(\frac{r}{R_0}\right)^6} \qquad \text{(S2)}$$

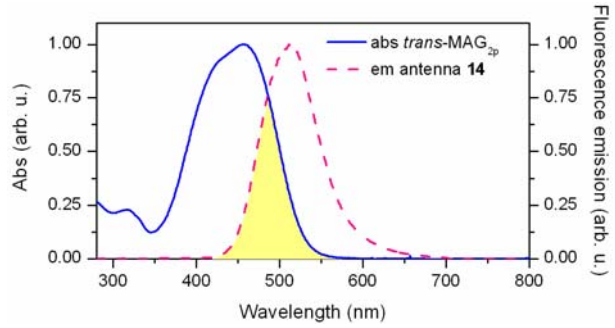

Figure S4. Spectral overlap between the absorption spectrum of the antenna-less *trans*-MAG$_{2p}$ (azobenzene acceptor) and the emission spectrum of **14** (naphtalene donor) in 80% PBS : 20% DMSO. From Marta Gascón-Moya.

Figure S5. Action spectra of LiGluR PTLs in HEKcells.

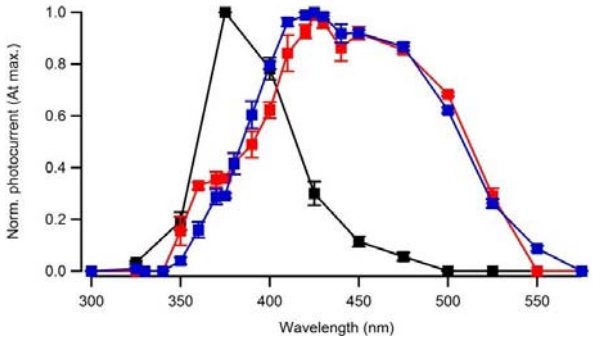

Figure S5. Normalized one-photon action spectra of LiGluR conjugated to MAG (black), MAG$_{2p}$ (blue) and MAGA$_{2p}$ (red) (N = 2 cells, N = 3 to 8 cells and N = 4 to 10 cells, respectively). To obtain the action spectra, whole-cell voltage-clamp measurements (such as those in **Fig. 3a** of the article) were registered with light pulses ranging from 300 nm to 550 nm. Before averaging over different cells, wavelength-dependent current amplitudes were normalized to the maximum photocurrent along the spectral range measured for each cell. Errors are s.e.m.

Figure S6. Characterization of calcium entry through LiGluR-MAG$_{2p}$ by calcium imaging.

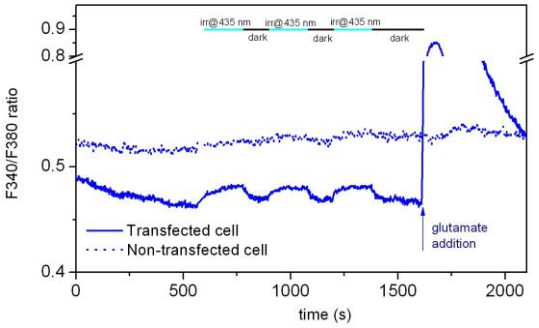

Figure S6. F340/F380 ratio measured for 35 min in two selected ROIs corresponding to a LiGluR-MAG$_{2p}$ expressing HEK cell (continuous line) and to a non-expressing HEK cell (control, dotted line) loaded with fura-2 AM. Fluorescence images were obtained every 5 s at 340 nm and 380 nm, 30 ms exposure time for each. Bar indicates alternated pulses of whole-field one-photon stimulation of 3 min at 435 nm (cyan) with dark periods of 4 min (black). At the end of the protocol, external solution containing 100 μM of glutamate was perfused for 1 min and after washed out. Illumination at 435 nm light opens LiGluR-MAG$_{2p}$, and calcium increases into the cell cytoplasm on the expressing cell and not on the control cell. Calcium ions permeate through LiGluR-MAG$_{2p}$, however its application for triggering calcium-dependent processes is limited by the small increase induced by light with respect to the full activation of LiGluR with glutamate. Figure from Marta Gascón-Moya.

Figure S7. Control of multiphoton stimulation of LiGluR expressing cells without PTL conjugation.

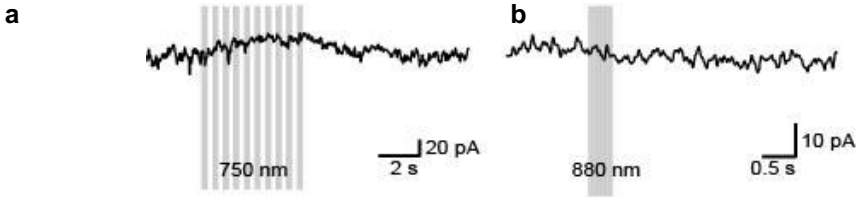

Figure S7. Control experiments were performed to discard any photoinduced unspecific effect on the cell membrane. To do this control, HEK293 cells were transfected with GluK2-L439C and they were incubated only with concanavalin A, as described in the Supproting Information. Two-photon stimulation conditions were applied that are equivalent to: **(a)** those used to activate LiGluR-MAG (λ

=750 nm, 10 scans of 0.4 s each, 51 mW on sample, 20x/0.95-NA objective); **(b)** those used to activate LiGluR-MAG_{2p} (λ =880 nm, 0.4 s scan, 36 mW on sample, 20x/0.95-NA objective). Two-photon stimulation under these conditions did not induce inward currents to transfected cells that were not treated with photoswitchable compounds.

Figure S8. LiGluR multiphoton current amplitude dependence on power.

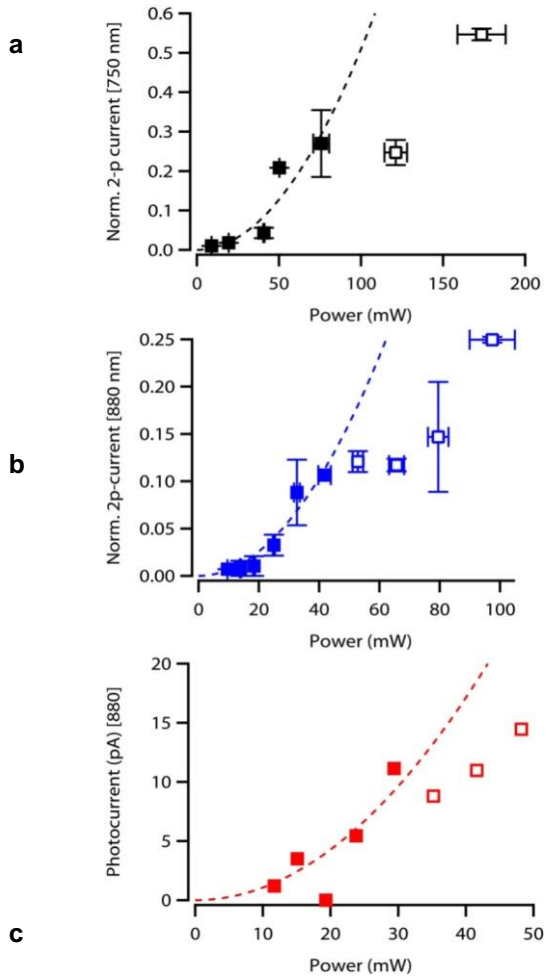

Figure S8. Dependence of the multiphoton photoresponse on laser intensity for each LiGluR PTL: **(a)** MAG (λ=750 nm, 10 scans of 0.4 s each, 20x/0.5-NA objective, *N*=1-3 cells), **(b)** MAG_{2p} (λ=880 nm, 0.4 s scan, 20x/0.95-NA objective, *N*=2 cells), **(c)** $MAGA_{2p}$ (λ=880 nm, 1 scan of 0.4 s, 20x/0.95-NA objective, *N*=1 cell). Laser intensities are given as the powers measured on sample, while photocurrents have been averaged over the different cells measured. At low and intermediate laser intensities, LiGluR photoresponse obeys

a squared power function for the three PTLs, which indicates that it arises from a two-photon absorption process. At high laser intensities, the quadratic dependence is lost, which we ascribe to saturation of the optical transition and/or cell photodamage. Therefore, all further measurements were conducted at lower laser intensities.

Figure S9. Repeated two-photon stimulation of LiGluR-MAG and LiGluR-MAG$_{2p}$.

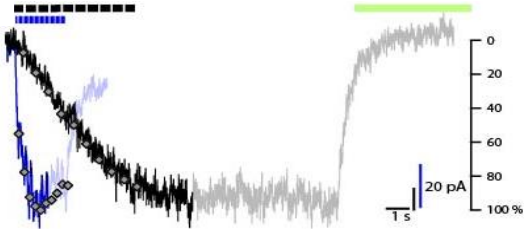

Figure S9. Typical photocurrent traces of single cells expressing LiGluR-MAG (black) and LiGluR-MAG$_{2p}$ (blue). Bars indicate the stimulation scans applied and grey dots show the photocurrent values obtained at the end of each scan in percentage (right axis). LiGluR-MAG$_{2p}$ opens with a faster kinetics, it reaches the saturation level earlier (three 0.4-s-pulses are needed to get 90% of maximum signal) and it rapidly closes after excitation is stopped. Excitation conditions: LiGluR-MAG: λ =820 nm, 10 scans of 0.4 s at 47 mW using a 20x/NA-0.5 objective, black bars; LiGluR-MAG$_{2p}$: λ =900 nm, 10 scans of 0.16 s at 39 mW using a 20x/NA-0.5 objective, blue bar.

Table S1. Optimal parameters for the one-photon activation of LiGluR with different PTLs.

	$\lambda_{trans \rightarrow cis}$ (nm)	$\lambda_{cis \rightarrow trans}$ (nm) or τ_{OFF} (s)	$\mathbf{I_{max}}$ (pA)	**% of 100 µM Glutamate**
MAG	375	500 nm	700 ± 300	60 ±10 (2)
MAG_{2p}	425	0.15 ± 0.01 s (7)	340 ± 50 (4)	27 ± 3 (5)
$MAGA_{2p}$ (sensitized excitation)	375	n.d.	12 ± 4 (6)	2.1 ± 0.6 (6)
$MAGA_{2p}$ (azo excitation)	425	0.265 ± 0.003 (4)	30 ± 9 (6)	6 ± 1 (6)

In brackets number of cells averaged. n.d. means not determined.

Table S2. Optimal parameters for the two-photon activation of LiGluR with different PTLs.

	$\lambda_{trans \rightarrow cis}$ (nm)	**Laser Power** (mW)	**Time scan** (s)	$\lambda_{cis \rightarrow trans}$ (nm) or τ_{OFF} (s)	$\mathbf{I_{max}}$ (pA)
MAG (3)	820	50	0.4x10	500 nm (NIR not tested)	117 ± 5
MAG_{2p}	900	30	1.25	0.159 ± 0.007 s (3)	32 ± 12 (3)
$MAGA_{2p}$ (4) (sensitized excitation)	740	30	1.25	n.d.	5.8 ± 1.5
$MAGA_{2p}$ (4) (azo excitation)	880	25	1.25	n.d.	4.8 ± 0.3

In brackets number of cells averaged. n.d. means not determined.

Figure S10. Control for stimulation of LiGluR-MAG astrocyte by calcium imaging

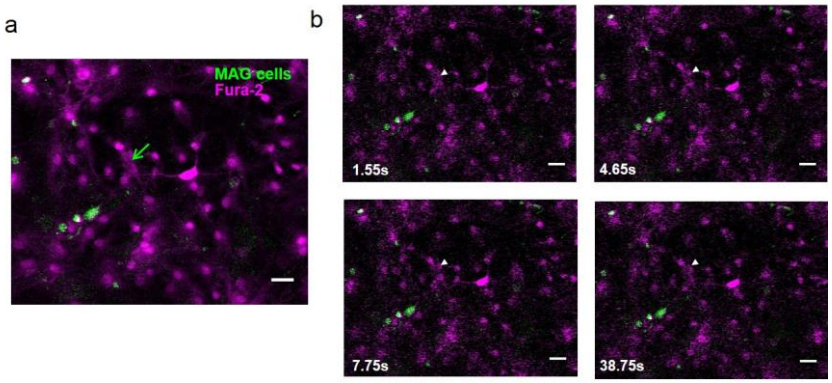

Figure S10. (a and b) Two-photon calcium imaging of cultured astrocytes loaded with Fura-2 (in purple, λ=800 nm) overlapped with an image of GFP fluorescence (in green, λ=900 nm) to identify astrocytes expressing LiGluR-MAG with a 20x/0.5-NA objective. **(a)** Scale bar 50 μm. **(b)** Images at 1.55, 4.65, 7.75 and 38.75 s after targeting the astrocyte pointed with the arrow that does not express GFP with two-photon stimulation (20 targets, 16-pixel diameter, 100 ms per point at 800 nm, 60 mW on sample). Scale bar 20 μm**.**

Movie S1. Two-photon calcium imaging of cultured astrocytes and two-photon stimulation of a LiGluR-MAG positive astrocyte.

Movie of two-photon calcium imaging of cultured astrocytes expressing LiGluR-MAG and loaded with Fura-2, showed in **Figure 6**. The astrocyte expressing GluK2-L439C-eGFP indicated with the arrow (**Fig. 6a**) was targeted with two-photon stimulation (20 targets, 16-pixel diameter, 10 ms per target at λ=800 nm, 60 mW on sample). The movie was recorded immediately after the stimulation (raster-scanning, 100 frames, 1.55 s per image, excitation at λ=800 nm). Scale bar 20 μm.

Movie S2. Two-photon calcium imaging of cultured astrocytes and two-photon stimulation of control astrocytes not expressing LiGluR

Movie of two-photon calcium imaging of cultured astrocytes expressing LiGluR-MAG and loaded with Fura-2, showed in **Figure S10**. For the control, a non-expressing GluK2-L439C-eGFP astrocyte (indicated with the arrow in **Fig. S10**) was targeted with the following stimulation: 20 targets, 16-pixel diameter, 100 ms per point at λ=800 nm, 60 mW on sample and immediately the images were recorded (raster scanning, 100 frames, 1.55 s per image, excitation at λ=800 nm). Scale bar 20 μm.

AVÍS IMPORTANT

El text del capítol 4 ha estat retirat seguint instruccions de l'autora de la tesi, en existir participació d'empreses, existir conveni de confidencialitat o existeix la possibilitat de generar patents

AVISO IMPORTANTE

El texto del capítulo 4 ha sido retirado siguiendo instrucciones de la autora, al existir participación de empresas, convenio de confidencialidad o la posibilidad de generar patentes.

IMPORTANT NOTICE

The text of chapter 4 has been withdrawn on the instructions of the author, as there is participation of undertakings, confidentiality agreement or the ability to generate patent

Chapter 5
Conclusions

The main conclusions drawn from this work are:

- LiGluR permeates enough calcium to trigger Ca^{2+}-dependent secretion, independently of the activation of endogenous VGCC. In consequence, LiGluR expression in hippocampal neurons enables direct and reversible control of neurotransmission with light.
- Amperometric and capacitance measurements demonstrate that LiGluR supports optical control of the physiological molecular mechanism governing exocytosis.
- As an exogenous protein, LiGluR is weakly coupled to the exocytic molecular machinery, which delays the onset of photosecretion, and requires higher calcium influx than VGCC to trigger neurotransmission.
- The graded behavior of LiGluR upon illumination at different wavelengths allows modulating the rate of secretion and APs in chromaffin cells and neurons, respectively.
- LiGluR stands as the best optical tool to reversibly control Ca^{2+}-regulated processes such as neurotransmission.
- LiGluR can be activated by two-photon stimulation when it is conjugated to the photoswitches MAG, MAG_{2p} or $MAGA_{2p}$, suggesting that multiphoton excitation can be applied to other azobenzene-based photoswitches.

- LiGluR responses display different photochemical properties depending on the attached PTL. Two-photon activation of MAG induces a slow and step-function opening of the receptor. In contrast, two-photon activation of LiGluR-MAG_{2p} or LiGluR-$MAGA_{2p}$ is faster and the channel closes spontaneously, enabling singe-wavelength operation of LiGluR.
- MAG_{2p} and $MAGA_{2p}$ are rationally designed MAG derivatives that provide visible absorption, fast thermal relaxation and high two-photon isomerization efficacy based on push-pull substitutions and sensitization of the azobenzene photoisomerization.
- Two-photon stimulation of LiGluR in neurons and astrocytes enables photoactivation with cellular or subcellular resolution.
- A new PTL design method is presented that allows chemically modifying endogenous kainate receptors to photocontrol their activity. PTL length is identified as a critical parameter to obtain optimized photoresponses in GluK1.
- The method to photoswitch endogenous GluK1 receptors can be applied to photosensitize genetically unmodified dorsal root ganglion neurons. The procedure might be extended to study other endogenous receptors under physiological conditions, and give rise to novel optopharmacological therapies.

Chapter 6

Resum:
Control de la neurotransmissió amb llum mitjançant receptors de glutamat fotocommutables

Capítol 1: Introducció

Quan el potencial d'acció (AP) arriba al terminal presinàptic, els canals de calci voltatge-dependents (VGCC) s'obren donant a lloc una entrada de calci (Ca^{2+}) que desencadena la fusió de les vesícules sinàptiques que contenen els neurotransmissors. Subseqüentment, en l'espai sinàptic els neurotransmissors alliberats s'uneixen i activen els receptors postsinàptics induint una resposta elèctrica a la cèl·lula postsinàptica. (**Fig.1.1a**)

Aquest procés de neurotransmissió permet que l'impuls nerviós es propagui d'una neurona a una altra en les sinapsis químiques, que es podrien veure com la unitat funcional del cervell. Com la neurotransmissió és la base de la comunicació entre neurones, aquest procés ha de ser extremadament ràpid i sincronitzat (**Fig. 1.1b**). De fet, aquesta seqüència d'esdeveniments involucrats en la neurotransmissió tenen lloc en menys d'un mil·lisegon, que sorprenentment és el mateix rang de temps en què s'obern els canals voltatge dependents (KATZ and MILEDI 1965, Sabatini and Regehr 1996, Borst and Sakmann 1996).

En l'últim mig segle, s'han fet molts avenços en el coneixement del procés de neurotransmissió, empesos per l'aparició de tècniques noves com el patch-clamp (Neher and Sakmann 1976), la microscòpia electrònica (Heuser et al. 1979) i la de fluorescència (Robinson et al. 1995), l'obtenció d'imatges de super-resolució (Liu et al. 2011, Nair et al. 2013), la manipulació genètica (Fernández-Chacón et al. 2001) o l'estimulació òptica (Neher and Zucker 1993, Watanabe et al. 2013, Banghart et al. 2004, Szobota et al. 2007). Encara queden dubtes per resoldre com ara: quin element molecular és el sensor de Ca^{2+} per la neurotransmissió, quins mecanismes hi ha darrere el reciclatge de vesícules o com es regula la plasticitat sinàptica. Les sinapsis s'adapten contínuament al senyal que reben, el processen i seguidament envien la resposta adequada fent que el cervell sigui capaç d'aprendre, tenir un comportament, emmagatzemar memòries o prendre decisions. Encara no sabem els mecanismes que s'amaguen darrere tota aquesta regulació del cervell, però segurament les sinapsis juguen un paper important, i es necessiten noves eines per a investigar les seves funcions.

La llum té avantatges excepcionals per la manipulació de les funcions biològiques (Miesenbock 2009, Gorostiza and Isacoff 2008b): no és invasiva i normalment no interfereix amb el sistema que s'estudia. El control òptic de l'activitat proteica té una alta resolució espacial, a més a més, de l'estímul es pot fer un patró d'il·luminació i és controlable al nivell dels mil·lisegons. L'any 2002, Miesenbock va visualitzar l'oportunitat de controlar l'activitat neuronal utilitzant proteïnes sensibles a la llum (Zemelman et al. 2002). Pocs anys més tard, aquesta idea es va millorar amb el desenvolupament dels canals iònics fotocommutables (Banghart et al. 2004) i per la introducció d'opsines bacterianes (proteïnes naturalment sensibles a la llum) (Boyden et al. 2005) en cèl·lules neuronals.

L'ús de proteïnes naturalment sensibles a la llum al camp de la neurobiologia ha accelerat el coneixement del cervell. Els actuadors optogenètics, representats principalment per opsines, s'han enfocat en la manipulació directa del potencial de membrana, sent eines excel·lents per activar i silenciar neurones (Kasparov and Herlitze 2013). Tanmateix l'activitat de cada neurona és el resultat coordinat de l'acció d'un gran nombre de participants com poden ser canals iòncs, receptors de membrana o processos intracel·lulars. Per tal de comprendre més enllà el procés

neuronal, mantenint una mínima invasivitat, aquests elements endògens haurien de ser el centre de les noves estratègies per la manipulació òptica de la seva funció.

La modificació química de proteïnes neuronals amb fotocommutadors sintètics s'està encarregant d'aquesta qüestió. L'interès de desplegar el control per llum a totes les proteïnes neuronals possibles es veu reflecit en el gran nombre de lligands fotocommutables que s'han desenvolupat els últims anys, adreçats a tots els tipus de canals iònics i receptors.

La sensibilitat a la llum es pot adquirir utilitzant lligands que commuten entre una forma activa i una d'inactiva amb la llum. Els lligands poden ser bloquejadors de porus, agonistes i antagonistes ortostèrics i moduladors al·lostèrics. Estan units a un grup regulat per llum format per un grup fotocròmic com l'azobenzè, que amb la fotoisomerització pateix un canvi de polaritat, de geometria i de distància d'extrem a extrem de la molècula. Aquest canvi regulat per llum es pot aprofitar per alterar les propietats dels lligands (afinitat, caràcter d'agonista o antagonista) o l'accessibilitat del lligand al centre actiu de la proteïna. Els fotocommutadors sintètics es poden classificar com a lligands fotocròmics solubles (PCLs) si estan lliures en solució, o com a lligands units fotocommutables (PTLs) si s'uneixen covalentment a la proteïna. El desenvolupament d'aquests lligands regulats per llum ha donat lloc als camps de l'optofarmacologia (incloent-hi compostos que poden actuar a receptors endògens) i la farmacologia optogenètica (quan el PTL està covalentment unit a un residu mutat de la proteïna, normalment un receptor) (Kramer, Mourot, and Adesnik 2013).

Objectius

Ajuntant les necessitats de noves eines per la manipulació de la neurotransmissió, amb les perspectives que ofereixen els fotocommutados aquesta tesis ha estat enfocada en l'ús de receptors de glutamat activables per llum (LiGluRs) pel control de l'activitat neuronal (i.e. generació d'AP) i dels processos de neurosecressió.

La possibilitat de sensibilitzar els receptors endògens mitjançant fotocommutadors units a la proteïna evitaria que s'alteressin genèticament les condicions fisiològiques de la neurona degudes a la sobreexpressió. També ens ofereix l'oportunitat d'estudiar el rol dels receptors *in situ*, o bé, els processos en que estan involucrats sense cap

tipus d'alteració del sistema (per exemple la neurotransmissió). A més a més, els fotocommutadors sintètics normalment estan controlats per llum violeta que no té penetrància en teixits, danya les cèl·lules i té una capacitat limitada per enfocar en la direcció axial. Una millora del mètode d'estimulació dels fotocommutadors és necessària si es vol controlar l'activitat dels receptors *in situ* en teixit intacte.

El gran objectiu d'aquesta tesi és utilitzar els receptors endògens de les neurones pel control òptic de l'activitat neuronal i del procés de neurotransmissió, i sent capaços d'estimular aquests receptors en volums petits (per exemple, terminals sinàptics). D'aquesta manera, la llum és una eina única per conèixer la fisiologia neuronal i entendre el funcionament dels circuits neuronals: des de la integració dels inputs sinàptics en neurones individuals, a l'operativitat d'estructures cerebrals. Per tal d'assolir aquesta meta, en aquesta tesi hem plantejat tres objectius diferents:

- Controlar directament la neurotransmissió amb llum, aprofitant la permeabilitat del Ca^{2+} dels receptors de glutamat per manipular la $[Ca^{2+}]$ intracel·lular i desencadenar l'exocitosi dels neurotransmissors. Aquest objectiu està desenvolupat al **capítol 2**.
- Demostrar l'excitabilitat per dos fotons dels receptors de glutamat modificats químicament amb fotocommutadors basats en l'azobenzè. Aquest objectiu és la base del **capítol 3**.
- Desenvolupar un mètode eficient i versàtil pel fotocontrol de receptors endògens utilitzant lligands covalents, es descriu en el **capítol 4**.

Capítol 2: Control reversible de processos regulats per Ca^{2+} per mitjà del LiGluR.

El Ca^{2+} és un missatger secundari de molts processos cel·lulars, per exemple és l'activador de l'exocitosi i en conseqüència de la neurotransmissió (veure **secció 1.1**). Actualment, hi ha poques eines ideades per la manipulació de la $[Ca^{2+}]$ intracel·lular. En aquest capítol, el nostre objectiu és demostrar que el LiGluR, que és permeable a Ca^{2+}, pot ser utilitzat com a eina per controlar reversiblement la neurosecreció, afectant directament la $[Ca^{2+}]$ intracel·lular. Per tal d'assolir aquest objectiu, LiGluR es va expressar en cultius primaris de cèl·lules cromafins bovines. Aquestes cèl·lules

neuroendocrines actuen com a terminals presinàptics gegants, i es mantenen com un model clàssic per estudiar l'exocitosi. Es va mesurar la secreció en les cèl·lules cromafins per mitjà de dues tècniques: l'amperometria i la mesura de la capacitància de membrana. Mentrestant l'activació del LiGluR es va controlar amb il·luminació amb llum de 380 nm, per l'obertura del canal, o bé amb llum a 500 nm, pel tancament d'aquest. El següent pas va ser millorar l'aplicació del LiGluR, a l'hora d'ampliar aquest control a una sinapsi química real, en cultius de neurones hipocampals.

Les troballes principals d'aquest treball han estat:

- La secreció, mesurada per amperometria, és induïda quan s'obre LiGluR amb llum en cèl·lules cromafins, mantenint els VGCC bloquejats. La secreció activada per llum assoleix una freqüència de 2 a 4 Hz, valor típic per cèl·lules cromafins. L'explosió d'espigues s'inicia amb un retard de pocs segons, i progressivament s'atura un cop el LiGluR és tancat amb llum a 500 nm. Aquest procés es pot repetir reversiblement fins que el reservori de grànuls secretoris de les cèl·lules s'exhaureix (veure **secció 2.1**, **Fig. 1** i **2**).
- L'anàlisi de la forma de les espigues amperomètriques induïdes per llum revela que la càrrega alliberada a cada esdeveniment es correspon amb els valors normals per cèl·lules cromafins. Tanmateix, els esdeveniments estimulats per llum es caracteritzen per una cinètica més lenta que podria ser resultat d'un alliberament més lent de catecolamines o bé per la detecció difusa d'un esdeveniment normal (veure **secció 2.1 Fig. 3**).
- La mesura directa del component de Ca^{2+} dels corrents de LiGluR conjuntament amb la mesura dels canvis de capacitància de la membrana mostren que:
    - Els corrents de Ca^{2+} a través de LiGluR, que corresponen al ~10% del fotocorrent total, són els responsables de desencadenar la fusió de grànuls secretors (**secció 2.1**, **Fig. 4**).
    - La dependència de la secreció activada per llum amb l'entrada de Ca^{2+} s'ajusta a una funció quadràtica (**secció 2.1**, **Fig. 5c**), similar al cas descrit per altres sinapsis (Leão and von Gersdorff 2009). Aquest

descobriment, evidencia que el LiGluR és capaç d'activar els mecanismes moleculars de la exocitosi depenent de Ca^{2+} de manera artificial.

- Del mateix ajust de les dades de secreció induïda per llum a la mateixa funció, s'ha calculat una constant dues vegades més petita en comparació a l'obtinguda per la secreció induïda per despolarització. Aquesta diferència de valors ens indica que l'exocitosi és més eficientment desencadenada per l'entrada de Ca^{2+} a través dels VGCC.

- L'acoblament entre els LiGluR i el sensor de Ca^{2+} de l'exocitosi es va estudiar mitjançant l'aplicació intracel·lular de quelants de Ca^{2+} exògens, BAPTA i EGTA (**secció 2.1**, **Fig. 6**). Els experiments mostren que la secreció activada per llum és més sensible als dos quelants, BAPTA i EGTA, que l'activada per despolarització. Aquesta diferència de sensibilitat apunta a acoblament més feble de l'entrada de Ca^{2+} per llum (per exemple, podria ser degut a una major distància entre el punt de secreció i els LiGluR), que també explicaria l'eficàcia menor de l'entrada de Ca^{2+} i induïda per llum i el retard en l'inici de la secreció detectat per amperometria.

- L'activació de la neurotransmissió per llum es va estudiar amb el següent mètode en cultius de neurones hipocampals: es va registrar el potencial de membrana de neurones LiGluR(-) que visualment se sobreposaven amb neurones LiGluR(+), i per tant potencialment estaven connectades (**secció 2.3**, **Fig. 3b**). Els VGCC es van bloquejar per evitar l'entrada de Ca^{2+} per la despolarització de la neurona LiGluR(+). Llavors, es va aplicar el pols de llum i es va generar un tren de potencials d'acció, que progressivament es va atenuar un cop el LiGluR es va tancar (**secció 2.3**, **Fig 3d**). La freqüència màxima assolida pel tren d'AP és de 6 Hz, de mitjana. Tal com s'ha observat en les cèl·lules cromafins, hi ha un retard més llarg de l'habitual entre l'inici de l'estímul de llum i la generació del primer AP (Sabatini and Regehr 1996).

- Aprofitant la dependència de l'amplitud del corrent del LiGluR amb la longitud d'ona de la il·luminació (Gorostiza et al. 2007) (**secció 2.3**, **Fig. 2a**), l'entrada

de Ca^{2+} a través del canal pot ser ajustada òpticament. En cèl·lules cromafins, la freqüència de secreció es va ajustar segons la longitud d'ona de l'estímul (**secció 2.3**, **Fig. 2b**). De la mateixa manera, la secreció estimulada per llum en neurones LiGluR(+) permet una neurotransmissió modulada pel color de la llum, i en conseqüència un control de la freqüència que dispara la neurona postsinàptica.

- L'entrada de Ca^{2+} mitjançada pel LiGluR és prou gran per desencadenar l'exocitosi regulada en cèl·lules cromafins i neurones. A més a més, la (neuro)secreció induïda per llum és modulada segons la longitud d'ona de la il·luminació. Aquesta nova aplicació del LiGluR obre la possibilitat de controlar reversiblement l'activitat a sinapsis individuals, que podria ajudar a entendre les propietats computacionals de les neurones i desenteranyinar el funcionament del circuit cerebral.

Aquest estudi ha estat publicat en dos articles. El primer es focalitza en la manipulació amb llum de l'exocitosi en cèl·lules cromafins, mentre que el segon s'ha utilitzat el mateix procediment per regular directament la neurotransmissió en neurones.

- Les **seccions 2.1** i **2.2** reprodueixen el següent article:

Izquierdo-Serra, D. Trauner, A. Llobet, and P. Gorostiza (2013). Optical control of calcium-regulated exocytosis. Biochimica et Biophysica Acta-General Subjects 1830(3):2853-60. doi: 10.1016/j.bbagen.2012.11.003

- La **secció 2.3** reprodueix la segona part d'aquest estudi*:*

Izquierdo-Serra M, Trauner D, Llobet A and Gorostiza P (2013) Optical modulation of neurotransmission using calcium photocurrents through the ion channel LiGluR. Front. Mol. Neurosci. 6:3. 10.3389/fnmol.2013.00003.

Capítol 3: Estimulació cel·lular per dos fotons de fotocommutadors basats en l'azobenzè.

Un mètode efectiu per tal d'interrogar les funcions neuronals en teixits intactes, amb una resolució cel·lular i subcel·lular ha de tenir una elevada resolució en 3D i ha de penetrar els teixits. L'excitació per multifotó amb llum infraroja propera (NIR) permet una estimulació amb aquestes característiques, i fins ara s'ha aplicat a actuadors

òptics tals com els compostos engabiats o l'optogènetica. Tanmateix, l'estimulació per dos fotons de fotocommutadors sintètics encara no ha estat estudiada. En aquest capítol, s'ha estudiat l'estimulació per dos fotons del LiGluR, incloent-hi el disseny, la síntesi i les aplicacions de dos compostos nous, basats en l'estructura de MAG, que volen millorar l'absorció a dos fotons del commutador azobenzè. El compost MAG_{2p} és un derivat amb l'espectre d'absorbància desplaçat cap al vermell amb una relaxació tèrmica ràpida. El segon compost és una modificació del MAG_{2p} ($MAGA_{2p}$), en la que s'incorpora una antena recol·lectora de llum amb la idea de sensitibitzar la isomerització de l'azobenzè per mitjà de transmissió d'energia per ressonància (RET) al grup fotoisomeritzable (veure estructures a la **secció 3.1,Fig. 1**).

Les troballes principals d'aquest projecte són:

- La caracterització fotoquímica dels nous PTLs pel LiGluR, Mag_{2p} i $MAGA_{2p}$, presenten un desplaçament cap a la dreta en l'espectre d'absorbància en comparació amb el compost original MAG (veure **secció 3.1**, **Fig. 2**), amb el pic de màxima absorbància situat a ~475 nm. Aquest canvi de l'espectre d'absorbància està acompanyat d'un escurçament de la vida mitjana de l'isòmer *cis* (veure **secció 3.2**, **Fig S2**). Com a conseqüència, aquests compostos relaxen tèrmicament de *cis* a *trans* en qüestió de mil·lisegons, permetent la completa operativitat del LiGluR amb una sola longitud d'ona. Les propietats fotoquímiques descrites pels nous compostos lliures en solució són transtuïdes al LiGluR un cop són conjugats amb el receptor, aquest pot ser activat amb il·luminació a 425 nm i tancat espontàniament a la fi del pols de llum (veure **secció 3.1**, **Fig. 3a** i **secció 3.2**, **Fig. S5** i **Taula S1**).
- L'excitació directa de l'antena col·lectora de llum del $MAGA_{2p}$ amb llum a 355 nm, aconseguiex sensitibitzar la fotoisimerització de *trans* a *cis*, originant una major fotoconversió de $MAGA_{2p}$ respecte al compost MAG_{2p}, tant amb el compost lliure en solució (veure **secció 3.1**, **Fig.2** i **secció 3.2**, **Fig. S3** i **S4**) , com quan es troba conjugat al receptor (veure **secció 3.2**, i **Fig. S5**).
- L'activació òptima per dos fotons del LiGluR-MAG, mesurada per patch clamp, s'obté amb repetides estimulacions amb llum a 820 nm (veure **secció 3.1**, **Fig. 3** i **4** i **secció 3.2 Taula S2**), i es tanca reversiblement després d'aplicar llum a

500 nm. Aquesta activació està caracteritzada per respostes petites a l'estimulació per dos fotons, d'entre 5 i 10 pA. Tanmateix, l'estabilitat tèrmica del *cis*-MAG permet l'acumulació de canals en estat obert després de repetir varis escombrats d'estimulació i deixa que s'assoleixin corrents per sobre els 100 pA.

- L'activació òptima per dos fotons del LiGluR-MAG_{2p} es dóna quan s'usa llum a 900 nm, sent suficients entre un i pocs escàners cel·lulars per obtenir el corrent màxim (32 ± 12 pA de mitjana), que reversiblement disminueix un cop acaba l'estímul (veure **secció 3.1**, **Fig. 3** i **4** i **secció 3.2**, **Taula S2**).
- L'activació per dos fotons del LiGluR-$MAGA_{2p}$ succeeix a dos rangs de l'espectre separats. Escàners de la cèl·lula individuals saturen els corrents de LiGluR a 880 nm (5.8 ± 1.5 pA, de mitjana, corresponent a l'absorbància directa de l'azobenzè) i 740 nm (4.8 ± 0.3 pA, de mitjana, corresponent a l'antena sensitibitzadora) (veure **seccions 3.1**, **Fig. 3** i **4** i **secció 3.2**, **Table S2**). Semblant al cas de MAG_{2p}, els corrents disminueixen espontàniament en acabar l'estímul.
- Els compostos desplaçats cap al vermell tenen una major ràtio 2P/1P de corrent LiGluR entre respecte MAG (veure **secció 3.1**, **Fig. 4**), indicant que posseeixen una major eficiència a l'hora d'activar LiGluR per dos fotons. Aquest fet ésta recolzat per l'estimulació més breu i menor potència que són necessàries per obtenir corrents saturats un cop LiGluR és conjugat amb MAG2p i MAGA2p.
- El compost de relaxació ràpida i d'operativitat amb una sola longitud d'ona, LiGluR-MAG_{2p} es va utilitzar per induir corrents i activar neurones hipocamapls amb estimulació per dos fotons, i en alguns casos es van desencadenar trens d'AP (veure **secció 3.1**, **Fig. 5**). En contraposició, el compost biestable LiGluR-MAG indueix corrents a cultius d'astròcits amb una resolució cel·lular i subcel·lular, a causa de l'estimulació per dos fotons (veure **secció 3.1, Fig. 6**). Aquests corrents indueixen onades de calci als astròcits veïns (veure **secció 3.1, Fig. 6 i secció 3.2, Fig. S10** i **Movie S1 i S2**).

AVÍS IMPORTANT

El text de les pàgines 172 a 174 ha estat retirat seguint instruccions de l'autora de la tesi, en existir participació d'empreses, existir conveni de confidencialitat o existeix la possibilitat de generar patents

AVISO IMPORTANTE

El texto de las páginas 172 a 174 ha sido retirado siguiendo instrucciones de la autora, al existir participación de empresas, convenio de confidencialidad o la posibilidad de generar patentes.

IMPORTANT NOTICE

The text of pages from 172 to 174 has been withdrawn on the instructions of the author, as there is participation of undertakings, confidentiality agreement or the ability to generate patent

Capítol 5: Conclusions

Les principals conclusions que es poden extreure d'aquest treball són:

- El LiGluR és suficientment permeable a Ca^{2+} per a activar secreció dependent de Ca^{2+}, independentment de l'activació dels VGCC endògens. De la mateixa manera, l'expressió de LiGluR en neurones hipocampals permet un control directe i reversible del procés de neurotransmissió amb llum.
- Mitjançant la tècnica d'amperometria i de mesura de la capacitància s´ha demostrat que LiGluR és capaç d'activar la maquinària molecular fisiològica que regeix l'exocitosi.
- Sent una proteïna exògena, el LiGluR està dèbilment acoblat a la maquinària molecular exocítica. Aquest fet dóna lloc a un retard en l'inici de la fotosecreció i requereix una entrada de Ca^{2+} major que la necessària pels VGCC per desencadenar la neurotransmissió.
- L'obertura gradual de LiGluR, segons la longitud d'ona a la qual és il·luminat, permet la modulació segons el color de la llum de la freqüència de secreció i d'aparició de potencials d'acció.
- D'aquesta manera, LiGluR és manté com la millor eina diponible enfocada al control de processos dependents de Ca^{2+}, tals com la neurotransmissió.
- LiGluR pot ser activat mitjançant l'excitació de dos fotons estan conjugat amb qualsevol dels tres PTLs descrits al capítol 3: MAG, MAG_{2p} i $MAGA_{2p}$. Fet que suggereix que l'estimulació multifotó es pot aplicar a altres fotocommutadors basats en un grup azobenzè.
- Les propietats fotoquímiques dels corrents induïts pel LiGluR són diverses segons el PTL que ha estat conjugat. L'activació per dos fotons del compost MAG resulta en una obertura del receptor lenta i esglaonada. Per contra, l'activació per dos fotons de LiGluR-MAG_{2p} or LiGluR-$MAGA_{2p}$ és més ràpida i el receptor tanca espontàniament, permetent una completa operativitat del receptor LiGluR amb l'ús d'una sola longitud d'ona.

- MAG_{2p} i $MAGA_{2p}$ són derivats del compost MAG dissenyats racionalment per proporcionar absorció de llum visible, una relaxació tèrmica ràpida i una eficiència d'isomerització per dos fotons més elevada. El disseny està basat en substitucions en grups pròxims a l'azobenzè i la sensibilització de la fotoisomerització d'aquest grup.
- L'estimulació per dos fotons del LiGluR expressat en neurones i astròcits permet l'activació d'aquestes cèl·lules amb resolució cel·lular i subcel·lular.
- Per mitjà del mètode presentat al capítol 4, els receptors endògens poden ser modificats químicament per tal de controlar la seva activitat amb llum. La llargada i flexibilitat dels compostos són dos paràmetres crítics que cal optimitzar si es vol obtenir la millor fotoresposta i minimitzar l'activitat basal.
- El mètode per fotocommutar els receptors GluK1 endògens es pot aplicar per fotosensitibitzar neurones del gangli de l'arrel dorsal no modificades genèticament. El procediment es podria estendre per estudiar altres receptors endògens en condicions fisiològiques, donant lloc a noves teràpies optofarmacològiques.

Acknowledgements

Vull agrair l'ajuda i la disponibilitat dels laboratoris amb qui hem col·laborat, i/o he visitat durant el doctorat. Començant pel cop de mà inicial rebut pel department, al complert, de Neurobiologia Cel·lular i Molecular, un suport que hem tingut en tot moment: gràcies pels mil consells i ajuda que m´heu donat. Agradecer también a Guillermo Álvarez de Toledo y Margarita Segovia por la paciencia en enseñarme las técnicas de amperometria y *cell-attached*. Many thanks to Rafael Yuste and all the members of his lab for their kind help and support. No em vull oblidar de l'Oscar Seira, del laboratori de l´Antonio del Rio i del Gerard Callejo del laboratori de Xavier Gasull per ajudar-me a aconseguir el cultiu de DRGs. Finalmente agradecer a Juan Lerma y a los miembros de su laboratorio, especialmente Sergio Valbuena, por permitirme realizar los experimentos finales de esta tesis.

We thank Ehud Isacoff for providing us the GluK2-L439C-eGFP construct, Miguel Valverde for the construct of VGCC P/Q-type, Geoffrey Swanson for the GluK1(Q)-2b(GGAA) and Dirk Trauner for providing MAG compound.

Agraeixo a CIBER-BBN per la beca d'iniciació a la inverstigació disfrutada durant el primer any de formació, i al Ministerio de Educación per la beca rebuda de *Formación de Profesorado Universitario* (FPU, AP2008-03313). Agraeixo també al projecte FOCUS de la Comissió Europea (FP7-ICT-2009-270483).

En les següents línies voldria agrair d'una manera més personal, a cada un dels que heu fet possible que existeixi aquesta tesi.

Començant pel Pau, gràcies per ensenyar-me tot el que sé de ciència i una mica més. Una vegada vaig dir que als agraïments posaria allò que sempre dius: *prova això que només són 5 minuts*; en aquestes pàgines hi ha una recol·lecta d'uns quants 5 minuts. Al final, sembla que així comencen els experiments bonics, en 5 minuts. Vull agrair-te, sobretot, la teva part de responsabilitat en el fet que aquest anys hagi pogut dedicar-me al que m'agrada, i ho hagi gaudit (... més del que esperava).

Gràcies a tots els companys del grup, sou unes persones extraordinàries. Gràcies al Marcel i l'Andrés per la paciència i ser els primers que em vau ensenyar el món dels laboratoris. Marisabel i Núria sou un pou d'experiència, aniré recordant les vostres paraules allà on vagi. Silvia, gràcies per compartir constantment el teu punt de vista, ha estat sempre utilíssim! Ets brillant. Ari, gràcies per la teva disponibilitat, per donar el 200% de tu a cada cosa que fas, ets sempre una garantia d'èxit. Se'm fa estrany posar-te dins la gent del grup, ja que portem molts anys plegades, Helena; que maco ha estat tenir-te a prop aquest temps. Vull agrair també l'estudiant de secundària Júlia pels bons moments que vam passar fent el treball. Fa pocs mesos que has arribat, però t´has espavilat de seguida, i has estat essencial en aquesta recta final, gràcies Aida.

Encara que alguns sigueu del grup us volia mencionar a part: Antonio, Ana, Marta, Amadeu, Jordi, els *químics*; cap d'aquestes històries hagués estat possible sense la vostra feina. Gràcies per l'esforç extra que heu de fer per entendre els capricis dels *biòlegs*.

El *set up* m'ha estat a punt de guanyar si no hagués estat pels vostres consells Artur, Ana Priscil·la, David Albrecht, Fran, Marcel, Marisabel i David Soto. I em toca també mencionar a tota la quarta i cinquena planta de Bellvitge que segur que us he demanat de tot durant aquests anys!

Gràcies a tots aquells que heu fet que desconnecti. Santi, contigo una no deja de aprender cosas nuevas, un placer compartir horas de trabajo, y cervezas de viernes. A vosaltres també, gràcies per *la* millor cervesa de la setmana i les nits de divendres, Joan i Diana. Dianeta, gracias por ayudar a hacer realidad un pequeño gran sueño que tenía de hace mucho tiempo. Gracias Thomas por descubrirnos Barcelona.

Gracias Cristina por los cuscus de pipas de calabaza, y lo que estos conllevan. Gràcies Rocco i Núria per les visites carregades de xocolata i ànims.

A dues grans persones que vaig conèixer a la carrera. Carmen gràcies per ser-hi, tot i la distància. Natàlia, fer la carrera i la tesi i amb tu ha estat una experiència intensa, inoblidable i meravellosa, gràcies per cada moment que has estat aquí.

A tots els tiets, tietes, cosins i cosines; també als tiets i tietes 'postissos' que tinc la sort de tenir. Grazie a Rosa e ed Enzo per l'estate ad Amalfi.

Per suposat no podia faltar la meva gran família, el meu petit orgull.

Jordi, mare, pare, i Fina, gràcies i gràcies pel recolzament que he rebut durant aquesta tesi, i sempre. M'ho poseu tot una mica més fàcil (gairebé sempre). També gràcies als que acabeu de fer que tot això vagi sobre rodes, Miquel i Sergi. Petita, tens tants anys com els que he dedicat a fer aquest treball, ets un amor de persona, gràcies Laura per totes les abraçades!

Sempre has estat al meu costat, hi ets i hi seràs, així que no podies faltar en aquesta llista, Lidia.

Finalment, Carlo. Aquests anys, en aquesta tesi, has estat el millor recolzament, el millor crític, l'ajuda més gran que he tingut en tots els sentits, mil gràcies bitxo. Ets increïble, tenir-te a prop és el que m'omple de forces cada matí i em fa sortir de casa amb un somriure. Et trobaré tan a faltar!

References

A. Catterall, William, Edward Perez-Reyes, Terrance P. Snutch, and Joerg Striessnig. 2013. "Voltage-gated calcium channels, introduction. Last modified on 14/08/2013. Accessed on20/02/2014. http://www.iuphar-db.org/DATABASE/FamilyIntroductionForward?familyId=80." IUPHAR database (IUPHAR-DB).

Abrams, Z. R., A. Warrier, Y. Wang, D. Trauner, and X. Zhang. 2012. "Tunable oscillations in the Purkinje neuron." *Phys Rev E Stat Nonlin Soft Matter Phys* 85 (4 Pt 1):041905. doi: 10.1103/PhysRevE.85.041905

Adler, E. M., G. J. Augustine, S. N. Duffy, and M. P. Charlton. 1991. "Alien intracellular calcium chelators attenuate neurotransmitter release at the squid giant synapse." *J Neurosci* 11 (6):1496-507.

Alabi, A. A., and R. W. Tsien. 2012. "Synaptic vesicle pools and dynamics." *Cold Spring Harb Perspect Biol* 4 (8):a013680. doi: 10.1101/cshperspect.a013680.

Albillos, A., G. Dernick, H. Horstmann, W. Almers, G. Alvarez de Toledo, and M. Lindau. 1997. "The exocytotic event in chromaffin cells revealed by patch amperometry." *Nature* 389 (6650):509-12. doi: 10.1038/39081.

Alivisatos, A. P., M. Chun, G. M. Church, K. Deisseroth, J. P. Donoghue, R. J. Greenspan, P. L. McEuen, M. L. Roukes, T. J. Sejnowski, P. S. Weiss, and R. Yuste. 2013. "Neuroscience. The brain activity map." *Science* 339 (6125):1284-5. doi: 10.1126/science.1236939.

Alvarez de Toledo, G., R. Fernández-Chacón, and J. M. Fernández. 1993. "Release of secretory products during transient vesicle fusion." *Nature* 363 (6429):554-8. doi: 10.1038/363554a0.

Alés, E., L. Tabares, J. M. Poyato, V. Valero, M. Lindau, and G. Alvarez de Toledo. 1999. "High calcium concentrations shift the mode of exocytosis to the kiss-and-run mechanism." *Nat Cell Biol* 1 (1):40-4. doi: 10.1038/9012.

Araya, R., J. Jiang, K. B. Eisenthal, and R. Yuste. 2006. "The spine neck filters membrane potentials." *Proc Natl Acad Sci U S A* 103 (47):17961-6. doi: 10.1073/pnas.0608755103.

Bahn, S., B. Volk, and W. Wisden. 1994. "Kainate receptor gene expression in the developing rat brain." *J Neurosci* 14 (9):5525-47.

Banghart, M., K. Borges, E. Isacoff, D. Trauner, and R. H. Kramer. 2004. "Light-activated ion channels for remote control of neuronal firing." *Nat Neurosci* 7 (12):1381-6. doi: 10.1038/nn1356.

Banghart, M. R., A. Mourot, D. L. Fortin, J. Z. Yao, R. H. Kramer, and D. Trauner. 2009. "Photochromic blockers of voltage-gated potassium channels." *Angew Chem Int Ed Engl* 48 (48):9097-101. doi: 10.1002/anie.200904504.

Bartels, E., N. H. Wassermann, and B. F. Erlanger. 1971. "Photochromic activators of the acetylcholine receptor." *Proc Natl Acad Sci U S A* 68 (8):1820-3.

Bean, B. P. 2007. "The action potential in mammalian central neurons." *Nat Rev Neurosci* 8 (6):451-65. doi: 10.1038/nrn2148.

Beaudoin, G. M., S. H. Lee, D. Singh, Y. Yuan, Y. G. Ng, L. F. Reichardt, and J. Arikkath. 2012. "Culturing pyramidal neurons from the early postnatal mouse hippocampus and cortex." *Nat Protoc* 7 (9):1741-54. doi: 10.1038/nprot.2012.099.

Bennett, M. K., N. Calakos, and R. H. Scheller. 1992. "Syntaxin: a synaptic protein implicated in docking of synaptic vesicles at presynaptic active zones." *Science* 257 (5067):255-9.

Bettler, B., J. Boulter, I. Hermans-Borgmeyer, A. O'Shea-Greenfield, E. S. Deneris, C. Moll, U. Borgmeyer, M. Hollmann, and S. Heinemann. 1990. "Cloning of a novel glutamate receptor subunit, GluR5: expression in the nervous system during development." *Neuron* 5 (5):583-95.

Borst, J. G., and B. Sakmann. 1996. "Calcium influx and transmitter release in a fast CNS synapse." *Nature* 383 (6599):431-4. doi: 10.1038/383431a0.

Bowie, D., and M. L. Mayer. 1995. "Inward rectification of both AMPA and kainate subtype glutamate receptors generated by polyamine-mediated ion channel block." *Neuron* 15 (2):453-62.

Boyden, E. S., F. Zhang, E. Bamberg, G. Nagel, and K. Deisseroth. 2005. "Millisecond-timescale, genetically targeted optical control of neural activity." In *Nat Neurosci*, 1263-8. United States.

Branco, T., B. A. Clark, and M. Häusser. 2010. "Dendritic discrimination of temporal input sequences in cortical neurons." *Science* 329 (5999):1671-5. doi: 10.1126/science.1189664.

Brejc, K., W. J. van Dijk, R. V. Klaassen, M. Schuurmans, J. van Der Oost, A. B. Smit, and T. K. Sixma. 2001. "Crystal structure of an ACh-binding protein reveals the ligand-binding domain of nicotinic receptors." *Nature* 411 (6835):269-76. doi: 10.1038/35077011.

Browne, L. E., J. P. Nunes, J. A. Sim, V. Chudasama, L. Bragg, S. Caddick, and R. Alan North. 2014. "Optical control of trimeric P2X receptors and acid-sensing ion channels." *Proc Natl Acad Sci U S A* 111 (1):521-6. doi: 10.1073/pnas.1318582111.

Bucurenciu, I., A. Kulik, B. Schwaller, M. Frotscher, and P. Jonas. 2008. "Nanodomain coupling between Ca2+ channels and Ca2+ sensors promotes fast and efficient transmitter release at a cortical GABAergic synapse." *Neuron* 57 (4):536-45. doi: 10.1016/j.neuron.2007.12.026.

Bureau, I., G. M. Shepherd, and K. Svoboda. 2004. "Precise development of functional and anatomical columns in the neocortex." *Neuron* 42 (5):789-801. doi: 10.1016/j.neuron.2004.05.002.

Burré, J., M. Sharma, T. Tsetsenis, V. Buchman, M. R. Etherton, and T. C. Südhof. 2010. "Alpha-synuclein promotes SNARE-complex assembly in vivo and in vitro." *Science* 329 (5999):1663-7. doi: 10.1126/science.1195227.

Callaway, E. M., and L. C. Katz. 1993. "Photostimulation using caged glutamate reveals functional circuitry in living brain slices." *Proc Natl Acad Sci U S A* 90 (16):7661-5.

Caporale, N., K. D. Kolstad, T. Lee, I. Tochitsky, D. Dalkara, D. Trauner, R. Kramer, Y. Dan, E. Y. Isacoff, and J. G. Flannery. 2011. "LiGluR restores visual responses in rodent models of inherited blindness." *Mol Ther* 19 (7):1212-9. doi: 10.1038/mt.2011.103.

Catterall, W. A. 2000. "Structure and regulation of voltage-gated Ca2+ channels." *Annu Rev Cell Dev Biol* 16:521-55. doi: 10.1146/annurev.cellbio.16.1.521.

Catterall, W. A., E. Perez-Reyes, T. P. Snutch, and J. Striessnig. 2005. "International Union of Pharmacology. XLVIII. Nomenclature and structure-function relationships of voltage-gated calcium channels." *Pharmacol Rev* 57 (4):411-25. doi: 10.1124/pr.57.4.5.

Chabala, L. D., and H. A. Lester. 1986. "Activation of acetylcholine receptor channels by covalently bound agonists in cultured rat myoballs." *J Physiol* 379:83-108.

Chambers, J. J., M. R. Banghart, D. Trauner, and R. H. Kramer. 2006. "Light-induced depolarization of neurons using a modified Shaker K(+) channel and a molecular photoswitch." *J Neurophysiol* 96 (5):2792-6. doi: 10.1152/jn.00318.2006.

Changeux, J. P., and S. J. Edelstein. 1998. "Allosteric receptors after 30 years." *Neuron* 21 (5):959-80.

Choquet, D., and A. Triller. 2013. "The dynamic synapse." *Neuron* 80 (3):691-703. doi: 10.1016/j.neuron.2013.10.013.

Chow, B. Y., X. Han, A. S. Dobry, X. Qian, A. S. Chuong, M. Li, M. A. Henninger, G. M. Belfort, Y. Lin, P. E. Monahan, and E. S. Boyden. 2010. "High-performance genetically targetable optical neural silencing by light-driven proton pumps." *Nature* 463 (7277):98-102. doi: 10.1038/nature08652.

Chow H., Robert, and Ludolf von Rüden. 1995a. "Electrochemical Detection of secretion from single cells." In *Single-Channel Recording*, edited by Bert Sakmann and Erwin Neher, 245-275. New York: Plenum Press.

Chow H., Robert, and Ludolf von Rüden. 1995b. "Electrochemical Detection of secretion from single cells." In *Single-Channel Recording*, edited by Bert Sakmann and Erwin Neher. New York: Plenum Press.

Chow, R. H., L. von Rüden, and E. Neher. 1992. "Delay in vesicle fusion revealed by electrochemical monitoring of single secretory events in adrenal chromaffin cells." *Nature* 356 (6364):60-3. doi: 10.1038/356060a0.

Cohen, F. S., and G. B. Melikyan. 2004. "The energetics of membrane fusion from binding, through hemifusion, pore formation, and pore enlargement." *J Membr Biol* 199 (1):1-14.

Colonnier, M. 1968. "Synaptic patterns on different cell types in the different laminae of the cat visual cortex. An electron microscope study." *Brain Res* 9 (2):268-87.

Conley, Edward C. 1996. *The ion channel Facts Book I: extracellular ligand-gated ion channels*. Vol. I. London: Academic Press Limited.

Connolly, C. N., and K. A. Wafford. 2004. "The Cys-loop superfamily of ligand-gated ion channels: the impact of receptor structure on function." *Biochem Soc Trans* 32 (Pt3):529-34. doi: 10.1042/BST0320529.

Del Castillo, J., and B. Katz. 1954a. "Quantal components of the end-plate potential." *J Physiol* 124 (3):560-73.

Del Castillo, J., and B. Katz. 1954b. "The effect of magnesium on the activity of motor nerve endings." *J Physiol* 124 (3):553-9.

Denk, W., J. H. Strickler, and W. W. Webb. 1990. "Two-photon laser scanning fluorescence microscopy." *Science* 248 (4951):73-6.

Denker, A., and S. O. Rizzoli. 2010. "Synaptic vesicle pools: an update." *Front Synaptic Neurosci* 2:135. doi: 10.3389/fnsyn.2010.00135.

Dernick, G., L. W. Gong, L. Tabares, G. Alvarez de Toledo, and M. Lindau. 2005. "Patch amperometry: high-resolution measurements of single-vesicle fusion and release." In *Nat Methods*, 699-708. United States.

Dernick, Gregor, Guillermo Alvarez de Toledo, and Manfred Lindau. 2007. "The Patch Amperometry Technique: Design of a Method to Study Exocytosis of Single Vesicles." In *Electrochemical Methods for Neuroscience*, edited by Adrian C Michael and Laura M Borland. Pennsylvania: CRC Press.

Dodge, F. A., Jr., and R. Rahamimoff. 1967. "Co-operative action a calcium ions in transmitter release at the neuromuscular junction." *J Physiol* 193 (2):419-32.

Dormán, G., and G. D. Prestwich. 1994. "Benzophenone photophores in biochemistry." *Biochemistry* 33 (19):5661-73.

Doumazane, E., P. Scholler, L. Fabre, J. M. Zwier, E. Trinquet, J. P. Pin, and P. Rondard. 2013. "Illuminating the activation mechanisms and allosteric properties of metabotropic glutamate receptors." *Proc Natl Acad Sci U S A* 110 (15):E1416-25. doi: 10.1073/pnas.1215615110.

Duchen, M.R, J. Millar, and T.J. Biscoe. 1990. "Voltammetric measurement of catecholamine release from isolated rat chromaffin cells." *Journal of Physiology* 426.

Dulubova, I., M. Khvotchev, S. Liu, I. Huryeva, T. C. Südhof, and J. Rizo. 2007. "Munc18-1 binds directly to the neuronal SNARE complex." *Proc Natl Acad Sci U S A* 104 (8):2697-702. doi: 10.1073/pnas.0611318104.

Dulubova, I., S. Sugita, S. Hill, M. Hosaka, I. Fernandez, T. C. Südhof, and J. Rizo. 1999. "A conformational switch in syntaxin during exocytosis: role of munc18." *EMBO J* 18 (16):4372-82. doi: 10.1093/emboj/18.16.4372.

Egebjerg, J., and S. F. Heinemann. 1993. "Ca2+ permeability of unedited and edited versions of the kainate selective glutamate receptor GluR6." *Proc Natl Acad Sci U S A* 90 (2):755-9.

Eggermann, E., I. Bucurenciu, S. P. Goswami, and P. Jonas. 2012. "Nanodomain coupling between Ca^{2+} channels and sensors of exocytosis at fast mammalian synapses." *Nat Rev Neurosci* 13 (1):7-21. doi: 10.1038/nrn3125.

Ellis-Davies, G. C. 2007. "Caged compounds: photorelease technology for control of cellular chemistry and physiology." *Nat Methods* 4 (8):619-28. doi: 10.1038/nmeth1072.

Ellis-Davies, G. C. 2013. "A chemist and biologist talk to each other about caged neurotransmitters." *Beilstein J Org Chem* 9:64-73. doi: 10.3762/bjoc.9.8.

Ellis-Davies, G. C., and J. H. Kaplan. 1994. "Nitrophenyl-EGTA, a photolabile chelator that selectively binds Ca2+ with high affinity and releases it rapidly upon photolysis." *Proc Natl Acad Sci U S A* 91 (1):187-91.

Engels, J., and E. J. Schlaeger. 1977. "Synthesis, structure, and reactivity of adenosine cyclic 3',5'-phosphate benzyl triesters." *J Med Chem* 20 (7):907-11.

Ertel, E. A., K. P. Campbell, M. M. Harpold, F. Hofmann, Y. Mori, E. Perez-Reyes, A. Schwartz, T. P. Snutch, T. Tanabe, L. Birnbaumer, R. W. Tsien, and W. A. Catterall. 2000. "Nomenclature of voltage-gated calcium channels." *Neuron* 25 (3):533-5.

Evanko, D. 2005. "Primer: spying on exocytosis with amperometry." *Nat Methods* 2 (9):650. doi: 10.1038/nmeth0905-650.

Fatt, P., and B. Katz. 1952. "Spontaneous subthreshold activity at motor nerve endings." *J Physiol* 117 (1):109-28.

Fehrentz, T., C. A. Kuttruff, F. M. Huber, M. A. Kienzler, P. Mayer, and D. Trauner. 2012. "Exploring the pharmacology and action spectra of photochromic open-channel blockers." *Chembiochem* 13 (12):1746-9. doi: 10.1002/cbic.201200216.

Felder, C. B., R. C. Graul, A. Y. Lee, H. P. Merkle, and W. Sadee. 1999. "The Venus flytrap of periplasmic binding proteins: an ancient protein module present in multiple drug receptors." *AAPS PharmSci* 1 (2):E2.

Fenno, L., O. Yizhar, and K. Deisseroth. 2011. "The development and application of optogenetics." *Annu Rev Neurosci* 34:389-412. doi: 10.1146/annurev-neuro-061010-113817.

Fernandez-Alfonso, T., and T. A. Ryan. 2008. "A heterogeneous "resting" pool of synaptic vesicles that is dynamically interchanged across boutons in mammalian CNS synapses." *Brain Cell Biol* 36 (1-4):87-100. doi: 10.1007/s11068-008-9030-y.

Fernández-Chacón, R., A. Königstorfer, S. H. Gerber, J. García, M. F. Matos, C. F. Stevens, N. Brose, J. Rizo, C. Rosenmund, and T. C. Südhof. 2001. "Synaptotagmin I functions as a calcium regulator of release probability." *Nature* 410 (6824):41-9. doi: 10.1038/35065004.

Fino, E., R. Araya, D. S. Peterka, M. Salierno, R. Etchenique, and R. Yuste. 2009. "RuBi-Glutamate: Two-Photon and Visible-Light Photoactivation of Neurons and Dendritic spines." *Front Neural Circuits* 3:2. doi: 10.3389/neuro.04.002.2009.

Fisher, J. L., and D. D. Mott. 2011. "Distinct functional roles of subunits within the heteromeric kainate receptor." *J Neurosci* 31 (47):17113-22. doi: 10.1523/JNEUROSCI.3685-11.2011.

Fisher, J. L., and D. D. Mott. 2012. "The auxiliary subunits Neto1 and Neto2 reduce voltage-dependent inhibition of recombinant kainate receptors." *J Neurosci* 32 (37):12928-33. doi: 10.1523/JNEUROSCI.2211-12.2012.

Fisher, J. L., and D. D. Mott. 2013. "Modulation of homomeric and heteromeric kainate receptors by the auxiliary subunit Neto1." *J Physiol* 591 (Pt 19):4711-24. doi: 10.1113/jphysiol.2013.256776.

Fortin, D. L., M. R. Banghart, T. W. Dunn, K. Borges, D. A. Wagenaar, Q. Gaudry, M. H. Karakossian, T. S. Otis, W. B. Kristan, D. Trauner, and R. H. Kramer. 2008. "Photochemical control of endogenous ion channels and cellular excitability." *Nat Methods* 5 (4):331-8. doi: 10.1038/nmeth.1187.

Fortin, D. L., T. W. Dunn, A. Fedorchak, D. Allen, R. Montpetit, M. R. Banghart, D. Trauner, J. P. Adelman, and R. H. Kramer. 2011. "Optogenetic photochemical control of designer K+ channels in mammalian neurons." *J Neurophysiol* 106 (1):488-96. doi: 10.1152/jn.00251.2011.

Gao, Y., S. Zorman, G. Gundersen, Z. Xi, L. Ma, G. Sirinakis, J. E. Rothman, and Y. Zhang. 2012. "Single reconstituted neuronal SNARE complexes zipper in three distinct stages." *Science* 337 (6100):1340-3. doi: 10.1126/science.1224492.

Gee, Kyle R., Raymond Wieboldt, and George P. Hess. 1994. "Synthesis and Photochemistry of a New Photolabile Derivative of GABA-Neurotransmitter Release and Receptor Activation in the Microsecond Time Region." *Journal of the American Chemical Society* 116 (18):8366-8367. doi: 10.1021/ja00097a054.

Geppert, M., B. T. Archer, and T. C. Südhof. 1991. "Synaptotagmin II. A novel differentially distributed form of synaptotagmin." *J Biol Chem* 266 (21):13548-52.

Gereau, Robert W., and Geoffrey T. Swanson. 2008. *The glutamate receptors*. Edited by Kim A. Neve: Humana Press.

Gillis D., Kevin. 1995. "Membrane capacitance measurements." In *Single-channel recording*, edited by Bert Sakmann and Erwin Neher, 155-198. New York: Plenum Press.

Goda, Y., and C. F. Stevens. 1994. "Two components of transmitter release at a central synapse." *Proc Natl Acad Sci U S A* 91 (26):12942-6.

Gong, L. W., G. A. de Toledo, and M. Lindau. 2007. "Exocytotic catecholamine release is not associated with cation flux through channels in the vesicle membrane but Na+ influx through the fusion pore." *Nat Cell Biol* 9 (8):915-22. doi: 10.1038/ncb1617.

Gonon, F., R. Cespuglio, J. L. Ponchon, M. Buda, M. Jouvet, R. N. Adams, and J. F. Pujol. 1978. "[In vivo continuous electrochemical determination of dopamine release in rat neostriatum]." *C R Acad Sci Hebd Seances Acad Sci D* 286 (16):1203-6.

Gorostiza, P., and E. Isacoff. 2007. "Optical switches and triggers for the manipulation of ion channels and pores." *Mol Biosyst* 3 (10):686-704. doi: 10.1039/b710287a.

Gorostiza, P., and E. Y. Isacoff. 2008a. "Nanoengineering ion channels for optical control." *Physiology (Bethesda)* 23:238-47. doi: 10.1152/physiol.00018.2008.

Gorostiza, P., and E. Y. Isacoff. 2008b. "Optical switches for remote and noninvasive control of cell signaling." *Science* 322 (5900):395-9. doi: 10.1126/science.1166022.

Gorostiza, P., M. Volgraf, R. Numano, S. Szobota, D. Trauner, and E. Y. Isacoff. 2007. "Mechanisms of photoswitch conjugation and light activation of an ionotropic glutamate receptor." *Proc Natl Acad Sci U S A* 104 (26):10865-70. doi: 10.1073/pnas.0701274104.

Gray, E. G. 1959. "Electron microscopy of synaptic contacts on dendrite spines of the cerebral cortex." *Nature* 183 (4675):1592-3.

Halliwell, R. F., J. A. Peters, and J. J. Lambert. 1989. "The mechanism of action and pharmacological specificity of the anticonvulsant NMDA antagonist MK-801: a voltage clamp study on neuronal cells in culture." *Br J Pharmacol* 96 (2):480-94.

Hamill, O. P., A. Marty, E. Neher, B. Sakmann, and F. J. Sigworth. 1981. "Improved patch-clamp techniques for high-resolution current recording from cells and cell-free membrane patches." *Pflugers Arch* 391 (2):85-100.

Hanson, P. I., R. Roth, H. Morisaki, R. Jahn, and J. E. Heuser. 1997. "Structure and conformational changes in NSF and its membrane receptor complexes visualized by quick-freeze/deep-etch electron microscopy." *Cell* 90 (3):523-35.

Harata, N., T. A. Ryan, S. J. Smith, J. Buchanan, and R. W. Tsien. 2001. "Visualizing recycling synaptic vesicles in hippocampal neurons by FM 1-43 photoconversion." *Proc Natl Acad Sci U S A* 98 (22):12748-53. doi: 10.1073/pnas.171442798.

Harlow, M. L., J. A. Szule, J. Xu, J. H. Jung, R. M. Marshall, and U. J. McMahan. 2013. "Alignment of synaptic vesicle macromolecules with the macromolecules in active zone material that direct vesicle docking." *PLoS One* 8 (7):e69410. doi: 10.1371/journal.pone.0069410.

Harvey, J. H., and D. Trauner. 2008. "Regulating enzymatic activity with a photoswitchable affinity label." *Chembiochem* 9 (2):191-3. doi: 10.1002/cbic.200700570.

Hermanson, Greg T. 2008a. "Chapter 2 - The Chemistry of Reactive Groups." In *Bioconjugate Techniques (Second Edition)*, edited by Greg T. Hermanson, 169-212. New York: Academic Press.

Hermanson, Greg T. 2008b. "Chapter 17 - Chemoselective Ligation: Bioorthogonal Reagents." In *Bioconjugate Techniques (Second Edition)*, edited by Greg T. Hermanson, 666-706. New York: Academic Press.

Heuser, J. E., and T. S. Reese. 1981. "Structural changes after transmitter release at the frog neuromuscular junction." *J Cell Biol* 88 (3):564-80.

Heuser, J. E., T. S. Reese, M. J. Dennis, Y. Jan, L. Jan, and L. Evans. 1979. "Synaptic vesicle exocytosis captured by quick freezing and correlated with quantal transmitter release." *J Cell Biol* 81 (2):275-300.

Hilf, R. J., and R. Dutzler. 2009. "A prokaryotic perspective on pentameric ligand-gated ion channel structure." *Curr Opin Struct Biol* 19 (4):418-24. doi: 10.1016/j.sbi.2009.07.006.

Hille, Bertil. 2001. *Ion Channel of Excitable Membranes*. London ed. Sunderland: Sinauer Associates, Inc.

Hodgkin, A. L., and A. F. Huxley. 1952. "A quantitative description of membrane current and its application to conduction and excitation in nerve." *J Physiol* 117 (4):500-44.

Horn, R., and A. Marty. 1988. "Muscarinic activation of ionic currents measured by a new whole-cell recording method." *J Gen Physiol* 92 (2):145-59.

Hua, Y., and R. H. Scheller. 2001. "Three SNARE complexes cooperate to mediate membrane fusion." *Proc Natl Acad Sci U S A* 98 (14):8065-70. doi: 10.1073/pnas.131214798.

Huettner, J. E. 1990. "Glutamate receptor channels in rat DRG neurons: activation by kainate and quisqualate and blockade of desensitization by Con A." *Neuron* 5 (3):255-66.

Härd, T., P. Fan, and D. R. Kearns. 1990. "A fluorescence study of the binding of Hoechst 33258 and DAPI to halogenated DNAs." *Photochem Photobiol* 51 (1):77-86.

Ishizuka, T., M. Kakuda, R. Araki, and H. Yawo. 2006. "Kinetic evaluation of photosensitivity in genetically engineered neurons expressing green algae light-gated channels." *Neurosci Res* 54 (2):85-94. doi: 10.1016/j.neures.2005.10.009.

Izquierdo-Serra, M., D. Trauner, A. Llobet, and P. Gorostiza. 2013a. "Optical control of calcium-regulated exocytosis." *Biochimica Et Biophysica Acta-General Subjects* 1830 (3):2853-2860. doi: 10.1016/j.bbagen.2012.11.003.

Izquierdo-Serra, M., D. Trauner, A. Llobet, and P. Gorostiza. 2013b. "Optical modulation of neurotransmission using calcium photocurrents through the ion channel LiGluR." *Front Mol Neurosci* 6:3. doi: 10.3389/fnmol.2013.00003.

Janovjak, H., S. Szobota, C. Wyart, D. Trauner, and E. Y. Isacoff. 2010. "A light-gated, potassium-selective glutamate receptor for the optical inhibition of neuronal firing." *Nat Neurosci* 13 (8):1027-32. doi: 10.1038/nn.2589.

Kaech, S., and G. Banker. 2006. "Culturing hippocampal neurons." *Nat Protoc* 1 (5):2406-15. doi: 10.1038/nprot.2006.356.

Kandel R., Eric, James Schwartz H., and Thomas Jessel M. 1991. *Principles of neural science*. Fourth Edition ed. United States of America: McGraw-HIll.

Kaplan, J. H., and G. C. Ellis-Davies. 1988. "Photolabile chelators for the rapid photorelease of divalent cations." *Proc Natl Acad Sci U S A* 85 (17):6571-5.

Kaplan, J. H., B. Forbush, and J. F. Hoffman. 1978. "Rapid photolytic release of adenosine 5'-triphosphate from a protected analogue: utilization by the Na:K pump of human red blood cell ghosts." *Biochemistry* 17 (10):1929-35.

Kasparov, S., and S. Herlitze. 2013. "Optogenetics at a crossroads?" *Exp Physiol* 98 (5):971-2. doi: 10.1113/expphysiol.2012.070797.

Kato, H. E., F. Zhang, O. Yizhar, C. Ramakrishnan, T. Nishizawa, K. Hirata, J. Ito, Y. Aita, T. Tsukazaki, S. Hayashi, P. Hegemann, A. D. Maturana, R. Ishitani, K. Deisseroth, and O. Nureki. 2012. "Crystal structure of the channelrhodopsin light-gated cation channel." In *Nature*, 369-74. England.

Katz, B., and R. Miledi. 1965. "The measurement of synaptic delay, and the time course of acetylcholine release at the neuromuscular junction." *Proc R Soc Lond B Biol Sci* 161:483-95.

Katz, B., and R. Miledi. 1967a. "Ionic requirements of synaptic transmitter release." *Nature* 215 (5101):651.

Katz, B., and R. Miledi. 1967b. "A study of synaptic transmission in the absence of nerve impulses." *J Physiol* 192 (2):407-36.

Kawate, T., J. C. Michel, W. T. Birdsong, and E. Gouaux. 2009. "Crystal structure of the ATP-gated P2X(4) ion channel in the closed state." *Nature* 460 (7255):592-8. doi: 10.1038/nature08198.

Keith, R. K., R. E. Poage, C. T. Yokoyama, W. A. Catterall, and S. D. Meriney. 2007. "Bidirectional modulation of transmitter release by calcium channel/syntaxin interactions in vivo." *J Neurosci* 27 (2):265-9. doi: 10.1523/JNEUROSCI.4213-06.2007.

Kienzler, M. A., A. Reiner, E. Trautman, S. Yoo, D. Trauner, and E. Y. Isacoff. 2013. "A red-shifted, fast-relaxing azobenzene photoswitch for visible light control of an ionotropic glutamate receptor." *J Am Chem Soc* 135 (47):17683-6. doi: 10.1021/ja408104w.

Kissinger, P. T., J. B. Hart, and R. N. Adams. 1973. "Voltammetry in brain tissue--a new neurophysiological measurement." *Brain Res* 55 (1):209-13.

Kleinlogel, S., K. Feldbauer, R. E. Dempski, H. Fotis, P. G. Wood, C. Bamann, and E. Bamberg. 2011. "Ultra light-sensitive and fast neuronal activation with the Ca(2)+-permeable channelrhodopsin CatCh." In *Nat Neurosci*, 513-8. United States.

Klippenstein, V., V. Ghisi, M. Wietstruk, and A. J. Plested. 2014. "Photoinactivation of glutamate receptors by genetically encoded unnatural amino acids." *J Neurosci* 34 (3):980-91. doi: 10.1523/JNEUROSCI.3725-13.2014.

Kramer, R. H., A. Mourot, and H. Adesnik. 2013. "Optogenetic pharmacology for control of native neuronal signaling proteins." *Nat Neurosci* 16 (7):816-23. doi: 10.1038/nn.3424.

Lakowicz, J. R. 2006. *Principles of Fluorescence Spectroscopy*. NewYork, USA: Springer.

Lee, C. J., H. Kong, M. C. Manzini, C. Albuquerque, M. V. Chao, and A. B. MacDermott. 2001. "Kainate receptors expressed by a subpopulation of developing nociceptors rapidly switch from high to low Ca2+ permeability." *J Neurosci* 21 (13):4572-81.

Lee, H. K., Y. Yang, Z. Su, C. Hyeon, T. S. Lee, H. W. Lee, D. H. Kweon, Y. K. Shin, and T. Y. Yoon. 2010. "Dynamic Ca2+-dependent stimulation of vesicle fusion by membrane-anchored synaptotagmin 1." *Science* 328 (5979):760-3. doi: 10.1126/science.1187722.

Lemoine, D., C. Habermacher, A. Martz, P. F. Méry, N. Bouquier, F. Diverchy, A. Taly, F. Rassendren, A. Specht, and T. Grutter. 2013. "Optical control of an ion channel gate." *Proc Natl Acad Sci U S A* 110 (51):20813-8. doi: 10.1073/pnas.1318715110.

Lerma, J. 2006. "Kainate receptor physiology." *Curr Opin Pharmacol* 6 (1):89-97. doi: 10.1016/j.coph.2005.08.004.

Lerma, J., and J. M. Marques. 2013. "Kainate receptors in health and disease." *Neuron* 80 (2):292-311. doi: 10.1016/j.neuron.2013.09.045.

Leslie, B. J., and P. J. Hergenrother. 2008. "Identification of the cellular targets of bioactive small organic molecules using affinity reagents." *Chem Soc Rev* 37 (7):1347-60. doi: 10.1039/b702942j.

Lester, H. A., and H. W. Chang. 1977. "Response of acetylcholine receptors to rapid photochemically produced increases in agonist concentration." *Nature* 266 (5600):373-4.

Lester, R. A., M. L. Quarum, J. D. Parker, E. Weber, and C. E. Jahr. 1989. "Interaction of 6-cyano-7-nitroquinoxaline-2,3-dione with the N-methyl-D-aspartate receptor-associated glycine binding site." *Mol Pharmacol* 35 (5):565-70.

Leszczyszyn, D. J., J. A. Jankowski, O. H. Viveros, E. J. Diliberto, J. A. Near, and R. M. Wightman. 1990. "Nicotinic receptor-mediated catecholamine secretion from individual chromaffin cells. Chemical evidence for exocytosis." *J Biol Chem* 265 (25):14736-7.

Levitz, J., C. Pantoja, B. Gaub, H. Janovjak, A. Reiner, A. Hoagland, D. Schoppik, B. Kane, P. Stawski, A. F. Schier, D. Trauner, and E. Y. Isacoff. 2013. "Optical control of metabotropic glutamate receptors." *Nat Neurosci* 16 (4):507-16. doi: 10.1038/nn.3346.

Leão, R. M., and H. von Gersdorff. 2009. "Synaptic vesicle pool size, release probability and synaptic depression are sensitive to Ca2+ buffering capacity in the developing rat calyx of Held." *Braz J Med Biol Res* 42 (1):94-104.

Li, D., K. Herault, E. Y. Isacoff, M. Oheim, and N. Ropert. 2012. "Optogenetic activation of LiGluR-expressing astrocytes evokes anion channel-mediated glutamate release." In *J Physiol*, 855-73. England.

Li, F., D. Kümmel, J. Coleman, K. M. Reinisch, J. E. Rothman, and F. Pincet. 2014. "A Half-Zippered SNARE Complex Represents a Functional Intermediate in Membrane Fusion." *J Am Chem Soc*. doi: 10.1021/ja410690m.

Li, X., D. V. Gutierrez, M. G. Hanson, J. Han, M. D. Mark, H. Chiel, P. Hegemann, L. T. Landmesser, and S. Herlitze. 2005. "Fast noninvasive activation and inhibition of neural and network activity by vertebrate rhodopsin and green algae channelrhodopsin." *Proc Natl Acad Sci U S A* 102 (49):17816-21. doi: 10.1073/pnas.0509030102.

Lima, S. Q., and G. Miesenböck. 2005. "Remote control of behavior through genetically targeted photostimulation of neurons." *Cell* 121 (1):141-52. doi: 10.1016/j.cell.2005.02.004.

Lin, J. Y. 2011. "A user's guide to channelrhodopsin variants: features, limitations and future developments." *Exp Physiol* 96 (1):19-25. doi: 10.1113/expphysiol.2009.051961.

Lindau, M., and J. M. Fernandez. 1986. "IgE-mediated degranulation of mast cells does not require opening of ion channels." *Nature* 319 (6049):150-3. doi: 10.1038/319150a0.

Lindau, M., and B. D. Gomperts. 1991. "Techniques and concepts in exocytosis: focus on mast cells." *Biochim Biophys Acta* 1071 (4):429-71.

Lindau, M., and E. Neher. 1988. "Patch-clamp techniques for time-resolved capacitance measurements in single cells." *Pflugers Arch* 411 (2):137-46.

Littleton, J. T., M. Stern, K. Schulze, M. Perin, and H. J. Bellen. 1993. "Mutational analysis of Drosophila synaptotagmin demonstrates its essential role in Ca(2+)-activated neurotransmitter release." *Cell* 74 (6):1125-34.

Liu, K. S., M. Siebert, S. Mertel, E. Knoche, S. Wegener, C. Wichmann, T. Matkovic, K. Muhammad, H. Depner, C. Mettke, J. Bückers, S. W. Hell, M. Müller, G. W. Davis, D. Schmitz, and S. J. Sigrist. 2011. "RIM-binding protein, a central part of the active zone, is essential for neurotransmitter release." *Science* 334 (6062):1565-9. doi: 10.1126/science.1212991.

Llinás, R. R. 1977. "Depolarization-release coupling systems in neurons." *Neurosci Res Program Bull* 15 (4):555-687.

Lomant, A. J., and G. Fairbanks. 1976. "Chemical probes of extended biological structures: synthesis and properties of the cleavable protein cross-linking reagent [35S]dithiobis(succinimidyl propionate)." *J Mol Biol* 104 (1):243-61.

Losonczy, A., and J. C. Magee. 2006. "Integrative properties of radial oblique dendrites in hippocampal CA1 pyramidal neurons." *Neuron* 50 (2):291-307. doi: 10.1016/j.neuron.2006.03.016.

Machado, D. J., M. S. Montesinos, and R. Borges. 2008. "Good practices in single-cell amperometry." *Methods Mol Biol* 440:297-313. doi: 10.1007/978-1-59745-178-9_23.

Mao, T., D. Kusefoglu, B. M. Hooks, D. Huber, L. Petreanu, and K. Svoboda. 2011. "Long-range neuronal circuits underlying the interaction between sensory and motor cortex." In *Neuron*, 111-23. United States: 2011 Elsevier Inc.

Marques, J. M., R. J. Rodrigues, S. Valbuena, J. L. Rozas, S. Selak, P. Marin, M. I. Aller, and J. Lerma. 2013. "CRMP2 tethers kainate receptor activity to cytoskeleton dynamics during neuronal maturation." *J Neurosci* 33 (46):18298-310. doi: 10.1523/JNEUROSCI.3136-13.2013.

Matsuzaki, M., G. C. Ellis-Davies, T. Nemoto, Y. Miyashita, M. Iino, and H. Kasai. 2001. "Dendritic spine geometry is critical for AMPA receptor expression in hippocampal CA1 pyramidal neurons." *Nat Neurosci* 4 (11):1086-92. doi: 10.1038/nn736.

Matsuzaki, M., T. Hayama, H. Kasai, and G. C. Ellis-Davies. 2010. "Two-photon uncaging of gamma-aminobutyric acid in intact brain tissue." *Nat Chem Biol* 6 (4):255-7. doi: 10.1038/nchembio.321.

Matthews, G., and P. Fuchs. 2010. "The diverse roles of ribbon synapses in sensory neurotransmission." *Nat Rev Neurosci* 11 (12):812-22. doi: 10.1038/nrn2924.

Mayer, A., W. Wickner, and A. Haas. 1996. "Sec18p (NSF)-driven release of Sec17p (alpha-SNAP) can precede docking and fusion of yeast vacuoles." *Cell* 85 (1):83-94.

Mayer, M. L. 2005. "Crystal structures of the GluR5 and GluR6 ligand binding cores: molecular mechanisms underlying kainate receptor selectivity." *Neuron* 45 (4):539-52. doi: 10.1016/j.neuron.2005.01.031.

McCleskey, E. W., A. P. Fox, D. H. Feldman, L. J. Cruz, B. M. Olivera, R. W. Tsien, and D. Yoshikami. 1987. "Omega-conotoxin: direct and persistent blockade of specific types of calcium channels in neurons but not muscle." *Proc Natl Acad Sci U S A* 84 (12):4327-31.

McMahon, H. T., M. Missler, C. Li, and T. C. Südhof. 1995. "Complexins: cytosolic proteins that regulate SNAP receptor function." *Cell* 83 (1):111-9.

Miesenbock, G. 2009. "The optogenetic catechism." In *Science*, 395-9. United States.

Mintz, I. M., V. J. Venema, K. M. Swiderek, T. D. Lee, B. P. Bean, and M. E. Adams. 1992. "P-type calcium channels blocked by the spider toxin omega-Aga-IVA." *Nature* 355 (6363):827-9. doi: 10.1038/355827a0.

Misura, K. M., R. H. Scheller, and W. I. Weis. 2000. "Three-dimensional structure of the neuronal-Sec1-syntaxin 1a complex." *Nature* 404 (6776):355-62. doi: 10.1038/35006120.

Mittelstaedt, T., E. Alvaréz-Baron, and S. Schoch. 2010. "RIM proteins and their role in synapse function." *Biol Chem* 391 (6):599-606. doi: 10.1515/BC.2010.064.

Mochida, S., Z. H. Sheng, C. Baker, H. Kobayashi, and W. A. Catterall. 1996. "Inhibition of neurotransmission by peptides containing the synaptic protein interaction site of N-type Ca2+ channels." *Neuron* 17 (4):781-8.

Mohrmann, R., H. de Wit, M. Verhage, E. Neher, and J. B. Sørensen. 2010. "Fast vesicle fusion in living cells requires at least three SNARE complexes." *Science* 330 (6003):502-5. doi: 10.1126/science.1193134.

Molleman, Areles. 2003. *Patch Clamping*. England: John Wiley&Sons Ltd.

Mosharov, E. V., and D. Sulzer. 2005. "Analysis of exocytotic events recorded by amperometry." In *Nat Methods*, 651-8. United States.

Mott, D. D., A. Rojas, J. L. Fisher, R. J. Dingledine, and M. Benveniste. 2010. "Subunit-specific desensitization of heteromeric kainate receptors." *J Physiol* 588 (Pt 4):683-700. doi: 10.1113/jphysiol.2009.185207.

Mourot, A., T. Fehrentz, and R. H. Kramer. 2013. "Photochromic potassium channel blockers: design and electrophysiological characterization." *Methods Mol Biol* 995:89-105. doi: 10.1007/978-1-62703-345-9_7.

Mourot, A., T. Fehrentz, Y. Le Feuvre, C. M. Smith, C. Herold, D. Dalkara, F. Nagy, D. Trauner, and R. H. Kramer. 2012. "Rapid optical control of nociception with an ion-channel photoswitch." *Nat Methods* 9 (4):396-402. doi: 10.1038/nmeth.1897.

Mourot, A., M. A. Kienzler, M. R. Banghart, T. Fehrentz, F. M. Huber, M. Stein, R. H. Kramer, and D. Trauner. 2011. "Tuning photochromic ion channel blockers." *ACS Chem Neurosci* 2 (9):536-43. doi: 10.1021/cn200037p.

Murphy, K. P., G. P. Reid, D. R. Trentham, and T. V. Bliss. 1997. "Activation of NMDA receptors is necessary for the induction of associative long-term potentiation in area CA1 of the rat hippocampal slice." *J Physiol* 504 (Pt 2):379-85.

Murthy, V. N., and P. De Camilli. 2003. "Cell biology of the presynaptic terminal." *Annu Rev Neurosci* 26:701-28. doi: 10.1146/annurev.neuro.26.041002.131445.

Mädler, S., C. Bich, D. Touboul, and R. Zenobi. 2009. "Chemical cross-linking with NHS esters: a systematic study on amino acid reactivities." *J Mass Spectrom* 44 (5):694-706. doi: 10.1002/jms.1544.

Nagel, G., T. Szellas, W. Huhn, S. Kateriya, N. Adeishvili, P. Berthold, D. Ollig, P. Hegemann, and E. Bamberg. 2003. "Channelrhodopsin-2, a directly light-gated cation-selective membrane channel." *Proc Natl Acad Sci U S A* 100 (24):13940-5. doi: 10.1073/pnas.1936192100.

Nair, D., E. Hosy, J. D. Petersen, A. Constals, G. Giannone, D. Choquet, and J. B. Sibarita. 2013. "Super-resolution imaging reveals that AMPA receptors inside synapses are dynamically organized in nanodomains regulated by PSD95." *J Neurosci* 33 (32):13204-24. doi: 10.1523/JNEUROSCI.2381-12.2013.

Neher, E. 1993. "Cell physiology. Secretion without full fusion." *Nature* 363 (6429):497-8. doi: 10.1038/363497a0.

Neher, E., and A. Marty. 1982. "Discrete changes of cell membrane capacitance observed under conditions of enhanced secretion in bovine adrenal chromaffin cells." *Proc Natl Acad Sci U S A* 79 (21):6712-6.

Neher, E., and B. Sakmann. 1976. "Single-channel currents recorded from membrane of denervated frog muscle fibres." *Nature* 260 (5554):799-802.

Neher, E., B. Sakmann, and J. H. Steinbach. 1978. "The extracellular patch clamp: a method for resolving currents through individual open channels in biological membranes." *Pflugers Arch* 375 (2):219-28.

Neher, E., and R. S. Zucker. 1993. "Multiple calcium-dependent processes related to secretion in bovine chromaffin cells." In *Neuron*, 21-30. United States.

Newcomb, R., B. Szoke, A. Palma, G. Wang, X. Chen, W. Hopkins, R. Cong, J. Miller, L. Urge, K. Tarczy-Hornoch, J. A. Loo, D. J. Dooley, L. Nadasdi, R. W. Tsien, J. Lemos, and G. Miljanich. 1998. "Selective peptide antagonist of the class E calcium channel from the venom of the tarantula Hysterocrates gigas." *Biochemistry* 37 (44):15353-62. doi: 10.1021/bi981255g.

Nikolenko, V., K. E. Poskanzer, and R. Yuste. 2007. "Two-photon photostimulation and imaging of neural circuits." In *Nat Methods*, 943-50. United States.

Numano, R., S. Szobota, A. Y. Lau, P. Gorostiza, M. Volgraf, B. Roux, D. Trauner, and E. Y. Isacoff. 2009. "Nanosculpting reversed wavelength sensitivity into a photoswitchable iGluR." *Proc Natl Acad Sci U S A* 106 (16):6814-9. doi: 10.1073/pnas.0811899106.

O'Connor, D. T., S. K. Mahata, M. Mahata, Q. Jiang, V. Y. Hook, and L. Taupenot. 2007. "Primary culture of bovine chromaffin cells." In *Nat Protoc*, 1248-53. England.

Oron, D., E. Papagiakoumou, F. Anselmi, and V. Emiliani. 2012. "Two-photon optogenetics." *Prog Brain Res* 196:119-43. doi: 10.1016/B978-0-444-59426-6.00007-0.

Ortells, M. O., and G. G. Lunt. 1995. "Evolutionary history of the ligand-gated ion-channel superfamily of receptors." *Trends Neurosci* 18 (3):121-7.

Packer, A. M., D. S. Peterka, J. J. Hirtz, R. Prakash, K. Deisseroth, and R. Yuste. 2012. "Two-photon optogenetics of dendritic spines and neural circuits." *Nat Methods* 9 (12):1202-5. doi: 10.1038/nmeth.2249.

Palma-Cerda, F., C. Auger, D. J. Crawford, A. C. Hodgson, S. J. Reynolds, J. K. Cowell, K. A. Swift, O. Cais, L. Vyklicky, J. E. Corrie, and D. Ogden. 2012. "New caged neurotransmitter analogs selective for glutamate receptor sub-types based on methoxynitroindoline and nitrophenylethoxycarbonyl caging groups." *Neuropharmacology* 63 (4):624-34. doi: 10.1016/j.neuropharm.2012.05.010.

Pang, Z. P., and T. C. Südhof. 2010. "Cell biology of Ca2+-triggered exocytosis." *Curr Opin Cell Biol* 22 (4):496-505. doi: 10.1016/j.ceb.2010.05.001.

Papagiakoumou, Eirini, Aurelien Begue, Ben Leshem, Osip Schwartz, Brandon M. Stell, Jonathan Bradley, Dan Oron, and Valentina Emiliani. 2013. "Functional patterned multiphoton excitation deep inside scattering tissue." *Nat Photon* 7 (4):274-278.

Partin, K. M., D. K. Patneau, C. A. Winters, M. L. Mayer, and A. Buonanno. 1993. "Selective modulation of desensitization at AMPA versus kainate receptors by cyclothiazide and concanavalin A." *Neuron* 11 (6):1069-82.

Paternain, A. V., A. Cohen, Y. Stern-Bach, and J. Lerma. 2003. "A role for extracellular Na+ in the channel gating of native and recombinant kainate receptors." *J Neurosci* 23 (25):8641-8.

Penner, Reindhold. 1995. "A practical guide to patch clamping." In *Single-Channel Recording*, edited by Bert Sakmann and Erwin Neher. New York: Plenum Press.

Petreanu, L., T. Mao, S. M. Sternson, and K. Svoboda. 2009. "The subcellular organization of neocortical excitatory connections." In *Nature*, 1142-5. England.

Polosukhina, A., J. Litt, I. Tochitsky, J. Nemargut, Y. Sychev, I. De Kouchkovsky, T. Huang, K. Borges, D. Trauner, R. N. Van Gelder, and R. H. Kramer. 2012. "Photochemical restoration of visual responses in blind mice." *Neuron* 75 (2):271-82. doi: 10.1016/j.neuron.2012.05.022.

Purves, Dale, George J Augustine, David Fitzpatrick, Lawrence C Katz, Anthony-Samuel LaMantia, James O McNamara, and S Mark Williams. 2001. "Electrochemical Equilibrium in an Environment with More Than One Permeant Ion." http://www.ncbi.nlm.nih.gov/books/NBK11111/.

Rae, J., K. Cooper, P. Gates, and M. Watsky. 1991. "Low access resistance perforated patch recordings using amphotericin B." *J Neurosci Methods* 37 (1):15-26.

Randall, A., and R. W. Tsien. 1995. "Pharmacological dissection of multiple types of Ca2+ channel currents in rat cerebellar granule neurons." *J Neurosci* 15 (4):2995-3012.

Raster, P., A. Späth, S. Bultakova, P. Gorostiza, B. König, and P. Bregestovski. 2013. "New GABA amides activating GABAA-receptors." *Beilstein J Org Chem* 9:406-10. doi: 10.3762/bjoc.9.42.

Reiter, A., A. Skerra, D. Trauner, and A. Schiefner. 2013. "A photoswitchable neurotransmitter analogue bound to its receptor." *Biochemistry* 52 (50):8972-4. doi: 10.1021/bi4014402.

Ren, Z., N. J. Riley, L. A. Needleman, J. M. Sanders, G. T. Swanson, and J. Marshall. 2003. "Cell surface expression of GluR5 kainate receptors is regulated by an endoplasmic reticulum retention signal." *J Biol Chem* 278 (52):52700-9. doi: 10.1074/jbc.M309585200.

Rettig, J., Z. H. Sheng, D. K. Kim, C. D. Hodson, T. P. Snutch, and W. A. Catterall. 1996. "Isoform-specific interaction of the alpha1A subunits of brain Ca2+ channels with the presynaptic proteins syntaxin and SNAP-25." *Proc Natl Acad Sci U S A* 93 (14):7363-8.

Rial Verde, E. M., L. Zayat, R. Etchenique, and R. Yuste. 2008. "Photorelease of GABA with Visible Light Using an Inorganic Caging Group." *Front Neural Circuits* 2:2. doi: 10.3389/neuro.04.002.2008.

Rivera, R., J. L. Rozas, and J. Lerma. 2007. "PKC-dependent autoregulation of membrane kainate receptors." *EMBO J* 26 (20):4359-67. doi: 10.1038/sj.emboj.7601865.

Rizzoli, S. O., and W. J. Betz. 2005. "Synaptic vesicle pools." *Nat Rev Neurosci* 6 (1):57-69. doi: 10.1038/nrn1583.

Rizzoli, S. O., and R. Jahn. 2007. "Kiss-and-run, collapse and 'readily retrievable' vesicles." *Traffic* 8 (9):1137-44. doi: 10.1111/j.1600-0854.2007.00614.x.

Robinson, I. M., J. M. Finnegan, J. R. Monck, R. M. Wightman, and J. M. Fernandez. 1995. "Colocalization of calcium entry and exocytotic release sites in adrenal chromaffin cells." *Proc Natl Acad Sci U S A* 92 (7):2474-8.

Sabatini, B. L., and W. G. Regehr. 1996. "Timing of neurotransmission at fast synapses in the mammalian brain." *Nature* 384 (6605):170-2. doi: 10.1038/384170a0.

Sakaba, T. 2008. "Two Ca(2+)-dependent steps controlling synaptic vesicle fusion and replenishment at the cerebellar basket cell terminal." *Neuron* 57 (3):406-19. doi: 10.1016/j.neuron.2007.11.029.

Sandoz, G., J. Levitz, R. H. Kramer, and E. Y. Isacoff. 2012. "Optical control of endogenous proteins with a photoswitchable conditional subunit reveals a role for TREK1 in GABA(B) signaling." *Neuron* 74 (6):1005-14. doi: 10.1016/j.neuron.2012.04.026.

Scanziani, M., and M. Hausser. 2009. "Electrophysiology in the age of light." In *Nature*, 930-9. England.

Schanze, Kirk S., T. Fleming Mattox, and David G. Whitten. 1983. "Solvent effects on the thermal cis-trans isomerization and charge-transfer absorption of 4-(diethylamino)-4'-nitroazobenzene." *The Journal of Organic Chemistry* 48 (17):2808-2813. doi: 10.1021/jo00165a005.

Schiavo, G., M. Matteoli, and C. Montecucco. 2000. "Neurotoxins affecting neuroexocytosis." *Physiol Rev* 80 (2):717-66.

Schikorski, T., and C. F. Stevens. 2001. "Morphological correlates of functionally defined synaptic vesicle populations." *Nat Neurosci* 4 (4):391-5. doi: 10.1038/86042.

Schneggenburger, R., A. C. Meyer, and E. Neher. 1999. "Released fraction and total size of a pool of immediately available transmitter quanta at a calyx synapse." *Neuron* 23 (2):399-409.

Schwiening, C. J. 2012. "A brief historical perspective: Hodgkin and Huxley." *J Physiol* 590 (Pt 11):2571-5. doi: 10.1113/jphysiol.2012.230458.

Sharma, M., J. Burré, P. Bronk, Y. Zhang, W. Xu, and T. C. Südhof. 2012. "CSPα knockout causes neurodegeneration by impairing SNAP-25 function." *EMBO J* 31 (4):829-41. doi: 10.1038/emboj.2011.467.

Sharma, M., J. Burré, and T. C. Südhof. 2011. "CSPα promotes SNARE-complex assembly by chaperoning SNAP-25 during synaptic activity." *Nat Cell Biol* 13 (1):30-9. doi: 10.1038/ncb2131.

Sheng, M., and E. Kim. 2011. "The postsynaptic organization of synapses." *Cold Spring Harb Perspect Biol* 3 (12). doi: 10.1101/cshperspect.a005678.

Sheng, Z. H., J. Rettig, M. Takahashi, and W. A. Catterall. 1994. "Identification of a syntaxin-binding site on N-type calcium channels." *Neuron* 13 (6):1303-13.

Shi, L., Q. T. Shen, A. Kiel, J. Wang, H. W. Wang, T. J. Melia, J. E. Rothman, and F. Pincet. 2012. "SNARE proteins: one to fuse and three to keep the nascent fusion pore open." *Science* 335 (6074):1355-9. doi: 10.1126/science.1214984.

Sigworth, F. J., and E. Neher. 1980. "Single Na+ channel currents observed in cultured rat muscle cells." *Nature* 287 (5781):447-9.

Silman, I., and A. Karlin. 1969. "Acetylcholine receptor: covalent attachment of depolarizing groups at the active site." *Science* 164 (3886):1420-1.

Singer, Dafna, Martin Biel, Iliana Lotan, Veit Folckerzi, Franz Hofmann, and Nathan Dascal. 1991. "The roles of the subunits in the function of the calcium channel." *Science* 253 (5027):4.

Sobolevsky, A. I., M. P. Rosconi, and E. Gouaux. 2009. "X-ray structure, symmetry and mechanism of an AMPA-subtype glutamate receptor." *Nature* 462 (7274):745-56. doi: 10.1038/nature08624.

Sommer, B., M. Köhler, R. Sprengel, and P. H. Seeburg. 1991. "RNA editing in brain controls a determinant of ion flow in glutamate-gated channels." *Cell* 67 (1):11-9.

Stawski, P., M. Sumser, and D. Trauner. 2012. "A photochromic agonist of AMPA receptors." *Angew Chem Int Ed Engl* 51 (23):5748-51. doi: 10.1002/anie.201109265.

Stein, M., A. Breit, T. Fehrentz, T. Gudermann, and D. Trauner. 2013. "Optical control of TRPV1 channels." *Angew Chem Int Ed Engl* 52 (37):9845-8. doi: 10.1002/anie.201302530.

Stein, M., S. J. Middendorp, V. Carta, E. Pejo, D. E. Raines, S. A. Forman, E. Sigel, and D. Trauner. 2012. "Azo-propofols: photochromic potentiators of GABA(A) receptors." *Angew Chem Int Ed Engl* 51 (42):10500-4. doi: 10.1002/anie.201205475.

Stevens, C. F., and J. H. Williams. 2007. "Discharge of the readily releasable pool with action potentials at hippocampal synapses." *J Neurophysiol* 98 (6):3221-9. doi: 10.1152/jn.00857.2007.

Sutton, R. B., D. Fasshauer, R. Jahn, and A. T. Brunger. 1998. "Crystal structure of a SNARE complex involved in synaptic exocytosis at 2.4 A resolution." *Nature* 395 (6700):347-53. doi: 10.1038/26412.

Swanson, G. T., D. Feldmeyer, M. Kaneda, and S. G. Cull-Candy. 1996. "Effect of RNA editing and subunit co-assembly single-channel properties of recombinant kainate receptors." *J Physiol* 492 (Pt 1):129-42.

Szobota, S., P. Gorostiza, F. Del Bene, C. Wyart, D. L. Fortin, K. D. Kolstad, O. Tulyathan, M. Volgraf, R. Numano, H. L. Aaron, E. K. Scott, R. H. Kramer, J. Flannery, H. Baier, D. Trauner, and E. Y. Isacoff. 2007. "Remote control of neuronal activity with a light-gated glutamate receptor." In *Neuron*, 535-45. United States.

Szobota, S., and E. Y. Isacoff. 2010. "Optical control of neuronal activity." *Annu Rev Biophys* 39:329-48. doi: 10.1146/annurev.biophys.093008.131400.

Szobota, S., C. McKenzie, and H. Janovjak. 2013. "Optical control of ligand-gated ion channels." *Methods Mol Biol* 998:417-35. doi: 10.1007/978-1-62703-351-0_32.

Szymanski, W., J. M. Beierle, H. A. V. Kistemaker, W. A. Velema, and B. L. Feringa. 2013. "Reversible Photocontrol of Biological Systems by the Incorporation of Molecular Photoswitches." *Chemical Reviews* 113 (8):6114-6178. doi: 10.1021/cr300179f.

Sätzler, K., L. F. Söhl, J. H. Bollmann, J. G. Borst, M. Frotscher, B. Sakmann, and J. H. Lübke. 2002. "Three-dimensional reconstruction of a calyx of Held and its postsynaptic principal neuron in the medial nucleus of the trapezoid body." *J Neurosci* 22 (24):10567-79.

Söllner, T., M. K. Bennett, S. W. Whiteheart, R. H. Scheller, and J. E. Rothman. 1993. "A protein assembly-disassembly pathway in vitro that may correspond to sequential steps of synaptic vesicle docking, activation, and fusion." *Cell* 75 (3):409-18.

Söllner, T., S. W. Whiteheart, M. Brunner, H. Erdjument-Bromage, S. Geromanos, P. Tempst, and J. E. Rothman. 1993. "SNAP receptors implicated in vesicle targeting and fusion." *Nature* 362 (6418):318-24. doi: 10.1038/362318a0.

Südhof, T. C. 2012. "Calcium control of neurotransmitter release." *Cold Spring Harb Perspect Biol* 4 (1):a011353. doi: 10.1101/cshperspect.a011353.

Südhof, T. C. 2013. "Neurotransmitter release: the last millisecond in the life of a synaptic vesicle." *Neuron* 80 (3):675-90. doi: 10.1016/j.neuron.2013.10.022.

Takamori, S., M. Holt, K. Stenius, E. A. Lemke, M. Grønborg, D. Riedel, H. Urlaub, S. Schenck, B. Brügger, P. Ringler, S. A. Müller, B. Rammner, F. Gräter, J. S. Hub, B. L. De Groot, G. Mieskes, Y. Moriyama, J. Klingauf, H. Grubmüller, J. Heuser, F. Wieland, and R. Jahn. 2006. "Molecular anatomy of a trafficking organelle." *Cell* 127 (4):831-46. doi: 10.1016/j.cell.2006.10.030.

Tanabe, T., H. Takeshima, A. Mikami, V. Flockerzi, H. Takahashi, K. Kangawa, M. Kojima, H. Matsuo, T. Hirose, and S. Numa. 1987. "Primary structure of the receptor for calcium channel blockers from skeletal muscle." *Nature* 328 (6128):313-8. doi: 10.1038/328313a0.

Tang, M., K. A. Pelkey, D. Ng, E. Ivakine, C. J. McBain, M. W. Salter, and R. R. McInnes. 2011. "Neto1 is an auxiliary subunit of native synaptic kainate receptors." *J Neurosci* 31 (27):10009-18. doi: 10.1523/JNEUROSCI.6617-10.2011.

Thirumurugan, P., D. Matosiuk, and K. Jozwiak. 2013. "Click chemistry for drug development and diverse chemical-biology applications." *Chem Rev* 113 (7):4905-79. doi: 10.1021/cr200409f.

Tochitsky, I., M. R. Banghart, A. Mourot, J. Z. Yao, B. Gaub, R. H. Kramer, and D. Trauner. 2012. "Optochemical control of genetically engineered neuronal nicotinic acetylcholine receptors." *Nat Chem* 4 (2):105-11. doi: 10.1038/nchem.1234.

tom Dieck, S., L. Sanmartí-Vila, K. Langnaese, K. Richter, S. Kindler, A. Soyke, H. Wex, K. H. Smalla, U. Kämpf, J. T. Fränzer, M. Stumm, C. C. Garner, and E. D. Gundelfinger. 1998. "Bassoon, a novel zinc-finger CAG/glutamine-repeat protein selectively localized at the active zone of presynaptic nerve terminals." *J Cell Biol* 142 (2):499-509.

Traynelis, S. F., L. P. Wollmuth, C. J. McBain, F. S. Menniti, K. M. Vance, K. K. Ogden, K. B. Hansen, H. Yuan, S. J. Myers, and R. Dingledine. 2010. "Glutamate receptor ion channels: structure, regulation, and function." *Pharmacol Rev* 62 (3):405-96. doi: 10.1124/pr.109.002451.

Tucker, W. C., T. Weber, and E. R. Chapman. 2004. "Reconstitution of Ca2+-regulated membrane fusion by synaptotagmin and SNAREs." *Science* 304 (5669):435-8. doi: 10.1126/science.1097196.

Tye, K. M., and K. Deisseroth. 2012. "Optogenetic investigation of neural circuits underlying brain disease in animal models." *Nat Rev Neurosci* 13 (4):251-66. doi: 10.1038/nrn3171.

Valera, S., N. Hussy, R. J. Evans, N. Adami, R. A. North, A. Surprenant, and G. Buell. 1994. "A new class of ligand-gated ion channel defined by P2x receptor for extracellular ATP." *Nature* 371 (6497):516-9. doi: 10.1038/371516a0.

van den Bogaart, G., and R. Jahn. 2011. "Counting the SNAREs needed for membrane fusion." *J Mol Cell Biol* 3 (4):204-5. doi: 10.1093/jmcb/mjr004.

Venkatachalam, K., and C. Montell. 2007. "TRP channels." *Annu Rev Biochem* 76:387-417. doi: 10.1146/annurev.biochem.75.103004.142819.

Verhage, M., A. S. Maia, J. J. Plomp, A. B. Brussaard, J. H. Heeroma, H. Vermeer, R. F. Toonen, R. E. Hammer, T. K. van den Berg, M. Missler, H. J. Geuze, and T. C. Südhof. 2000. "Synaptic assembly of the brain in the absence of neurotransmitter secretion." *Science* 287 (5454):864-9.

Vervaeke, K., A. Lorincz, Z. Nusser, and R. A. Silver. 2012. "Gap junctions compensate for sublinear dendritic integration in an inhibitory network." *Science* 335 (6076):1624-8. doi: 10.1126/science.1215101.

Vodovozova, E. L. 2007. "Photoaffinity labeling and its application in structural biology." *Biochemistry (Mosc)* 72 (1):1-20.

Volgraf, M., P. Gorostiza, R. Numano, R. H. Kramer, E. Y. Isacoff, and D. Trauner. 2006. "Allosteric control of an ionotropic glutamate receptor with an optical switch." In *Nat Chem Biol*, 47-52. United States.

Volgraf, M., P. Gorostiza, S. Szobota, M. R. Helix, E. Y. Isacoff, and D. Trauner. 2007. "Reversibly caged glutamate: a photochromic agonist of ionotropic glutamate receptors." *J Am Chem Soc* 129 (2):260-1. doi: 10.1021/ja067269o.

Vyleta, N. P., and P. Jonas. 2014. "Loose coupling between Ca2+ channels and release sensors at a plastic hippocampal synapse." *Science* 343 (6171):665-70. doi: 10.1126/science.1244811.

Walter, A. M., K. Wiederhold, D. Bruns, D. Fasshauer, and J. B. Sørensen. 2010. "Synaptobrevin N-terminally bound to syntaxin-SNAP-25 defines the primed vesicle state in regulated exocytosis." *J Cell Biol* 188 (3):401-13. doi: 10.1083/jcb.200907018.

Wang, X., M. Kibschull, M. M. Laue, B. Lichte, E. Petrasch-Parwez, and M. W. Kilimann. 1999. "Aczonin, a 550-kD putative scaffolding protein of presynaptic active zones, shares homology regions with Rim and Bassoon and binds profilin." *J Cell Biol* 147 (1):151-62.

Wang, Y., M. Okamoto, F. Schmitz, K. Hofmann, and T. C. Südhof. 1997. "Rim is a putative Rab3 effector in regulating synaptic-vesicle fusion." *Nature* 388 (6642):593-8. doi: 10.1038/41580.

Watanabe, S., B. R. Rost, M. Camacho-Pérez, M. W. Davis, B. Söhl-Kielczynski, C. Rosenmund, and E. M. Jorgensen. 2013. "Ultrafast endocytosis at mouse hippocampal synapses." *Nature* 504 (7479):242-7. doi: 10.1038/nature12809.

Watson, B. O., V. Nikolenko, and R. Yuste. 2009. "Two-photon imaging with diffractive optical elements." *Front Neural Circuits* 3:6. doi: 10.3389/neuro.04.006.2009.

Weiss, N., and G. W. Zamponi. 2012. "Regulation of voltage-gated calcium channels by synaptic proteins." *Adv Exp Med Biol* 740:759-75. doi: 10.1007/978-94-007-2888-2_33.

Wieboldt, R., K. R. Gee, L. Niu, D. Ramesh, B. K. Carpenter, and G. P. Hess. 1994. "Photolabile precursors of glutamate: synthesis, photochemical properties, and activation of

glutamate receptors on a microsecond time scale." *Proc Natl Acad Sci U S A* 91 (19):8752-6.

Wightman, R. M., J. A. Jankowski, R. T. Kennedy, K. T. Kawagoe, T. J. Schroeder, D. J. Leszczyszyn, J. A. Near, E. J. Diliberto, and O. H. Viveros. 1991. "Temporally resolved catecholamine spikes correspond to single vesicle release from individual chromaffin cells." *Proc Natl Acad Sci U S A* 88 (23):10754-8.

Wiser, O., M. K. Bennett, and D. Atlas. 1996. "Functional interaction of syntaxin and SNAP-25 with voltage-sensitive L- and N-type Ca2+ channels." *EMBO J* 15 (16):4100-10.

Wofsy, Leon, Henry Metzger, and S. J. Singer. 1962. "Affinity Labeling—a General Method for Labeling the Active Sites of Antibody and Enzyme Molecules*." *Biochemistry* 1 (6):1031-1039. doi: 10.1021/bi00912a013.

Wyart, C., F. Del Bene, E. Warp, E. K. Scott, D. Trauner, H. Baier, and E. Y. Isacoff. 2009. "Optogenetic dissection of a behavioural module in the vertebrate spinal cord." *Nature* 461 (7262):407-10. doi: 10.1038/nature08323.

Xu, J., T. Mashimo, and T. C. Südhof. 2007. "Synaptotagmin-1, -2, and -9: Ca(2+) sensors for fast release that specify distinct presynaptic properties in subsets of neurons." *Neuron* 54 (4):567-81. doi: 10.1016/j.neuron.2007.05.004.

Xu, J., Z. P. Pang, O. H. Shin, and T. C. Südhof. 2009. "Synaptotagmin-1 functions as a Ca2+ sensor for spontaneous release." *Nat Neurosci* 12 (6):759-66. doi: 10.1038/nn.2320.

Xu, W., W. Morishita, P. S. Buckmaster, Z. P. Pang, R. C. Malenka, and T. C. Südhof. 2012. "Distinct neuronal coding schemes in memory revealed by selective erasure of fast synchronous synaptic transmission." *Neuron* 73 (5):990-1001. doi: 10.1016/j.neuron.2011.12.036.

Yip, G. M., Z. W. Chen, C. J. Edge, E. H. Smith, R. Dickinson, E. Hohenester, R. R. Townsend, K. Fuchs, W. Sieghart, A. S. Evers, and N. P. Franks. 2013. "A propofol binding site on mammalian GABAA receptors identified by photolabeling." *Nat Chem Biol* 9 (11):715-20. doi: 10.1038/nchembio.1340.

Yizhar, O., L. E. Fenno, T. J. Davidson, M. Mogri, and K. Deisseroth. 2011. "Optogenetics in neural systems." *Neuron* 71 (1):9-34. doi: 10.1016/j.neuron.2011.06.004.

Yue, L., M. Pawlowski, S. S. Dellal, A. Xie, F. Feng, T. S. Otis, K. S. Bruzik, H. Qian, and D. R. Pepperberg. 2012. "Robust photoregulation of GABA(A) receptors by allosteric modulation with a propofol analogue." *Nat Commun* 3:1095. doi: 10.1038/ncomms2094.

Zemelman, B. V., G. A. Lee, M. Ng, and G. Miesenböck. 2002. "Selective photostimulation of genetically chARGed neurons." *Neuron* 33 (1):15-22.

Zemelman, B. V., N. Nesnas, G. A. Lee, and G. Miesenbock. 2003. "Photochemical gating of heterologous ion channels: remote control over genetically designated populations of neurons." *Proc Natl Acad Sci U S A* 100 (3):1352-7. doi: 10.1073/pnas.242738899.

Zhai, R. G., and H. J. Bellen. 2004. "The architecture of the active zone in the presynaptic nerve terminal." *Physiology (Bethesda)* 19:262-70. doi: 10.1152/physiol.00014.2004.

Zhang, F., L. P. Wang, M. Brauner, J. F. Liewald, K. Kay, N. Watzke, P. G. Wood, E. Bamberg, G. Nagel, A. Gottschalk, and K. Deisseroth. 2007. "Multimodal fast optical interrogation of neural circuitry." *Nature* 446 (7136):633-9. doi: 10.1038/nature05744.

Zhang, W., F. St-Gelais, C. P. Grabner, J. C. Trinidad, A. Sumioka, M. Morimoto-Tomita, K. S. Kim, C. Straub, A. L. Burlingame, J. R. Howe, and S. Tomita. 2009. "A transmembrane

accessory subunit that modulates kainate-type glutamate receptors." *Neuron* 61 (3):385-96. doi: 10.1016/j.neuron.2008.12.014.

Zhou, Z., and S. Misler. 1995. "Amperometric detection of stimulus-induced quantal release of catecholamines from cultured superior cervical ganglion neurons." *Proc Natl Acad Sci U S A* 92 (15):6938-42.

Ziff, E. B. 1997. "Enlightening the postsynaptic density." *Neuron* 19 (6):1163-74.

Appendices

A. Protocols

A.1 Primary culture of bovine chromaffin cells and viral infection

Primary culture

Bovine cromaffin cells culture is from bovine adrenal glands, we obtain 3 or 4 fresh glands from the slaughter house and process them not later than 30-45 min from the moment they have been cut out from the cow. Chromaffin cells are located at the medula of the adrenal gland, thus the culture consist on cleaning the glands, isolating the medula, digesting it to obtain individual cells and finally purify chromaffin cells by sucessive centrigufations. Further information about the culture can also be found on (O'Connor et al. 2007).

Required special reagents:

Reagent	Supplier	Reference
DMEM:F12	Invitrogen	113020-074
FBS	Reactiva	04-007-1A
P/S	Sigma-Aldrich	P7081
Collagenase	Sigma-Aldrich	C9891-500MG
Protease	Sigma-Aldrich	P5147-1G
Percoll	GE Healthcare	17-0891-02
Poly-L-Lysine	Sigma-Aldrich	P4832

Solution recipes

- Buffer A 1x (filtered)

Reagent	Concentration (mM)	Quantity for 1 L (g)
NaCl	140	8.18
KCl	2.5	0.19
$MgCl_2$	1	0.095
HEPES	10	2.38
	pH 7.42	
	Osm 280 mOsm·Kg^{-1}	

- Buffer 10x (filtered)

Reagent	Concentration (mM)	Quantity for 100 mL (g)
NaCl	1400	8.18
KCl	25	0.19
$MgCl_2$	10	0.095
HEPES	100	2.38
	pH 7.42	

- Chromaffin culture media

Reagent	Concentration	Quantity for 500 mL (mL)
DMEM:F12		42
FBS	15%	7.5
P/S	1%	0.5

Equipment:

Culture hood, 37 ºC water bath, 37 ºC incubator with agitation, centrifuge, ultracentrifuge, 37 ºC CO_2 incubator

To prepare before:

- Pre-warmed 500 mL of buffer A 1x (for 2 to 3 adrenal glands)
- In the culture hood:
  - plastic bag
  - scissors (rounded and sharp), scalpel, tweezers in a beaker with ethanol
  - 10 mL syringe
  - Plastic petri dish, 12 cm diameter.
  - Holder
  - 75 cm^2 culture flask
  - Autoclaved material: cloth, funnel, 100 mL and 250 mL beaker and 30 mL ultracentrifuge tube
- Enzymatic solutions:

- 50 mL of 1 mg/mL protease with buffer A 1x
- 50 mL of 1 mg/mL collagenase with buffer A 1x

Filtrate solutions using a syringe and 22 µm filter, and warm them at 37 ºC.

- 12-well plate with poly-L-Lysine treated coverslips (15 mm diameter, number 1). See **section A.4** for the procedure for coverslips treatment.

Procedure:

1. Remove the surrounding fat tissue from 3 glands using the rounded scissors (**Fig. A1**). Be careful not to damage the gland.

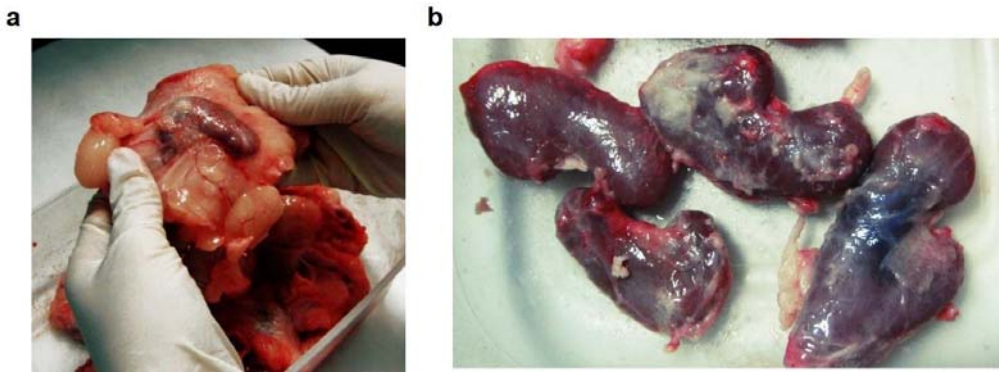

Figure A1. The bovine adrenal gland. (**a**) Adrenal gland covered with fat tissue. The fat tissue help to maintain the temperature of the gland during the transport from the slaughter house to the laboratory. (**b**) Appearance of the bovine adrenal gland once they have been cleaned. Images provided by Júlia Sala Jarque.

2. Clean the blood from inside the glands. With the 10 mL syringe filled 10 mL of warm protease solution, inject the solution *via* the adrenal vein until the gland is inflated. Then pump the liquid up and down, doing some pressure to the gland with the hands to help the blood to exit. Discard the effluent liquid into the 250 mL autoclaved beaker. Finally, inflate the gland with new protease solution, and place it in the beaker. Repeat the procedure for each gland, and cover them with the rest of protease solution. Incubate them at 37 ºC for 12 min.

!! An extensive washing will help to diminish red blood cells in the culture.

3. To isolate the medulla, open the gland by cutting it with the small scissors from the adrenal vein following the external edge of the gland (**Fig. A2**). Place the gland opened like a book (as it is shown in **Figure A2**) in the petri dish. Using the tweezers to hold the cortex and a NUM scalpel, peel out the medulla and place it in the 75 cm^2 sterile flask, with few milliliters of buffer A 1x. After collecting all medullas, add the 50 mL of collagenase solution and incubate it for 25 min at 37 ºC, with gentle agitation (220 rpm).

!! To obtain a cell culture free of fibroblast, no piece of cortex tissue should be taken, as fibroblast are located in this part of the tissue.

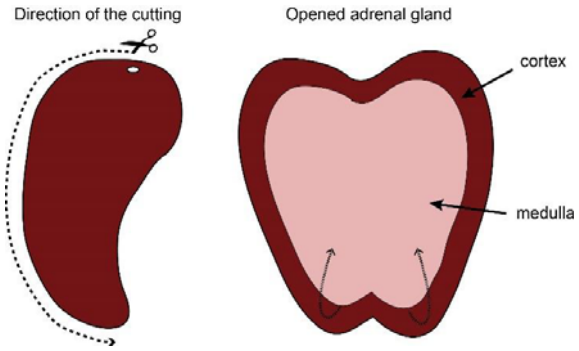

Figure A2. Isolation of the medulla. Scheme of the intact gland showing the direction of the cut (left) done in order to open the adrenal gland (right). To separate the medulla, where the chromaffin cells are, it is peeled from the bottom to the top.

4. Place metal holder with the funnel inside the culture hood, and with the cloth placed on the funnel, filter the collagenase solution with the digested medulla through the cloth to two 50 mL sterile falcon tubes. Fill them up to 30-40 mL with buffer A 1x and centrifuge 15 min at 400*g*.

5. Meanwhile, prepare the percoll solution to isolate chromaffin cells by means of density gradient centrifuge. Mix the secified quantity of percoll and Buffer A 10x in a 30 mL sorval centrifuge tube.

Reagent	Final concentration	Quantity (mL)

Percoll	45%	13.5
Buffer A 10x	1x	1.5
Cell suspension		15

6. When the centrifuge is finished, discard supernatant and resuspend the 2 cell pellets in a final volume of 15 mL Buffer A 1x. Add the 15 mL of cell suspension into the percoll tube.
7. Centrifuge at 20000*g* for 20 min at 8-10 ºC. After the density gradient centrifuge, cell debris will be at the upper portion of the gradient, chromaffin cell band will be the in the middle, and red blood cells accumulate into the bottom of the tube.
8. Discard the debris layer. Carefully collect the middle band containing chromaffin cells and trespass it to a 50 mL sterile falcon tube (it corresponds to 7 mL approximately). Avoid taking red blood cells. When the chromaffin cell band has a silver tone, it is a good indicative of a healthy primary culture.
9. Add up to 20 mL of chromaffin culture media, and pellet cells by centrifuging 10 min at 400*g*.
10. Discard supernatant and resuspend cells in 10 mL of chromaffin media culture.
11. Filter the cell suspension with a 100-µm cell strainer filter (BD Falcon, ref. 352360). Count cells.

!! Typically we obtained 40 to 50 million of cells using 3-4 adrenal glands.

12. Plate chromaffin cells in fresh poly-L-Lysine treated coverslips (15 mm diameter, number 1) on a 12-well plate at a density of 250000 cells per well.
13. Maintain cell culture in a 37 ºC and 5% CO_2 incubator.

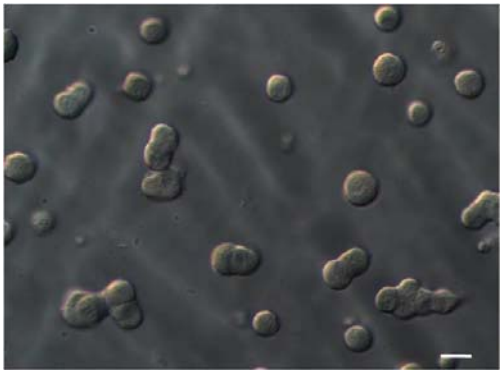

Figure A3. Differential Interference Contrast (DIC) image of chromaffin cells plated in a Poli-L-Lysine treated coverslip, 24 h after isolation. Cultured chromaffin cells have a characteristic round shape. Scale bar 12 µm.

Infection of chromaffin cells with Ad5 viruses

Exogen genes are tipically difficut to express in bovine chromaffin cells. Marcel Ruíz-Mejías optimized the method in the lab. After trying several methods such as lipofectamin, conventional electroporation or nucleofection, he found that viral infection was the best method of inserting our construct, as approximatedly 50% of chromaffin cells were sucessfully expressing the gene.

Ad5 viruses were produced by CBATEG (Universitat Autònoma de Barcelona), and carried the GluK2-L439C-eGFP construct under control of CMV promoter. Viruses were stored at -80 ºC in 50 µL aliquotes of virus with a infectious virus titer about $3.7x10^9$ IU/mL. Each aliquote was maximally unfrozen twice.

!! Some precautions for manipulation of virus: always wear golves. Use pipette tips with filter. All material that have been in contact with viruses should be inmersed in bleach for at least 1 h, before throwing away or cleaning it. Clean the culture hood with bleach and switch the UV lamp on for 1 h, before using it again.

Procedure for viral infection of chromaffin cell culture (24 h post chromaffin cell isolation):

1. Unfreeze the virus aliquote in ice.

2. Remove half of the medium of each well (0.5 mL) and put it into a 25 cm^2 flask, keep the medium in the CO_2 incubator for using it later.
3. Add virus particles to cells at a final rate of 57.6 and 28.8 infections particles per cell.
4. Put cells back to the incubator for 60-90 min. (rate and time should be optimized for each batch of viruses)
5. After incubation, remove cell media with the viruses (throw it in a tube with bleach). Add the 0.5 mL reserved old media per well, and fill them up to 1 mL with fresh chromaffin culture media.
6. Place the cells back to the CO_2 incubator. We used infected cells with the higher rate of infectious particles after 24 h of infection, and the ones treated with the lower rate 48 h.

!! The contstruct GluK2-L439C-eGFP expressed on chromaffin cells (or in neurons, but not in HEK cells) agregates inside the cell after 48 h of expression.

A.2 Hippocampal neuronal culture and transfection

Primary culture

The following protocol is for obtaining a dissociated neuronal culture from 6 hippocampi of 3 postnatal rats P1 to P3. It is a modified protocol from (Halliwell, Peters, and Lambert 1989). Complementary information can be found in the following references (Beaudoin et al. 2012, Kaech and Banker 2006)

Required special reagents:

Reagent	Supplier	Reference	Stock concentration
HBSS +Ca^{2+} and +Mg^{2+}	Invitrogen	24020-091	-
MEM	Sigma-Aldrich	51412C	-
Neurobasal A	Invitrogen	10888-022	-
Trypsin (Type XI) from bovine pancreas	Sigma-Aldrich	T1005	1.25% or 12.5 mg/mL
BSA	Sigma-Aldrich	A7906	-
Ovomucoid (Trypsin inhibitor from chicken egg white)	Sigma-Aldrich	T9253	-
B-27 Serum-Free Suppleent	Invitrogen	17504-044	50x
FBS (heat inactivated)	Invitrogen	10500-056	-
Horse Serum (heat inactivated)	Sigma-Aldrich	H1270	-
P/S	Sigma-Aldrich	P0781	10000 IU/mL / 10 mg/mL
GlutaMax	Invitrogen	A12860	100x
L-glutamine	Sigma-Aldrich	G7513	200 mM
Ara C	Sigma-Aldrich	C6645	10 mM
Sigmacote	Sigma-Aldrich	SL2	-
Poly-D-Lysine	Sigma-Aldrich	P1024	0.1 mg/mL

Solution recipe:

- Basic stock solutions:
    - 15mL of HEPES 1M, filtered.
    - 15 mL of glucose 2.5 M, filtered.
- Trypsin stock:
    - Add 2 mL of HEPES 1 M to 18 mL of HBSS (+Ca^{2+} and +Mg^{2+})
    - Add 250 mg of Trypsin, and store it in 0.5 mL aliquots at -20 ºC
- Enzymatic solution (6 mL, prepare fresh on the day)

Reagent	Final concentration	Quantity for 6 mL
HBSS	-	5.5 mL
Trypsin (1.25% (w/v))	0.1% (w/v)	0.5 mL

- Ovomucoid solution (6 mL)

Reagent	Final concentration	Quantity for 6 mL
BSA	10 mg/mL	60 mg
Ovomucoid	10 mg/mL	60 mg
HEPES (1M)	20 mM	120 µL

- Plating Medium (PM) (8 mL)

Reagent	Final concentration	Quantity for 8 mL (µL)
MEM	-	7.048 mL
Heat-inactived FBS	5% (v/v)	400
Heat-inactived Horse Serum	5% (v/v)	400
P/S (10000 IU/mL and 10 mg/mL)	10 IU/mL and 10 µg/mL	8
L-glutamine (200 mM)	2 mM	80
Glucose (2.5 M)	20 mM	64

- Maintenance medium (50 mL)

Reagent	Final concentration	Quantity for 25 mL (µL)
Neurobasal A	-	47.6 mL
B-27 (50x)	5% (v/v)	1 mL
P/S (10000 IU/mL and 10 mg/mL)	5 IU/mL and 5 µg/mL	250
GlutaMAX (100x)	0.5x	250
Glucose (2.5 M)	15 mM	665

Equipment:

Dissecting microscope with illumination source, culture hood, centrifuge, 37 ºC CO_2 incubator

To prepare before:

- Autoclaved Sterile glass Pasteur pipettes with 4 different diameter, treated with Sigmacote, to avoid cell adhesion to the negative charged glass.
- Filtrate and pre-warm (37 ºC) all solutions:
    - Enzyme solution 6 mL in 7-cm diameter petri Dish (prepare the day of the dissection)
    - HBSS (2 x 5 mL) in 15 mL centrifuge tube
    - Plating medium (2 mL) in 15 ml centrifuge tube
    - Ovomucoid solution (6 mL) in 15 ml centrifuge tube
    - Plating medium (6 mL) in 15 mL centrifuge tube
    - Maintenance medium (50 mL) in 50 mL centrifuge tub
- In the dissection hood:
    - Tray with Ice
    - 3x 100 mL beakers (a layer of agar in the bottom of the glass is recommended for not damaging dissecting tools) filled with ethanol, distilled water or HBSS.

- The following dissecting tools: Big Scissors, small scissors, 2x scalpel (style 10), Small spatula, 2x jeweler tweezers (#5), iris tweezers – serrated curved, Iris Eye dressing tweezers-serrated, sterile plastic Pasteur pipettes
- 2x sterile Pasteur pipettes with end cut
- 3-cm diameter petri dish with HBSS (1 per brain + 1 for all hippocampi), in ice
- 3-cm diameter petri dish empty
- Plastic bag
- 7-cm diameter petri dish filled with freeze water (1 per brain)

- 24-well plate with poly-D-Lysine treated coverslips (12-mm diameter, number 1). See **section A.4** for the detailed protocol of coverslip treatment.

Procedure:

1. Kill three or four postnatal rat pups using an approved method of euthanasia, and separate the head from the body.
2. Dissect and place hippocampi in chilled HBSS.

Hippocampus dissection (any alternative method to isolate hippocampus can be used). Work always on a cold surface.

a. Hold rat head from the nose using the curve tweezers and peel the skin by cutting the laterals and top with scissors. Remove some fat tissue from caudal side.

b. Being carefully, with short movements, open the head following the middle line from back to front using the small scissors. Then, make two perpendicular cuts following the tiny white lines.

c. Remove the cranium film to access to the brain (with serrated forceps), and take the cerebellum out using a spatula.

d. Take the brain from the bottom (also with the spatula) and put it into a 3 cm-petri dish with chilled HBSS.

e. Using a sterile scalpel, cut the brain in two following the middle line.

f. Facing the inner part of the half-brain up, remove all the white brain tissue that is covering the hippocampus using the pair of 'Jeweler' forceps. Remove until hippocampus can be distinguished.

g. Peel out the meninges (full of red globules) that wrap the hippocampus, leaving it as clean as possible.

h. Release the hippocampus. It is fixed to the brain from the upper side and the laterals. Introduce the forceps closed into the upper cleft, and then open in order to break the union. Repeat it along all the line and with the laterals.

i. When the hippocampus is completely separated, remove using the forceps the transparent tissue, which does not contain neurons.

j. Transfer the hippo to a 3 cm-petri dish with HBSS in ice using a plastic Pasteur pipette with the end cut. Repeat steps from f to j for each half-brain.

3. Chop each hippo into 4-5 pieces. (Everything in the culture hood from here onwards).

4. Transfer all pieces of hippocampus to the pre-warmed enzyme solution using a plastic Pasteur pipette. Incubate them at 37 ºC for 10 min.

!! To minimizing the HBSS volume trespassed try to sediment the pieces of hippocampus in the pipette.

5. To wash trypsin, trespass the pieces of hippocampus to the prepared tube with 5 mL of pre-warmed HBSS and resuspend by gentle flicking. Repeat the procedure for the second HBSS tube prepared.

6. Transfer the pieces of hippocampus to the tube with plating medium (2 mL) and triturate into single cell suspension. Gently make hippocampal pieces pass through the Sigmacote-treated pipettes starting from the bigger diameter until the smaller one. Pipette the suspension 10 times in each pipette, until the suspension is homogeneous.

!! It is a critical step. Move the liquid through the pipette slowly and avoid doing any bubble.

7. Carefully layer dissociated cells on top of 6 mL ovomucoid solution. First remove any bubbles from top of ovomucoid solution, then take cells into one of the Pasteur pipettes and very gently place tip at solution interface and bleed cell suspension slowly onto the ovomucoid solution, so that cells remain in very top layer. When cells are pelleted, they cross the protein rich medium of the ovomucoid solution and it seems that protect them.
8. Centrifuge 400*g* for 10 min.
9. Discard the supernatant.
10. Resuspend cells in 6 mL of plating medium (1 mL/hippo), and transfer it to a 50 mL falcon tube. Using a Sigmacote-treated Pasteur pipette mix fairly vigorously (doing bubbles!) [Although many cells die, the culture results much healthy].
11. Filter the cell suspension with a 100-µm cell strainer filter (BD Falcon, ref. 352360)
12. Plate 50000 cells per well using a small volume of 100-300 µL, in a 24-well plate with poly-D-Lysine treated coverslips. Place them into the 37 ºC and 5% CO_2 incubator for 1.5 -2 h, while they are attaching to the surface.

!! The neuronal density is critical for a proper development of neurons, and to create a functional neuronal net. The density of 50000 cells per well has been will only work when all neurons are on the coverslip, thus it is CRITICAL to put the cell suspension as a bubble on the coverslip being carefully not to break the bubble.

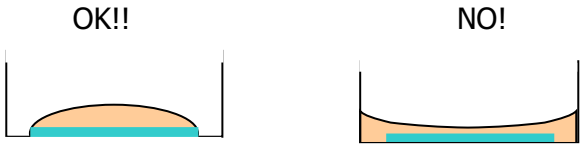

13. Add 0.8 mL of pre-warmed Maintenance Medium once the neurons are attached on the coverslip.
14. On day 2-3, it is needed an anti-mitotic treatment with AraC 5 µM, to avoid fibroblast and astrocyte proliferation. For 24-well plate, prepare 12 mL of maintenance media with AraC (1:1000, stock 10 mM). Remove 0.5 mL of the old media from each well, and then add 0.5 mL with AraC-fresh media.
15. Change half of the media every 3-4 days.

Transfecting neurons with liposomal reagent

In this work, neurons have also been transfected using the calcium phosphate method. This procedure is already described in detail in the **section 3.2**. Here we explain the procedure used when transfection was done with the liposomal transfection reagent Lipofectamine 2000 (Life technologies). Different times, and ratios of transfection reagent and DNA have been tested following the recommendations of from the manufacturer, the best conditions to successfully transfect neurons and keeping them healthy were finally used.

Neurons were transfected with the plasmid pcDNA3 containing the construct GluK2-L439C-eGFP under the control of CMV virus.

Procedure:

Neurons were transfected on *in vitro* day 7 to 12 with Lipofectamine 2000 transfection reagent. The following protocol is for the transfection of ONE well from a 24-well plate.

1. In two separated eppendorff tubes prepare the DNA and Lipofectamine mixture. Incubate 5 min at room temperature.

Reagent	DNA Mix	Lipofectamine Mix
MEM (Sigma, 51412C)	50	50
DNA	0.8 µg	-
Lipofectamine 2000	-	2 µL

2. Add drop by drop the DNA mix onto the Lipofectamine mix and gentle shake it. Incubate 20 min at room temperature.

3. Meanwhile, remove the old media from the neuronal culture, and keep it in the 37 ºC and 5% CO_2 incubator to use it after transfection. Add 0.4 mL of pre-warmed fresh MEM and put neurons back to the incubator.
4. After 20 min incubation add dropwise the 100 µL of the Lipofectamine/DNA mixture to the well. Incubate neurons with the DNA and lipofectamine for 2 h at 37 ºC and 5% of CO_2.
5. Remove the media with DNA and Lipofectamine, wash 3 times with 1 mL of pre-warmed MEM and put back the reserved old media.

6.

A.3 Primary culture of DRG neurons

GluK1 expression in DRG neurons is time dependent (Bahn, Volk, and Wisden 1994), there is a peak of expression of this receptor in neonatal pups (P0 and P1). The subpopulation of DRG neurons that express GluK1 are the small-middle sized (around 20 pF) (Lee et al. 2001). GluK1 currents recording is also time limited, DRG culture neurons are characterized by a rounded body and a small neurites. In the differentiated DRG neuron, GluK1 is expressed at the edge of this neurites, thus the high-resistance access of neurites limits the recording of GluK1 currents. In consequence, they can only be recordered immediately after cell dissection or before 48 h after plating the cells.

This protocol has been modified from the original one written by Sergio Valbuena Alvarez (Juan Lerma laboratory).

Required special reagents:

Reagent	Supplier	Reference	Stock concentration
HBSS no Ca^{2+} no Mg^{2+}	Invitrogen	14175-053	
DMEM with Glutamax	Invitrogen	31966-021	
Collagengase	Sigma-aldrich	C5894	75 mg/mL
DNase	Sigma-aldrich	D5025	5 mg/mL, dissolve in 0.15 M Na
Tripsin	Sigma-aldrich	T7409	1.25% or 12.5 mg/mL
FCS	Invitrogen		
P/S			
NGF	Sigma-aldrich	N0513	10 µg/mL
BDNF	Sigma-aldrich	B3795	20 µg/mL
Poly-L-Lysine	Sigma-aldrich	P7280	250 µg/mL
Laminin	Sigma-aldrich	L2020	1 mg/mL

Solution recipes:

- DRG culture medium:

Reagent	Final concentration	Quantity for 20 mL (mL)
DMEM with Glutamax		18
FCS	10%	2
P/S	1%	0.2
In the final media, it is added:		
NGF	10 ng/mL	
BDNF	20 ng/mL	

Equipment:

Dissecting microscope, culture hood, centrifuge, 37 ºC CO_2 incubator

Procedure**:**

1. Isolation of dorsal root ganglia (DRGs)

    a. Decapitate one mouse (P0-P1). Make two longitudinally cuts, one on each side of the body, above the shoulder and hip joints. Starting by sectioning the ribs and moving until the tail.

    b. Cut transversally behind the hip joint, to isolate the spinal column. Remove the skin that is bound to the dorsal part of the spinal column.

    c. Place the spinal column on a 60-mm diameter dish with cold PBS, dorsal side down. Remove, with number 5 forceps, the organs bound to the column, until the ventral side of it is completely visible.

    d. Make two longitudinal cuts on the ventral side very near from the column. Then remove, with forceps, the spinal cord. Meninges will be visible attached to the internal lateral sides of the spinal column. Remove them. DRGs will then be visible in the intervertebral spaces.

    e. Cut the spinal column in two symmetric pieces and place them in a clean 35-mm diameter dish with cold HBSS. Extract DRGs with sharp number 55 forceps, introducing the tips into the intervertebral spaces and grabbing each ganglion from behind, trying not to grab the body of the ganglion to avoid damaging cells. Approximately 30 to 40

DRGs can be extracted from one mouse. Place the DRGs in a clean 35-mm diameter dish with HBSS.

2. Once you have finished the dissection, put the DRGs in a 15 mL Falcon tube using a glass pipette (rinse the pipette with the medium on the plate a few times before taking the DRGs, to prevent them from sticking to the glass). Adjust the volume to 2.5 mL with HBSS.
3. Add collagenase to a final concentration of 1.25 mg/mL (43 µL of 75 mg/mL stock), DNAse to a final concentration of 50 µg/mL (40 µL of 5 mg/mL stock) and trypsin to 0.125 % (250 µL of 12.5 mg/mL stock).
4. Incubate at 37 ºC for 40 min.
5. Remove the medium carefully after allowing DRG to sediment in the bottom of the tube. Add 5 mL of DRG culture medium prepared without NGF/BDNF.
6. Wait for the DRGs to fall to the bottom again and remove 4 mL of the medium.
7. Add 15 µL of DNase (5 mg/mL stock) and dissociate the DRGs in the remaining 1 mL of medium with a fire-polished Pasteur pipette:
    a. Flame two glass pipettes: make one with a more widely open tip, and the other one with a narrower opening, it should not be too narrow because it may damage cells.
    b. Pass the DRG culture medium through the bigger diameter pipette 10 times, it is recommended to wet the pipette before to prevent DRGs from sticking onto the glass.
    c. Pass DRGs through the second pipette 5-10 times, gently pipetting up and down. Try not to make bubbles. DRGs are completely dissociated when the medium appears homogeneous and no single DRGs can be distinguished any more.
8. Centrifuge 5 min at 400*g*. Remove the supernatant.

9. Add 1 mL of DRG culture medium complete with NGF/BDNF, mix gently and count cells.

10. Plate neurons at the desired concentration on poly-L-Lysine/Laminin treated coverslips (see **section A.4** for coverslip treatment protocol). This coverslip treatment is critical for a good development of DRG neurons. Cells will attach completely to the substrate 3-4 h after plating, they can be patched by then.

A.4 Coverslip treatment

Poly-L-Lysine treated coverslips

- Poly-L-Lysine (Sigma, P4832) sterile-filtered 0.01%.

Coverslip treatment:

1. Incubate 100 sterile coverslips with 3-5 mL of poly-L-Lysine in a sterile 6-cm diameter petri dish for 1-2 h at 37 ºC, or O/N at room temperature.
2. Remove poly-L-Lysine and extenisvly wash them with autoclaved MilliQ (3 to 5 times).
3. Let coverslips dry in the culture hood with the air flow on. Do not swith UV on!
4. Use them, or PLL-coverslips can be kept on the fridge for a while (dry or on PBS solution, it depends on the lab).

Poly-L-Lysine/Laminin treated coverslips

- Poly-L-Lysine (Sigma, P4832) sterile-filtered 0.01%.
- Laminin (Sigma, L2020) stock at 1 mg/mL

This coverslip treatment is critical for primary cultures of DRG neurons.

1. Poly-L-Lysine treatment.
    - Incubate coverslips with 1/100 dilution of PLL 0.01%, O/N at room temperature.
    - Wash with PBS with Ca^{2+} 4x if is diluted PLL or 6x if 0.01% PLL was used. PLL excess is toxic for cells!
2. Laminin treatment (laminin helps neurons to develop neurofilaments).
    - Prepare 5 mL of PBS 1 mM Ca^{2+} (add 5 µL of 1 M $CaCl_2$) and filtrate it.

- Dilute Laminin to 4 ug/mL (add 4 ug of 1 mg/mL Laminin to 1 mL of PBS with Ca^{2+} solution).

!! Use always PBS with Ca^{2+}, Laminin needs Ca^{2+} to be effective.

- On PLL-coverslips, add 200 µL of laminin solution, incubate O/N at 37 ºC.
- Before plating cells, aspirate laminin to dry coverslips.

Alternatively, Laminin can be diluted at 16 µg/mL, then the coverslip treatment can be reduced to 4 h at 37 ºC.

Poly-D-Lysine treated coverslips

- Poly-D-Lysine (Sigma, P1024) stock at 1 mg/mL in MiliQ, and filtrated.

Coverslip treatment:

1. Incubate sterile coverslips with Poly-D-Lysine 1 mg/mL for 1-2 h at 37 ºC or O/N at room temperature. If coverslips are incubated individually add 200 µL per coverslip (12 mm diameter) or 5 µg/cm^2.
2. Remove Poly-D-Lysime solution. It can be recycled 1-2 times.
3. Wash coverslips 3 times with PBS and 3 times with MilliQ.
4. Let coverslips dry for 30-60 min in the culture hood with the air flow on, but do not switch UV light on. For drying, put them in the support you will use, they stick on the surface! And it may be difficult to remove them.

Collagenase treated coverslips

- Collagen (from rat tail, Sigma, C7661) stock solution: Dilute collagen at 50 µg/mL with acetic acid 20 mM. Do not filtrate!

Coverslip treatment:

1. Incubate coverslips with collagen solution at 50 µg/mL for 1-2 h at 37 ºC. If coverslips are incubated individually add 180 µL per coverslip (15 mm diameter), or 5-10 µg/cm^2.

2. Remove collagen solution. It can be recycled 2-3 times.
3. Wash coverslips 3 times with PBS and 3 times with MilliQ.
4. Let coverslips dry for 30-60 min in the culture hood with the air flow on and UV light on to sterize (collagen solution can not be filtered). Put them in the support you will use, they stick on the surface!

A.5 Carbon fiber microelectrodes

Carbon-fiber electrodes (CFE) are commercially available (e.g. HEKA) or they can be home-made. There are different alternatives to fabricate the electrodes (Chow H. and von Rüden 1995b, Machado, Montesinos, and Borges 2008). The method we performed consist on isolating single carbon-fiber electrodes with polyethylene leaving with the end of the fiber exposed. The protected CFE is assembled into a glass tube filled with conducting solution. Whit this strategy, the CFE can be mounted on the same patch-clamp headstage used for electrophysiology.

CFE fabrication

1. Under magnifying glass and bright illumination, carefully inserte a single carbon microfiber of 12-µm diameter into polyethylene (PE) tubing of 0.4 x 0.2 mm, previously filled with acetone to reduce static attraction between the plastic and the carbon fiber. Then, remove acetone by capillarity, being careful not to not break the carbon fiber.
2. Connect a platinum loop to a voltage generator and place it under the magnifying glass, it have to be heated up to 200º C. Melt the PE, previously cannulated with the carbon fiber. Firmly suspende the PE tubing in the center of the loop by grasping each ends with the hands. When the middle section of the PE tubing melts (the plastic becomes totally transparent), apply tension, *constantly and slowly*, to stretch the plastic and leave a thin layer of plastic wrapping the carbon fiber.

!! The PE should be in tight contact with the carbon fiber electrode, to avoid leakage of the electrode solution, and the thickness of the PE wrapping should be as thick as the carbon fiber.

3. Remove from the loop the plastic covered carbon fiber, and cut with a *clean* scalpel blade at the middle, resulting in two electrode tip assemblies. Then, cut the opposite end, leaving approximately 1 cm of tube.
4. Mount each tip into a glass capillary that fits on the patch-clamp headstage and glue it with epoxide.

5. Carefully inspect, under the magnifying glass, the tip of the electrode. All electrodes with an abnormal morphology should be discarded (e.g. the PE is not perfectly wrapping the carbon fiber electrode).
6. The electrodes with good appearance are back-filled with 3 M KCl solution and bubbles are removed by gentle hitting the electrode with the fingers.

!! For a proper conduction of the signal, all bubbles must be removed.

7. The tip end needs to be clean before using the electrode with cells or before testing it. Heat the tip using the platinum loop, to retract the plastic covering the carbon fiber, and cut it about 100 µm with a new scalpel blade.

!! The end of the tip should be a straight for a correct quantification of the released molecules.

8. Place the electrode in the patch-clamp headstage with the Ag/AgCl electrode. And it is ready to measure secretion or to be tested.

CFE testing

Conductivity of each electrode tip was tested immersing it into 10 mM $Fe(CN)_6$ in 0.1 M KCl solution, pH 6.8 with Ag/AgCl electrode reference. Two symmetric ramps from +700mV to -300 mV and from -300 mV to +700 mV at 100 mV/s scan rate were applied using EPC-10 amplifier from HEKA (Germany). Therefore if there was a good conductivity a symmetric current response was expected (if not, the electrode tip was discarded) (Schulte, 1996).

B. Abbreviations

	1P	One-photon
	2P	Two-photon
	5-HT	5-hydroxytryptamine
A	Ad5	Adenovirus serotype 5
	AMPA	α-Amino-3-hydroxy-5-methyl-4-isoxazolepropionic acid
	AMPAR	AMPA receptor
	AP	Action potential
	AP-5	2-Amino-5-phosphonopentanoic acid
	AraC	Cytosine β-D-arabinofuranoside hydrochloride
	ATP	Adenosine triphosphate
B	BAPTA	1,2-bis(o-aminophenoxy)ethane-N,N,N',N'-tetraacetic acid
	BDNF	Brain-derived neurotrophic factor
	BSA	Bovine Serum Albumin
C	cDNA	Complementary DNA
	CDNI-GABA	4-carboxymethoxy-5,7-dinitroindolinyl-GABA
	CFE	Carbon fiber microelectrodes
	ChR2	Channelrhodopsin-2
	C_m	Membrane capacitance
	CNB-glu	α-carboxy-ortho-nitrobenzyl-glutamate
	CNS	Centran nervous system
	CNS	Central nervous system
	Con A	Concanavalin A
	CSP	Cysteine string protein
D	DC	Direct current
	DMEM	Dulbecco's Minimal Essential Medium
	DM-nitrophen	1-(2-nitro-4,5-dimethoxyphenyl)-N,N,N',N'-tetrakis[(oxycarbonyl)methyl]-1,2-ethanediamine
	DMSO	Dimethyl sulfoxide
	DNQX	6,7-dinitroquinoxaline-2,3-dione

	DRG	Dorsal Root Ganglion
E	eGFP	Enhanced GFP
	EGTA	Ethylene glycol tetraacetic acid
F	FCS	Fetal Calf Serum
G	GABA	γ-aminobutyric acid receptors
	GluK1, GluK2 and GluK5	Kainate Receptor type 1,2 and 5
	GlyR	Glycine receptors
	GPCRs	G protein-coupled receptor
H	HBSS	Hanks' Balanced Salt solution
	HEK293 tsA201	Human Embrionic Kidney cell line stably expressing SV40 temperature-sensitive T antigen.
	HEPES	2-[4-(2-hydroxyethyl)piperazin-1-yl]ethanesulfonic acid
	HyLighter	Hyperpolarizing light-gated channel
I	iGluR	Ionotropic glutamate receptor
K	KAR	Kainate receptor
	Laser	Light amplification by stimulated emission of radiation
	LED	Light-emitting diodes
L	LBD	Ligand Binding Domain
	LiGluR	Light-gated Glutamate Receptor
M	MAG	Maleimide-Azobenzene-Glutamate
	MEM	Minimum Essential Medium
	mGluR	Metabotropic glutamate receptor
	MNI-glu	4-methoxy-7- nitroindolinyl-glutamate
	Munc-13	Mammalian uncoordinated-13
	Munc-18	Mammalian uncoordinated-18
N	nAChR	Nicotinic acetylcholine receptors
	Neto	Neuropilin and Tolloid like proteins
	NGF	Nerve growth factor
	NHS	N-Hydroxysuccinimide
	NIR	Near-Infrared ratiation
	NMDA	N-methyl-D-aspartate

	NMDAR	NMDA receptor
	NMDG	N-Methyl-D-glucamin
	NP-EGTA	Nitrophenyl-EGTA
	NpHR	Halorhodopsin
	NSF	*N*-ethylmaleimide-sensitive factor
P	P/S	Penicillin/Streptomycin
	PCL	Photochromic Tethered Ligand
	PE	Polyethylene
	PLL	Poly-L-Lysine
	PSD	Postsynaptic density
	PTL	Photoswitchable Tethered Ligand
Q	QBr	Quaternary ammonium salt- benzyl bromide group
R	RET	Resonant electronic energy transfer
	RIM	Rab3-interacting molecule
	RIM-BP	Rab3-interacting molecule binding protein
	R_m	Membrane resistance
	RRP	Readily releasable pool
	RuBi-glu	Ruthenium-bipyridine- triphenylphosphine-gluamate
S	SM	Sec1/Munc18-like proteins
	SNAP	Soluble NSF attachment proteins
	SNAP-25	Synaptosome-associated protein of 25 kDa
	SNARE	Soluble NSF attachment receptor proteins
T	TEA	Tetraethylamonium
	TTX	Tetrodotoxin
U	UV	Ultra-violet
	UPLC	Ultra Performance Liquid Chromatography
V	VAMP	Vesicle-associated membrane protein
	VGCC	Voltage-gated calcium channels
	V_h	Holding voltage
	V_m	Membrane voltage
W	Wt	Wild-type